

Universiteit
Leiden
The Netherlands

From fetus towards adult : maturation and functional analysis of pluripotent stem cell-derived cardiomyocytes

Catarino Ribeiro, M.

Citation
Catarino Ribeiro, M. (2016, October 13). *From fetus towards adult : maturation and functional analysis of pluripotent stem cell-derived cardiomyocytes*. Retrieved from https://hdl.handle.net/1887/43479

Version:	Not Applicable (or Unknown)
License:	Licence agreement concerning inclusion of doctoral thesis in the Institutional Repository of the University of Leiden
Downloaded from:	https://hdl.handle.net/1887/43479

Note: To cite this publication please use the final published version (if applicable).

Cover Page



Universiteit Leiden



The handle http://hdl.handle.net/1887/43479 holds various files of this Leiden University dissertation

Author: Catarino Ribeiro, Marcelo
Title: From fetus towards adult : maturation and functional analysis of pluripotent stem cell-derived cardiomyocytes
Issue Date: 2016-10-13

From Fetus towards Adult

Maturation and functional analysis of pluripotent stem cell-derived cardiomyocytes

Marcelo Catarino Ribeiro

Promotor: Prof. Dr. Christine Mummery

Co-Promotor: Prof. Dr. Robert Passier

Promotiecommissie:

- Prof. dr. R.C. Hoeben

- Prof.dr. T. Schmidt (Leiden Institute of Physics)

- Prof. dr. M.J.T.H. Goumans

- Dr. E. Danen (LACDR)

Colophon

From Fetus towards Adult - Maturation and functional analysis of pluripotent stem cell-derived cardiomyocytes

This thesis was prepared at the Department of Anatomy & Embryology of the Leiden University Medical Center, Leiden, The Netherlands

Copyright © 2016 Marcelo C. Ribeiro

All rights reserved. No part of this book may be reproduced or transmitted, in any form or by any means, without permission in writing of the author. The copyright of the article that have been published or have been accepted for publication has been transferred to the respective journals.

The research described in this thesis as well as its publication was supported by a grant of Fundamenteel Onderzoek der Materie (FOM).

Financial support by the Dutch Heart Foundation and by the Stichting Proefdiervrij for the publication of this thesis is gratefully acknowledged.

ISBN: 978-90-9029874-0

Cover: Roeland Reitsema, Matthew Schriock and Marcelo C. Ribeiro

Design and Lay-out: Marcelo C. Ribeiro

Printing: Uitgeverij BOXpress || proefschriftmaken.nl

From Fetus towards Adult

Maturation and functional analysis of pluripotent stem cell-derived cardiomyocytes

Proefschrift

ter verkrijging van

de graad van Doctor aan de Universiteit Leiden,

op gezag van Rector Magnificus prof.mr. C.J.J.M. Stolker,

volgens besluit van het College voor Promoties

te verdedigen op donderdag 13 oktober 2016 klokke 16.15 uur

door

Marcelo Catarino Ribeiro

geboren op 18 oktober

1987, Lissabon

Esta tese é dedicada aos meus pais

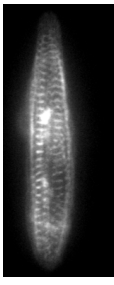
Contents

Chapter 1	General Introduction	9
	Scope of this thesis	18
Chapter 2	Mimicking the in vivo microenvironment in a cell culture dish	27
Chapter 3	Functional maturation of human pluripotent stem cell derived cardiomyocytes in vitro – correlation between contraction force and electrophysiology *Biomaterials. 2015; 51:138–50*	45
Chapter 4	Contractile defect caused by mutation in MYBPC3 revealed under conditions optimized for human PSC-cardiomyocyte function *Adapted from CellReports. 2015; (13):1–13*	73
Chapter 5	Alpha-Actinin-mCherry fusion protein – Building a paramount new tool for cardiomyocyte analysis	103
Chapter 6	Hypertrophic Cardiomyopathy - Impaired sarcomeric motion and contractile dysfunction caused by defective MYBPC3 in hPSC derived cardiomyocytes	123
Chapter 7	Expansion and developmental patterning of human PSC-derived cardiovascular progenitors *Nat Biotechnol. 2015; 33(9):1–12*	141
Chapter 8	General discussion and future perspectives	169
	Summary/ Resumo/ Samenvatting	179/ 184/ 189
	Acknowledgements	193
	Curriculum Vitae	195
	List of Publications	196



Chapter 1

General Introduction



Human pluripotent stem cells (hPSC)

Human embryonic stem cells (hESC), derived from the inner cell mass (ICM) of late blastocyst stage embryos, were first isolated and maintained in culture in 1998 [1]. HESCs have the ability to undergo unlimited self-renewal and are pluripotent, i.e. have the capacity to differentiate into all ~220 somatic cell types in the adult organism and germ cells [2],[3]. hESC are typically characterized by the expression of transcription factors OCT3/4 [4], NANOG [5] and SOX2 [6], which play an important role in the maintenance of their pluripotent state. Additional cell surface markers such as SSEA3, SSEA4, TRA-1-60, TRA-1-80 and TRA-2-49/6E (alkaline phosphatase) are used to distinguish pluripotent hESC from other cell-types [1],[7],[8]. Although, many studies have shown the utility of hESC in biomedical research after their differentiation to specialized cell-types, ethical issues on their origin limited their widespread use for both research and clinical applications.

In 2006, groundbreaking work of the group of Shinya Yamanaka demonstrated the generation of pluripotent stem cells by reprogramming mouse adult cells *in vitro* through overexpression of only 4 transcription factors associated with pluripotency, i.e. Sox2, Oct3/4, c-Myc, and Klf4 [9]. In 2007, the groups of Yamanaka and Thomson independently described this reprogramming for the first time in adult human skin fibroblasts using a similar approach [10,11]. It was demonstrated that these reprogrammed cells, called induced pluripotent stem (iPS) cells, were comparable to hESC, with respect to their morphology, molecular markers and functional characteristics, including self-renewal and differentiation capacity. In addition, human iPS cells resemble the hESC in other aspects, including proliferation, teratoma formation, and promoter- and telomerase activities [10]. Differences in gene expression and methylation state between hiPS cells and hESC have been described [10] when small samples have been compared but overall they seem very similar. The first approaches used integrating retroviral vectors to introduce the reprogramming transcription factors, but later induced pluripotency without the integration of transgenes [12–14]. Banks of hiPS cells from multiple individuals could support *in vitro* studies at the population level for disease modeling, tissue engineering and drug toxicity. Due to their human origin, the tools created with hiPS technology are expected to be more predictive and relevant to human conditions than existing animal or cell line based models.

hPSC cultures

hPSCs self-renewal *in vitro* is rather complex and still under intensive study. Initially hPSC cultures were maintained on mouse embryonic fibroblast (MEF) feeder layers in fetal calf serum (FCS); however, FCS-based media introduced variation in culture and differentiation. Some advances have been made regarding the use of defined medium for sustaining the hPSC self-renewal in culture. Several factors have been reported to be important for the maintenance of pluripotent stem cells *in vitro*. In particular, basic fibroblast growth factor 2 (bFGF) has a pivotal role in hPSC stability and maintenance [15]. Activin A, a member of the transforming growth factor-b family is thought to be important in combination with bFGF for self-renewal of hPSC [16,17]. It has been suggested that the mechanism consists of promoting the expression of the transcription factors needed for self-renewing, such as Oct3/4 and Nanog, through the induction of Smad2/3 [18]. Furthermore, data have been

published demonstrating a crucial role for Phosphoinositide 3-kinases (PI3K) signaling in hESC self-renewal. PI3K appears to be involved in inhibiting differentiation of hESCs as well as in the self-renewal regulatory pathway. Therefore, the presence of PI3K agonists, such as insulin/IGF type molecules, in the culture medium is important for cell survival and self-renewal by inhibiting differentiation [19]. In addition, PI3K suppresses the activity of glycogen synthase kinase-3 (GSK3). Suppression of GSK3 is mandatory for pluripotency maintenance [20]. Furthermore, the production of a completely defined culture medium is essential in the development of large scale culture systems for differentiation purposes and for enabling high throughput *in vitro* screening. The first fully defined medium was made commercially available in 2006 . However, the costs of some components in the medium made it too expensive for daily research use [21]. Therefore modifications were made to develop an alternative, named mTeSR1. Five years later, based on the mTeSR1 formulation Chen et al. decreased the components necessary for hPSC maintenance to 8, the E8 medium containing insulin, selenium, transferrin, L-ascorbic acid, FGF2 and TGFβ in DMEM/F12 [22]. This fully defined medium is now widely used as the starting point for differentiation protocols.

Cardiac differentiation



Initially cardiomyocytes were generated from hESC during "spontaneous" differentiation that takes place when the cells are grown as aggregates in suspension called embryoid bodies (EBs) [23] . A more robust and efficient protocol was later described using END-2 co-culture to differentiate hESC into cardiomyocytes [24]. This protocol was further improved by removal of serum and insulin [25,26]. Presently, there are several methods described for efficient differentiation of human pluripotent stem cells into cardiomyocytes often tailored to the particular hESC or hiPSC. Most efficient are based on defined, serum free medium (methods reviewed in Mummery et al 2012 [27]). Among the more widely used are those based on the serum-free defined media called APEL (albumin, polyvinyl alcohol, essential lipids)[28] or BPEL, a variant of APEL where albumin is replaced by BSA [29]. Since signaling events during early cardiogenesis are highly conserved between species, lessons from cardiac development have been very important for stepwise efficient differentiation of hPSCs to cardiomyocytes. The major signaling pathways involved in cardiogenesis are initiated by ligands of the Transforming growth factor beta family (TGF-β), the wingless/INT proteins (WNTs) and the fibroblast growth factors (FGFs) (reviewed in [30]). Studies on early development have demonstrated that the TGF-β family signaling proteins Activin or nodal are important in the induction of mesoderm specification prior to gastrulation in Xenopus and chick embryos [31,32]. Activin/Nodal signaling pathway activates downstream SMAD proteins type 2 and 3, which have an important role in embryonic development and organ growth. Bone morphogenic proteins (BMPs) also play a role. Among its members BMP4 has a pivotal role in cardiac development, acting via the SMAD (type1,3,5) and MAPK pathways to promote cardiogenesis [33]. The Wnt family are signaling proteins that play a regulatory role in many different developmental processes, including cell survival, migration, proliferation, cell-fate specification and adhesion [34]. Wnt signaling can be divided into two distinct pathways, referred to as canonical and non-canonical. Initial findings suggested a clear functional separation of these signaling pathways, where β-cat-

enin-dependent canonical Wnt pathway is thought to play an inhibitory role on cardiac specification [35,36], as opposed to the cardiovascular development promoting role of the β-catenin-independent non-canonical Wnt signaling [37],[38]. Currently, different studies suggest more complex function of the canonical Wnt pathway in the temporal specification of cardiac commitment. Expression of canonical Wnt ligands before gastrulation promotes mesoderm induction [39], whereas activation of the canonical Wnt pathway during late cardiac differentiation blocks the expression of cardiac genes [40]. Recent completely defined protocols were developed using cytokines BMP4 and Activin A together with a GSK3 inhibitor that acts as a potent Wnt activator to initiate cardiomyocyte differentiation and later removed in a time dependent manner, recapitulating the development cardiac induction signaling *in vivo* [28]. An alternative format of differentiation have been developed using monolayer culture on a specific extracellular matrix (ECM) (e.g. Matrigel) in serum free medium (RPMI/B27 or APEL) in combination with similar cytokine cocktail and timing as the EB methods; cardiomyocyte yields of 30% have been reported [28,41]. More recent advances however, now enable the production of cultures containing 85% or more cardiomyocytes across different hESC and hiPSC lines. This was achieved through the use of RPMI medium in combination with defined chemicals (Wnt activator Chir99021 and Wnt inhibitor Wnt-C59) on hPSC cultures maintained in animal component-free medium (E8) [42]. Further increases in purity of the cardiomyocytes culture have been achieved by taking advantage of the cardiomyocyte's ability to use l-Lactate as an energy source. The use of l-Lactate as a replacement of Glucose as energy substrate eliminates the non-cardiomyocytes from the culture, increasing the cardiomyocytes yield to 95% [42,43]. Other selection methods include the use of cardiomyocte cell surface markers like Sirpα in combination with VECAM [44,45] or cell type specific reporters (review den Hartogh and Passier 2016 [46])

hPSC derived cardiomyocyte phenotype

These recent advances in robust cardiomyocyte differentiation procedures enables the use of hPSC-derived cardiomyocytes for (hPSC-CM) in the fields of disease modeling or drug toxicity screening, which are of interest for both the academic and the industrial research communities. HPSC-CMs based models have the inherent advantage of being human, making them closer to the clinic reality then the established animal models. Moreover, these cells can be generated from any individual as hiPSC, enabling the disease modeling of particular individuals, bridging the *in vitro* phenotype and the clinical symptoms in order to understand the disease mechanism. Despite the advantages of this model, the use of hPSC-technology is still limited by the immature phenotype of the cardiomyocytes. Although hPSC-CMs express cardiac-specific genes, which are necessary for action potential (AP) induction and contractile function, their electrophysiological and contractile properties resemble those of human fetal cardiomyocytes [24]. In particular the APs of hPSC-CM have low resting membrane potentials (~-63mV), low upstroke velocities (~20V/s) and short AP amplitudes (~90mV) in comparison to the adult situation (-85mV, 270V/s and 106mV, respectively)[47]. This immature phenotype is also observed in cell morphology with a variable shape, partially disarrayed sarcomeres and a smaller cell size [48],[49] (**Figure 1**). Additionally, the T-tubules, which are key components of excitation–contraction coupling

mechanism in adult cardiomyocytes, are not present in hPSC-CM, making this feature a hallmark of cardiomyocyte maturation [50]. Mitochondrial structure and function play an important role during development. hPSC-CM have long and slender mitochondria located around the nucleus [51] and use glycolysis as a major energy source, which is comparable to fetal cardiomyocytes, as opposed to the crystal-like lattice pattern distributed throughout the cell [52] and use of fatty acids as energy source in adult cardiomyocytes [53]. Different studies have shown that the gene profiles of hPSC-CM have a higher degree of similarity with fetal than with adult cardiomyocytes [54],[55].

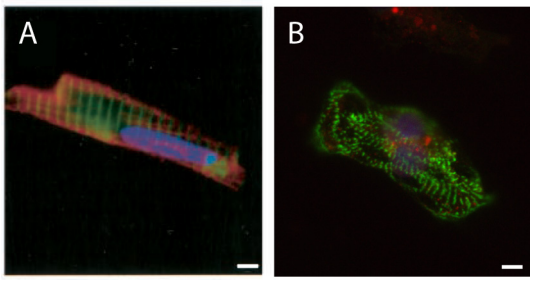


Figure 1- Cardiomyocyte structure. **A.** Human adult cardiomyocytes (Adapted from C. Mummery et. al 2003). **B.** Human stem cell derived cardiomyocytes. Both stained for α-actinin (green), MLC-2v (red) and nuclei (blue).



Maturation of hPSC-CM *in vitro*

Although several studies have shown the potential of hPSC-CM for disease modeling, drug toxicity screening and cell-based therapies, it is crucial to drive hPSC-CM towards a mature phenotype. During cardiac development *in vivo*, cardiomyocytes are exposed to different maturation cues, varying from circulating factors in the blood, to cell-cell interactions, extracellular matrix components to electrical and mechanical signals for a prolonged time allowing cardiomyocytes to develop an adult phenotype and function. Different approaches have been applied to mimic the conditions present in the development of adult heart. The effect of long term culture on hPSC-CM maturation have been described with variable outcomes [56–58]. The most striking change has been reported by Lundy et al. in 2013 by culturing hPSC-CM on glass for periods up to 120 days, leading to improved morphology, sarcomeric structure and length, calcium handling and electrophysiological properties [56]. Interestingly, the commonly used cell culture surfaces such as plastic or glass for cell culture have Young's modulus of ≈2 GPa and ≈50 GPa, respectively, which are 5 to 6 orders of magnitude stiffer than ≈24.4kPa measured on the native heart tissue [59]. Different studies have described that culturing neonatal rat ventricular myocytes (NRVM) on substrates with physiological-like stiffness improved their sarcomere structure, cell aspect ratio and contractile forces [60,61]. Moreover, cardiomyocyte length/width ratio has been proposed as a measure of maturity and disease [62,63]. Cell shape plays an important role in cardiomyocyte function since changes in cytoskeletal architecture have been described to regulate gene expression [64], impulse propagation [65], excitability [66] and contraction [62,67]. Morphology of healthy adult ventricular cardiomyocytes is characterized by an elongated shape with a length/width ratios of 7:1 *in vivo* [68]. Accordingly, restraining cardiomyo-

cyte shape to an adult like length/width ratio, with techniques like microcontact-printing or defined topology, can enhance its sarcomere structure and contractile performance[62]. Furthermore, 2D monolayer cultures lack endogenous 3D biophysical properties crucial for cardiomyocyte development such as electical impulse and mechanical loading. Electrical stimulation have been shown to improve NRVM alignment and ultrastructural organization and to increase contraction amplitude [69]. In 2011 Tulloch et al. were the first to show improvements of hPSC-CM sarcomere alignment and physiological hypertrophy by mechanically stretching cells cast in a 3D collagen gel [70]. Later, a combination of collagen type I and a suture wire in a PDMS channel template created a 3D microenvironment with architectural and electrical cues conducive for hPSC-CM maturation. This so-called 3D biowire platform induced physiological hypertrophy with maturation of contractile apparatus, improvements in calcium handling and electrophysiology properties of hPSC-CM *in vitro* [71]. Although 3D structures are a better representatives of the environment *in vivo* they are still deprived of the biochemical cues present in the blood during development and adult stages. Despite its complexity some components present in human serum such as hormones, growth factors and adrenergic receptor agonists have been described to play a role in cardiomyocyte maturation. Triiodothyronine (T3) is a thyroid hormone involved in numerous physiological processes throughout the body, related to growth and development. More specifically for the development of the heart, T3 has been shown to affect heart rate and metabolism [72]. In addition, T3 has been shown enhance the expression of cardiac genes such as NKX2.5, MYH6, MLC2v, SERCA, RYR2, KCND3 and PGC1α [73,74], which have pivotal roles in cardiomyocyte differentiation and function including electrophysiology [75], calcium handling and contraction force [76]. Furthermore, Insulin-like growth factor 1 (IGF-1) is known to promote cell growth, proliferation, survival and metabolism (reviewed in Troncoso et al. 2014[77]). IGF-1 activates the phosphatidylinositol-3 kinase (PI3K)/Akt pathway, Ras/Raf/ Mitogen-activated protein kinase (MEK) and consequently the extracellular signal-regulated kinase (ERK) pathway, which are major pathways involved in protein production leading to metabolic changes, cell growth and at a later stage cardiomyocyte hypertrophy [78]. Although IGF-1 have been shown to inhibit cardiomyocyte formation [26], its role in promoting migration, proliferation, and survival of cardiac progenitor cells has been established [79,80], making it a potential effector in hPSC-CM maturation.

Cardiac hypertrophy

Cardiac hypertrophy is a process characterized by an increase in cell size with increased protein synthesis and sarcomere assembly. Since mammalian cardiomyocytes rapidly fail to retain their ability to divide, cardiomyocyte hypertrophy accompanied with fibroblast and endothelial proliferation is the major process responsible for the development of the adult size heart. This developmental enlargement of cardiomyocytes is referred to as physiological hypertrophy [48]. During postnatal physiological hypertrophy the contractile apparatus matures, there is a switch to a fatty acid based metabolism and T-tubules develop, improving the excitation contraction coupling efficiency [81]. Physiological hypertrophy also occurs in adult hearts during female pregnancy or extreme exercise by increasing 10–20% heart weight, in order to handle the necessary cardiac output, in a fully reversible man-

ner[82,83]. In contrast, pathological hypertrophy is defined as an overall increase in the size of cardiomyocytes compensating for impaired cardiac function where there is loss of cardiomyocytes (as occurs after myocardial infarction) or pressure overload (aortic stenosis, high blood pressure) or genetic causes. In addition to an increase in cardiomyocyte size, pathological cardiac hypertrophy is characterized by fibroblast proliferation and interstitial fibrosis leading to worsened cardiac function and an increased mortality. Cardiomyopathies can be classified in two different categories: Concentric (hypertrophic cardiomyopathy) or Eccentric (dilated cardiomyopathy). Concentric hypertrophy is evidenced by thicker/wider cardiomyocytes with length/width ratio of 5:1 or lower, which generates a thickening of the cardiac wall and consequently a decrease in ventricular volume [68]. On the other hand, cardiomyocytes in eccentric hypertrophy display an elongated shape with a length/width of 10:1 or greater, leading to a disproportionally thin cardiac walls and ventricular volume overload [63]. Despite the differences between these two extreme phenotypes, both conditions lead to the same outcome: a decrease in cardiac output leading to cardiac failure. An important molecular marker of pathological hypertrophy is the induction or reactivation of genes such as c-jun, c-fos, c-myc, atrial natriuretic peptide (ANP), α-myosin heavy chain (α-MHC) and skeletal alpha actin (SKA), which are also important during development[84].

Molecular pathways in hypertrophy



Cardiac hypertrophy is originated from the cardiomyocyte response to mechanical and neurohormonal stimuli such as angiotensin II, IGF-1, endothelin-1, adrenaline, etc. Although there is some insight on the initial triggers of hypertrophy, the mechanisms underlying progression of pathological hypertrophy are still intensively studied. Several molecular pathways have been described to be involved in the initiation and progression of cardiac hypertrophy. The Phosphoinositide 3-kinase (PI3K)/Akt pathway plays a major role in cardiac hypertrophy and serves as a nodal point that is directly activated by tyrosine kinase receptors such as IGF-R, TGFβ-R (transforming growth factor β-receptor), FGF-R (fibroblast growth factor-receptor), as well as β-adrenergic G protein coupled receptors [85]. The 3-kinase (PI3K)/Akt pathway promotes hypertrophy through mediation of two direct target proteins, mTOR (mammalian target of Rapamycin) and glycogen synthase kinase 3β (GSK3β)[86]. Another important pathway in hypertrophy is the MAPK signalling cascades (mitogen activated protein kinases). These cascades are involved in protein production, cell proliferation, growth and survival, and can be activated by different stimuli as mechanical stress and growth promoting factors (ET-1, AngiotensineII, Phenylephrine and TGF-β). Downstream of these cascades are the Extracellular signal receptor-Regulated Kinase (ERKs), c-jun NH2-terminal Kinase (JNKs) and p38 MAPK, which are known to induce cell growth, increase in protein synthesis and hypertrophy specific gene expression [87,88]. The calcineurin/nuclear factor of activated T-cells (NFAT) was one of the first pathways described as playing a role in hypertrophy. In this pathway, calcineurin is induced by mechanical and/or neurohormonal stimuli to regulate NFAT dephosphorylation [89], leading to nuclear translocation where it can activate transcription factors involved in hypertrophy such as GATA-4 and MEF2 [90]. Furthermore, this process can be inhibited by a class of histone deacetylases (HDACIIa) as they repress transcription of GATA-4, MEF2 and NFAT. On the other hand the class I HDACs are known for their pro-hypertrophic role in the heart

as they are involved in the regulation of growth proliferation and differentiation [91]. The interleukin-6 family of cytokines are known to induce cardiac hypertrophy by binding to a common receptor unit glycoprotein 130 (gp130) and consequently activating the (PI3K)/Akt, MAPK and Janus Associated Kinase/signal transducers and activators of transcription (JAK/STAT) pathways [92]. The JAK/STAT signalling pathway has been implicated as important key in cardiac pathophysiology[93] (**Figure 2**). Dysregulation of this pathway has been described in pressure overload induced hypertrophy [94].

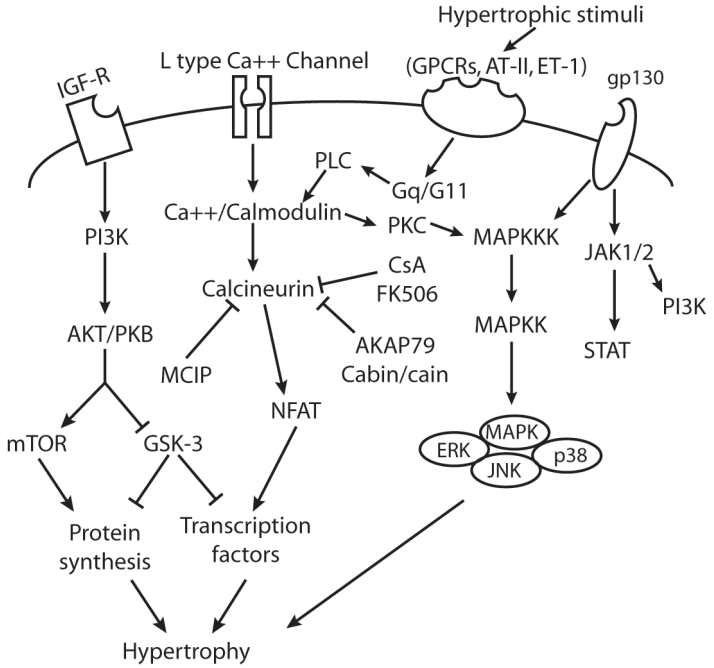


Figure 2- Different mechanisms leading to hypertrophy. Activation of the IGF receptor, L-Type calcium channel or G protein coupled receptors by hypertrophic stimuli leads to the activation of PI3K, Calcineurin and MAP kinase pathways, respectively. The activation of these pathways result in an upregulation or activation of transcription factors involved in protein synthesis and cell growth, the building blocks of hypertrophy. (Figure adapted from Agrawal et al 2010, with permission)

MYBPC3 in Hypertrophic Cardiomyopathy

Hypertrophic cardiomyopathy (HCM) is the most common genetic cardiovascular disease with a prevalence of 1:500 in general population [95] (**Figure 3**). The clinical signs and symptoms for HCM include palpitations, dizziness, syncope and sudden cardiac death (SCD), with the latter often being the first symptom. Genetic linkage studies revealed nine different chromosomal loci, with the preponderance of genes encoding cardiac sarcomeric proteins [96–99] inherited in a dominant autosomal manner. The genes most frequently mutated encode β-myosin heavy chain (35%), myosin binding protein C (20%), troponin T (5%) and α-tropomyosin (<3%), which are proteins with pivotal roles in the cardiomyocyte contraction mechanism [100]. Such mutations can arise de novo or be familial and passed

on from each generation. In the Netherlands nearly 35% of the familial hypertrophic cardiomyopathy are caused by founder mutations in the MYBPC3 gene, which encompass a Guanine duplication in exon 25 (2373dupG) or a Cysteine and threonine deletion from exon 29 (2864_2865delCT)[101]. Although these mutations are predicted to encode a truncated MYBPC3 version, such protein is not found in patient material. Moreover, the amount of the wild-type MYBPC3 has been shown to be reduced by 33% in these patients, suggesting haploinsufficiency as a trigger of the disease mechanism [101]. The cardiac MYBPC3 is present in the C zones of the A band as 9 transverse stripes 43nm apart [102]. This protein is composed of 11 domains named C0-C10 from the N- to the C-terminus and by a linker amino acid sequence (MYBPC motif) between C1 and C2 with four phosphorylation sites. The MYBPC3 interacts with different sarcomeric proteins via de different protein domains. The C0 and C1 are anchored on the actin filaments, allowing the MYBPC motif to interact with the myosin head during contraction. The C2 to C4 domains work as an arm connecting the thin to the thick filament. Furthermore, two predictive models have been suggested describing the interaction between C5 and C10 domains and components of the thick filament [103],[104]. The most accredited model describes a trimeric collar constituted by the C5 to C10 domains of three different MYBPC3 wrapped around the myosin, titin and light meromyosin (LMM). This anchoring is further stabilized by the interaction between domains of the different MYBPC3 (C5:C8 and C7:C10)[105]. Functionally, the MYBPC3 restrains the distance between the thick and the thin filaments and acts as a physical holder of the myosin heads at a specific distance of the actin filament, reducing the probability of their interaction during diastole. Importantly, low levels or absence of MYBPC3 leads to a hypertrophic cardiomyopathy phenotype characterized by an eccentric left ventricular hypertrophy with myocardial disarray, diastolic dysfunction and interstitial fibrosis[106,107].

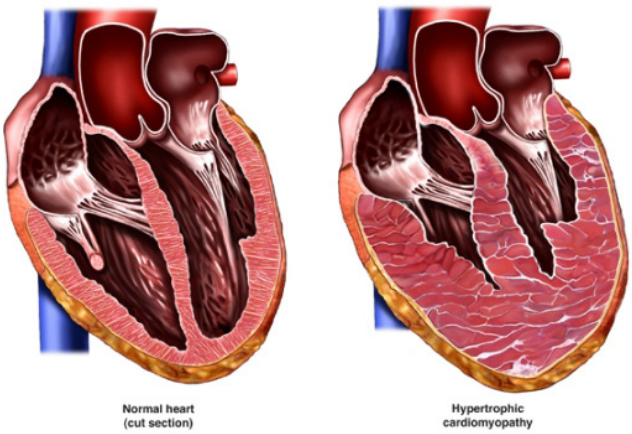


Figure 3- Hypertrophic cardiomyopathy illustration. The hypertrophic heart (right) displays thicker ventricular walls due to the increase in interstitial fibrosis and cardiomyocyte size, decreasing the ventricular volume capacity. (http://www.extremehealthradio.com/i-no-longer-have-hypertrophic-cardiomyopathy)

Scope of this thesis

This thesis describes different approaches for studying human stem cell cardiomyocyte differentiation and their maturation in health and disease using state-of-the-art technologies. By integrating stem cell biology with other disciplines of molecular biology, imaging, biomaterials and biophysics, we were able to address different biological questions. In **Chapter 2** we tested different biocompatible materials for hPSC-CM culture in order to partially mimic the *in vivo* microenvironment using soft substrate stiffness and controlling cell shape. Moreover, we describe the combination of cell traction force measurement technique with μcontact-printing and its application in the assessments of contraction force of single hPSC-CM. In **Chapter 3** a comparative analysis on contraction force was performed between hPSC-CM and primary human fetal cardiomyocytes on the same substrate. Moreover, by adjusting the culture conditions we assessed changes in maturation stage of hPSC-CM by measuring contraction force and electrophysiology in identical cardiomyocytes. In Chapter 4 we describe a combination of different molecules to induce maturation of hPSC-CM *in vitro*. We further use this maturation technology to assess contraction differences on hiPSC-CM derived from patients with a Dutch founder mutation in the MYBPC3 protein. In Chapter 5 we develop a genetically engineered α-actinin-mCherry fusion to study sarcomere development, structure and function of hPSC-CM with live imaging. In Chapter 6 we apply the technology and initial findings of chapters 4 and 5 to develop a hESC-CM based disease model, where we assess changes in calcium kinetics, contraction force and sarcomeric structure caused by the absence of the MYBPC3 protein. In Chapter 7 we make use of an inducible cMYC overexpression to arrest cardiac progenitors in their multipotent state. We were able to expand and differentiate these cardiac progenitors to cardiomyocytes, smooth muscle and endothelial cells. Moreover, within the cardiomyocyte lineage we were able to specifically differentiate the cardiac progenitors to nodal-like or working myocardium *in vitro*. Finally, in Chapter 8 the content of the experimental chapters is discussed and future perspectives in this field are proposed.

References

1. Thomson JA, Itskovitz-eldor J, Shapiro SS, et al. Embryonic Stem Cell Lines Derived from Human Blastocysts. Science (80-). 1998;282(5391):1145-1147.

2. Shimosato D, Shiki M, Niwa H. Extra-embryonic endoderm cells derived from ES cells induced by GATA factors acquire the character of XEN cells. BMC Dev Biol. 2007;7(Icm):80. doi:10.1186/1471-213X-7-80.

3. Fujikura J, Yamato E, Yonemura S, et al. Differentiation of embryonic stem cells is induced by GATA factors. Genes Dev. 2002;16(7):784-789. doi:10.1101/gad.968802.

4. Nichols J, Zevnik B, Anastassiadis K, et al. Formation of pluripotent stem cells in the mammalian embryo depends on the POU transcription factor Oct4. Cell. 1998;95(3):379-391. http://www.ncbi.nlm.nih.gov/pubmed/9814708.

5. Mitsui K, Tokuzawa Y, Itoh H, et al. The homeoprotein Nanog is required for maintenance of pluripotency in mouse epiblast and ES cells. Cell. 2003;113(5):631-642. http://www.ncbi.nlm.nih.gov/pubmed/12787504.

6. Avilion A a, Nicolis SK, Pevny LH, Perez L, Vivian N, Lovell-Badge R. Multipotent cell lineages in early mouse development depend on SOX2 function. Genes Dev. 2003;17(1):126-140. doi:10.1101/gad.224503.

7. Brimble SN, Sherrer ES, Uhl EW, et al. The cell surface glycosphingolipids SSEA-3 and SSEA-4 are not essential for human ESC pluripotency. Stem Cells. 2007;25(1):54-62. doi:10.1634/stemcells.2006-0232.

8. Reubinoff BE, Pera MF, Fong CY, Trounson a, Bongso a. Embryonic stem cell lines from human blastocysts: somatic differentiation in vitro. Nat Biotechnol. 2000;18(4):399-404. doi:10.1038/74447.

9. Takahashi K, Yamanaka S. Induction of Pluripotent Stem Cells from Mouse Embryonic and Adult Fibroblast Cultures by Defined Factors. Cell. 2006;126(4):663-676. doi:10.1016/j.cell.2006.07.024.

10. Takahashi K, Tanabe K, Ohnuki M, et al. Induction of pluripotent stem cells from adult human fibroblasts by defined factors. Cell. 2007;131(5):861-872. doi:10.1016/j.cell.2007.11.019.

11. Yu, Vodyanik, Smuga-Otto, et al. Induced Pluripotent Stem Cell Lines Derived from Human Somatic Cells. Science (80-). 2007;318(5858):1917-1920. doi:10.1126/science.1151526.

12. Yu J, Hu K, Smuga-Otto K, et al. Human induced pluripotent stem cells free of vector and transgene sequences. Science. 2009;324(5928):797-801. doi:10.1126/science.1172482.

13. Nishimura K, Sano M, Ohtaka M, et al. Development of defective and persistent Sendai virus vector: a unique gene delivery/expression system ideal for cell reprogramming. J Biol Chem. 2011;286(6):4760-4771. doi:10.1074/jbc.M110.183780.

14. González F, Boué S, Belmonte JCI. Methods for making induced pluripotent stem cells: reprogramming à la carte. Nat Rev Genet. 2011;12(4):231-242. doi:10.1038/nrg2937.

15. Levenstein ME, Ludwig TE, Xu R-H, et al. Basic fibroblast growth factor support of human embryonic stem cell self-renewal. Stem Cells. 2006;24(3):568-574. doi:10.1634/stemcells.2005-0247.

16. Wang G, Zhang H, Zhao Y, et al. Noggin and bFGF cooperate to maintain the pluripotency of human embryonic stem cells in the absence of feeder layers. Biochem Biophys Res Commun. 2005;330(3):934-942. doi:10.1016/j.bbrc.2005.03.058.

17. Vallier L, Alexander M, Pedersen R a. Activin/Nodal and FGF pathways cooperate to maintain pluripotency of human embryonic stem cells. J Cell Sci. 2005;118:4495-4509. doi:10.1242/



jcs.02553.

18. Babaie Y, Herwig R, Greber B, et al. Analysis of Oct4-dependent transcriptional networks regulating self-renewal and pluripotency in human embryonic stem cells. Stem Cells. 2007;25(2):500-510. doi:10.1634/stemcells.2006-0426.

19. McLean AB. Activin A Efficiently Specifies Definitive Endoderm from Human Embryonic Stem Cells Only When Phosphatidylinositol 3-Kinase. Stem Cells. 2007:29-38. doi:10.1634/stemcells.2006-0219.S.

20. Sato N, Meijer L, Skaltsounis L, Greengard P, Brivanlou AH. Maintenance of pluripotency in human and mouse embryonic stem cells through activation of Wnt signaling by a pharmacological GSK-3-specific inhibitor. Nat Med. 2004;10(1):55-63. doi:10.1038/nm979.

21. Ludwig TE, Levenstein ME, Jones JM, et al. Derivation of human embryonic stem cells in defined conditions. Nat Biotechnol. 2006;24(2):185-187. doi:10.1038/nbt1177.

22. Chen G, Gulbranson DR, Hou Z, et al. Chemically defined conditions for human iPSC derivation and culture. Nat Methods. 2011;8(5):424-429. doi:10.1038/nmeth.1593.

23. Kehat I, Kenyagin-Karsenti D, Snir M, et al. Human embryonic stem cells can differentiate into myocytes with structural and functional properties of cardiomyocytes. J Clin Invest. 2001;108(3):407-414. doi:10.1172/JCI12131.

24. Mummery C, Ward-van Oostwaard D, Doevendans P, et al. Differentiation of human embryonic stem cells to cardiomyocytes: role of coculture with visceral endoderm-like cells. Circulation. 2003;107(21):2733-2740. doi:10.1161/01.CIR.0000068356.38592.68.

25. Mummery CL, Ward D, Passier R. Differentiation of Human Embryonic Stem Cells to Cardiomyocytes by Coculture with Endoderm in Serum-Free Medium. In: Current Protocols in Stem Cell Biology. John Wiley & Sons, Inc.; 2007. doi:10.1002/9780470151808.sc01f02s2.

26. Freund C, Ward-van Oostwaard D, Monshouwer-Kloots J, et al. Insulin Redirects Differentiation from Cardiogenic Mesoderm and Endoderm to Neuroectoderm in Differentiating Human Embryonic Stem Cells. Stem Cells. 2008;26(3):724-733. doi:10.1634/stemcells.2007-0617.

27. Mummery CL, Zhang J, Ng ES, Elliott D a, Elefanty AG, Kamp TJ. Differentiation of human embryonic stem cells and induced pluripotent stem cells to cardiomyocytes: a methods overview. Circ Res. 2012;111(3):344-358. doi:10.1161/CIRCRESAHA.110.227512.

28. Elliott D a, Braam SR, Koutsis K, et al. NKX2-5(eGFP/w) hESCs for isolation of human cardiac progenitors and cardiomyocytes. Nat Methods. 2011;8(12):1037-1040. doi:10.1038/nmeth.1740.

29. Ng ES, Davis R, Stanley EG, Elefanty AG. A protocol describing the use of a recombinant protein-based, animal product-free medium (APEL) for human embryonic stem cell differentiation as spin embryoid bodies. Nat Protoc. 2008;3(5):768-776. doi:10.1038/nprot.2008.42.

30. Olson EN, Schneider MD. Sizing up the heart: development redux in disease. Genes Dev. 2003;17(16):1937-1956. doi:10.1101/gad.1110103.

31. Johansson BM, Wiles M V. Evidence for involvement of activin A and bone morphogenetic protein 4 in mammalian mesoderm and hematopoietic development. Mol Cell Biol. 1995;15(1):141-151.

32. Ladd a N, Yatskievych T a, Antin PB. Regulation of avian cardiac myogenesis by activin/TGFbeta and bone morphogenetic proteins. Dev Biol. 1998;204:407-419. doi:10.1006/dbio.1998.9094.

33. van Wijk B, Moorman AFM, van den Hoff MJB. Role of bone morphogenetic proteins in cardiac differentiation. Cardiovasc Res. 2007;74(2):244-255. doi:10.1016/j.cardiores.2006.11.022.

34. Nusse R. Wnt signaling in disease and in development. Cell Res. 2005;15(1):28-32. doi:10.1038/sj.cr.7290260.

35. Marvin MJ, Di Rocco G, Gardiner A, Bush SM, Lassar AB. Inhibition of Wnt activity induces heart formation from posterior mesoderm. Genes Dev. 2001;15:316-327. doi:10.1101/gad.855501.

36. Schneider V a., Mercola M. Wnt antagonism initiates cardiogenesis in Xenopus laevis. Genes Dev. 2001;15:304-315. doi:10.1101/gad.855601.

37. Eisenberg C a., Eisenberg LM. WNT11 promotes cardiac tissue formation of early mesoderm. Dev Dyn. 1999;216(November 1998):45-58. doi:10.1002/(SICI)1097-0177(199909)216:1<45::AID-DVDY7>3.0.CO;2-L.

38. Pandur P, Lasche M, Eisenberg LM, Kuhl M. Wnt-11 activation of a non-canonical Wnt signalling pathway is required for cardiogenesis. Nature. 2002;418(August):17-19. doi:10.1038/nature00909.1.

39. Ueno S, Weidinger G, Osugi T, et al. Biphasic role for Wnt/beta-catenin signaling in cardiac specification in zebrafish and embryonic stem cells. Proc Natl Acad Sci U S A. 2007;104(23):9685-9690. doi:10.1073/pnas.0702859104.

40. Naito AT, Shiojima I, Akazawa H, et al. Developmental stage-specific biphasic roles of Wnt/beta-catenin signaling in cardiomyogenesis and hematopoiesis. Proc Natl Acad Sci U S A. 2006;103:19812-19817. doi:10.1073/pnas.0605768103.

41. Laflamme M a, Chen KY, Naumova A V, et al. Cardiomyocytes derived from human embryonic stem cells in pro-survival factors enhance function of infarcted rat hearts. Nat Biotechnol. 2007;25(9):1015-1024. doi:10.1038/nbt1327.

42. Burridge PW, Matsa E, Shukla P, et al. Chemically defined generation of human cardiomyocytes. Nat Methods. 2014;11(8):855-860. doi:10.1038/nmeth.2999.

43. Tohyama S, Hattori F, Sano M, et al. Distinct metabolic flow enables large-scale purification of mouse and human pluripotent stem cell-derived cardiomyocytes. Cell Stem Cell. 2013;12(1):127-137. doi:10.1016/j.stem.2012.09.013.

44. Elliott DA, Braam SR, Koutsis K, et al. for isolation of human cardiac progenitors and cardiomyocytes. Nat Methods. 2011;(october):1-7. doi:10.1038/nmeth.1740.

45. Dubois NC, Craft AM, Sharma P, et al. SIRPA is a specific cell-surface marker for isolating cardiomyocytes derived from human pluripotent stem cells. Nat Biotechnol. 2011;29(11):1011-1018. doi:10.1038/nbt.2005.

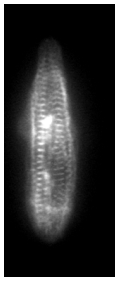
46. Den Hartogh SC, Passier R. Concise Review: Fluorescent Reporters in Human Pluripotent Stem Cells: Contributions to Cardiac Differentiation and Their Applications in Cardiac Disease and Toxicity. Stem Cells. 2016;34(1):13-26. doi:10.1002/stem.2196.

47. Koncz I, Szél T, Bitay M, et al. Electrophysiological effects of ivabradine in dog and human cardiac preparations: potential antiarrhythmic actions. Eur J Pharmacol. 2011;668(3):419-426. doi:10.1016/j.ejphar.2011.07.025.

48. Maillet M, van Berlo JH, Molkentin JD. Molecular basis of physiological heart growth: fundamental concepts and new players. Nat Rev Mol Cell Biol. 2013;14(1):38-48. doi:10.1038/nrm3495.

49. Yang X, Pabon L, Murry CE. Engineering adolescence: maturation of human pluripotent stem cell-derived cardiomyocytes. Circ Res. 2014;114(3):511-523. doi:10.1161/CIRCRESAHA.114.300558.

50. Ziman AP, Gómez-Viquez NL, Bloch RJ, Lederer WJ. Excitation-contraction coupling chang-



es during postnatal cardiac development. J Mol Cell Cardiol. 2010;48(2):379-386. doi:10.1016/j.yjmcc.2009.09.016.

51. Gherghiceanu M, Barad L, Novak A, et al. Cardiomyocytes derived from human embryonic and induced pluripotent stem cells: Comparative ultrastructure. J Cell Mol Med. 2011;15(11):2539-2551. doi:10.1111/j.1582-4934.2011.01417.x.

52. Schaper J, Meiser E, Stämmler G. Ultrastructural morphometric analysis of myocardium from dogs, rats, hamsters, mice, and from human hearts. Circ Res. 1985;56:377-391. doi:10.1161/01.RES.56.3.377.

53. Lopaschuk GD, Jaswal JS. Energy metabolic phenotype of the cardiomyocyte during development, differentiation, and postnatal maturation. J Cardiovasc Pharmacol. 2010;56(2):130-140. doi:10.1097/FJC.0b013e3181e74a14.

54. Synnergren J, Améen C, Jansson A, Sartipy P. Global transcriptional profiling reveals similarities and differences between human stem cell-derived cardiomyocyte clusters and heart tissue. Physiol Genomics. 2012;44(4):245-258. doi:10.1152/physiolgenomics.00118.2011.

55. Xu XQ, Soo SY, Sun W, Zweigerdt R. Global expression profile of highly enriched cardiomyocytes derived from human embryonic stem cells. Stem Cells. 2009;27(9):2163-2174. doi:10.1002/stem.166.

56. Lundy SD, Zhu W-Z, Regnier M, Laflamme M a. Structural and functional maturation of cardiomyocytes derived from human pluripotent stem cells. Stem Cells Dev. 2013;22(14):1991-2002. doi:10.1089/scd.2012.0490.

57. Snir M, Kehat I, Gepstein A, et al. Assessment of the ultrastructural and proliferative properties of human embryonic stem cell-derived cardiomyocytes. Am J Physiol Heart Circ Physiol. 2003;285(6):H2355-H2363. doi:10.1152/ajpheart.00020.2003.

58. Kadota S, Minami I, Morone N, Heuser JE, Agladze K, Nakatsuji N. Development of a reentrant arrhythmia model in human pluripotent stem cell-derived cardiac cell sheets. Eur Heart J. 2013;34(15):1147-1156. doi:10.1093/eurheartj/ehs418.

59. Mirsky I, Parmley WW. Assessment of passive elastic stiffness for isolated heart muscle and the intact heart. Circ Res. 1973;33:233-243. doi:10.1161/01.RES.33.2.233.

60. Jacot JG, McCulloch AD, Omens JH. Substrate stiffness affects the functional maturation of neonatal rat ventricular myocytes. Biophys J. 2008;95(7):3479-3487. doi:10.1529/biophysj.107.124545.

61. Chopra A, Tabdanov E, Patel H, Janmey PA, Yasha J, Kresh JY. Cardiac myocyte remodeling mediated by N-cadherin-dependent mechanosensing Cardiac myocyte remodeling mediated by N-cadherin-dependent mechanosensing. Changes. 2011;(January). doi:10.1152/ajpheart.00515.2010.

62. Kuo P-L, Lee H, Bray M-A, et al. Myocyte shape regulates lateral registry of sarcomeres and contractility. Am J Pathol. 2012;181(6):2030-2037. doi:10.1016/j.ajpath.2012.08.045.

63. Gerdes a. M, Kellerman SE, Moore J a., et al. Structural remodeling of cardiac myocytes in patients with ischemic cardiomyopathy. Circulation. 1992;86(2):426-430. doi:10.1161/01.CIR.86.2.426.

64. Pijnappels D a, Schalij MJ, Ramkisoensing A a, et al. Forced alignment of mesenchymal stem cells undergoing cardiomyogenic differentiation affects functional integration with cardiomyocyte cultures. Circ Res. 2008;103(2):167-176. doi:10.1161/CIRCRESAHA.108.176131.

65. Kléber AG, Rudy Y. Basic mechanisms of cardiac impulse propagation and associated arrhythmias. Physiol Rev. 2004;84(2):431-488. doi:10.1152/physrev.00025.2003.

66. Walsh KB, Parks GE. Changes in cardiac myocyte morphology alter the properties of voltage-gated ion channels. Cardiovasc Res. 2002;55(1):64-75. http://www.ncbi.nlm.nih.gov/pubmed/12062709.

67. Feinberg AW, Feigel A, Shevkoplyas SS, Sheehy S, Whitesides GM, Parker KK. Muscular thin films for building actuators and powering devices. Science. 2007;317(5843):1366-1370. doi:10.1126/science.1146885.

68. Gerdes a M, Capasso JM. Structural remodeling and mechanical dysfunction of cardiac myocytes in heart failure. J Mol Cell Cardiol. 1995;27:849-856.

69. Radisic M, Park H, Shing H, et al. Functional assembly of engineered myocardium by electrical stimulation of cardiac myocytes cultured on scaffolds. Proc Natl Acad Sci U S A. 2004;101(52):18129-18134. doi:10.1073/pnas.0407817101.

70. Tulloch NL, Muskheli V, Razumova M V., et al. Growth of engineered human myocardium with mechanical loading and vascular coculture. Circ Res. 2011;109(1):47-59. doi:10.1161/CIRCRESAHA.110.237206.

71. Nunes SS, Miklas JW, Liu J, et al. Biowire: a platform for maturation of human pluripotent stem cell-derived cardiomyocytes. Nat Methods. 2013;10(8):781-787. doi:10.1038/nmeth.2524.

72. Brent G a. Science in medicine Mechanisms of thyroid hormone action. Sci Med. 2012;122(9):3035-3043. doi:10.1172/JCI60047.three.

73. Klein I, Danzi S. Thyroid disease and the heart. Circulation. 2007;116(15):1725-1735. doi:10.1161/CIRCULATIONAHA.106.678326.

74. Weitzel JM, Radtke C, Seitz HJ. Two thyroid hormone-mediated gene expression patterns in vivo identified by cDNA expression arrays in rat. Nucleic Acids Res. 2001;29(24):5148-5155. http://www.pubmedcentral.nih.gov/articlerender.fcgi?artid=97559&tool=pmcentrez&rendertype=abstract.

75. Lee Y-K, Ng K-M, Chan Y-C, et al. Triiodothyronine promotes cardiac differentiation and maturation of embryonic stem cells via the classical genomic pathway. Mol Endocrinol. 2010;24(9):1728-1736. doi:10.1210/me.2010-0032.

76. Yang X, Rodriguez M, Pabon L, et al. Tri-iodo-l-thyronine promotes the maturation of human cardiomyocytes-derived from induced pluripotent stem cells. J Mol Cell Cardiol. 2014;72:296-304. doi:10.1016/j.yjmcc.2014.04.005.

77. Troncoso R, Ibarra C, Vicencio JM, Jaimovich E, Lavandero S. New insights into IGF-1 signaling in the heart. Trends Endocrinol Metab. 2014;25(3):128-137. doi:10.1016/j.tem.2013.12.002.

78. Song Y-H, Godard M, Li Y, Richmond SR, Rosenthal N, Delafontaine P. Insulin-like growth factor I-mediated skeletal muscle hypertrophy is characterized by increased mTOR-p70S6K signaling without increased Akt phosphorylation. J Investig Med. 2005;53:135-142. doi:10.2310/6650.2005.00309.

79. Kawaguchi N, Smith AJ, Waring CD, et al. c-kitpos GATA-4 high rat cardiac stem cells foster adult cardiomyocyte survival through IGF-1 paracrine signalling. PLoS One. 2010;5(12). doi:10.1371/journal.pone.0014297.

80. Linke A, Müller P, Nurzynska D, et al. Stem cells in the dog heart are self-renewing, clonogenic, and multipotent and regenerate infarcted myocardium, improving cardiac function. Proc Natl Acad Sci U S A. 2005;102:8966-8971. doi:10.1073/pnas.0502678102.

81. Hopkins SF, McCutcheon EP, Wekstein DR. Postnatal changes in rat ventricular function. Circ Res. 1973;32:685-691. doi:10.1161/01.RES.32.6.685.



82. Schannwell CM, Zimmermann T, Schneppenheim M, Plehn G, Marx R, Strauer BE. Left ventricular hypertrophy and diastolic dysfunction in healthy pregnant women. Cardiology. 2002;97:73-78. doi:10.1159/000057675.

83. Sugishita Y, Koseki S, Matsuda M, Yamaguchi T, Ito I. Myocardial mechanics of athletic hearts in comparison with diseased hearts. Am Heart J. 1983;105:273-280.

84. Rohini A, Agrawal N, Koyani CN, Singh R. Molecular targets and regulators of cardiac hypertrophy. Pharmacol Res. 2010;61(4):269-280. doi:10.1016/j.phrs.2009.11.012.

85. Oudit GY, Crackower M a., Eriksson U, et al. Phosphoinositide 3-Kinase γ-Deficient Mice Are Protected From Isoproterenol-Induced Heart Failure. Circulation. 2003;108:2147-2152. doi:10.1161/01.CIR.0000091403.62293.2B.

86. Lupu F, Terwilliger JD, Lee K, Segre G V, Efstratiadis a. Roles of growth hormone and insulin-like growth factor 1 in mouse postnatal growth. Dev Biol. 2001;229:141-162. doi:10.1006/dbio.2000.9975.

87. Lamortes VJ, Thorburns J, Abshers D, et al. Gq- and Ras-dependent Pathways Mediate Hypertrophy of Neonatal Rat Ventricular Myocytes following cw , -Adrenergic Stimulation *. Biol Chem. 1994;269(18):13490-13496.

88. Wang Y. Signal transduction in cardiac hypertrophy - Dissecting compensatory versus pathological pathways utilizing a transgenic approach. Curr Opin Pharmacol. 2001;1:134-140. doi:10.1016/S1471-4892(01)00029-7.

89. De Windt LJ, Lim HW, Bueno OF, et al. Targeted inhibition of calcineurin attenuates cardiac hypertrophy in vivo. Proc Natl Acad Sci U S A. 2001;98(6):3322-3327. doi:10.1073/pnas.031371998.

90. Morimoto T, Hasegawa K, Kaburagi S, et al. Phosphorylation of GATA-4 is involved in a1-adrenergic agonist- responsive transcription of the endothelin-1 gene in cardiac myocytes. J Biol Chem. 2000;275(18):13721-13726. doi:10.1074/jbc.275.18.13721.

91. Kee HJ, Kook H. Roles and targets of class I and IIa histone deacetylases in cardiac hypertrophy. J Biomed Biotechnol. 2011;2011:928326. doi:10.1155/2011/928326.

92. Kunisada K, Hirota H, Fujio Y, et al. Activation of JAK-STAT and MAP Kinases by Leukemia Inhibitory Factor Through gp130 in Cardiac Myocytes. Circ . 1996;94 (10):2626-2632. doi:10.1161/01.CIR.94.10.2626.

93. Harada M, Qin Y, Takano H, et al. G-CSF prevents cardiac remodeling after myocardial infarction by activating the Jak-Stat pathway in cardiomyocytes. Nat Med. 2005;11(3):305-311. doi:10.1038/nm1199.

94. Pan J, Fukuda K, Kodama H, et al. Role of Angiotensin II in Activation of the JAK/STAT Pathway Induced by Acute Pressure Overload in the Rat Heart. Circ Res . 1997;81 (4):611-617. doi:10.1161/01.RES.81.4.611.

95. Maron BJ. Hypertrophic cardiomyopathy: A Systematic Review. Clin Cardiol. 2002;287(10):1308-1320. doi:10.1016/j.cpcardiol.2004.01.001.

96. Jarcho JA, McKenna W, Pare JA, Solomon SD, Holcombe RF, Dickie S. Mapping a gene for familial hypertrophic cardiomyopathy to chromosome 14q1. N Engl J Med. 1989;321:1372-1378.

97. Geisterfer-Lowrance AAT, Kass S, Tanigawa G, et al. A molecular basis for familial hypertrophic cardiomyopathy: A β cardiac myosin heavy chain gene missense mutation. Cell. 1990;62(5):999-1006. doi:10.1016/0092-8674(90)90274-I.

98. Watkins H, MacRae C, Thierfelder L, et al. A disease locus for familial hypertrophic cardiomyo-

pathy maps to chromosome 1q3. Nat Genet. 1993;3(4):333-337. http://dx.doi.org/10.1038/ng0493-333.

99. Thierfelder L, Watkins H, MacRae C, et al. α-tropomyosin and cardiac troponin T mutations cause familial hypertrophic cardiomyopathy: A disease of the sarcomere. Cell. 1994;77(5):701-712. doi:10.1016/0092-8674(94)90054-X.

100. Maron BJ, Maron MS. Hypertrophic cardiomyopathy. Lancet. 381(9862):242-255. doi:10.1016/S0140-6736(12)60397-3.

101. van Dijk SJ, Dooijes D, Remedios C Dos, et al. Cardiac myosin-binding protein C mutations and hypertrophic cardiomyopathy: haploinsufficiency, deranged phosphorylation, and cardiomyocyte dysfunction. Circulation. 2009;119(11):1473-1483. doi:10.1161/CIRCULATIONAHA.108.838672.

102. Luther PK, Bennett PM, Knupp C, et al. Understanding the Organisation and Role of Myosin Binding Protein C in Normal Striated Muscle by Comparison with MyBP-C Knockout Cardiac Muscle. J Mol Biol. 2008;384(1):60-72. doi:10.1016/j.jmb.2008.09.013.

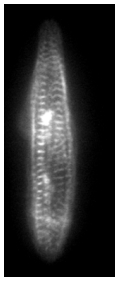
103. Squire JM, Luther PK, Knupp C. Structural evidence for the interaction of C-protein (MyBP-C) with actin and sequence identification of a possible actin-binding domain. J Mol Biol. 2003;331(03):713-724. doi:10.1016/S0022-2836(03)00781-2.

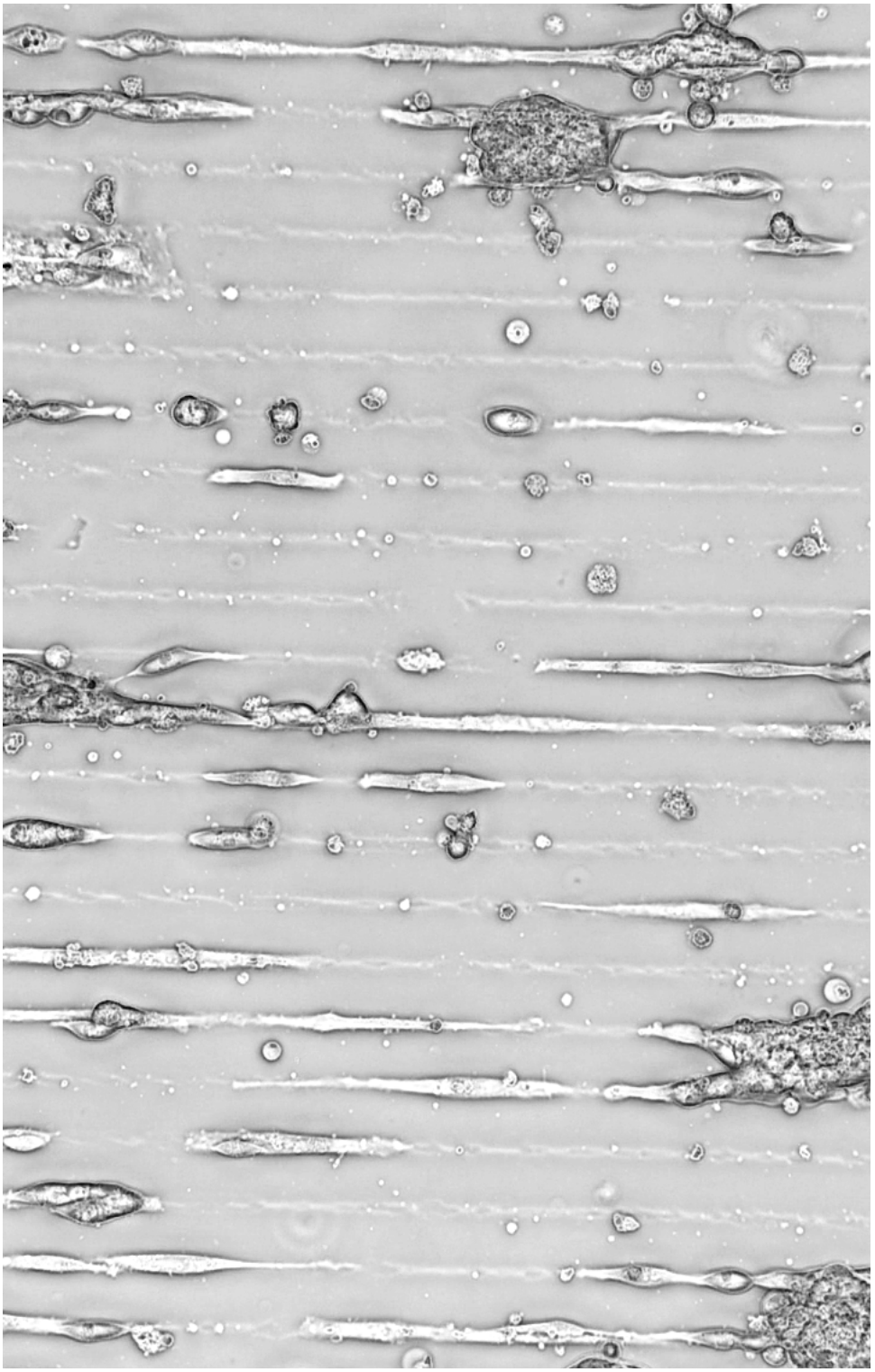
104. Moolman-Smook J, Flashman E, De Lange W, et al. Identification of novel interactions between domains of myosin binding protein-C that are modulated by hypertrophic cardiomyopathy missense mutations. Circ Res. 2002;91:704-711. doi:10.1161/01.RES.0000036750.81083.83.

105. Schlossarek S, Mearini G, Carrier L. Cardiac myosin-binding protein C in hypertrophic cardiomyopathy: mechanisms and therapeutic opportunities. J Mol Cell Cardiol. 2011;50(4):613-620. doi:10.1016/j.yjmcc.2011.01.014.

106. Harris SP, Bartley CR, Hacker T a., et al. Hypertrophic cardiomyopathy in cardiac myosin binding protein-C knockout mice. Circ Res. 2002;90:594-601. doi:10.1161/01.RES.0000012222.70819.64.

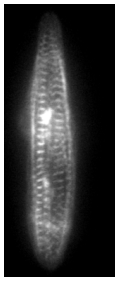
107. Carrier L, Knöll R, Vignier N, et al. Asymmetric septal hypertrophy in heterozygous cMyBP-C null mice. Cardiovasc Res. 2004;63:293-304. doi:10.1016/j.cardiores.2004.04.009.





Chapter 2

Mimicking the *in vivo* microenvironment in a cell culture dish



Marcelo C. Ribeiro[1], Quentin Jallerat[2,3], John M. Szymanski[2,3], Rachelle N. Palchesko[2,3], Stephanie S. Chang[4], Cristina D'Aniello[1], Jantine Monshouwer-Kloots[1], Antonio Gouveia[1], Yu-li Wang[4], Adam W. Feinberg[4,5], Christine L. Mummery[1] and Robert Passier[1]

[1]Department of Anatomy & Embryology, Leiden University Medical Center, Leiden, The Netherlands

[2]Department of Biomedical Engineering, Carnegie Mellon University, Pittsburgh, Pennsylvania, United States of America

[3]Department of Materials Science and Engineering, Carnegie Mellon University, Pittsburgh, Pennsylvania, United States of America

Abstract

The *in vivo* microenvironment plays a major role in the regulation of cell homeostasis and function. This microenvironment is extremely complex which makes it difficult to mimic *in vitro*. Polydimethylsiloxane (PDMS) and polyacrylamide are currently used as cell compatible substrates with tunable stiffness capabilities. We assessed differences in differentiation efficiency of human embryonic stem cell derived cardiomyocytes (hESC-CM) on PDMS with stiffness resembling the native tissue in combination with different extracellular matrix proteins. Furthermore, we combined the tunable substrates with μcontact-printing technique to pattern cardiomyocytes into a more physiological relevant shape and developed it to a high throughput system. This combination was further used to assess the contraction force output of single hESC and human induced pluripotent stem cell derived cardiomyocytes (hPSC-CM) and its response to adrenergic stimuli.

In this study we show that *in vivo* stiffness and cellular patterning can be mimicked *in vitro* and used to measure contractile output of single hPSC-CM.

Introduction

The current standard materials for cell culture use polyethylene (plastic) or silica (glass) based surfaces for cell culture due to an efficient and low-cost manufacturing procedure. Nevertheless, these substrates are very different from the natural environment that cells encounter in the human body. In the plastic or glass culture dish, cells are in contact with a 2 dimensional (2D) surface that has a Young's modulus of 5 to 6 orders of magnitude stiffer than the human tissue[1]. Moreover, under these conditions cell-to-cell contact is predominantly restrained to the peripheries of cells. Furthermore, cells within the *in vivo* situation are in general part of a highly organized 3D structure consisting of multiple interacting and/or communicating cell-types. These differences are more profound in organs with mechanical functions such as the heart, since the mechanical loading and electrical stimulus, fundamental for proper cardiomyocyte function, are absent or underdeveloped in standard cell or tissue cultures. Various methods have been applied to mimic the *in vivo* environment, including the development of biocompatible polymer scaffolds[2] for 2D or 3D cultures, which have been used in combination with μcontact-printing for cell shape regulation and orientation[3], mechanical[4] or electrical[5] stimulation and cell co-cultures[6].



Biocompatible scaffolds can be made from natural or synthetic sources and have different characteristics with respect to properties such as architecture, cyto-compatibility, bioactivity and mechanical properties[7]. The most widely used scaffolds for cell culture are Polydimethylsiloxane (PDMS) and hydrogel (e.g. Matrigel or Polyacrylamide) based due its versatility, low cost, biocompatibility, tunability over a wide range of Young's modulus, light transparency and low light scattering.

PDMS is a silicon-based organic polymer comprised of repeating units of -O-Si(CH3)2-. PDMS is considered to be extremely useful for microfabrication and biological applications based on the following: i) it can produce features at the micron scale and be released from the template without damaging it; ii) it is optically transparent down to the 280nm; iii) it cures at low temperatures; iv) it is nontoxic to cells *in vitro* or *in vivo* (biocompatible); v) the chemistry of its surface can be altered, vi) it can be reversibly deformed[8]. Although PDMS is nonreactive due to its closed chemistry composition, exposing it to air plasma induces a transition of its surface from hydrophobic to hydrophilic by introduction of polar groups (Si-OH) at the expense of the methyl groups (Si-CH3), allowing protein anchorage such as extracellular matrix components (ECM) to the surface in a specific pattern. Such characteristic enabled the development of the μcontact-printing technique that is comprised by the patterning of ECM proteins with features at a scale of 1μm onto an activated PDMS surface. When attached the cells acquire the printed shape[3]. Furthermore, the Young's modulus of PDMS can be varied from 5 kPa to 1.72 MPa by mixing versions of PDMS with different composition (Sylgard 527 and Sylgard 184)[9]. This combination of technologies creates a relatively inexpensive cellular environment with similar stiffness and cell architecture to the *in vivo* situation that can be applied to the standard cell culture.

Polyacrylamide is a synthetic hydrogel-based polymer formed by acrylamide repeats ((C3H5NO)n) co-polymerized with bis-acrylamide (N,N-methylene-bis-acrylamide). Although this polymer is not used generally for microfabrication it has similar cell culture

applicabilities as PDMS, as it is suitable for cell culture, μcontact-printable and its Young's modulus can be varied between 5 and 100kPa[10],[11]. One advantage of polyacrylamide over PDMS is that it is a liquid prior to polymerization and is hydrophilic as a polymer, allowing the encapsulation of cells or water-soluble molecules. These characteristics enabled development of model to measure traction force during the dynamic process of cell migration[12] and have been recently used for measuring traction force of stem cell-derived cardiomyocytes[13],[11]. Cell's attachment on a substrate is implemented by the anchorage of an assembly of membrane proteins - focal adhesions, to the ECM proteins of the substrate. The anchorage of the focal adhesions is a dynamic process that changes over time, allowing the cells to change position or migrate through the substrate. Attachment and locomotion are processes that can be described as forces applied by the cell thought the focal adhesions onto the substrate. If the substrate is elastic and has a low Young's modulus, the cell is able to deform it during attachment or migration.

In this chapter we describe the development and adaptation of soft substrates, μcontact-printing and contraction force techniques onto human pluripotent stem cell derived cardiomyocyte differentiation, culture and analysis.

Materials and Methods

Human embryonic stem cell culture and differentiation

The human embryonic stem cell (hESC) line HES3-NKX2-5-eGFP, described previously[14] in which one allele of the cardiac transcription factor NKX2-5 was replaced by GFP, was used to allow selection of cardiomyocytes after differentiation. Human induced pluripotent stem cells (hiPS) were generated from skin fibroblasts obtained from a healthy female individual, after written informed consent and following approval by the Leiden University ethics committees, using a non-integrating Sendai virus to deliver the four reprogramming factors OCT4, SOX2, KLF4, and MYC [15]. Both cell-lines were maintained on irradiated mouse embryonic fibroblasts (MEFs) and differentiation was performed by two different methods, 1) Monolayer differentiation was performed in a 6-well plate, coated with Matrigel where 300.000 hESC were seeded at day 0 in BSA polyvinylalcohol essential lipids medium (BPEL) [16] together with 20ng/ml BMP4 (R&D), 20ng/ml Activin A (Miltenyi), 1.5μM chir99021 (Axon Medchem). The medium was refreshed after 3 days with BPEL supplemented with 5μM XAV-939. 2) For spin embryoid body (EB) differentiations 30.000 hESC were seeded per well in a V-shaped 96-well plate in BPEL containing 35ng/ml BMP4 (R&D), 30ng/ml Activin A (Miltenyi), 30ng/ml VEGF (Miltenyi), 40ng/ml SCF (Miltenyi), 1.5μM chir99021 (Axon Medchem)[14]. At day 3, medium was refreshed with BPEL. GFP-positive spin EBs started beating between day 7 and 10 of differentiation. Dissociation of both monolayer and spin EB-derived cardiomyocytes was performed at day 20 with 1x TryplE select for 10 mins at 37 ^{o}C.

Gene expression analysis

HESC-derived cardiomyocytes (15 days of differentiation of HES3-NKX2-5-eGFP) were purified by FACS sorting for GFP expression. RNA was isolated from purified cardiomyocytes

using the RNeasy-MicroKit (Qiagen) and reverse transcribed to cDNA using the Iscript cDNA kit (BioRad). Gene expression analysis was performed by q-PCR using IQ SYBR Green (BioRad). The samples were normalized to the house keeping gene human Acidic Ribosomal Protein (RPLP). The primers used are listed in supplementary Table 1.

Spin Coating

Spin coating was performed using spin coater WS-650MZ-23NPP (Laurell) for coating surfaces with solutions/polymers at high-speed rotation. A drop of freshly mixed PDMS was added to the center of the coverslip and we used the following protocol for optimal and evenly spreading of the polymer evenly.

Time (s)	RPM	Acceleration
5	500	100
5	1000	200
10	3000	300
60	4000	400
15	2000	200
10	1000	100
5	500	100

Fluorescent conjugation of fibronectin

The fibronectin was conjugated with Alexa Flour 546 Maleimide (Invitrogen) in a 8M Guanidine Hydrochloride (Sigma) solution for 1h, followed by dialysis overnight in PBS using a Slide-A-Lyzer Dialysis cassette.

μcontact-printing technique

The procedure was started by coating an in-house available PDMS stamp containing line features of 20μm thick spaced 20μm apart (20x20) with 50μg/ml Fibronectin for 1h. The liquid was aspirated and the stamp was dipped on PBS for a short wash, and dried with a nitrogen gun before stamping the fibronectin onto the PDMS surface activated by UV-Ozone treatment. The quality of the stamping was checked under a fluorescence microscope.

Cardiomyocyte isolation and culture

Chick cardiomyocytes (CMs) were isolated from day 7–8 (HH stages 30–32) White Leghorn embryos and are not considered live vertebrate animals under US Public Health Service policy. For each isolation, 7–15 hearts were dissected, cut into small pieces and digested in 3 mL of 0.05% Trypsin-EDTA (Sigma-Aldrich) for 7 min. The supernatant was carefully collected, added to seeding medium (M199 medium, 10% heat-inactivated FBS, 1% penicillin/streptomycin) and filtered through a 40-μm cell strainer to isolate individual cells. The 7-min incubation was repeated three times so that the hearts were completely digested while minimizing cytotoxicity by long exposure to trypsin. The cell solution was then centrifuged at 50g for 10 min and resuspended in 30 mL of seeding medium. Fibroblasts were removed by selective adhesion by pre-plating successively for 45-min incubations in T75 cell culture flasks. The supernatant, enriched in CMs, was centrifuged at 50g for 10 min then resuspended in seeding medium at 7.5 × 105 cells/mL. PDMS substrates were placed in a 6-well plate, 200 μL of the cell suspension was pipetted on top and incubated for 2 h to



allow cells to attach and then the wells were filled with additional seeding medium. On the next day, the medium was replaced with a maintenance medium containing a reduced level of 2% heat-inactivated FBS to minimize fibroblast proliferation.

Immunocytochemistry and sarcomere structure evaluation

Cells were fixed with 4% paraformaldehyde for 20mins and washed three times with PBS. Cells were permeabilized with 0.1% Triton for 8mins and blocked with 4% swine serum for 1h at room temperature (RT). For identification of sarcomeres and cell boundaries the samples were incubated with the primary antibodies mouse anti α-actinin (Sigma-Aldrich A7811) diluted 1:800 and rabbit anti pan-cadherin (Sigma-Aldrich C3678) diluted 1:200 for 1h at RT. The samples were washed three times 10 mins with PBS with 0.05% tween20 and incubated with the secondary antibodies donkey anti mouse IgG Cy3 (Jackson ImmunoResearch Europe 715-165-150) and donkey anti rabbit IgG A488 (Invitrogen A-21206) both diluted 1:200 for 1h at RT

Traction force technique

The traction force microscopy technique makes use of fluorescent carboxylate-modified microspheres embedded in the polyacrylamide gel to track such substrate deformation. By taking into account the displacement of the microspheres, the Young's modulus of the polyacrylamide and the thickness of the gel, Dr. Micah Dembo together with Dr. Yu-li Wang developed the LIBTRC software package that translates the substrate deformation into a force.

1% gelatin was made from porcine skin powder (Sigma Aldrich) and autoclaved. The gelatin was further oxidized with 3.5mg/ml Sodium Periodate (Sigma Aldrich) for 45mins at room temperature and used to coat the 20x20 lines stamp for 1h. The stamp was then dried with a nitrogen gun and used to stamp a 15mm glass coverslip. The polyacrylamide solution was prepared with a final concentration of 0.1% bis-acrylamide (Bio-Rad), 5% acrylamide (Bio-Rad) and 10mM HEPES pH 8.5 in distilled water, followed by centrifugation for 1 min at 10.000RPM for degassing. 0.006% (m/v) of ammonium persulphate (Sigma-Aldrich) and a 1:1000 dilution of 0.2-μm fluorescent beads (Ex/Em: 660/680nm - Molecular Probes) were added to the solution and briefly vortexed. The gel polymerization was initiated with TEMED (Bio-Rad) and 9.2μl of the final solution was added to a 25mm coverslip treated with plus Bind-Silane solution (GE Healthcare). The μcontact-printed 15mm coverslip was applied on top of the drop with the gelatin lines facing the gel. After 20 min of polymerization the 15mm coverslip was removed and the 25mm coverslip was mounted onto a well of a glass bottomed 6-well plate (Mattek), replacing the initial glass. The polymerized gel has a Young's modulus of 5.8 kPa [17]. The plates were sterilized under UV light for 30mins and the gels were rehydrated with 1xPBS for another 30mins. Before cell seeding the gels were equilibrated in culture medium for 15mins.

Statistics

The different groups were compared using one-way A-NOVA followed by Bonferroni. Significance was attributed to comparisons with values of $P < 0.05$*; $P < 0.01$**; $P < 0.001$***. All error bars represent SEM.

Results

Previous studies have shown the effect of substrate stiffness on stem cell differentiation[18]. In this chapter we studied the effect of substrate stiffness on human pluripotent stem cell-derived differentiation to cardiomyocytes. In order to culture cells on substrates with a stiffness which is comparable to the fetal heart *in vivo*, we combined two different PDMS formulations, Sylgard 527 and Sylgard 184 (Dow Corning), as described by Palchesko et.al[9]. The elastic modulus (y in kPa) in function of the percentage of the polymer Sylgard 184 (x) in a 184/527 mixture can be calculated by the following equations:

For low percentages of Sylgard 184 (0-20%) the regime is non-linear:

$$y=0.3236x^2+2.0606x+5 \quad 1)$$

For higher percentages of Sylgard 184 (20-100%) the regime is linear:

$$y=18.591x-156.87 \quad 2)$$

Previously, the embryonic heart has been described to generate a maximal contractile work output on matrixes with elasticity E≈11-17kPa[19]. In order to mimic the embryonic conditions *in vitro* PDMS with an estimated Young's modulus of 15kPa, was made using a combination of 96.78% of Sylgard 527 and 3.22% of Sylgard 184 and used as a substrate for cardiac differentiation. Plastic 6-well plates were coated with a layer of 15kPa PDMS and cured for 3h at 60ºC. The PDMS was then activated using a plasma cleaner and coated with various the respective ECM components. In order to additionally assess the best ECM for cardiac differentiation on this substrate each PDMS well was coated with either with Matrigel, 50µg/ml Fibronectin (BD), 50µg/ml Laminin (Sigma) and 0.1% Gelatine (Sigma). The monolayer differentiation was started at day 0 in every substrate. At day 1 and 2 the wells with PDMS coated with Fibronectin, Laminin and Gelatine were clumped in suspension whereas the cells on Matrigel coated PDMS and plastic control were attached and displaying normal morphology. As the differentiation progressed the cells in suspension attached as all conditions showed cell attachment and proliferation at day 3. At day 7 cells were visibly expressing GFP in all conditions. However, at day 14 there were obvious differences in monolayer morphology. A flat uniform beating cell layer was observed in both Matrigel conditions, whereas Laminin-coating resulted in beating cell layers with more evident three-dimensional structures on PDMS substrates in comparison with the plastic control. The cells on the Fibronectin coated PDMS displayed a string-like web on the PDMS that was only attached to the surface on the edges. Gelatine surface conditions resulted in floating beating spheroids (**Figure 1A**). At day 15 the cells were dissociated and FACS sorted for GFP. FACS analysis showed a modest increase in differentiation efficiency from 57% in the Matrigel coated plastic to 71% in the Matrigel coated PDMS (N=2). There was also an increase in cardiomyocyte differentiation efficiency to 65% in Laminin coated PDMS in comparison to Matrigel coated plastic control, but no change in Gelatine coated PDMS (55%) and a decrease in Fibronectin coated PDMS (19%). Despite no study clearly reporting it, there is generally accepted that hPSC differentiation protocols to cardiomyocytes are inconsistent through time. Due to the differences in colony morphology the RNA from GFP+ sorted cells were isolated for gene expression analysis. Preliminary Q-PCR analysis indicat-



ed no changes in expression of genes encoding for structural, sarcomeric and/or contractile proteins (ACTN2 and MYBPC3) in any conditions. MLC2V expression was decreased in PDMS/Matrigel conditions, indicating a decrease in ventricular specification on PDMS with Matrigel or a decrease in levels of maturation. The same holds true for Laminin. In contrast Gelatine-coating displayed an increase in MLC2V expression. As a marker of calcium handling CASQ2 expression is elevated in cardiomyocytes differentiated in Laminin, Fibronectin and Gelatine. On the other hand cardiomyocytes in these conditions also displayed increased expression of the hypertrophic marker ANF (**Figure 1B**).

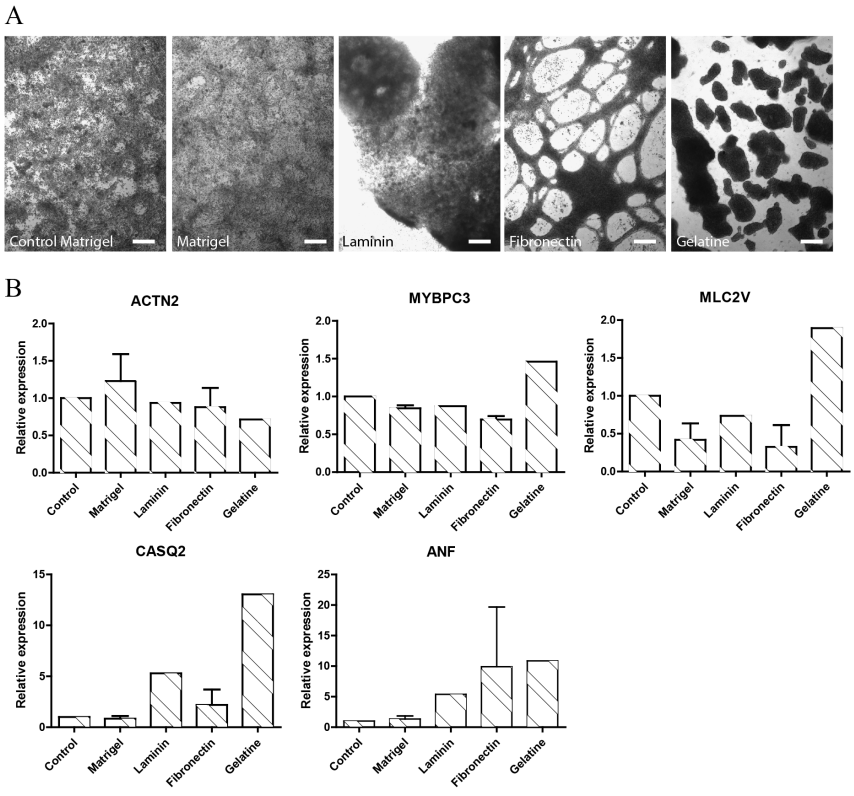


Figure 1 – Cardiomyocyte differentiation on different substrates. **A.** Representative pictures of hESC-CM culture morphology in plastic coated with Matrigel (Control Matrigel) and with PDMS coated with Matrigel, Laminin, Fibronectin and Gelatin (Bar-100μm). **B.** Relative expression levels of ACTN2, MYBPC3, MLC2V, CASQ2 and ANF in cardiomyocytes cultures in different substrate conditions (Control, Matrigel and Fibronectin N=2, Laminin and Gelatine N=1).

Since cell shape is known to be important for cardiomyocyte morphology and function [3,20] we applied μcontact-printing of ECM substrates on PDMS. To increase the applicability of this procedure we prepared coverslips coated with PDMS with and without the use of a spin-coater, which is not readily available in a standard cell biology lab. For this 100μl of PDMS was added onto the center of a glass 25mm coverslip and incubated overnight at room temperature. The next day the coverslips were fully covered with PDMS and were cured for 2h at 60ºC. Fibronectin was used for μcontact-printing since it has been

used frequently for this procedure[21]. In order to immediately visualize the outcome of the fibronectin was conjugated with Alexa Flour 546 Maleimide (Invitrogen). Two different stiffnesses were tested during this experiment ranging between the softer 5 kPa (0% Sylgard 184) and the stiff 1.72 MPa (100% Sylgard 184). On the stiff PDMS the μcontact-printing was successful in both spin-coated and non-spin-coated conditions, displaying uniform line pattern (**Figure 2A**). On the soft PDMS the μcontact-printing was only successful on spin-coated condition, whilst on the non-spin-coated PDMS the lines were not present or with large gaps in between (**Figure 2B**). The same μcontact-printing pattern was observed on PDMS with Young's modulus of 24kPa (data not show), indicating that μcontact-printing without a spin coater cannot be successfully applied to PDMS substrates with a lower Young's modulus range. The patterned lines on the spin coated PDMS were subsequently tested for cell culturing. First we used cardiomyocytes of chicken embryos, which were isolated and seeded on patterned coverslips at a density of 200.000 cells per cm2. The following day the cells were nicely attached and acquired the shape of the lines in both conditions (Figure 2C and D).

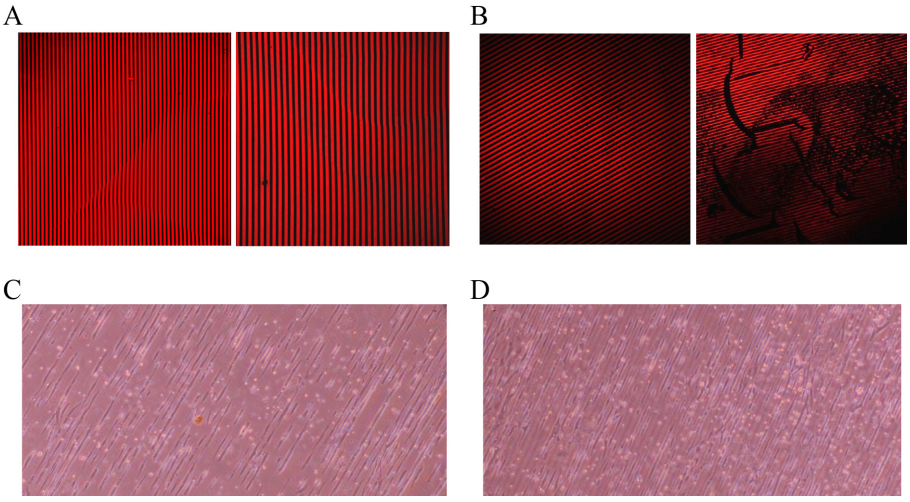


Figure 2- μcontact-printing of fibronectin-546 on PDMS with different Young's Modulus. **A.** μcontact-printed fibronectin lines 15 and 20μm wide onto spin coated (left-15x magnification) or non-spin coated (right-15x magnification) PDMS with ≈1.72MPa (stiff). **B.** μcontact-printed 15 and 20μm wide fibronectin lines onto spin coated (left-10x magnification) or non-spin coated (right-5x magnification) PDMS with ≈5kPa (soft). **C.** Chick primary cardiomyocytes aligned on stiff spin coated PDMS with μcontact-printed lines displayed on **2A** (10x magnification). **D.** Chick primary cardiomyocytes aligned on soft PDMS with μcontact-printed lines displayed on **2B** (10x magnification).

In order to test whether human-derived cardiomyocytes would attach and function, we cultured hESC-CMs on PDMS with a stiffness which is comparable to the adult heart (Young's modulus of 24kPa) was prepared, mimicking the elastic stiffness described in the adult heart muscle[1]. Alexa Fluor 548 labeled fibronectin was successfully μcontact-printed on PDMS in a configuration of 20μm wide 20μm interspaced lines and 50μm x50μm squares, although it was not uniformly distributed in the latter situation (**Figure 3A** and **B**). hESC-

CM were seeded on the patterned PDMS at a density of 200.000 cells per cm2. After 16 hours, although cardiomyocytes were nicely attached on the lines, there was a clear difference when compared to primary chick cardiomyocytes: the majority of the hESC-CM aggregated and bridged between lines (**Figure 3C**). On squares cell attachment was not very effective and hESC-CM formed spheroids instead of spread out single cells (Figure 3D). After 8 days of culture on the lines most of the hESC-CM remained attached and beating. Nevertheless, the aggregates had a more compact morphology and more single cells were aligned. Attachment of the hESC-CM on squares decreased and cells maintained a spheroid-like morphology at 8 days of culture (**Figure 3E** and **F**). The cells were then fixed in 4% paraformaldehyde and immunostained for α-actinin. HESC-CM on the lines showed aligned sarcomeres perpendicular to the direction of the patterned lines (**Figure 3G**). Cardiomyocytes that bridged the lines displayed a more disorganized sarcomere structure (**Figure 3G**). In an attempt to reduce the bridging effect by hESC-CM, fibronectin was μcontact printed on PDMS with patterns of 20μm lines interspaced at 100μm. Although the lines were successfully printed on the PDMS, the distance between lines in combination with the elasticity of the PDMS caused undesirable contact between the PDMS surface and the ceiling of the stamp, transferring a visible amount of fibronectin on the surface between lines (**Figure 4A**). Next, in order to avoid such contact μcontact-printing was performed without pressing the stamp on the surface, which indeed resulted in a clean space between lines but unfortunately also resulted in a decreased quality of the printed lines (**Figure 4B**). Following seeding of hESC-CM on these patterns of spaced lines, we observed that attachment was reduced and restricted to the edges of the coverslip (**Figure 4C**). Moreover, removal of aggregates by filtering cardiomyocytes with a 70μm cell strainer before seeding, still resulted in formation of aggregates and bridging 100μm space between the lines (**Figure 4C**).

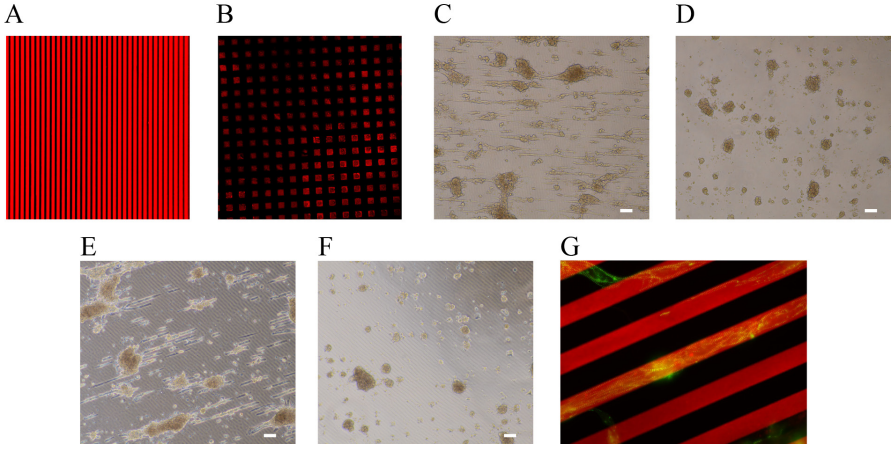


Figure 3- Culturing hESC-CM on μcontact-printed substrate with tissue-like stiffness. **A.** μcontact-printed 20μm wide fibronectin lines on spin coated PDMS with Young's Modulus of 24kPa. **B.** μcontact-printed 50x50μm fibronectin squares on spin coated PDMS with Young's Modulus of 24kPa. **C.** and **D.** hESC-CM seeded on fibronectin lines and squares from **3A** and **3B**, respectively. **E.** and **F.** hESC-CM cultured for 8 days on fibronectin lines and squares from **3A** and **3B**, respectively. **G.** α-actinin staining (green) of hESC-CM cultured on 20μm wide fibronectin lines (red). White bars- 50μm

Even with the undesirable bridging between the lines, the μcontact-printing technique still has potential added value when applied to high throughput screenings, as in this set up the percentage of cardiomyocytes effectively aligned can be picked and further analyzed. In order to prepare this μcontact-printing procedure for high throughput screening, instead of spin-coating single coverslips, 96-well format plates were used combined with 55mm x 75mm x 0.15mm glass (half the size of the bottom of a 96 well plate) purchased from Grace-bio and spin-coated with PDMS using a 50mm round chuck. The PDMS coating was initially only uniformly distributed in the 55mm diameter circle at the center of the coverslip and displayed a stringy pattern on the edges due to air bubbles trapped within the PDMS (**Figure 5A**). Different approaches such a decreasing the spinning speed, increasing the time of the top speed step, or pre-coating the entire coverslip with PDMS did not eliminate the stringy pattern. Despite the differences in uniformity the μcontact-printing was successfully performed on the uniformly coated circle in the center of the coverslip (**Figure 5B**). The μcontact-printed coverslip was glued to a bottomless 96 well plate (Nunc) using high vacuum grease (Dow Corning) (**Figure 5C**). HESC-CM attached to the lines as shown before (**Figure 5D**). In addition, no visible leak was observed between the different wells, demonstrating the feasibility to further develop this platform for high throughput assays.

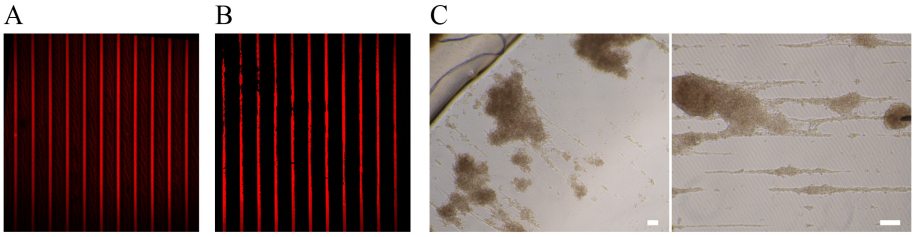


Figure 4 – Culturing hESC-CM on 100μm spaced lines. **A.** μcontact-printed 20μm wide fibronectin lines interspaced by 100 μm applying pressure on the stamp. **B.** μcontact-printed 20μm wide fibronectin lines interspaced by 100 μm without applying pressure on the stamp. **C.** hESC-CM cultured on lines showed in **4A** and **4B** with visible cell aggregates and bridging between lines (top-left shows the edge of the gel). White bars- 50μm

Measuring contractile function of cardiomyocytes is important for obtaining a better understanding of heart development and disease, and drug-induced cardiotoxicity. As introduced earlier traction force microscopy has been applied to assess the displacement of the substrate upon contraction of single cardiomyocytes[11],[13]. Displacement is recorded by video imaging and following software analysis computed to force applied by the cell per unit of area (mN/mm2), which are known as units of stress. In order to adapt this technique to our current set up we combined it with the μcontact-printing technique. Polyacrylamide (5%) gels embedded with fluorescent beads and gelatin printed lines were seeded with hESC-CM (**Figure 6A** and **B**). Nevertheless, cell attachment of hESC-CM to gelatin printed lines was poor if cardiomyocytes were derived from spin EBs or from monolayer differentiations on Matrigel. These problems were solved by dissociating these hESC-CM and pre-plating as a monolayer on 0.1% gelatin coated wells for 5 days or/and by equilibrating the gels in medium containing 10% fetal calf serum (Sigma) for 30mins prior to cell seeding. Initial contraction measurements revealed forces of 0.271±0.02mN/mm2 and 0.253±0.02mN/

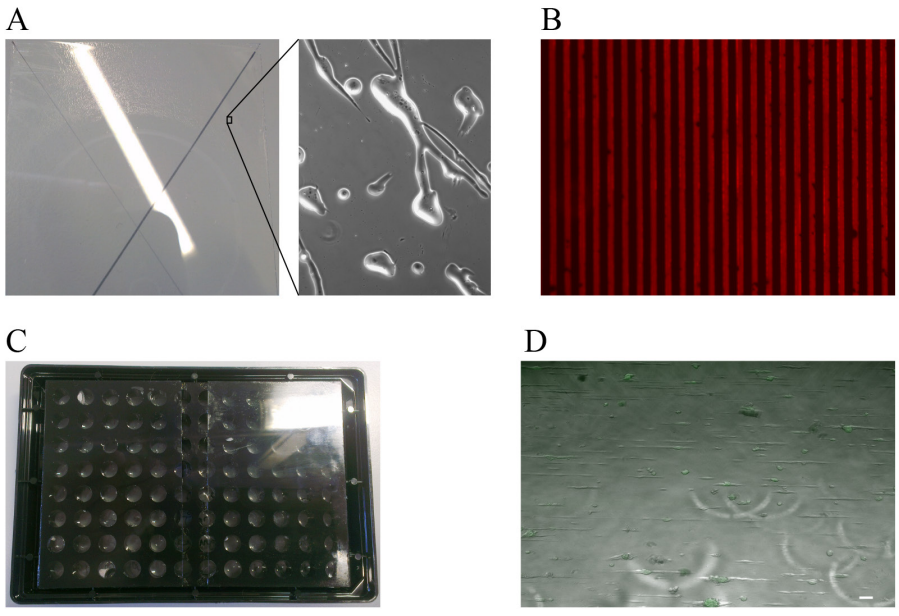


Figure 5- Up scaling μcontact-printing to 96 well format. **A.** 55mm x 75mm glass coverslip spin coated with PDMS displaying a flat uniform coating in center circle. The higher magnification (right side) shows the air bubbles trapped in the PDMS around the circle. **B.** μcontact-printed 20μm wide fibronectin-546 lines on the uniform PDMS coated center circle. **C.** Two spin coated 55mm x 75mm glass coverslip glued to the bottom of a 96well bottomless plate using high vacuum grease. **D.** hESC-CM cultured on the μcontact-printed 20μm wide fibronectin-546 lines (Green-GFP expression in cardiomyocytes). White bar- 50μm.

mm2 for hESC-CM and hiPSC-CM, respectively (**Figure 6C**). In order to measure contractility on substrates with a stiffness comparable to the heart, the acrylamide was increased to 10%, producing a polymerized gel with a Young's modulus of 18.4 kPa[11]. Contraction stress of hESC-CM and hiPSC-CM increased with the substrate stiffness (**Figure 6C**), indicating a correlation between contractile stress and substrate stiffness. Of note, cell alignment on the 18.4kPa polyacrylamide gels was poor in three consecutive experiments (**Figure 6D**), limiting the usage of this substrate for further experiments. Further characterization of hESC-CM was performed by analyzing their contraction performance after activation of the α and β adrenergic receptors with phenylephrine and isoprenaline, respectively. Phenylephrine induces an increase in beating rate and isoprenaline induces and increase in beating rate and contraction force in the adult heart [22,23]. Although both phenylephrine and isoprenaline induced an increase in beating frequency, no change in contraction force was observed as the net variation in contraction stress is close to null (**Figure 7A** and **B**).

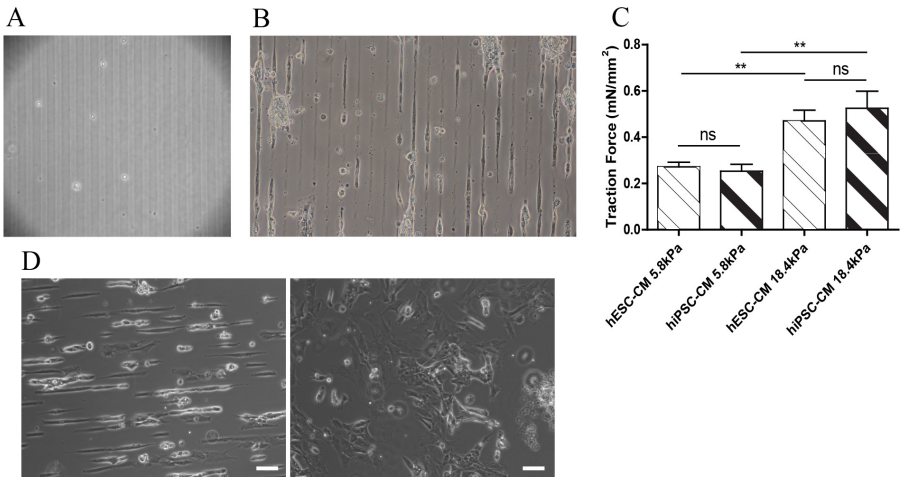
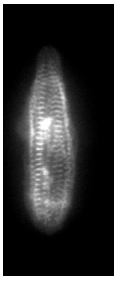


Figure 6- Contraction stress measurements using patterned polyacrylamide gels. **A.** 20 μm wide gelatin lines contact-printed onto 5.8kPa polyacrylamide gel. **B.** hESC-CM cultured on lines as shown in **6A. C.** Mean contraction stress generated by hESC-CM and hiPSC-CM in 5.8kPa (n=29 and n=12 respectively) and 18.4kPa (n=24 and n=13, respectively). **D.** hESC-CM aligned on a patterned polyacrylamide gel (5.8kPa) (left) but not aligned in patterned 18.4kPa polyacrylamide gel. White bar-50μm. ns = non-significant; **P<0.01



Discussion

This chapter describes the use of synthetic polymers as soft substrates for hESC-CM differentiation, maintenance and contractile analysis. These soft substrates were used in combination with μcontact-printing of different ECM proteins for cardiomyocyte alignment during culture and contraction force measurements. Additionally, we made the first steps for development of a 96 well-automated high throughput platform for functional analysis of human cardiomyocytes.

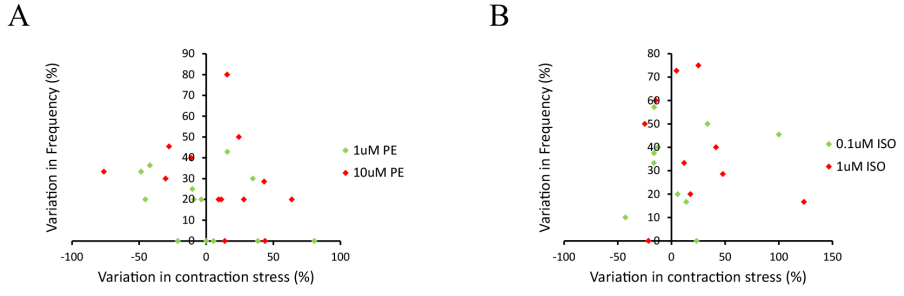


Figure 7- Chronotropic and inotropic effects of phenylephrine and isoprenaline on hESC-CM. **A.** Variation in beating frequency of each cell relative to its baseline frequency is plotted in function of the variation in contraction stress of that same cell, relative to its contraction stress baseline upon stimulus with 1μM or 10 μM phenylephrine. **B.** Variation in beating frequency of each cell relative to its baseline frequency plotted in function of the variation in contraction stress of that same cell relative to its contraction stress baseline upon stimulus with 0.1μM or 1 μM isoprenaline.

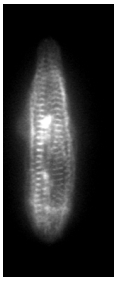
Standard cell cultures are realized on plastic substrates with a stiffness of several fold higher than tissues in the human body. Moreover, in general the stiffness of tissues during embryonic development are even softer than the adult counterparts[1],[19]. In order to consider this aspect for mimicking *in vivo* cardiac development, we differentiated hESC on PDMS with different stiffness by combining Sylgard 182 and 527. Results showed a modest increase in differentiation efficiency (from 57% to 71% GFP+ cells) under conditions, which are more comparable to the stiffness of the heart, although no obvious difference in morphology or gene expression were observed. These results are in disagreement with the decrease in cardiac differentiation efficiency on softer substrates described by Hazeltine et al.[24]. This discrepancy could be explained by the use of different substrates (polyacrylamide versus PDMS) and differences in cardiac differentiation and maintenance protocols. Furthermore, the soft PDMS substrate was also tested in combination with different ECM proteins for optimization of cardiac differentiation and maintenance. The most striking differences observed the lack of hESC attachment to the substrate until day 3 of differentiation when laminin, gelatin or fibronectin were used. This observation could be due to changes in conformation or availability of ECM protein upon interaction with activated PDMS, since the hydrophilic part of ECM proteins are bound to the PDMS leaving the hydrophobic part, less favorable, as the major anchor for cardiomyocytes. Moreover, the different ECMs induced different cardiomyocyte monolayer morphology by day 15, demonstrating the important role of ECM proteins in cardiac differentiation. Despite all ECM proteins promoting cardiogenesis, the efficiency was highest in combination with Matrigel. Recently Burridge et al. used Vitronectin as ECM protein for cardiac differentiation with better outcome than Matrigel[25], which may represent a good candidate for further improvement of this procedure. Although ACTN2 and MYBPC3 were not changed in any condition, preliminary results indicated an increase in MLC2V expression on gelatin, suggesting a more ventricular specification or maturation. Additional analysis would be required in order to make solid conclusions.

Besides the substrate stiffness, cell shape and geometry are among other parameters that influence cell differentiation and function. HPSC-derived cardiomyocytes are very similar to primary human fetal cardiomyocytes based on morphological (as well as molecular and functional) aspects, which is in contrast to the elongated, brick-like morphology of adult cardiomyocytes with length to width ratio of 7:1. In order to constrain the adult cardiomyocyte morphology *in vitro* we made use of μcontact-printing. We were able to show that this technique can be applied to spin-coated PDMS with Young's modulus ranging from 5kPa to 1.72MPa, but not on non-spin coated PDMS surfaces with low Young's modulus (5kPa). Human hESC-CM successfully attached and contracted on fibronectin printed lines, although bridging of hESC-CM between lines was frequently observed. This is in contrast to primary embryonic chick cardiomyocytes and neonatal rat ventricular cardiomyocytes[21], illustrating the difference between hESC-derived and primary cardiomyocytes.

The combination of culturing on soft transparent polymers (such as PDMS) with μcontact-printing has great potential advantages for high throughput screening since it allows imaging of cells in a micro-environment with an elasticity and geometry comparable to the *in vivo* situation and with higher degree of standardization and consequently a lower

degree of variation. This is crucial for successful implementation of hPSC-based assays for disease modeling, drug discovery and safety pharmacology. In line with this, it is encouraging that we have shown that it is feasible to use this technology in a custom-made 96-well plate format, allowing high throughput screening.

The combination of a soft flexible substrate embedded with fluorescent beads and μcontact-printing was applied for traction force measurements of single hPSC-CM. The initial values of contraction stress measured in hPSC-CM were congruent with previous studies on similar substrate stiffness[13]. We also demonstrated that contraction stress of both hESC-CM and hiPS-CM increased with the increase of substrate stiffness, which is in accordance with previous observations[11]. This observation is inherent to the complexity of the contraction machinery depicted by the Frank-Starling Law. Although there is no preloading stress (pressure generated by the blood volume in the ventricles at the end of diastole) in this 2D system, the afterload stress (pressure applied by the contracting ventricle walls during ejection) is mimicked by the elastic modulus of the substrate. At lower elastic modulus the pressure exerted by the substrate to the cell at the maximal contraction is lower than the stress applied by the cell on the substrate[19], meaning that in this setup the contraction stress measured is only influenced by the sarcomere dynamics and by cell size. Although this technique outputs an absolute value of stress, the dependence of this contraction stress value on the stiffness of the substrate limits the its comparison with other studies using different contraction force measurement setups (e.g. Force transducers). This limitation is inherent to the assumptions made on the cell attachment, substrate properties and bead location in order to translate the substrate deformation into a force/stress value using a mathematical algorithm, which are technically different from the assumptions made on the translation of the spring deflection into a force/stress in a force transducer apparatus. Measuring contraction stress in single cardiomyocytes will be important for functional analysis of specific cardiac disease and the effect of drugs on heart function. In this context, it has been previously shown that agonists of α/β adrenergic receptors, which are known to affect cardiac inotropy[22,23], did not affect contractile force in single hESC-CM[11], which may result from a low level of maturity of hESC-CM under the current *in vitro* conditions.



Conclusion

In this chapter we show that the tunability of different polymers can be used to mimic native tissue stiffness *in vitro*. Moreover, we showed prove of principle of combining tunable substrates with μcontact-printing and use it in a high throughput set up. Furthermore, this combination of techniques was used to measure contraction force of single hESC-CM and hiPSC-CM in different substrate stiffness together with its response on adrenergic stimuli. To conclude we established a 2D platform for culturing and analyzing hPSC-CM in a more native tissue-like environment.

References

[1] Mirsky I, Parmley WW. Assessment of passive elastic stiffness for isolated heart muscle and the intact heart. Circ Res. 1973;33:233–43.

[2] Jin R, Dijkstra PJ. Hydrogels for Tissue Engineering Applications. Biomed Appl Hydrogels Handb. 2001;101(7):203–25.

[3] Kuo P-L, Lee H, Bray M-A, Geisse N a, Huang Y-T, Adams WJ, et al. Myocyte shape regulates lateral registry of sarcomeres and contractility. Am J Pathol. Elsevier Inc.; 2012;181(6):2030–7.

[4] Nunes SS, Miklas JW, Liu J, Aschar-Sobbi R, Xiao Y, Zhang B, et al. Biowire: a platform for maturation of human pluripotent stem cell-derived cardiomyocytes. Nat Methods. 2013;10(8):781–7.

[5] Radisic M, Park H, Shing H, Consi T, Schoen FJ, Langer R, et al. Functional assembly of engineered myocardium by electrical stimulation of cardiac myocytes cultured on scaffolds. Proc Natl Acad Sci U S A. 2004;101(52):18129–34.

[6] Naito H, Melnychenko I, Didié M, Schneiderbanger K, Schubert P, Rosenkranz S, et al. Optimizing engineered heart tissue for therapeutic applications as surrogate heart muscle. Circulation. 2006;114:72–9.

[7] Chan BP, Leong KW. Scaffolding in tissue engineering: General approaches and tissue-specific considerations. Eur Spine J. 2008;17.

[8] Mcdonald JC, Duffy DC, Anderson JR, Chiu DT. Review - Fabrication of microfluidic systems in poly (dimethylsiloxane). Electrophoresis. 2000;21:27–40.

[9] Palchesko RN, Zhang L, Sun Y, Feinberg AW. Development of Polydimethylsiloxane Substrates with Tunable Elastic Modulus to Study Cell Mechanobiology in Muscle and Nerve. 2012;7(12).

[10] J. PELHAM R, Wang Y-L. Cell locomotion and focal adhesions are regulated by substrate flexibility. Proc Natl Acad Sci. 1997;94:13661–5.

[11] Hazeltine LB, Simmons CS, Salick MR, Lian X, Badur MG, Han W, et al. Effects of substrate mechanics on contractility of cardiomyocytes generated from human pluripotent stem cells. Int J Cell Biol. 2012;2012:508294.

[12] Dembo M, Wang Y. Stresses at the Cell-to-Substrate Interface during Locomotion of Fibroblasts. 1999;76(January):2307–16.

[13] Kita-Matsuo H, Barcova M, Prigozhina N, Salomonis N, Wei K, Jacot JG, et al. Lentiviral vectors and protocols for creation of stable hESC lines for fluorescent tracking and drug resistance selection of cardiomyocytes. PLoS One. 2009;4(4):e5046.

[14] Elliott D a, Braam SR, Koutsis K, Ng ES, Jenny R, Lagerqvist EL, et al. NKX2-5(eGFP/w) hESCs for isolation of human cardiac progenitors and cardiomyocytes. Nat Methods. 2011;8(12):1037–40.

[15] Nishimura K, Sano M, Ohtaka M, Furuta B, Umemura Y, Nakajima Y, et al. Development of defective and persistent Sendai virus vector: a unique gene delivery/expression system ideal for cell reprogramming. J Biol Chem. 2011;286(6):4760–71.

[16] Ng ES, Davis R, Stanley EG, Elefanty AG. A protocol describing the use of a recombinant protein-based, animal product-free medium (APEL) for human embryonic stem cell differentiation as spin embryoid bodies. Nat Protoc. 2008;3(5):768–76.

[17] Frey MT, Engler A, Discher DE, Lee J, Wang Y-L. Microscopic methods for measuring the elasticity of gel substrates for cell culture: microspheres, microindenters, and atomic force microscopy.

Methods Cell Biol. 2007;83(07):47–65.

[18] Wen JH, Vincent LG, Fuhrmann A, Choi YS, Hribar KC, Taylor-Weiner H, et al. Interplay of matrix stiffness and protein tethering in stem cell differentiation. Nat Mater. 2014;advance on(October).

[19] Engler AJ, Carag-krieger C, Johnson CP, Raab M, Tang H, Speicher DW, et al. Embryonic cardiomyocytes beat best on a matrix with heart-like elasticity : scar-like rigidity inhibits beating. J Cell Sci. 2008;121(Pt 22):3794–802.

[20] McCain ML, Yuan H, Pasqualini FS, Campbell PH, Parker KK. Matrix elasticity regulates the optimal cardiac myocyte shape for contractility. Am J Physiol Heart Circ Physiol. 2014;306(11):H1525–39.

[21] Feinberg AW, Feigel A, Shevkoplyas SS, Sheehy S, Whitesides GM, Parker KK. Muscular thin films for building actuators and powering devices. Science. 2007;317(5843):1366–70.

[22] Frishman WH. Cardiology patient page. Beta-adrenergic blockers. Circulation. 2003;107(18):e117–9.

[23] Landzberg JS, Parker JD, Gauthier DF, Colucci WS. Effects of myocardial alpha 1-adrenergic receptor stimulation and blockade on contractility in humans. Circulation. 1991;84(4):1608–14.

[24] Hazeltine LB, Badur MG, Lian X, Das A, Han W, Palecek SP. Temporal Impact of Substrate Mechanics on Differentiation of Human Embryonic Stem Cells to Cardiomyocytes. Acta Biomater. 2014;10(2):604–21.

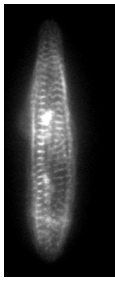
[25] Burridge PW, Matsa E, Shukla P, Lin ZC, Churko JM, Ebert AD, et al. Chemically defined generation of human cardiomyocytes. Nat Methods. 2014;11(8):855–60.





Chapter 3

Functional maturation of human pluripotent stem cell derived cardiomyocytes *in vitro* – correlation between contraction force and electrophysiology



Marcelo C. Ribeiro[1], Leon Tertoolen[1], Juan Antonio Guadix[1,2], Milena Bellin[1], Georgios Kosmidis[1], Cristina D'Aniello[1], Jantine Monshouwer-Kloots[1], Marie-Jose Goumans[3], Yu-li Wang[4], Adam W. Feinberg[4,5], Christine L. Mummery[1] and Robert Passier[1]

[1]Department of Anatomy & Embryology, Leiden University Medical Center, Leiden, The Netherlands

[2]Department of Animal Biology, University of Málaga, Málaga, Spain

[3]Department of Molecular Cell Biology, Cancer Genomics Centre, Centre for Biomedical Genetics, Leiden University Medical Center, Leiden, The Netherlands

[4]Department of Biomedical Engineering, Carnegie Mellon University, Pittsburgh, Pennsylvania, United States of America

[5]Department of Materials Science and Engineering, Carnegie Mellon University, Pittsburgh, Pennsylvania, United States of America

Biomaterials 2015;51:138–50

Abstract

Cardiomyocytes from human pluripotent stem cells (hPSC-CM) have many potential applications in disease modelling and drug target discovery but their phenotypic similarity to early fetal stages of cardiac development limits their applicability. In this study we compared contraction stresses of hPSC-CM to 2nd trimester human fetal derived cardiomyocytes (hFetal-CM) by imaging displacement of fluorescent beads by single contracting hPSC-CM, aligned by microcontact-printing on polyacrylamide gels. hPSC-CM showed distinctly lower contraction stress than cardiomyocytes isolated from hFetal-CM. To improve maturation of hPSC-CM *in vitro* we made use of commercial media optimized for cardiomyocyte maturation, which promoted significantly higher contraction stress in hPSC-compared with hFetal-CM. Accordingly, other features of cardiomyocyte maturation were observed, most strikingly increased upstroke velocities and action potential amplitudes, lower resting membrane potentials, improved sarcomeric organization and alterations in cardiac-specific gene expression. Performing contraction force and electrophysiology measurements on individual cardiomyocytes revealed strong correlations between an increase in contraction force and a rise of the upstroke velocity and action potential amplitude and with a decrease in the resting membrane potential.

We showed that under standard differentiation conditions hPSC-CM display lower contractile force than primary hFetal-CM and identified conditions under which a commercially available culture medium could induce molecular, morphological and functional maturation of hPSC-CM *in vitro*. These results are an important contribution for full implementation of hPSC-CM in cardiac disease modelling and drug discovery.

Introduction

The efficiency of cardiomyocyte differentiation of human pluripotent stem cells (hPSC) has greatly improved in recent years[1], with many reports describing more than 60% cardiomyocytes in differentiated cultures. For most laboratories, generating hPSC-derived cardiomyocytes (hPSC-CM) is no longer a major hurdle, providing opportunities for disease modelling, drug toxicity screening and identifying drug sensitivities of certain genotypes[2,3]. However, hPSC-CM are immature compared with human adult cardiomyocytes and express typical fetal cardiac genes [4], have immature electrophysiological properties such as low resting membrane potential and slow upstroke velocities[5], use glucose as major energy source as opposed to the fatty acids used by adult cardiomyocytes[6], have underdeveloped, (partially) disarrayed sarcomeres, heterogeneous shapes and are smaller in size [7,8]. Several studies have reported that the contraction stress of hPSC-CM using hydrogel-based technologies in two (2D) and three dimensions (3D) varied from 0.22±0.70mN/mm^2 to 11.8±4.5mN/mm^2 [9–12]. Furthermore, it has also been shown that contraction stress is dependent on substrate stiffness [13], emphasizing the necessity of using similar substrate stiffness for comparison of contraction stress values between different conditions.



Optimal implementation of hPSC-CM in human cardiac disease modelling and drug toxicity screening, would benefit from greater maturation of hPSC-CM. Therefore, it is important to understand which physiological parameters impact features of maturation. Candidate parameters that have been examined to date include long-term culture to mimic developmental gestation [14], substrate stiffness [15], cell patterning and alignment as occurs in the normal heart [16,17], electrical and mechanical stimulation [18], mechanical loading [19], interaction with other cell-types [20], and interference with signalling pathways thought to be of importance in heart development The outcomes of these studies have been variable: in assessing the effects of long-term culture, hPSC-CM were reported to withdraw from the cell-cycle and show ultrastructural maturation in 35 days [21] and increased conduction velocities in 2 months[22] but no improvements in contraction force were observed up to 2 or 3 months in culture [9,13] Following hPSC-CM for even longer, up to 4 months, both morphological and functional maturation were reported for both human embryonic stem cell (hESC) and human induced pluripotent stem cell (hiPS)-derived cardiomyocytes [14]. In assessing the role of substrate stiffness, neonatal rat ventricular myocytes (NRVM) cultured on a glass substrate (Young's Modulus ≈50 GPa), which is six orders of magnitude stiffer than heart tissue [23], showed decreased length to width ratios and increased stress fibre content compared to NRVM on substrates with Young's Modulus of 10kPa [15,23]. Both stiffness and cell shape have regulatory roles in cytoskeletal architecture and extra cellular matrix (ECM) coupling [24]. In turn, the cytoskeletal architecture is known to regulate gene expression [25], impulse propagation [26], excitability [27] and contraction [16,28], demonstrating the regulatory role of cell shape on cardiac function. *In vivo*, adult ventricular cardiomyocytes are elongated and aligned along one axis with length/width ratios of 7:1 [17,24]. Accordingly, restraining cell shape to a more elongated phenotype reminiscent of that of adult cardiomyocytes improves cardiomyocyte structure and function [16,29]. Thyroid hormones also have an important influence on cardiac structure, electrophysiological functions

and cardiac contractility in development *in vivo*[30], by directly regulating key structural and regulatory genes such as α-MHC and β-MHC, SERCA2, PLN, and various ion channels [31]. Moreover, triiodothyronine (T3) has been described as promoting electrophysiological and calcium handling maturation in mouse embryonic stem cell derived cardiomyocytes [32] and contraction maturation hiPS-CM [33].

Alterations in cardiomyocyte transcriptional, biochemical and functional cues, manifested by changes in electrophysiology, calcium handling, bioenergetics and contraction force, are inherent to progression from fetal to an adult state [8]. Consequently, *in vitro* cardiomyocyte maturation state can be assessed by analyses of these features. Nevertheless, the relationship and interdependence of these different parameters are poorly understood. Here, we found that hPSC-CM generate lower contraction stress than second trimester (16 week) human fetal cardiomyocytes (hFetal-CM) at the same substrate stiffness. Furthermore, by making use of different maturation media we were able to demonstrate that hPSC-CM displayed improved sarcomeric structure organization, stronger contraction stress, improved electrophysiological parameters and changes in gene expression compatible with a more developmentally advanced stage. Additionally, we assessed the relation between electrophysiology and contraction force during cardiomyocyte maturation by analysing these parameters on the same cardiomyocyte.

Materials and Methods

hESC and hiPS cell maintenance and differentiation to cardiomyocytes

Both hESC and hiPS lines were cultured on irradiated mouse embryonic fibroblasts (MEFs). Differentiation to cardiomyocytes was as described previously [34]. Briefly, spin embryoid bodies (spinEB) were formed by centrifugation of cells into aggregates in a 96-well format (Greiner) with BSA polyvinylalcohol essential lipids medium (BPEL) [35] together with 35ng/ml bone morphogenetic protein 4 (BMP4) (R&D), 30ng/ml Activin A (Miltenyi), 30ng/ml vascular endothelial cell growth factor (VEGF) (Miltenyi), 40ng/ml stem cell factor (SCF) (Miltenyi), 1.5μM CHIR99021 (Axon Medchem). The medium was refreshed on day 3 (**Supplementary Figure 1**). SpinEBs started beating between day 7 and 10 of differentiation.

Culturing and plating of hPSC derived cardiomyocytes

Two commercially available media, Cardiomyocyte medium (CA) and Maturation medium (MM) (available as Pluricyte Medium from Pluriomics BV), were used in a stepwise manner to mature hPSC-CM *in vitro*. CA and MM (containing T3 hormone) are serum-free, defined, nutrient-rich media that were pre-optimized for viability in culture and morphological maturation of hPSC-CMs. Differentiated cardiomyocytes were dissociated at day 10 with 1x TryplE select (Gibco) for 10 min and plated as single cells in BPEL on 0.1% gelatin (Sigma)-coated 6-well plates in order to change from a spinEB to a monolayer culture format. This step is crucial for proper cell attachment to the gelatin lines later on. On day 13, the medium was changed to BPEL or CA (**Supplementary Figure 1**). On day 20, one well of each condition was dissociated as described above and seeded on the polyacrylamide gel patterned with 1% gelatin lines, in the respective medium. The medium was refreshed the

next day and contraction and electrophysiological characteristics measured three days after plating. In the remaining culture wells the medium was changed to BPEL, CA and MM on day 20 as described in **Supplementary Figure 1**. The cells were cultured in the respective media for ten more days. As before, on day 30 the cells were dissociated with 10x Tryple select (Gibco) and seeded on the polyacrylamide gel patterned with 1% gelatin lines, in the respective medium. The cells were refreshed next day and contraction and electrophysiological characteristics measured three days after plating.

Human Fetal cardiomyocyte isolation and culture

Human fetal hearts were collected after elective abortion following individual informed consent, after approval by the Medical Ethical Committee of Leiden University Medical Center. The investigation conforms to the principles outlined in the Declaration of Helsinki. The fetal heart was examined for any apparent anomalies before single cell isolation. The hearts were cut into small pieces and subsequently dissociated in collagenase A (Roche) Calcium-free Tyrode's buffer. To minimize the amount of fibroblasts, the cells were pre-plated on a 10cm dish for 45 min. The remaining cells were plated directly on the polyacrylamide gel patterned with 1% gelatin lines and kept at 37ºC, 5%CO2. The medium was refreshed next day and measurements were made three days after plating.



Patterned Polyacrylamide gel fabrication

Patterned polyacrylamide gels were prepared as previously described [36]. Briefly, a polydimethylsiloxane (PDMS) stamp was incubated with 1% gelatin (Sigma) for 1h. The stamp was used to μcontact-print a pattern of 20μm wide gelatin lines with 20μm spacing onto 15mm coverslips. The polyacrylamide solution was prepared with a final concentration of 0.1% bis-acrylamide (Bio-Rad), 5% acrylamide (Bio-Rad) and 10mM HEPES pH 8.5 in distilled water, followed by centrifugation for 1 min at 10.000RPM for degassing. 0.006% (m/v) of ammonium persulphate (Sigma-Aldrich) and a 1:1000 dilution of 0.2-μm fluorescent beads (Ex/Em: 660/680nm - Molecular Probes) were added to the solution and briefly Vortexed. The gel polymerization was initiated with TEMED (Bio-Rad) and 9.2μl of the final solution was added to a 25mm coverslip treated with plus Bind-Silane solution (GE Healthcare). The μcontact-printed 15mm coverslip was placed on top of the drop with the gelatin lines facing the gel. After 20 min of polymerization, the 15mm coverslip was removed and a 25mm coverslip was mounted onto a well of a glass bottomed 6-well plate (Mattek), replacing the initial glass. The polymerized gel has a Young's modulus of 5.8 kPa [37].

Contraction force measurements

The contraction force measurements were performed as previously described [13]. Briefly, using a Leica AF-6000LX microscope with controlled temperature and CO2, 40x image series of brightfield and fluorescent beads were taken at 5 frames per second of aligned single self-pacing cardiomyocytes. Single frames from maximal relaxation and contraction of the brightfield and fluorescent image series were analyzed by the LIBTRC software package (kindly provided by Dr. Micah Dembo), creating a mask of the cell outline from the

brightfield image and a vector map from the difference between the relaxed and contracted fluorescent images. The vector map and the cell mask were used to calculate the total force that the cell applies on the substrate at its maximum peak of contraction. The contraction stress generated by the cardiomyocyte was calculated by dividing the total force by the cell surface area.

Electrophysiology

After contraction force measurements, the position of each cell was noted by its quadrant localization and by 10x and 40x brightfield images. Subsequently, the coverslips were transferred to the patch clamp electrophysiology set up. Measurements were performed with the amphothericin-perforated patch-clamp technique using the Axopatch 200B patch clamp amplifier (Molecular Devices Axon Instruments, U.S.A.) at 5 kHz in the fast current clamp mode.

Gene expression analysis

Cardiomyocytes derived from the HES3-NKX2-5-eGFP line [34] were cultured in the different test media (**Supplementary figure 1**) and purified by sorting on day 20 and 30 of differentiation. RNA from day 20 and 30 cells was isolated using the RNeasy-MicroKit (Qiagen) and Nucleo Spin RNA XS (Macherey-Nagel), respectively, and reverse transcribed to cDNA using the Iscript cDNA (BioRad). Gene expression analysis was performed by q-PCR using IQ SYBR Green (BioRad). The samples were normalized to the house keeping gene human Acidic Ribosomal Protein (RPLP).

Immunocytochemistry and sarcomere structure evaluation

After contraction measurements, the cells were fixed on the lines with 4% paraformaldehyde. For identification of sarcomeres and cell boundaries the samples were incubated with the primary antibodies mouse anti α-actinin (Sigma-Aldrich A7811) and rabbit anti pan-cadherin (Sigma-Aldrich C3678) followed by the secondary antibodies donkey anti mouse IgG Cy3 (Jackson ImmunoResearch Europe 715-165-150) and donkey anti rabbit IgG A488 (Santa Cruz Biotechnology sc-15368). The sarcomeric structure of individual cardiomyocytes was determined by grading the organization of α-actinin into four different classes of individual aligned cells at 40x using the AF-6000 Leica microscope [38]. Sarcomere profiles were constructed with the function Plot Profile of ImageJ. Software developed in house (LabVIEW, National Instruments Corporation, Austin, U.S.A.) was used to analyze the average spacing distance by the method of power spectral analysis applied to the profile data from ImageJ (μm/pixel).

Statistical analysis

Differences between the different groups were assessed by Student's t-test for comparison of two groups or one-way ANOVA followed by Bonferroni post-test for comparison of three or more groups. The differences in cell structure classification were assessed using Chi2 test. Significance was attributed to comparisons with values of $P < 0.05$*; $P < 0.01$**; $P < 0.001$***. All error bars represent SEM.

Results

Contraction stresses of hESC-CM and hiPS-CM are comparable

hESC-CM and hiPS-CM (hPSC-CM) were routinely differentiated and maintained in BPEL medium then dissociated on day 10 and plated on 0.1% gelatin (**Supplementary Figure 1**). To analyze cardiomyocyte function in physiologically relevant substrate dimensions and stiffness specifically, hPSC-CM were dissociated on differentiation day 20 and seeded on 20μm wide 1% gelatin lines that were μcontact-printed on polyacrylamide gel (**Figure 1A**). Three days after seeding, measurements of contraction force by spontaneously beating cardiomyocytes were performed by imaging displacement of fluorescent beads embedded in the gels (**Figure 1B**). From the contraction cycle, frames corresponding to maximal contraction and relaxation of single cardiomyocytes were compared and analyzed using LIBTRC traction force microscopy software, creating a vector heat-map with the total force produced by each cell at the peak of contraction (**Figure 1C**). To compensate for variation in contraction force (nN) induced by differences in cell size, total force was normalized to cell surface area (μm^2) and designated as contraction stress (mN/mm^2). First, we determined contraction stresses of hESC-CM and hiPS-CM under standard differentiation culture conditions (BPEL) on day 23. The contraction stress generated by hESC-CM and hiPS-CM were comparable (0.29±0.01 mN/mm^2 and 0.26±0.01 mN/mm^2, respectively; P=0.17) (**Figure 2A**). In accordance, cardiomyocyte morphology and sarcomeric organization were similar on micropatterned lines, demonstrated by expression and localization of sarcomeric protein α-actinin (**Figure 2B**). In accordance with contraction stress, hESC-CM and hiPS-CM have

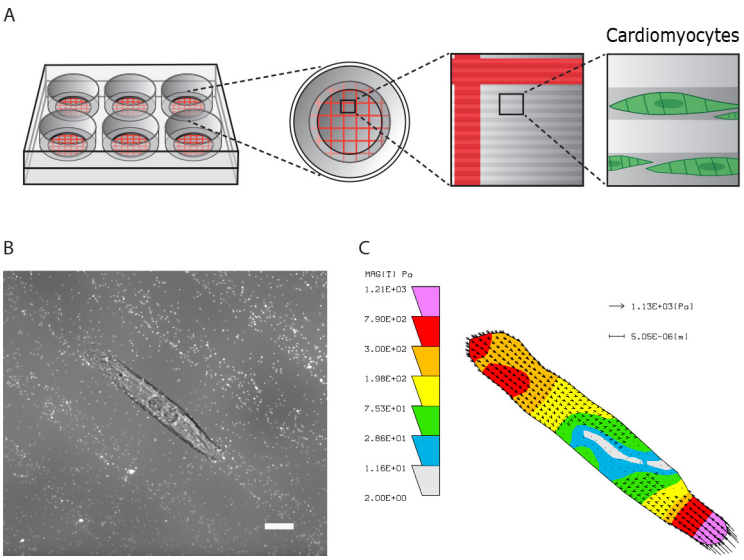


Figure 1- Schematic overview of measuring traction stress. **A.** A bottomless 6-well plate with the 25mm coverslips carrying the polyacrylamide gel with patterned gelatin (darker gray lines) and red quadrant grid. **B.** Merge of the bright field image of a single cardiomyocyte with the fluorescent image of the fluorescent beads embedded in the gel, representing the image acquisition during measurements. Scale bar 10μm. **C.** Heat map generated by the LIBTRC software representative of the traction stress applied by the cell on the substrate (1Pa=10-3mN/mm2).

similar cell surface area (hESC-CM 1050 ± 55.01μm2 versus hiPS-CM 1244 ± 49.92 μm2 P=0.055) (**supplementary Figure 3**)

hPSC-CMs generate less contraction stress than hFetal-CM

Since previous studies have reported that hPSC-CM resemble hFetal-CM based on gene expression [4], electrophysiology [5] and morphology [39] we assessed the degree of contraction maturity in relation to fetal developmental stage by comparing hPSC-CM to cardiomyocytes from second trimester human embryos. As reported previously, contraction stress generated by a single cardiomyocyte is intrinsically dependent on the stiffness of the substrate [13]. Therefore contraction stresses of all cardiomyocytes were determined on the same substrate. hFetal-CM isolated from hearts of 14 (N=1), 17 (N=2) and 19 (N=1) weeks of gestation fetuses were seeded onto 1% gelatin lines microcontact-printed on polyacrylamide gels and cultured for three days before contraction force measurements. Cardiomyocyte populations from all four human fetal hearts generated similar contraction stresses (14 weeks 0.42±0.04 mN/mm^2; 17 weeks 0.42±0.03 mN/mm^2; 19 weeks 0.39±0.02 mN/mm^2 P=0.78) (**Figure 2A**), indicating unchanged contraction stress levels of cardiomyocytes over this gestational period. However, in hESC-CM and hiPS-CM, contraction stresses were significantly lower than hFetal-CM (**Figure 2A** and **4B**). Correspondingly, α-actinin staining demonstrated greater sarcomeric organization (**Figure 2B**) in hFetal-CM than in hPSC-CMs. The cell surface areas of hFetal-CM were similar (1216 ± 44.60μm^2) to the hPSC-CM population (P=0.055) (**Supplementary Figure 3**).

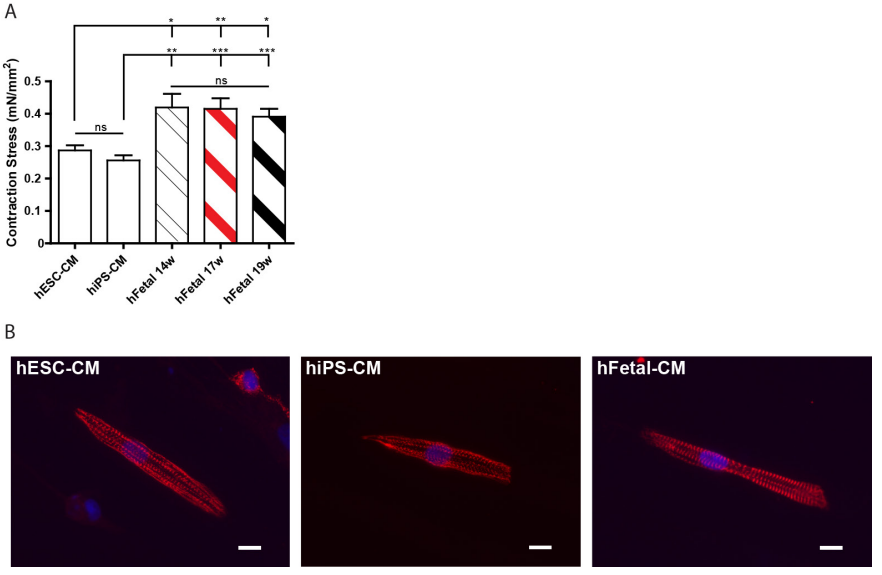


Figure 2- Comparison of contraction stresses between hPSC-CM and 2nd trimester hFetal-CM. **A.** Mean contraction stress generated by hESC-CM (n=45), hiPS-CM (n=45) and 14 week hFetal-CM (1 heart; n=16), 17 week hFetal-CM (average of 2 hearts; n=50) and 19 week hFetal-CM (1 heart; n=50). ns = non-significant; *P<0.05; **P<0.01; ***P<0.001. **B.** Representative images of α-actinin staining of hESC-CM, hiPS-CM and hFetal-CM. Scale bar 10 μm.

Improvement of hPSC-CM function in vitro

In order to improve contractile force in hPSC-CM, we introduced a step-wise change in culture conditions of the cardiomyocytes. We first changed the culture format from aggregates to monolayer on day 10. Three days after plating, the medium was changed to CA. After incubation of hESC-CM and hiPS-CM in CA for ten days (from day 13 to 23 - **Supplementary Figure 1**) contraction stress increased by 51% and 66%, respectively, compared to cardiomyocytes maintained in standard differentiation medium BPEL (hESC-CM in CA 0.43±0.03mN/mm^2 P<0.0001 and hiPS-CM in CA 0.43±0.02mN/mm^2 P<0.0001) (**Figure 3A**). Interestingly, the contraction stress generated by hPSC-CM maintained in CA reached similar levels to that in second trimester hFetal-CM (P= 0.6417) (**Figure 3A**), indicating progressive contractile maturation. Furthermore, the hPSC-CM population almost doubled in surface area in CA (hESC-CM in CA 2067±169.2µm^2 P<0.0001 and hiPS-CM in CA 1866±98.85µm^2 P<0.0001) (**Supplementary Figure 3**). Since contraction stresses of both hESC-CM and hiPS-CM populations in CA were similar, further functional analyses were performed on hESC-CM only. Since we used the hESC-NKX2-5-eGFP cardiac reporter line [34] we could sort single cardiomyocytes based on GFP expression.

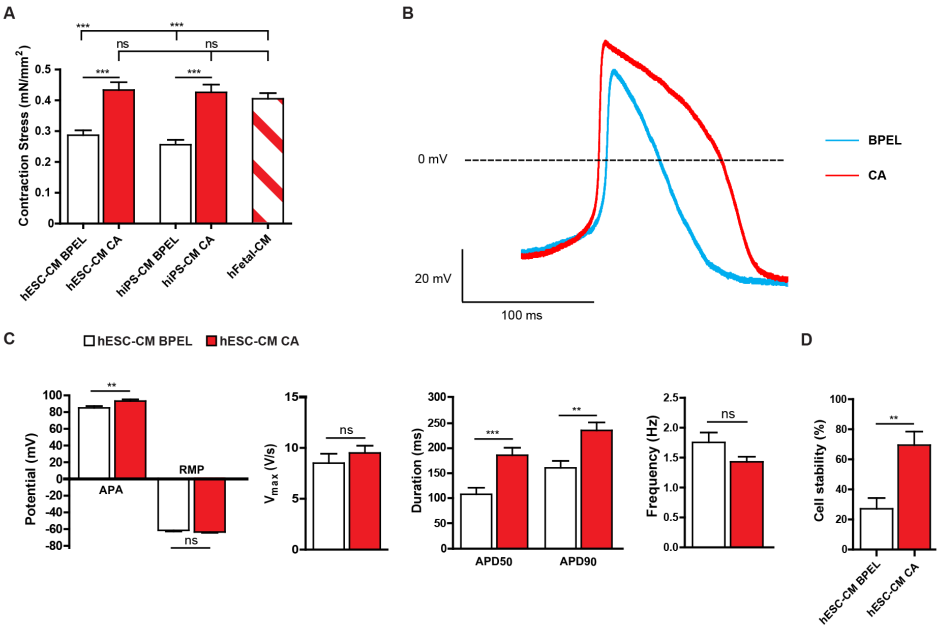


Figure 3- Functional improvement of hPSC-CM in vitro. **A.** Mean contraction stress at day 23 generated by hESC-CM in BPEL (n=45) and CA (n=41) and hiPS-CM in BPEL (n=45) and CA (n=43) and in hFetal-CM combined (mean of 4 hearts between week 14 and 19; n=116). **B.** Representative examples of spontaneous AP of hESC-CM in the two different media. **C.** Electrophysiological comparison between hESC-CM in BPEL (n=18) and in CA (n=24), with APA, APD50 and APD90, RMP, Vmax, and beating frequency. **D.** Percentage of stable hESC-CM in CA when compared to BPEL. ns = non-significant; **P<0.01; ***P<0.001.

In addition to contraction stress, electrophysiological analysis is an important functional readout for assessing maturity of cardiomyocytes [5]. Electrophysiological measurements were performed by patch-clamp on single hESC-CM previously maintained in control (BPEL) or in CA media. In order to compare changes in electrophysiological parameters with changes in contraction force, both assays were performed on the same cell. Contraction force was first determined in 15 to 20 cardiomyocytes per coverslip in control (BPEL) and CA, followed by electrophysiological measurements in Tyrode's solution. Action potential duration (APD) was significantly prolonged at 50% (APD50) and 90% (APD90) repolarization in CA, in both spontaneously beating and paced cardiomyocytes at all tested frequencies (1, 2, 3 Hz). Furthermore action potential amplitude (APA) was increased in spontaneously beating and 2Hz-paced cardiomyocytes, indicating more mature action potential (AP) shapes (**Figure 3B** and **3C**; **Supplementary Table 1**). Nevertheless, no differences on the upstroke velocity (Vmax) or resting membrane potential (RMP), important parameters reflecting cardiomyocyte maturity, were observed (**Figure 3C**; **Supplementary Table 1**). Besides the differences in contraction stress and electrophysiological measurements of hESC-CM cultured in BPEL or CA, there was also a clear difference in the "stability" of cardiomyocytes. Switching medium from that used for contraction force measurements to Tyrode's solution used for electrophysiology frequently resulted in a contractile arrest without measurable action potentials during patch-clamp. From hESC-CM cultured in BPEL only 25% (21 of 84) had measurable APs, while from the same population cultured in CA 65.9% (29 of 44) of the hESC-CM had measurable APs (**Figure 3D**), suggesting increased single cell stability *in vitro*.

To investigate a possible relationship between functional changes in contraction stress and electrophysiology and changes in gene expression, RNA from GFP/Nkx2.5 sorted hESC-CM cultured in BPEL and CA was isolated and quantified by q-PCR. Expression of cardiac genes showed no differences between groups (**Figure 4A**). To determine the level of morphological maturation, sarcomeric organization was analyzed. Sarcomeres in aligned hPSC-CM were immunostained for α-actinin and the sarcomere pattern in each cell was graded into four different classes [38]: Class I cells display a random or patterned dotted staining; Class II cells display parallel bands in less than 70% of the cell; Class III display parallel band patterned staining in more than 70% and less than 90% of the cell; Class IV display high sarcomeric organization with parallel bands in more than 90% of the cell (**Supplementary figure 2**). Both hESC-CM and hiPS-CM in CA displayed significant increases in sarcomeric organization relative to BPEL with a shift from class I to II (**Figure 4B** and **C**). Moreover, both cardiomyocyte populations displayed increased sarcomere length in CA compared to BPEL (hESC-CM – BPEL 1.66±0.01μm, CA 1.83±0.02μm, $P<0.0001$ and hiPS-CM - BPEL 1.68±0.02μm, CA 1.86±0.01μm, $P<0.0001$) (**Figure 4D**). Additionally, and in accordance with contraction stress, both sarcomeric organization and sarcomere length in CA were comparable to that of hFetal-CM (1.82±0.01μm, $P=0.3976$) (**Figure 4B, C** and **D**).

Increase in hPSC-CM maturity in vitro

Next, we investigated whether a further increase in cardiomyocyte maturation could be achieved by introducing another step of culture in a T3 thyroid hormone based matura-

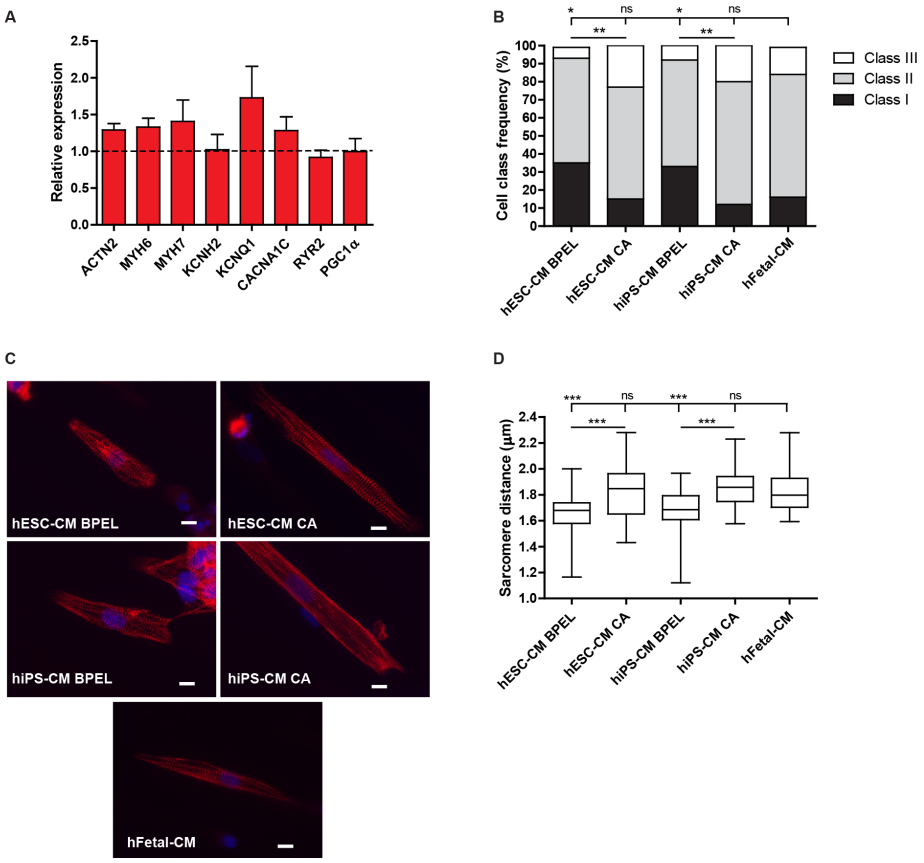


Figure 4- Characterization of gene expression and sarcomeric organization of hPSC-CM. **A.** Relative gene expression of cardiac genes by for hESC-CM in CA at day 23 compared to expression levels of these genes in hESC-CM in BPEL (dotted line). Expression levels were normalized to RPLP expression. **B.** Classification of sarcomeric organization of hFetal-CM (n=76) and hESC-CM and hiPS-CM in BPEL (n=77 and n=75, respectively) and CA (n=74 for both). **C.** Representative images of α-actinin staining (red) and nuclei (blue) of hESC-CM, hiPS-CM in BPEL and in CA, and of hFetal-CM. Scale bar 10 µm. **D.** Median, maximum and minimum sarcomere lengths of hESC-CM and hiPS-CM in BPEL (n=53 and n=58, respectively) and in CA (n=68 and n=65, respectively), and hFetal-CM (n=70). ns = non-significant; *P<0.05; **P<0.01; ***P<0.001.

tion medium (MM) for 10 additional days (**Supplementary Figure 1**). Recent studies have shown that T3 thyroid hormone has the potential to stimulate different characteristics of cardiomyocyte maturation [33]. Both hESC-CMs and hiPS-CMs cultured in MM showed an increase of 140% and 170% in contraction stress, respectively, compared to CMs cultured in BPEL or a 43% and 41% increase compared to CMs in CA media on day 33 (hESC-CM - BPEL 0.21±0.07mN/mm^2, CA 0.36±0.02mN/mm^2, MM 0.52±0.04mN/mm^2 P<0.0001) and (hiPS-CM - BPEL 0.18±0.02mN/mm^2, CA 0.36±0.02mN/mm^2, MM 0.51±0.04mN/mm^2 P<0.0001) (**Figure 5A**). Moreover, hPSC-CMs in MM displayed a higher contraction stress than hFetal-CM population (hESC-CM vs hFetal-CM P=0.0018; hiPS-CM vs hFetal-CM P=0.0084) (**Figure 5A**), indicating that hPSC-CM can be stimulated to mature further in their contractile output *in vitro*, beyond the force level of 2nd trimester human fetal cardiomy-



ocytes. Furthermore, culturing hESC-CM in MM did not increase their cell surface area in comparison with hESC-CMs in CA (hESC-CM in CA 1378±71.95µm^2 and hESC-CM in MM 1483±90.38µm2 P=0.36), while culturing hiPS-CM in MM increased their cell surface area in comparison with hiPS-CM in CA (hiPS-CM in CA 1445±74.39µm2 and hiPS-CM in MM 2169±110.2µm2 P<0.0001) (**Supplementary Figure 4**). We next examined the electrophysiological maturation state of hESC-CMs in MM by patch-clamp recordings at day 33. The Vmax was significantly increased in hESC-CM in MM in spontaneously beating cells and cells paced at 2 and 3Hz, whereas hESC-CMs in MM had a lower RMP at all frequencies, indicating electrophysiological maturation. In terms of AP shape, there was an increase in APA at all tested frequencies, together with an increase in ADP50 and ADP90 (**Figure 5B** and **5C**; **Supplementary table 2**). Furthermore, the number of stable cardiomyocytes capable of generating measurable APs upon medium switch following contraction force measurements increased in MM. Cardiomyocyte stability increased from 29.6% (21 of 71) in BPEL to 60.5% (23 of 38) in CA and to 85.3% (29 of 34) in MM (**Figure 5D**).

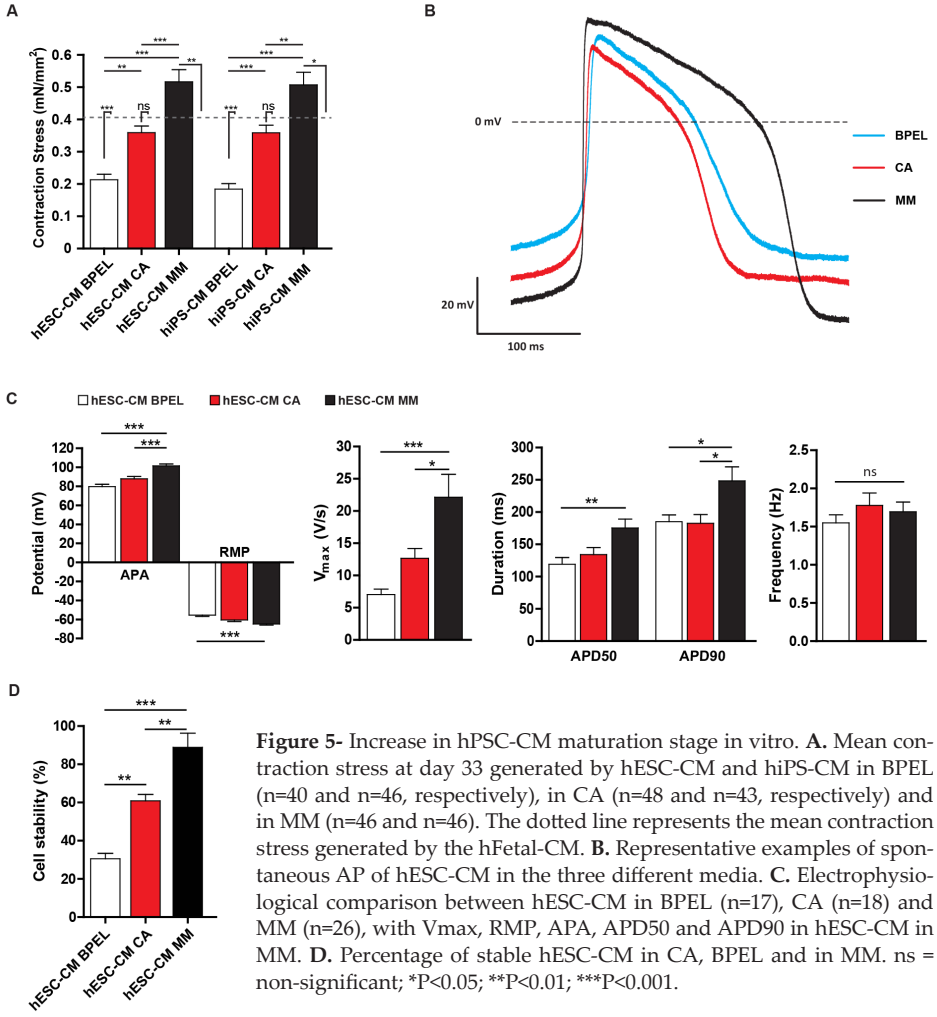


Figure 5- Increase in hPSC-CM maturation stage in vitro. **A.** Mean contraction stress at day 33 generated by hESC-CM and hiPS-CM in BPEL (n=40 and n=46, respectively), in CA (n=48 and n=43, respectively) and in MM (n=46 and n=46). The dotted line represents the mean contraction stress generated by the hFetal-CM. **B.** Representative examples of spontaneous AP of hESC-CM in the three different media. **C.** Electrophysiological comparison between hESC-CM in BPEL (n=17), CA (n=18) and MM (n=26), with Vmax, RMP, APA, APD50 and APD90 in hESC-CM in MM. **D.** Percentage of stable hESC-CM in CA, BPEL and in MM. ns = non-significant; *P<0.05; **P<0.01; ***P<0.001.

In order to shed light on possible molecular mechanisms underlying these functional changes we analyzed gene expression on NKX2-5-eGFP sorted hESC-CM. In agreement with functional maturation, a clear increase in expression of genes encoding sarcomeric proteins such as ACTN2, MYBPC3, MYH6, MYH7, TNNI3 was observed whereas expression of TNNI1 and of genes encoding calcium handling proteins like SERCA2, RYR2 and CACNA1C in MM cultured cells was unaltered (**Figure 6A**). Contractile maturation is therefore accompanied by upregulation of genes that are important for cardiac contractility, suggesting a causal relationship. Similarly, electrophysiological maturation is likely the result of increased expression of sodium and potassium channel encoding genes such as SCN5A, KCNH2, KCND3, KCNJ12 and KCNQ1, with a decrease in HCN4 (**Figure 6A**). Additionally, increased PGC1α expression suggested improvements in bioenergetics, since this gene has been previously shown to regulate mitochondrial biogenesis in these cells [38].

Correspondingly, hPSC-CM in MM displayed improved sarcomeric organization compared with cardiomyocytes in BPEL, although not significantly better than hPSC-CM maintained in CA (**Figure 6B** and **C**). Moreover, hPSC-CM in MM showed increased sarcomere length relative to hPSC-CM in BPEL and CA (hESC-CM – BPEL 1.44±0.05μm, CA 1.64±0.02μm, MM 1.85±0.02μm P<0.0001) and (hiPS-CM - BPEL 1.60±0.02μm, CA 1.79±0.02μm, MM 1.98±0.02μm P<0.0001) (**Figure 6D**). Of note, hiPS-CM in MM exhibited better sarcomeric organization and larger sarcomere length than hFetal-CM, indicating a higher level of structural maturation (**Figure 6B, C** and **D**)

Cardiomyocyte maturation can be assessed from the direct relationship between contraction force and electrophysiological parameters

Increased contractile force and electrophysiological parameters are important independent indicators of cardiomyocyte maturation. However, little is known about the relationship between the two during cardiomyocyte maturation process. Using the micropatterned polyacrylamide platform we were able to measure contraction force and carry out patch clamp electrophysiology in the same cells. On day 23, contraction force increase was directly proportional to the increase in APA, APD50 and APD90 (**Figure 7A**). However, contraction force did not appear to be correlated with Vmax or RMP at this stage (**Figure 7A**). Interestingly, at day 33 the increase of contraction force was strongly correlated with Vmax, RMP and APA but not with APD50 and APD90 (**Figure 7B**), indicating that during cardiomyocyte maturation, the different electrophysiological parameters are independently related to contraction force.

Discussion

In this study we have shown that cardiomyocytes derived from both hESC and hiPS have comparable contraction stress, but these are lower than those of second trimester hFetal-CM. By adjusting cardiomyocyte culture conditions in a step-wise manner, we were able to increase the contraction stress of single hPSC-CM to values higher than hFetal-CM, indicating cardiomyocyte maturation. Corroborating these findings, we also observed changes



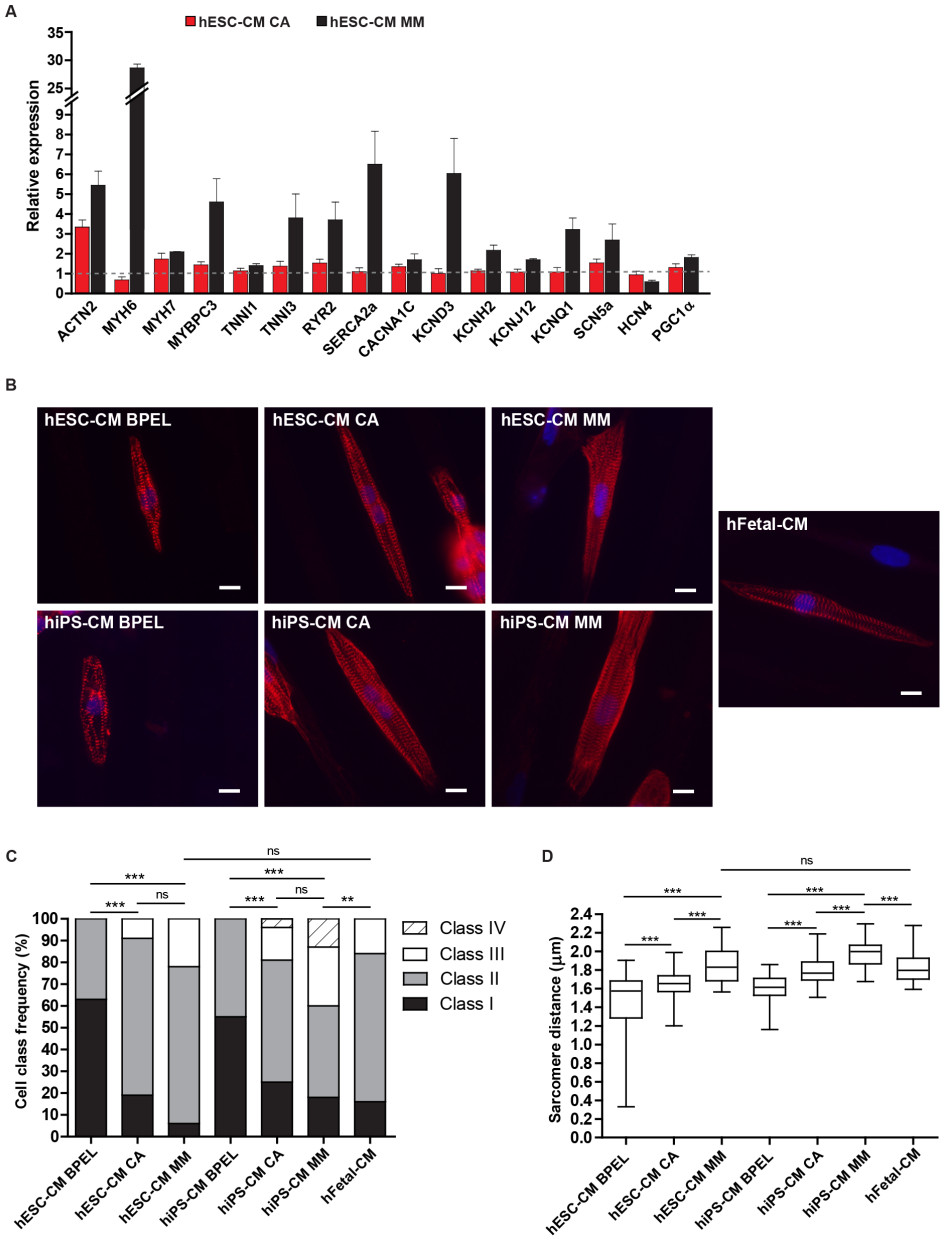


Figure 6- Changes in gene expression and sarcomeric organization of hPSC-CM in MM. **A.** Expression of genes encoding: sarcomeric proteins (ACTN2, MYH6, MHY7, MYBPC3, TNNI1, TNNI3), calcium handling channels (RYR2, SERCA2a, CACNA1C), membrane ion channels (KCND3, KCNH2, KCNJ12, KCNQ1, SCN5a, HCN4) and the mitochondrial master regulator PGC1α, normalized to RPLP expression. The dotted line represent gene expression levels in hESC-CM in BPEL **B.** Representative images of α-actinin staining (red) and nuclei (blue) of hESC-CM and hiPS-CM in BPEL, in CA and in MM, and of hFetal-CM. Scale bar 10 μm. **C.** Classification of sarcomere organization. HESC-CM and hiPS-CM in BPEL (both n=74), in CA (n=47 and n=45, respectively) and in MM (n=46 and n=46, respectively), and hFetal-CM (n=76). **D.** Median, maximum and minimum sarcomere lengths of hESC-CM and hiPS-CM in BPEL (n=38 and n=34, respectively), in CA (n=42 and n=44, respectively) and in MM (n=40 and n=43, respectively), and hFetal-CM (n=70). ns = non-significant; **P<0.01; ***P<0.001.

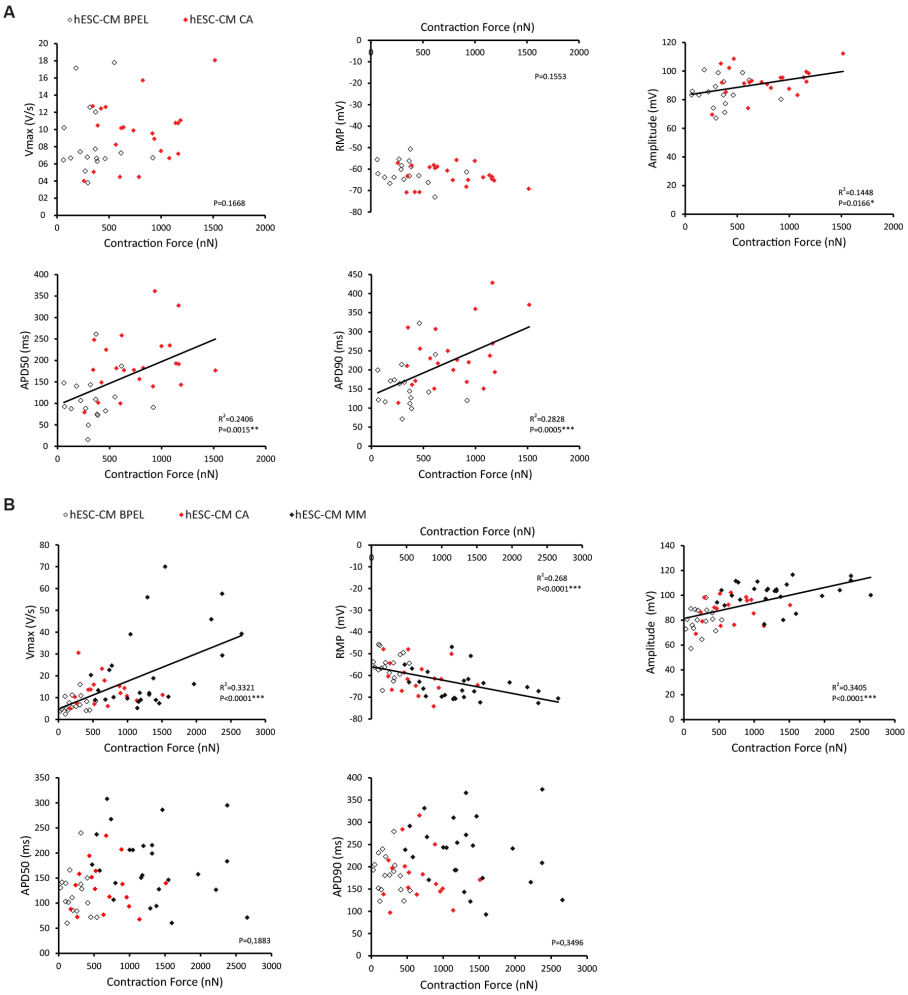
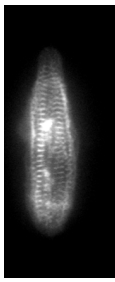


Figure 7- Relationship between different electrophysiology parameters and contraction force during cardiomyocyte maturation. **A.** Relation between contraction force (nN) and Vmax, RMP, APA, APD50 and APD90 in single hESC-CM at day 23 (n=42 including hESC-CM in BPEL (white) and in CA (red)). **B.** Relation between contraction force (nN) and Vmax, RMP, APA, APD50 and APD90 on single hESC-CM at day 33 (n=60 including hESC-CM in BPEL (white), in CA (red) and in MM (black)). The P values refer to significance in correlation between the two parameters. With P >0.05 no correlation was considered existent and therefore no linear regression line was drawn; With P<0.05* and P<0.01** a correlation was considered existent and a linear regression line was drawn (black line) with the respective R2. With P<0.0001*** a strong correlation was considered existent and a linear regression line was drawn (black line) with the respective R2.

in several electrophysiological parameters, sarcomeric organization and gene expression, all of which indicated cardiomyocyte maturation in culture. Interestingly, we observed a strong correlation between electrophysiological and contractile maturation measured in single cells, suggesting involvement of a common pathway for phenotypic and functional cardiomyocyte maturation.

Despite improvement in differentiation methods of hPSC-CM, their relative immaturity limits their possible application in disease modelling, drug discovery, safety pharmacology



and regenerative medicine. In order to overcome this hurdle, it is crucial to compare the phenotype and function of hPSC-CM with that of cardiomyocytes from the human heart. Previously, we have shown that hESC-CM and 16 week hFetal-CM were comparable at the electrophysiological level, whereas hESC-CM displayed less defined sarcomeric structures [5]. Others have compared transcriptional levels of cardiac genes of hESC-CM to those of 33-35 weeks fetal heart. However, no direct comparison of contraction stress between hPSC-CM and human primary cardiomyocytes has been made before. So far the contraction stress of 44±11.7mN/mm^2 measured in adult human papillary muscle strips have been used as a comparison reference value for tissue engineered cardiac patches [12,40]. However, even though 3D engineered tissues have a closer resemblance to the human heart, differences such as cellular composition, ratio of cardiomyocytes versus non-cardiomyocytes, cardiomyocyte orientation, extracellular components and variation in methodology for calculating contractile stress amplitudes [12], cause a considerable variation in the levels of contraction stress output. Although a continuous effort to mimic the human heart in all its complexity is crucial, development of simplified 2D platforms is necessary to complement 3D models, allowing assessment of molecular, phenotypic and functional changes of individual cells without interference from external factors. Our results showed similar contraction stress between hESC-CM and hiPS-CM (0.29±0.01mN/mm^2 and 0.26±0.01mN/mm^2, respectively), in agreement with previous reports [13]. These results are comparable to the 0.22±0.07mN/mm^2 reported for hESC-CM under similar substrate conditions [9]. Moreover, hPSC-CM showed lower contraction stress and sarcomeric organization than 14-19 week hFetal-CM, indicating an earlier maturation stage of these cardiomyocytes under standard culture conditions. Although it has been reported that expression of contractile and remodelling proteins progressed from the first to second trimester [41], not much is known on the functional progression of hFetal-CM during development. Here we have shown that contraction stresses of hFetal-CM are similar from gestation week 14 until 19.

In order to promote hPSC-CM maturation *in vitro* we made use of a commercial defined, nutrient-rich maturation media containing T3 hormone in combination with a more physiologically relevant substrate stiffness and micropatterned adhesive surfaces to standardize the cell shape [16,29]. Cardiomyocyte maturation was determined based on various molecular, phenotypic and functional parameters using combinations of different technologies.

We divided our approach in two steps by analysing hPSC-CM maturation progression at day 23, cultured for 10 days in CA, and at day 33, cultured for an additional 13 days in MM. At day 23, both hESC-CM and hiPS-CM cultured in CA increased their contraction stress by 51% and 66%, respectively, and remarkably achieved a level comparable to that of hFetal-CM. Although this progression in contractility was accompanied by a prolongation of the AP and increased APA amplitude to levels similar to those in human adult ventricular muscle [42], the values for Vmax and RMP, two important parameters of electrophysiological maturation, did not change. Nevertheless, sarcomeric organization and cell size increased, and there was a modest increase in the expression of genes encoding contractile sarcomeric proteins and ion channels. In agreement with these findings, a recent study by Feinberg and colleagues described that improvement in sarcomere organization led to increased APD, calcium transient kinetics and contraction stress [43], which is consistent

with functional maturation. Observed changes in sarcomeric organization and cell size are compatible with the physiological cardiac hypertrophy during development. However, it is worth noting that human adult ventricular myocytes have been reported to have surface areas of 12315±2103μm^2 in culture [44], which is approximately 6 fold higher than the average hPSC-CM under these culture conditions.

In the following step we prolonged hPSC-CM culture in a T3-based MM, achieving further cardiomyocyte maturation. hESC-CM and hiPS-CM in MM displayed a higher level of sarcomeric organization and increased their contraction stress by 140% and 170% respectively when compared to CMs cultured in BPEL and by 43% and 41% in comparison to CMs in CA. These results are in accordance with previously reported findings that T3 hormone increased contractile maturation in hiPS-CM [33]. Interestingly, both hESC-CM and hiPS-CM in MM generated significantly higher contraction stress than hFetal-CM. In agreement with increased contractility, gene expression analysis revealed increased expression of genes encoding contractile sarcomeric proteins such as ACTN2, MYBPC3, MYH6, MYH7 and TNNI3, which have all been described to have lower expression in hESC-CM than in human adult heart [45]. In particular the β-myosin heavy chain (MYH7) and troponin I type 3 (TNNI3) are major isoforms in the adult heart[46],[47] and their increase in expression has been previously linked to cardiomyocyte maturation [8]. Although the α-myosin heavy chain (MYH6) isoform is not the dominant MHC isoform in the adult human heart, its expression in adult human cardiomyocytes is higher than in hESC-CM [45]. Therefore, the nearly 30-fold upregulation of α-myosin heavy chain expression in hESC-CM in MM, is likely associated with cardiomyocyte maturation.

Progression in maturation was not only found in contraction but was also observed electrophysiologically. hESC-CM cultured in MM on polyacrylamide gels displayed overall improvements in electrophysiological maturation with a significant increase in the Vmax, APA, APD50, APD90 and a decrease in RMP at all tested frequencies. Although the AP amplitude, APD50 and APD90 of hESC-CM on MM reached levels similar to human adult ventricular myocytes [42], the levels of Vmax and RMP were still relatively low in comparison with the adult situation. Therefore, additional maturation steps are still required to reach levels in adult cardiomyocytes. Maintaining cardiomyocyte cultures for a prolonged time in MM may be sufficient to accomplish such goal, since a recent study described Vmax of 188.7±12.6V/s and RMP of -68.2±2.1mV in hESC-CM by culturing for ≤120 days [14].

In accordance with the functional improvements, hESC-CMs maintained in MM showed increased expression of distinct cardiac ion channel genes. In particular, KCNJ12 encoding the primary subunit of the inwardly rectifying potassium channel that contributes to IK1, the current responsible for lowering the RMP, was increased. Furthermore, the RMP itself influences the availability of the other ion channels in the membrane. Increased expression of the SCN5A gene encoding the alpha-subunit of the sodium channel conducting INa, together with a lower RMP, are responsible for the increase in the Vmax. Increased expression of KCND3, encoding a potassium voltage-gated channel conducting the transient outward potassium current (Ito1), promotes a more mature AP shape [48]. The KCNH2 and KCNQ1 genes encode the alpha-subunits of potassium channels responsible for the rapid



and slow delayed rectifier potassium currents (Ikr and IKs, respectively), therefore an increase in their expression advocates a faster repolarization of the cell membrane which can be linked to shorter AP duration. However, the APD50 and APD90 were prolonged in the hESC-CMs in MM, which may be explained by the increase in the availability of the L-type voltage-dependent calcium channel (where CACNA1C encodes the α-subunit), which is responsible for the inward flow of calcium and consequent membrane depolarization [49]. The net result is in agreement with electrophysiological maturation, since it has been shown previously that the expression of genes encoding ion channels is low in hESC-CM when compared to that in adult heart [4]. Furthermore, the funny current (If) channel HCN4, which delineates the cardiac conduction system and is important for pacemaking activity [50], is also expressed in early immature cardiomyocytes during embryonic development but not expressed in adult atrial or ventricular cardiomyocytes. Therefore, HCN4 downregulation in MM is also consistent with phenotypic maturation of cardiomyocytes of working myocardium. Furthermore, increased expression of genes responsible for calcium handling and metabolism was also observed, suggesting functional maturation of the calcium kinetics and metabolism. In summary, hESC-CM in MM displayed increased expression of genes responsible for contraction, calcium handling, electrophysiology and metabolism, all indicating a more advanced stage of cardiomyocyte maturation. These effects can at least partially be attributed to T3, since this has been described as directly inducing MYH6, SERCA2, KCND3 and PGC1α expression[31,51]. Each of these genes has a critical role in each functional component characteristic of cardiomyocytes, and their upregulation may influence the overall maturation. Furthermore, single cell stability increased significantly in MM compared to BPEL and CA; this could also be attributed to overall cardiomyocyte maturation. In accordance with the contractility, electrophysiological and gene expression maturation, the sarcomeric organization of hPSC-CM in MM improved significantly in comparison to hPSC-CM in BPEL. Corroborating this observation hPSC-CM, displayed a stepwise increase in sarcomere length from BPEL to CA and to MM, reaching lengths similar to those observed in 3D tissue patches [12]. Interestingly, at this stage hiPSC-CM displayed better sarcomeric organization, with highly organized sarcomeres filling more than 90% of the cell, and greater sarcomere lengths than hESC-CM. This difference is perhaps attributable to inherent differences between the cells lines. Additionally, hiPSC-CM show significantly increased sarcomeric organization in comparison to the hFetal-CM, demonstrating a more mature structure. Furthermore, an automated cell classification was developed, which validated the manual classification. This software is now available for further cell classification analysis.

Altogether, these improvements in cardiomyocyte contractility, electrophysiology, sarcomere organization and gene expression are indicative of an overall increase in the hPSC-CM maturation stage. These parameters together can be considered adequate reporters of maturation. Interestingly, this 2D platform allowed the measurement of contraction forces and electrophysiology of individual cells in different maturation stages, enabling us to determine the relationship between these two key characteristics during cardiomyocyte maturation. We observed that the increase in contraction force is only correlated with the increase in APD50, APD90 and APA on day 23, while on day 33 there was also a correlation between

Vmax, APA and RMP. Since CA does not induce progression in hESC-CM Vmax and RMP, there is no correlation between these parameters and the CA induced increase in contraction force. In MM, however, the biochemical cue from T3 promoted improvement in Vmax and RMP together with an improvement in contraction force. One possible explanation for these observations could be that changes in the electrophysiological parameters to a mature phenotype occur in a process-dependent fashion with parameters such as Vmax, APA and RMP as late-stage alterations. Alternatively, the lack of significant correlation of these electrophysiological parameters and contractility at day 23 in CA medium may suggest independent mechanisms of maturation at this stage. The presence of T3 in the late stage of maturation (MM) may directly affect regulation of genes encoding for sarcomeric and ion channels, suggesting a possible common pathway responsible for the synchronous progression of both electrophysiological parameters and contraction force. In this regard, it is of interest to note that T3 has been shown to increase the inward rectifying potassium Ik1 currents in guinea pig ventricular myocytes [52], which has a prominent effect on RMP (and Vmax), but also on shortening of APDs. These results indicate that different electrophysiological parameters correlate with the contractile force machinery in a distinct manner during maturation, which may be dependent on the stage or mechanism of maturation.



Conclusions

This is the first study directly comparing contraction stress generation between single hPSC-CM and single hFetal-CM on substrates with the same stiffness, establishing the contractile maturation level of hPSC-CM relative to a human fetal stage. Additionally, here we showed increased hPSC-CM maturation *in vitro*, with increased contractile force, electrophysiological maturation, improved sarcomeric organization and increased expression of cardiac specific genes. During this progression in maturation we established a correlation between contraction and electrophysiology. This improvement in cardiomyocyte phenotype is important for advancing applications of hPSC-CM in cardiac disease modelling, drug discovery and development and regenerative medicine.

Acknowledgments

The authors are grateful to Prof. Micah Dembo, Boston University, for providing the LIBTRC program package for computing traction forces and to Stephanie S. Chang for training on the traction force technique. The authors would also like to thank Matthew Birket and Dorien Ward-van Oostwaard for their technical support with cell culture.

References

[1] Mummery CL, Zhang J, Ng ES, Elliott D a, Elefanty AG, Kamp TJ. Differentiation of human embryonic stem cells and induced pluripotent stem cells to cardiomyocytes: a methods overview. Circ Res. 2012;111(3):344–58.

[2] Bellin M, Marchetto MC, Gage FH, Mummery CL. Induced pluripotent stem cells: the new patient? Nat Rev Mol Cell Biol. Nature Publishing Group; 2012;13(11):713–26.

[3] Davis RP, van den Berg CW, Casini S, Braam SR, Mummery CL. Pluripotent stem cell models of cardiac disease and their implication for drug discovery and development. Trends Mol Med. Elsevier Ltd; 2011;17(9):475–84.

[4] Synnergren J, Améen C, Jansson A, Sartipy P. Global transcriptional profiling reveals similarities and differences between human stem cell-derived cardiomyocyte clusters and heart tissue. Physiol Genomics. 2012;44(4):245–58.

[5] Mummery C, Ward-van Oostwaard D, Doevendans P, Spijker R, van den Brink S, Hassink R, et al. Differentiation of human embryonic stem cells to cardiomyocytes: role of coculture with visceral endoderm-like cells. Circulation. 2003;107(21):2733–40.

[6] Lopaschuk GD, Jaswal JS. Energy metabolic phenotype of the cardiomyocyte during development, differentiation, and postnatal maturation. J Cardiovasc Pharmacol. 2010;56(2):130–40.

[7] Maillet M, van Berlo JH, Molkentin JD. Molecular basis of physiological heart growth: fundamental concepts and new players. Nat Rev Mol Cell Biol. Nature Publishing Group; 2013;14(1):38–48.

[8] Yang X, Pabon L, Murry CE. Engineering adolescence: maturation of human pluripotent stem cell-derived cardiomyocytes. Circ Res. 2014;114(3):511–23.

[9] Kita-Matsuo H, Barcova M, Prigozhina N, Salomonis N, Wei K, Jacot JG, et al. Lentiviral vectors and protocols for creation of stable hESC lines for fluorescent tracking and drug resistance selection of cardiomyocytes. PLoS One. 2009;4(4):e5046.

[10] Stoehr A, Neuber C, Baldauf C, Vollert I, Friedrich FW, Flenner F, et al. Automated analysis of contractile force and Ca2+ transients in engineered heart tissue. Am J Physiol Heart Circ Physiol. 2014;306(9):H1353–63.

[11] Kensah G, Roa Lara A, Dahlmann J, Zweigerdt R, Schwanke K, Hegermann J, et al. Murine and human pluripotent stem cell-derived cardiac bodies form contractile myocardial tissue in vitro. Eur Heart J. 2013;34(15):1134–46.

[12] Zhang D, Shadrin IY, Lam J, Xian H-Q, Snodgrass HR, Bursac N. Tissue-engineered cardiac patch for advanced functional maturation of human ESC-derived cardiomyocytes. Biomaterials. Elsevier Ltd; 2013;34(23):5813–20.

[13] Hazeltine LB, Simmons CS, Salick MR, Lian X, Badur MG, Han W, et al. Effects of substrate mechanics on contractility of cardiomyocytes generated from human pluripotent stem cells. Int J Cell Biol. 2012;2012:508294.

[14] Lundy SD, Zhu W-Z, Regnier M, Laflamme M a. Structural and functional maturation of cardiomyocytes derived from human pluripotent stem cells. Stem Cells Dev. 2013;22(14):1991–2002.

[15] Jacot JG, McCulloch AD, Omens JH. Substrate stiffness affects the functional maturation of neonatal rat ventricular myocytes. Biophys J. 2008;95(7):3479–87.

[16] Kuo P-L, Lee H, Bray M-A, Geisse N a, Huang Y-T, Adams WJ, et al. Myocyte shape regulates lateral registry of sarcomeres and contractility. Am J Pathol. Elsevier Inc.; 2012;181(6):2030–7.

[17] Gerdes a. M, Kellerman SE, Moore J a., Muffly KE, Clark LC, Reaves PY, et al. Structural remodeling of cardiac myocytes in patients with ischemic cardiomyopathy. Circulation. 1992;86(2):426–30.

[18] Yang Xia, L.Maximilian Buja, Richard C. Scarpulla and JBM. Electrical stimulation of neonatal cardiomyocytes results in the sequential activation of nuclear genes governing mitochondrial. Proc Natl Acad Sci. 1997;94(October):11399–404.

[19] Mihic A, Li J, Miyagi Y, Gagliardi M, Li S-H, Zu J, et al. The effect of cyclic stretch on maturation and 3D tissue formation of human embryonic stem cell-derived cardiomyocytes. Biomaterials. Elsevier Ltd; 2014;35(9):2798–808.

[20] Kim C, Wong J, Wen J, Wang S, Wang C, Spiering S, et al. Studying arrhythmogenic right ventricular dysplasia with patient-specific iPSCs. Nature. Nature Publishing Group; 2013;494(7435):105–10.

[21] Snir M, Kehat I, Gepstein A, Coleman R, Itskovitz-Eldor J, Livne E, et al. Assessment of the ultrastructural and proliferative properties of human embryonic stem cell-derived cardiomyocytes. Am J Physiol Heart Circ Physiol. 2003;285(6):H2355–63.

[22] Kadota S, Minami I, Morone N, Heuser JE, Agladze K, Nakatsuji N. Development of a reentrant arrhythmia model in human pluripotent stem cell-derived cardiac cell sheets. Eur Heart J. 2013;34(15):1147–56.

[23] Chopra A, Tabdanov E, Patel H, Janmey P a, Kresh JY. Cardiac myocyte remodeling mediated by N-cadherin-dependent mechanosensing. Am J Physiol Heart Circ Physiol. 2011;300(4):H1252–66.

[24] McCain ML, Parker KK. Mechanotransduction: the role of mechanical stress, myocyte shape, and cytoskeletal architecture on cardiac function. Pflugers Arch. 2011;462(1):89–104.

[25] Pijnappels D a, Schalij MJ, Ramkisoensing A a, van Tuyn J, de Vries A a F, van der Laarse A, et al. Forced alignment of mesenchymal stem cells undergoing cardiomyogenic differentiation affects functional integration with cardiomyocyte cultures. Circ Res. 2008;103(2):167–76.

[26] Kléber AG, Rudy Y. Basic mechanisms of cardiac impulse propagation and associated arrhythmias. Physiol Rev. 2004;84(2):431–88.

[27] Walsh KB, Parks GE. Changes in cardiac myocyte morphology alter the properties of voltage-gated ion channels. Cardiovasc Res. 2002;55(1):64–75.

[28] Feinberg AW, Feigel A, Shevkoplyas SS, Sheehy S, Whitesides GM, Parker KK. Muscular thin films for building actuators and powering devices. Science. 2007;317(5843):1366–70.

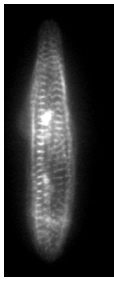
[29] Bray M-A, Sheehy SP, Parker KK. Sarcomere alignment is regulated by myocyte shape. Cell Motil Cytoskeleton. 2008;65(8):641–51.

[30] Pascual A, Aranda A. Thyroid hormone receptors, cell growth and differentiation. Biochim Biophys Acta. Elsevier B.V.; 2013;1830(7):3908–16.

[31] Klein I, Danzi S. Thyroid disease and the heart. Circulation. 2007;116(15):1725–35.

[32] Lee Y-K, Ng K-M, Chan Y-C, Lai W-H, Au K-W, Ho C-YJ, et al. Triiodothyronine promotes cardiac differentiation and maturation of embryonic stem cells via the classical genomic pathway. Mol Endocrinol. 2010;24(9):1728–36.

[33] Yang X, Rodriguez M, Pabon L, Fischer K a, Reinecke H, Regnier M, et al. Tri-iodo-l-thyronine promotes the maturation of human cardiomyocytes-derived from induced pluripotent stem cells. J Mol Cell Cardiol. Elsevier Ltd; 2014;72:296–304.



[34] Elliott D a, Braam SR, Koutsis K, Ng ES, Jenny R, Lagerqvist EL, et al. NKX2-5(eGFP/w) hESCs for isolation of human cardiac progenitors and cardiomyocytes. Nat Methods. 2011;8(12):1037–40.

[35] Ng ES, Davis R, Stanley EG, Elefanty AG. A protocol describing the use of a recombinant protein-based, animal product-free medium (APEL) for human embryonic stem cell differentiation as spin embryoid bodies. Nat Protoc. 2008;3(5):768–76.

[36] Rape AD, Guo W-H, Wang Y-L. The regulation of traction force in relation to cell shape and focal adhesions. Biomaterials. Elsevier Ltd; 2011;32(8):2043–51.

[37] Frey MT, Engler A, Discher DE, Lee J, Wang Y-L. Microscopic methods for measuring the elasticity of gel substrates for cell culture: microspheres, microindenters, and atomic force microscopy. Methods Cell Biol. 2007;83(07):47–65.

[38] Birket MJ, Casini S, Kosmidis G, Elliott D a, Gerencser A a, Baartscheer A, et al. PGC-1α and Reactive Oxygen Species Regulate Human Embryonic Stem Cell-Derived Cardiomyocyte Function. Stem Cell Reports. The Authors; 2013;1(6):560–74.

[39] Claire Robertson SCG. Maturation Phases of Human Pluripotent Stem Cell-Derived Cardiomyocytes. Stem Cells. 2013;31(5):1–17.

[40] Hasenfuss G, Mulieri L a., Blanchard EM, Holubarsch C, Leavitt BJ, Ittleman F, et al. Energetics of isometric force development in control and volume- overload human myocardium. Comparison with animal species. Circ Res. 1991;68(3):836–46.

[41] Iruretagoyena JI, Davis W, Bird C, Olsen J, Radue R, Teo Broman a, et al. Metabolic gene profile in early human fetal heart development. Mol Hum Reprod. 2014;20(7):690–700.

[42] Koncz I, Szél T, Bitay M, Cerbai E, Jaeger K, Fülöp F, et al. Electrophysiological effects of ivabradine in dog and human cardiac preparations: potential antiarrhythmic actions. Eur J Pharmacol. Elsevier B.V.; 2011;668(3):419–26.

[43] Feinberg AW, Alford PW, Jin H, Ripplinger CM, Werdich A a, Sheehy SP, et al. Controlling the contractile strength of engineered cardiac muscle by hierarchal tissue architecture. Biomaterials. Elsevier Ltd; 2012;33(23):5732–41.

[44] Li RK, Mickle D a, Weisel RD, Carson S, Omar S a, Tumiati LC, et al. Human pediatric and adult ventricular cardiomyocytes in culture: assessment of phenotypic changes with passaging. Cardiovasc Res. 1996;32(2):362–73.

[45] Xu XQ, Soo SY, Sun W, Zweigerdt R. Global expression profile of highly enriched cardiomyocytes derived from human embryonic stem cells. Stem Cells. 2009;27(9):2163–74.

[46] Gorza L, Mercadier JJ, Schwartz K, Thornell LE, Sartore S, Schiaffino S. Myosin types in the human heart. An immunofluorescence study of normal and hypertrophied atrial and ventricular myocardium. Circ Res. 1984;54(6):694–702.

[47] Saggin L, Gorza L, Ausoni S, Schiaffino S. Troponin I switching in the developing heart. J Biol Chem. 1989;264(27):16299–302.

[48] Adriana Blazeski LT. Cardiomyocytes derived from human induced pluripotent stem cells as models for normal and diseased cardiac electrophysiology and contractility. Prog Biophys Mol Biol. 2012;110(0):166–77.

[49] Kim C, Majdi M, Xia P, Wei K a, Talantova M, Spiering S, et al. Non-cardiomyocytes influence the electrophysiological maturation of human embryonic stem cell-derived cardiomyocytes during differentiation. Stem Cells Dev. 2010;19(6):783–95.

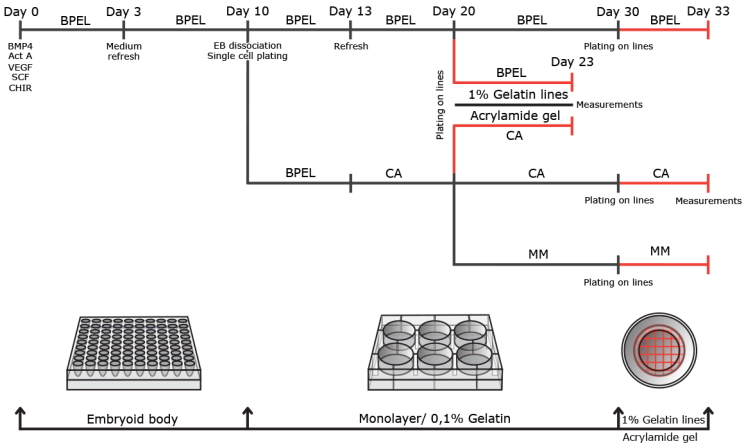
[50] Accili E a, Proenza C, Baruscotti M, DiFrancesco D. From funny current to HCN channels: 20 years of excitation. News Physiol Sci. 2002;17(6):32–7.

[51] Weitzel JM, Radtke C, Seitz HJ. Two thyroid hormone-mediated gene expression patterns in vivo identified by cDNA expression arrays in rat. Nucleic Acids Res. 2001;29(24):5148–55.

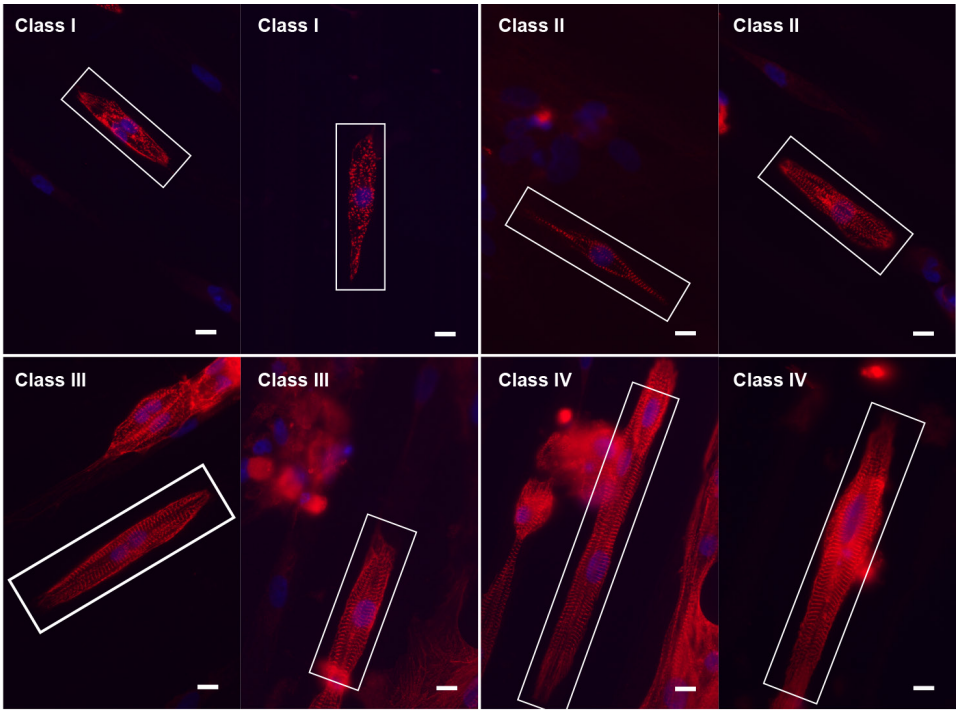
[52] Sakaguchi Y, Cui G, Sen L. Acute Effects of Thyroid Hormone on Inward Rectifier Potassium Channel Currents in Guinea Pig Ventricular Myocytes. Endocrinology. 1996;137(11):4744–51.



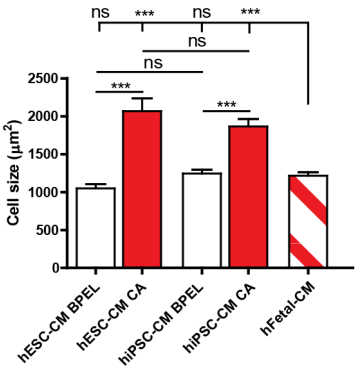
Supplementary figures



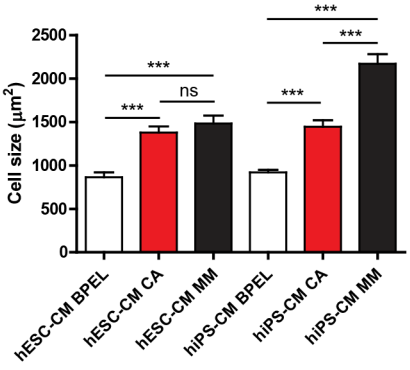
Supplementary Figure 1- Experimental schematic time line. Spin EB differentiation from day 0 to day 10 in a 96 well format. At day dissociation of Spin Ebs and plating on a 6 well plate with 30 Spin Ebs per well. Medium change three days later and culture as monlayer until time of dissociation. At day 20 one well of BPEL and CA were dissociated and plated on the gelatin lines for 3 days before measurements. The medium of remaining wells were changed and cultured for ten more days. At day 30 one well of BPEL, CA and MM were dissociated and plated on the gelatine lines three days before measurements.



Supplementary Figure 2- Classification for sarcomeric structure based on α-actinin staining. Top right panel- Example of class I cells displaying a random or patterned dotted staining. Top left panel- Example of class II cells displaying parallel band patterned staining in less than 70% of the cell. Bottom left panel- Example of class III cells displaying parallel band patterned staining in between 70% and 90% of the cell. Bottom right panel- Example of class IV cells displaying high sarcomeric organization with parallel band patterned staining in more than 90% of the cell.



Supplementary Figure 3- Cell size comparison between hESC-CM, hiPS-CM in different media and hFetal-CM. hESC-CM (n=45) and hiPS-CM (n=45) have comparable size. Both hESC-CM (n=41) and hiPS-CM (n=43) increase their size in CA medium. Both hESC-CM and hiPS-CM in BPEL have comparable size to hFetal-CM (n=116).



Supplementary Figure 4- Cell size comparison between hPSC-CM in different media. hESC-CM and hiPS-CM increase their size in CA and in MM in comparison to BPEL. hESC-CM does not increase their size in MM relative to CA, while hiPS-CM in MM display a significant increase in cell size in comparison to hiPs-CM in CA.



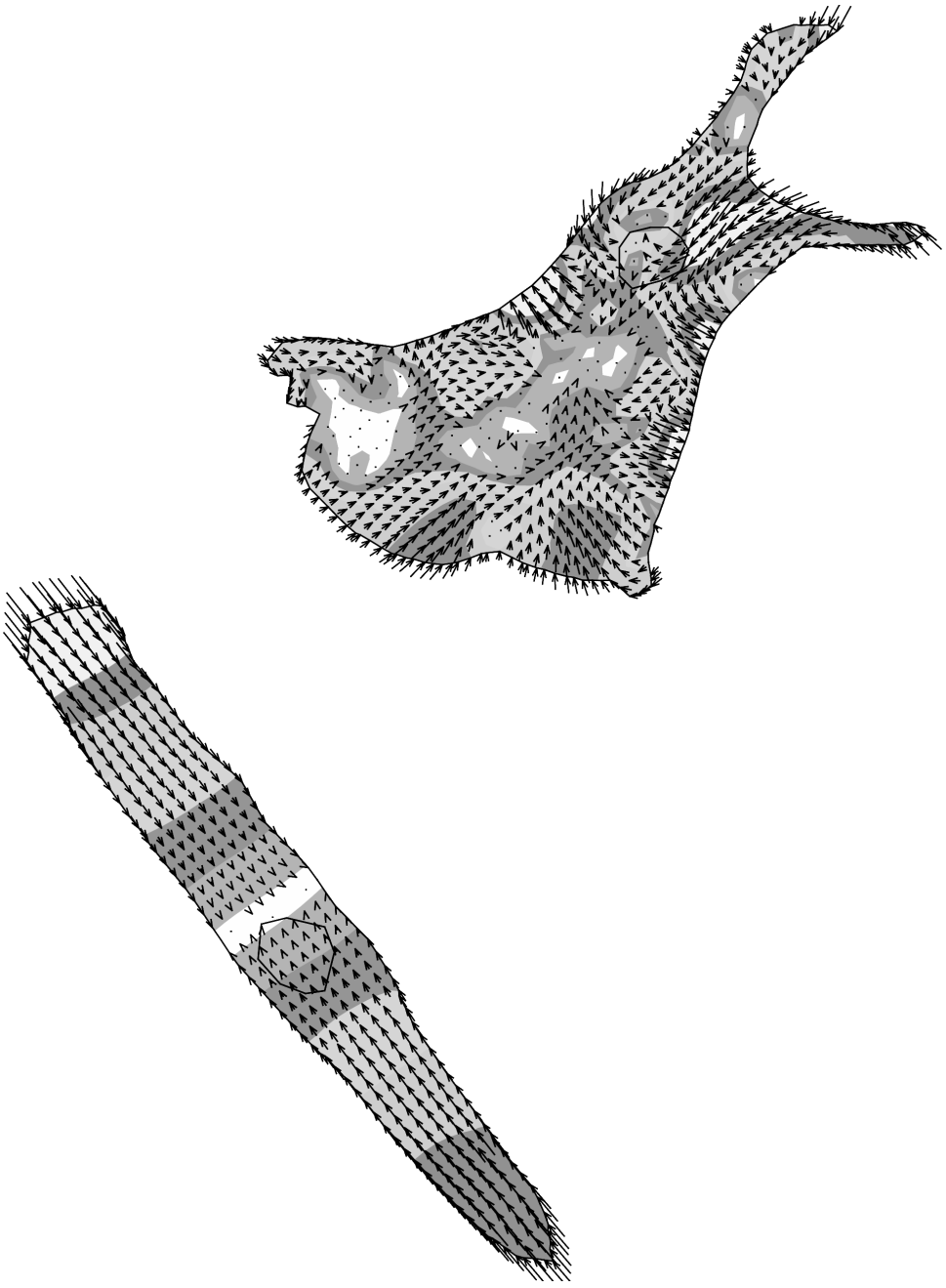
Table 1- Differences in electrophysiological parameters at day 23 at different frequency pacing.

Spontaneous		
	BPEL	CA
Vmax (V/s)	8.51±0.92	9.50±0.70
RMP (mV)	-61.47±1.20	-63.47±0.98
Amplitude (mV)	84.99±2.23	93.16±2.00**
APD50 (ms)	107.69±12.89	188.98±13.94***
APD90 (ms)	159.88±13.81	233.75±15.92**
n	18	24
1Hz		
	BPEL	CA
Vmax (V/s)	18.95±1.98	17.63±2.11
RMP (mV)	-62.92±1.42	-65.27±1.19
Amplitude (mV)	90.27±3.37	97.48±1.89
APD50 (ms)	97.70±12.94	222.64±40.53**
APD90 (ms)	145.00±26.26	249.82±30.05*
n	11	10
2Hz		
	BPEL	CA
Vmax (V/s)	19.22±2.29	18.94±2.37
RMP (mV)	-63.34±1.04	-66.13±1.22
Amplitude (mV)	90.32±2.52	96.89±2.31*
APD50 (ms)	101.56±9.66	143.02±11.56**
APD90 (ms)	133.85±9.42	179.22±11.04**
n	17	17
3Hz		
	BPEL	CA
Vmax (V/s)	22.42±3.26	20.25±2.51
RMP (mV)	-63.61±1.24	-66.55±1.21
Amplitude (mV)	90.92±2.81	97.97±2.33
APD50 (ms)	123.58±23.24	140.85±11.56**
APD90 (ms)	125.39±6.68	178.04±15.57**
n	18	15

Table 2- Differences in electrophysiological parameters at day 33 at different frequency pacing.

Spontaneous			
	BPEL	CA	MM
Vmax (V/s)	7.02 ±0.85	12.66±1.54	22.14±3.54*** †
RMP (mV)	-55.49±1.35	-60.51±1.72	-64.74±1.30***
Amplitude (mV)	79.70±2.42	87.95±2.39	101.54±1.94*** †††
APD50 (ms)	119.15±10.59	134.09±11.01	175.46±13.71**
APD90 (ms)	185.14±10.38	182.51±13.52	248.38±21.68* †
n	17	18	26
1Hz			
	BPEL	CA	MM
Vmax (V/s)	14.6±2.36	18.77±3.61	21.74±7.45
RMP (mV)	-55.17±1.88	-67.04±0.58***	-69.88±1.85***
Amplitude (mV)	84.62±3.07	93.81±1.60	107.59±2.29*** †
APD50 (ms)	102.02±16.56	123.30±18.01	222.08±37.00*
APD90 (ms)	161.50±21.73	178.24±24.41	347.68±47.44** ††
n	8	5	4
2Hz			
	BPEL	CA	MM
Vmax (V/s)	13.21±1.72	19.09±2.05	35.57±6.33*** †
RMP (mV)	-57.40±1.80	-64.28±1.08*	-67.52±1.45***
Amplitude (mV)	85.21±02.54	94.66±1.64*	106.88±1.67*** ††
APD50 (ms)	109.58±9.37	136.47±11.68	166.98±12.29**
APD90 (ms)	156.46±13.93	191.87±16.37	211.30±14.50*
n	16	11	14
3Hz			
	BPEL	CA	MM
Vmax (V/s)	11.90±1.26	23.08±5.23	39.47±7.13***
RMP (mV)	-57.01±1.44	-62.01±2.05	-64.40±1.67**
Amplitude (mV)	83.80±2.44	91.64±2.83	102.12±2.76*** †
APD50 (ms)	94.88±6.78	110.40±7.70	128.19±8.00**
APD90 (ms)	138.53±6.65	146.52±10.80	172.75±9.66
n	18	16	15





Chapter 4

Contractile defect caused by mutation in MYBPC3 revealed under conditions optimized for human PSC-cardiomyocyte function



Marcelo C Ribeiro[1,*], Matthew J Birket[1,*], Georgios Kosmidis[1], Dorien Ward[1], Ana Rita Leitoguinho[1], Vera van de Pol[1], Cheryl Dambrot[1,2], Harsha D Devalla[1], Richard P Davis[1], Pier G Mastroberardino[3], Douwe E Atsma[2], Robert Passier[1,ϕ], Christine L Mummery[1,ϕ]

[1]Department of Anatomy and Embryology, and 2 Department of Cardiology, Leiden University Medical Center, 2300 RC Leiden, The Netherlands.

[3]Erasmus Medical Center, 3015 GE Rotterdam, The Netherlands.

* Co-first author.

ϕ Co-last author.

Adapted from Cell reports 2015, 13: 1–13

Abstract

Maximizing baseline function of human pluripotent stem cell-derived cardiomyocytes (hPSC-CMs) is essential for their effective application in models of cardiac toxicity and disease. Here, we aimed to identify factors that would promote an adequate level of function to permit robust single cell contractility measurements in an induced PSC (hiPSC) model of hypertrophic cardiomyopathy (HCM). A simple screen revealed the collaborative effects of thyroid hormone, IGF-1 and the glucocorticoid analog dexamethasone on the electrophysiology, bioenergetics and contractile force generation of hPSC-CMs. In this optimized condition, hiPSC-CMs with mutations in MYBPC3, a gene encoding myosin-binding protein C and causing HCM, showed significantly lower contractile force generation than controls. This was recapitulated by direct knockdown of MYBPC3 in control hPSC-CMs, supporting a mechanism of haploinsufficiency. Modelling this disease *in vitro* using human cells is an important step towards identifying therapeutic interventions for HCM.

Introduction

Human pluripotent stem cells (hPSCs) are becoming increasingly used in biomedical research. Their extensive growth and differentiation potential enables routine production of cell types otherwise difficult to obtain. Cardiomyocytes are an important example, since collecting biopsies from the heart is highly invasive yet the cells they contain are those most pertinent to heart disease and drug-associated toxicity. Although many reports have now demonstrated the utility of hPSC-derived cardiomyocytes (hPSC-CMs) for modelling heart disease [1–4], the baseline functional performance of these cells is still less than that in adult heart tissue. Low maximum diastolic potential (MDP) and slow action potential upstroke velocities are frequently observed across all cardiomyocyte subtypes [5–7], coupled with a low force of contraction [8,9].

The poor functional output of hPSC-CMs is in large part due to their developmental immaturity [6]. While efforts are ongoing to advance the developmental state beyond their fetal equivalents, another important and valid approach is to also consider ways to maximise cell function more immediately, which might not necessarily be coupled to or regulated in the same way as developmental maturation. This might be achieved, for example, by improving aspects of cell metabolism and bioenergetics. Cardiomyocytes maintained outside their native environment within the heart may be disconnected from many factors important for their basic physiology, including relevant growth factor and hormone signalling, extracellular matrix proteins, other cell populations in the heart and mechanical- and electrical-stimulation. As protocols for hPSC-CM generation have improved and the generation of pure populations of cardiomyocytes in serum-free media well established, this separation becomes even more notable. Many physiological factors that would normally be circulating in the heart are absent under most basal culture conditions and it is unclear which should be provided in a defined formulation to promote optimal cardiomyocyte function in bioassay development.

The MDP is a fundamental determinant of excitability, and in cardiomyocytes from adult "working myocardium" is around -85 mV [10]. The lack of Ik1 current, due to low expression of the KCNJ2 gene, is one reason that ventricular- and atrial-like cardiomyocytes from hPSCs are insufficiently polarised [5,11,12]. However, many other factors affect the resting membrane potential. These include the activity of the energy demanding Na,K-ATPase, and potassium conductance as determined by other channels [13,14], which may also not be appropriately expressed or function optimally. The MDP is a strong predictor of contractile output in hPSC-CMs [9], and so improving MDP is an important prerequisite for faithfully modelling diseases affecting excitability or contractility.

One disease predicted to affect cardiomyocyte contractility is hypertrophic cardiomyopathy (HCM). HCM is highly prevalent, affecting 1:500 of the population and can be caused by mutations in various sarcomeric protein encoding genes [15]. Approximately 70% of cases are the result of mutations either in MYH7, encoding β-myosin heavy chain, or in MYBPC3, encoding cardiac myosin-binding protein C (cMyBP-C). As a disease with known genetic cause but ill-defined molecular pathogenesis, HCM is an excellent candidate for stem



cell modelling [16]. The absence of a cure or even an effective treatment strategy provides great urgency for *in vitro* human models to identify drugs able to restore contractile function and prevent the development of hypertrophy, cardiac remodelling and consequential arrhythmias. Induced pluripotent stem cells (hiPSCs) have already been generated from patients with mutations in MYH7 and MYBPC3, and cardiomyocytes derived from them [17–19], but their force generation, measured on physiologically-relevant substrate dimensions and stiffness, has not yet been described, and is currently hindered by poor baseline performance as noted above.

In this study, we began with a well characterised NKX2-5eGFP/w human embryonic stem cell (hESC) line, in which working cardiomyocytes are specifically marked by eGFP expression [20,21], to identify factors or combinations of factors which promoted an increase in their resting plasma membrane potential, or that had an anabolic effect, making the assumption that such factors could have functional benefit. We then tested these factors at the level of single cell traction force and action potential generation. Optimized conditions were then applied to an hiPSC model of MYBPC3 insufficiency and this revealed a contractile defect in cardiomyocytes derived from MYBPC3 mutation carriers.

Results

The identification of factors modulating hPSC-derived cardiomyocyte plasma membrane potential and size

Populations of cardiomyocytes were generated by monolayer differentiation of NKX2-5eGFP/w hESCs and these were maintained until day 16. To screen for modulators of resting plasma membrane potential ($\Delta\Psi p$), we assessed short-term accumulation of the cationic fluorescent probe tetramethylrhodamine methyl ester (TMRM) in cell suspensions. TMRM follows Nernstian behaviour across cell membranes, the early phase of TMRM accumulation into cells is dominated by the $\Delta\Psi p$, while with longer loading times the mitochondrial membrane potential and matrix volume contribute increasingly to total accumulation [22]. Time-course measurement of TMRM accumulation was performed from control conditions (**Figure 1a** and **b**). Based on this, 8 mins loading time was chosen for relative assessments of $\Delta\Psi p$, since this was in the linear phase of accumulation but gave signal substantially above background. Additionally, total cellular eGFP fluorescence was used as an estimate of cell size/volume, on the assumption that eGFP levels should correlate with total cell protein. There are several caveats to this reasoning, but modulators can be subsequently validated with more direct assays. In support of a general correlation, fetal calf serum exposure, known to increase the size of these cells [23], increased eGFP levels after 5 days of exposure (**Fig. S1**).

The following factors, each with putative roles in cardiomyocyte function, were tested: insulin-like growth factor 1 (IGF-1), the hedgehog signalling agonist SAG, the synthetic glucocorticoid dexamethasone (Dex), triiodothyronine hormone (T3), the α-adrenergic agonist phenylephrine (PE) and the β-adrenergic agonist isoproterenol (ISO) [24–29]. Testing was performed in a serum-free, low-insulin medium that has become a widely used standard for

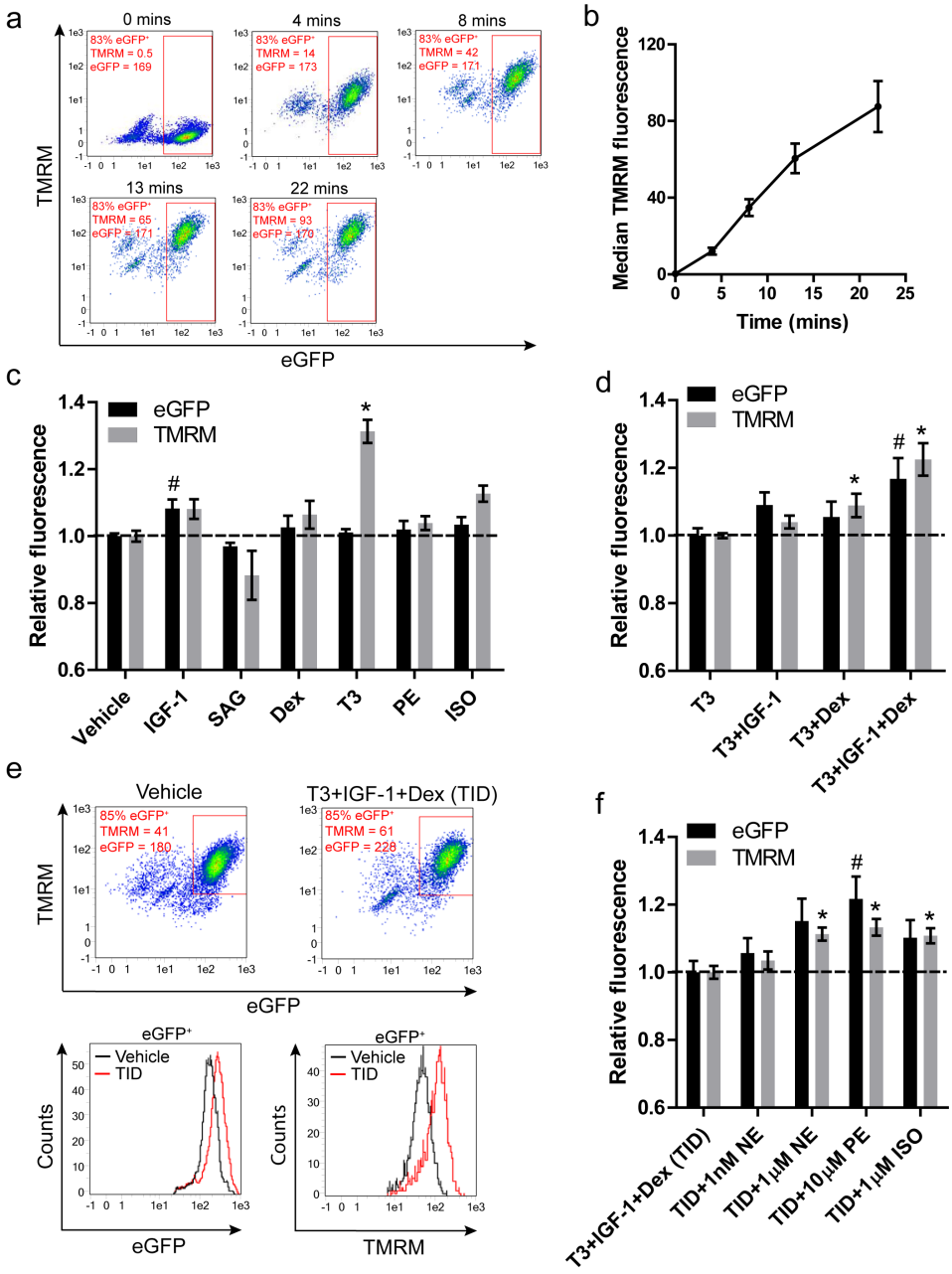


Figure 1- Using TMRM to identify modifiers of ΔΨp in hESC-derived NKX2-5+ cardiomyocytes. **A.** Time-course measurement of TMRM accumulation after cardiac differentiation of NKX2-5eGFP/w hESCs. FACS plots show eGFP and TMRM fluorescence after 0, 4, 8, 13 and 22 mins of loading with TMRM. A minor cross-bleed correction has been applied to all. **B.** Median TMRM fluorescence intensity in eGFP+ cells plotted against loading time. **C.** eGFP and TMRM fluorescence values in eGFP+ cardiomyocytes relative to a vehicle-only control after 5 days of incubation with the factors shown (n=6-34). **D.** eGFP and TMRM fluorescence values in eGFP+ cardiomyocytes relative to a T3-treated control after 5 days of incubation with the factors shown (n=10-22). **E.** Upper panel: example FACS

plots showing measurement of a vehicle-only control alongside a T3+IGF-1+Dex-treated sample. Lower panel: Histograms of eGFP and TMRM intensity in the eGFP+ populations as marked on the dot plots above. **F.** eGFP and TMRM fluorescence values in eGFP+ cardiomyocytes relative to a T3+IGF-1+Dex-treated sample after 5 days of incubation with the factors shown (n=11). Data are mean±SEM. The n signifies biological replicates. Statistical significance compared to the vehicle-only control was calculated using a one-way ANOVA with Dunnett's correction, # P<0.05 for eGFP fluorescence, * P<0.05 for TMRM fluorescence. See also Figure S1 and S2.

maintenance of these cells [30]. Contracting monolayers of differentiated cells (day 16) were maintained for 5 days in each test condition before measurement (**Figure 1c**). IGF-1 was the only factor to significantly increase eGFP fluorescence intensity, and TMRM accumulation increased only proportionally in this condition. IGF-1 may therefore mildly increase cell volume without affecting ΔΨp. T3 was the only factor that significantly increased TMRM accumulation, while eGFP fluorescence remained unaffected. This indicated an increase in ΔΨp by T3, but not in cell volume. While ISO mildly increased TMRM accumulation, neither ISO nor PE induced an increase in eGFP fluorescence; inconsistent with their established role as hypertrophic agonists in other cardiomyocyte systems but consistent with a reported variable response in some hPSC-CM lines [31–33]. Dex had little effect on either eGFP or TMRM, consistent with unpublished work from our group showing a lack of effect by Dex-alone on cardiomyocyte electrophysiology in hPSC-derived cardiomyocytes (Kosmidis et al. unpublished results), but inconsistent with its previously described role in cardiomyocyte maturation [28,34], suggesting that competence factors may be lacking.

These results support a role for T3 in determining ΔΨp in hPSC-derived cardiomyocytes, but not for maturation-related growth. To explore the possibility of enhancing this condition further, we tested the effect of additional IGF-1 or Dex compared to T3-alone (assigned as the new reference control and normalized to 1) (**Figure 1d**). The addition of IGF-1 again mildly increased eGFP levels over T3-alone, while T3+Dex mildly, but significantly increased TMRM accumulation. However, the combination of T3+IGF-1+Dex (TID) increased both eGFP and TMRM significantly, suggesting an enhancement in both size and possibly ΔΨp (**Figure 1e**), changes which could be associated with further improved cardiomyocyte function. The increased eGFP fluorescence with T3+IGF-1 and TID was not associated with, and therefore explained by, a relative increase in eGFP mRNA expression in these cells (**Fig. S2**). Upregulation (~4-fold) of the glucocorticoid-response gene FKBP5 confirmed increased glucocorticoid signalling by Dex (**Fig. S2**). The action of TID on eGFP levels and TMRM accumulation was confirmed in cardiomyocytes from an independent NKX2-5eGFP/w knock-in reporter M1 hESC line as well as an NKX2-5eGFP/w knock-in reporter hiPSC line (**Fig. S1**).

As insulin was present in the basal medium at 1 μg/ml for all these assays and at these concentrations can cross-react with the IGF-1 receptor, we separately tested the impact of insulin and IGF-1 in this T3+Dex condition. Addition of 1 μg/ml insulin-alone to the medium containing T3+Dex significantly increased eGFP fluorescence, but addition of 100 ng/ml IGF-1 increased eGFP fluorescence further and also increased TMRM accumulation (**Fig. S1**). This suggests that activation of the IGF receptor is the primary mediator of this response.

Importantly, in the presence of TID, cardiomyocytes responded appropriately to stimulation by the adrenergic agonists: norepinephrine (NE), PE or ISO, with an increase in eGFP fluorescence, suggesting that a baseline level of bioenergetic- or anabolic-activity may be important for this hypertrophic response (**Fig. 1f**). Relative eGFP mRNA expression was not significantly affected by these factors (**Fig. S2**). The action of adrenergic agonists did not, however, increase TMRM accumulation beyond the increase in eGFP intensity, suggesting increased TMRM was probably due to increased cell volume and not due to a further improvement in $\Delta\Psi p$ by these factors.

Bioenergetic response in cardiomyocytes by the concerted action of T3, IGF-1 and dexamethasone

The response to IGF-1 and Dex in terms of cardiomyocyte growth and $\Delta\Psi p$ suggests a possible synergistic role in metabolic stimulation. To test this, bioenergetic profiling of contracting cardiomyocyte monolayers was performed using the Seahorse XF24 Analyzer on cells treated during the same experimental time-course. Contraction rates, measured prior to analysis, were not significantly different between groups (**Figure 2a**). Under standard conditions (15 mM glucose, 0.5 mM sodium pyruvate) normalized to total cell protein, T3 mildly increased the oligomycin-sensitive respiration rate as previously reported (Yang et al., 2014), indicating increased mitochondrial ATP turnover (**Figure 2b and d**). Neither IGF-1 nor Dex stimulated this further, but the combination of TID did have a further stimulatory effect (TID: 213±4 vs Vehicle: 124±6 pmoles O2/min/10 μg cell protein; $p<0.05$). The anaerobic glycolytic rate (calculated as previously described by Mookerjee et al., 2015) was also significantly increased by TID (TID: 68±4 vs Vehicle: 34±4 pmoles H+/min/10 μg cell protein; $p<0.05$) (**Figure 2c**). A conversion of these values to ATP production rates (see Experimental procedures) showed a large increase (1.7-fold) in combined ATP turnover with TID (**Figure 2d**). The oligomycin-inhibited rates, the maximum uncoupled respiration rates induced by FCCP, and the non-mitochondrial rates, were not significantly different between conditions (**Figure 2b**). These results support a synergistic effect for the actions of IGF-1 and Dex on basal cell activity. Inhibition of both excitation and contraction by co-injection of nifedipine and blebbistatin decreased the mitochondrial respiration rate by 39.3±4.2% in the vehicle-only condition and 43.9±9.0% in TID (**Figure 1e**) after subtraction of a minor buffer-only injection effect. As the starting respiration rate was higher with TID this showed that the activity of these processes had increased at least proportionally by TID.

Sensitivity to substrate supply was assessed by examining the change in basal respiration rate and respiratory capacity on inhibition of either long-chain fatty acid uptake into mitochondria by the carnitine palmitoyl transferase inhibitor etomoxir (40 μM) or inhibition of mitochondrial pyruvate uptake by inhibition of the pyruvate transporter with UK5099 (5 μM). These experiments were performed in a more physiological medium containing 5.5 mM glucose, 0.15 mM sodium pyruvate and 100 μM palmitate. **Figure 2f** and **2g** show typical respiratory responses to etomoxir and UK5099 of cells from vehicle-only medium and TID-medium respectively. **Figure 2h** shows quantification of the sensitivity of basal and FCCP-stimulated mitochondrial respiration rates to these inhibitors. Basal respiration in cells from vehicle-only medium and TID-medium was inhibited 21.0±4.3% and 24.4±4.9%



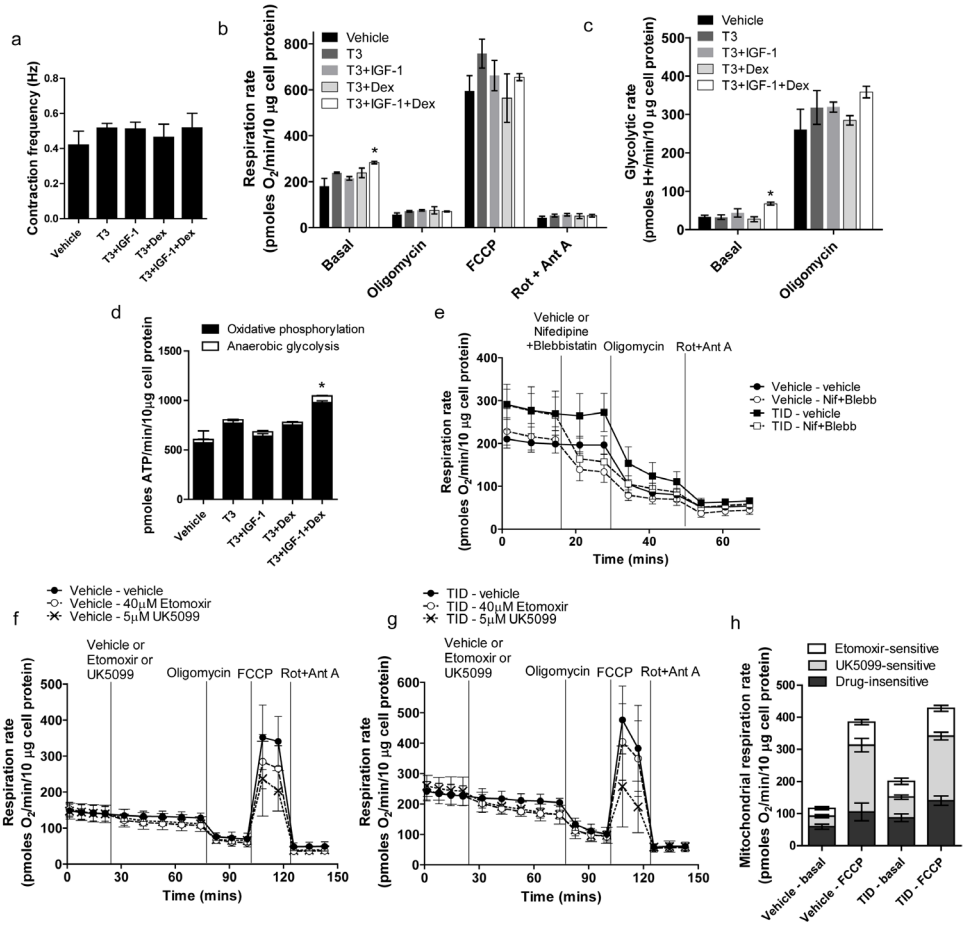


Figure 2- Bioenergetic profiling of hESC-derived cardiomyocytes. **A.** Contraction frequency in cardiomyocyte monolayers, treated for 5 days with the factors shown, prior to Seahorse measurement. **B.** Respiration rates in cardiomyocyte monolayers treated with the factors shown, normalized to cell protein. Basal = endogenous rate; Oligomycin = ATP synthase-inhibited rate; FCCP = maximum uncoupled rate; Rot + Ant A = non-mitochondrial respiratory rate. **C.** Glycolytic rate measured in parallel with respiration, normalized to cell protein. **D.** Theoretical basal ATP production rates from oxidative phosphorylation and anaerobic glycolysis calculated from measurements in B and C. **E.** Real-time respiration measurements of vehicle-only and TID-treated cells and response to injection of vehicle-only or nifedipine + blebbistatin, then oligomycin, and finally rotenone and antimycin A. **F.** Real-time respiration measurements of vehicle-only or **G.** TID-treated cells and response to injection of vehicle-only or 40 µM etomoxir or 5 µM UK5099, then oligomycin, FCCP, and finally rotenone and antimycin A. **H.** Sensitivity of basal and FCCP-stimulated mitochondrial respiration to etomoxir and UK5099 in vehicle-only or TID-treated cells. Bar data are mean±SEM from three independent experiments, each comprising 4-5 measurement wells per condition. Real-time respiration plots show data of a typical experiment mean±SD of individual wells. Statistical significance compared to the vehicle-only control was calculated using a one-way ANOVA with Dunnett's correction for b-d. * P<0.05. See also Figure S3.

respectively by etomoxir, and 27.7±4.2% and 31.9±3.3% respectively by UK5099. The basal respiration rate was again higher in TID-treated cells. FCCP-stimulated respiration in cells from vehicle-only medium and TID-medium was inhibited 18.5±2.1% and 20.2±2.2%

respectively by etomoxir, and 53.8±5.5% and 47.0±2.9% respectively by UK5099. Overall, these data suggest that TID increases the basal utilization of both glucose and fatty acids in cardiomyocytes in concert with increased ATP demand for excitation/contraction as well as other processes. In line with these changes, TID increased expression of PGC-1α and PGC-1β (**Fig. S2**), important regulators of myocardial FAO and mitochondrial function (Birket et al., 2013; Finck and Kelly, 2007). We additionally found that increased bioenergetic activity by TID exposure was associated with a decreased rate of dihydroethidium (DHE) oxidation, suggesting a decreased level of reactive oxygen species (**Fig. S3**), which may also support improved cardiomyocyte function.

Electrophysiological and contractile improvements by the concerted action of TID

To test whether the bioenergetic changes and improved resting $\Delta\Psi p$ resulted in improvements in electrophysiological function, action potentials were measured in spontaneously active cells. To focus on a possible effect of glucocorticoid signalling we measured cells maintained in three conditions: vehicle-only, T3+IGF-1 and TID. The results are shown in **Figure 3** and summarized in Table 1. The MDP was increased by both T3+IGF-1 and TID (**Figure 3b**), aligning well with our estimates by TMRM uptake. The amplitude of the AP was also increased progressively by both treatments (**Figure 3c**). Interestingly, while the upstroke velocity was not significantly increased by T3+IGF-1 it was markedly increased by TID, from 16±5 V/s to 59±6 V/s (**Figure 3d**; $p<0.05$). This specific effect was significantly blocked by 6 μM GSK650394, an inhibitor of the serum- and glucocorticoid inducible kinase SGK1 [35] which was previously shown to block cardiac sodium channel degradation, and which is activated by IGF-1 [36]. We confirmed SGK1 upregulation in response to Dex (**Figure 3g)**. SCN5A expression was not increased by dexamethasone (**Fig. S2**), and the inhibitor did not significantly affect any other aspect of the AP, together supporting this specific mechanistic explanation. Despite the increased MDP, AP frequency was increased by TID in this single cell format (**Figure 3f**), differing from measurements in the monolayer format in **Figure 2a**. In summary, the AP data also supports the conclusion that cardiomyocyte function was improved by the action of TID.

Table 1- Action potential parameters of single spontaneously active cardiomyocytes.

	Vehicle (n=12)	T3+IGF-1 (n=15)	T3+IGF-1+Dex (n=33)	TID+SGKi (n=16)
MDP (mV)	–66.9±1.2	–71.5±0.9*	–74.2±0.8*	–74.2±1.1*
dV/dt_{max} (V/s)	15.8±2.2	21.5±4.9	58.9±4.6*	36.5±5.6
APA (mV)	97±2	104±2*	112±2*	114±2*
APD_{50} (ms)	110±11	98±12	104±11	97±10
APD_{90} (ms)	146±14	125±13	134±11	124±10
Frequency (Hz)	1.6±0.2	2.1±0.2	2.5±0.2*	2.2±0.2
Capacitance (Cm)	20±3	17±1	25±2	24±3

Data are mean±SEM; TID+SGKi=T3+IGF-1+Dex+GSK650394, n=number of cells, MDP=maximal diastolic potential, dV/dtmax=maximal upstroke velocity, APA=action potential amplitude, APD50, and APD90=action potential duration at 50, and 90% repolarization, respectively. * $p<0.05$ compared to vehicle. One-Way ANOVA with a Tukey post-test.



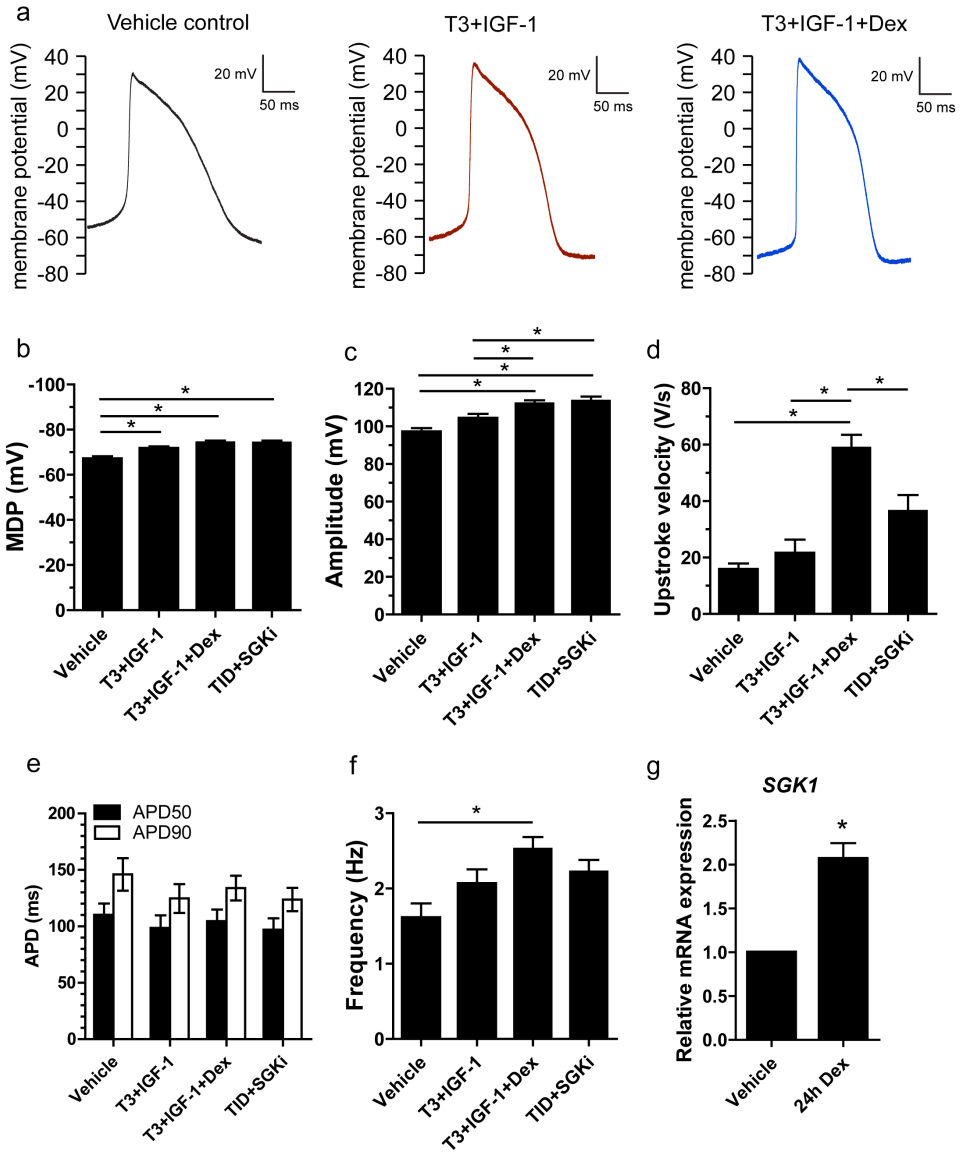


Figure 3- Cardiomyocyte action potential measurement. **A.** Typical examples of action potential (AP) traces from single spontaneously active cardiomyocytes maintained in the three conditions indicated. **B-G.** Average data of maximum diastolic potential (MDP), AP amplitude, AP upstroke velocity, and AP duration at 50% (APD50) and 90% (APD90) repolarization and AP frequency. SGKi = 5 day co-incubation with 6 μM GSK650394. Data are mean±SEM. Actual AP values and n values are shown in Table 1. Statistical significance was calculated using a one-way ANOVA with Tukey's multiple comparison test * P<0.05.

We next examined single cell contractility under the same maintenance conditions with the exception that cardiomyocytes were plated on soft micropatterned polyacrylamide gels (20 μm-wide gelatin lines) containing fluorescent micro-beads. Bead displacement was imaged during spontaneous contraction of individual cells and converted to a value of trac-

tion stress (**Figure 4a**), as previously described [9]. In vehicle-only medium, mean traction stress was 0.15±0.02 mN/mm^2; in T3+IGF-1 this was increased by 1.8-fold to 0.27±0.02 mN/mm^2 ($p<0.05$), and in TID medium it was increased by 2.9-fold to 0.44±0.04 mN/mm^2 ($p<0.05$) (**Figure 4b**). This corresponded to traction forces of 0.15±0.02 μN, 0.36±0.04 μN and 0.76±0.08 μN for vehicle-only, T3+IGF-1, and TID medium, respectively. The potentiated increase in traction stress by the addition of Dex, over the T3+IGF-1-condition, was significant ($p<0.05$). Cardiomyocyte area was increased 1.4-fold by T3+IGF-1 ($p<0.05$) and 1.8-fold by TID ($p<0.05$) (**Figure 4c**), although cells remained small compared to adult human equivalents (Ancey et al., 2003). The potentiated increase in cell area by Dex was significant ($p<0.05$), aligning with our estimates by eGFP intensity. Contraction frequency was increased by TID, however as the force-frequency relationship was negative in all conditions this did not explain the difference in traction stress between the conditions (**Figure 4d**). A co-staining of Troponin I and α-actinin showed that the structural organization of sarcomeres was improved by TID and sarcomeres were more uniform across the entire area of each cardiomyocyte (**Figure 4e** and **Fig. S4**). Expression of the contractility-related protein encoding genes: MYH6, ACTN2, MLC2V and SERCA2 were upregulated by TID, although they were not significantly different between T3+IGF-1 and TID (**Fig. S2**). T3 repressed MYH7 expression as previously reported (Iwaki et al., 2014). An increase in traction stress by TID was also recorded in cardiomyocytes from the M1 hESC line (**Fig. S4**).

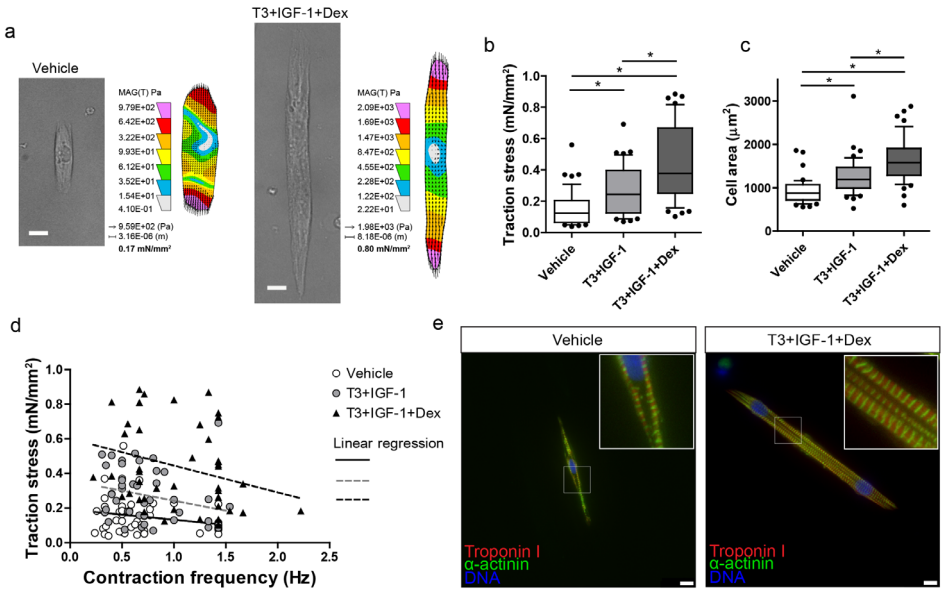


Figure 4- Single cardiomyocyte traction force measurement. **A.** Typical examples of single aligned (spontaneously contracting) cardiomyocytes from vehicle-only and T3+IGF-1+Dex containing medium, showing a brightfield image of the relaxed form and a heat map of traction stress applied to the substrate calculated from the mean of the traction stress vectors (corresponding to Supplementary video 1). **B.** Traction stress, **C.** cell area and **D.** Traction stress-frequency relationship, of single spontaneously contracting cardiomyocytes maintained in vehicle (n=44), T3+IGF-1 (n=44) and T3+IGF-1+Dex (n=45). **E.** Immunostaining of typical aligned cardiomyocytes from vehicle- and TID-containing medium. Box and whisker plots show the median, interquartile range and 10-90 percentile range. The n signifies the number of individual cells measured, acquired over 3 independent experiments. Statistical significance was calculated using a one-way ANOVA with Tukey's multiple comparison test * $P<0.05$. Scale bar = 10 μm. See also Figure S4.



Contractile dysfunction in a hiPSC model of hypertrophic cardiomyopathy

We have previously observed that single hiPSC-derived cardiomyocytes also generate very low contractile forces when maintained under standard basal conditions (~0.2 mN/mm^2) (Ribeiro et al., 2015 and unpublished observations). This creates a very low level of sensitivity for detecting defects in function, as even the control cells may be functioning far from their full dynamic range. Therefore we took the opportunity to apply the TID-containing medium to an hiPSC disease model in which the derivative cardiomyocytes carry a c.2373dupG mutation in MYBPC3 [17]. This mutation causes HCM in patients [37]. The mutant MYBPC3 hiPSC-CMs were compared to cardiomyocytes derived from two hiPSC lines generated from healthy controls. Cardiac functional data of the HCM patients is provided in Table S1. A significant decrease in MYBPC3 protein relative to α-actinin was observed in the cardiomyocytes from all three HCM lines compared to both controls when measured at day 25 of differentiation (**Figure 1a** and **b**).

Attempts to measure these hiPSC-CMs in medium without TID proved unsuccessful as even the control cells failed to reliably generate robust bead displacement. However, in medium containing TID, traction force on the polyacrylamide substrate could be measured in all cell populations. Under these conditions, traction stress was significantly decreased in all three mutant lines: HCM1 0.31±0.02 mN/mm^2, HCM2 0.30±0.03 mN/mm^2, HCM3 0.29±0.03 mN/mm2, compared to both controls: Con1 0.57±0.04 mN/mm^2, Con2 0.51±0.03 mN/mm^2; $p<0.05$ (**Figure 5c** and **d**). This corresponded to traction forces of 0.43±0.04 μN, 0.46±0.06 μN, 0.44±0.05 μN and 0.81±0.16 μN, 0.86±0.10 μN for HCM1, HCM2, HCM3 and Con1, Con2, respectively. A difference in cardiomyocyte size as measured by cell area, was not evident between the control and the mutant cells, suggesting an overt hypertrophic response had not occurred by this stage of development under these conditions (**Figure 5e**). Contraction frequencies were not different (**Fig. S4**).

Discussion

Using a simple flow cytometry based assay we have identified a combination of defined factors, namely thyroid hormone (T3), IGF-1 and the glucocorticoid dexamethasone, which together enhanced the functional properties of hPSC-derived cardiomyocytes. We observed that T3 principally increased the resting membrane potential ($\Delta\Psi p$), a critical factor in determining excitability and contractility, while IGF-1 and dexamethasone acted synergistically to stimulate cell energetics and traction force generation. In this optimized condition we assessed the impact of an HCM-causing mutation in MYBPC3, or gene knockdown. Decreased force generation was observed in both cases, recapitulating measurements in mutant mouse models and patient-derived cells, opening up the possibility of using this *in vitro*-based human model as a tool for future mechanistic studies and drug screening.

The positive influence of T3 on cardiomyocyte function is well supported in the literature. Levels increase markedly at birth in humans and have an important role in heart development and maturation [27,38]. T3 was previously shown to increase the activity of the Na,K-ATPase in cardiomyocytes [39], as well as increasing the Ik1 current [40], both of

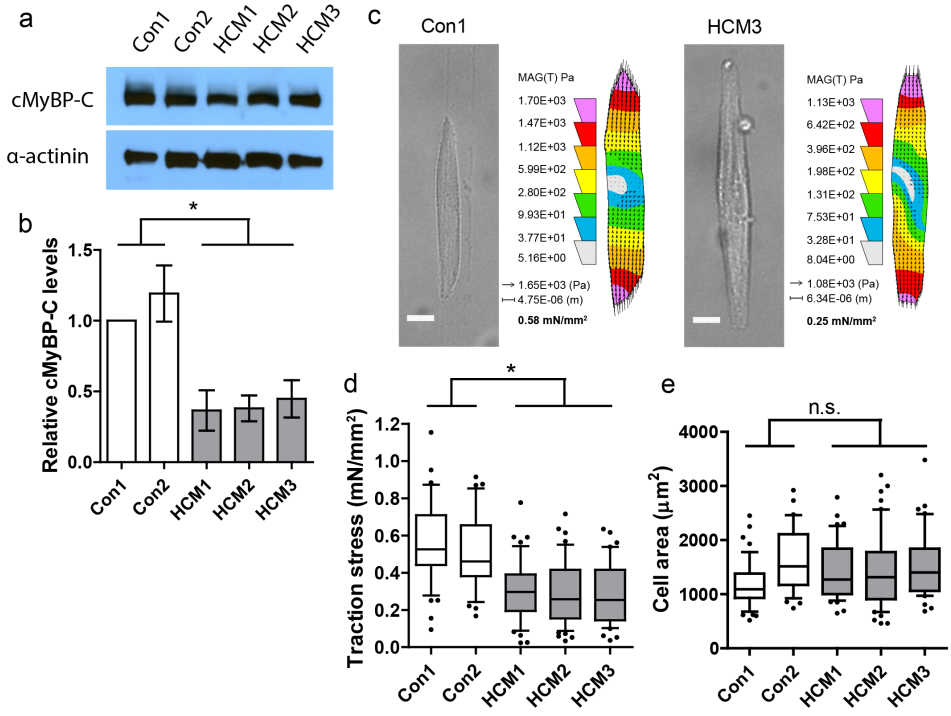
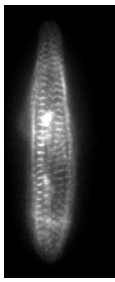


Figure 5- Single cell traction force measurements in cardiomyocytes with MYBPC3 mutation or MYBPC3 shRNA knockdown. **A.** Western blot of MYBPC3 protein from two control (Con1 and Con2) and three MYBPC3 mutation lines (HCM1, HCM2 and HCM3). α-actinin is shown as a loading control for cardiomyocyte input. **B.** Relative MYBPC3 levels normalized to α-actinin levels based on densitometry of Western blot data (n=3-6 lysates). **C.** Typical examples of single aligned (spontaneously contracting) cardiomyocytes from control (Con1) and MYBPC3 mutation (HCM3) lines, showing a brightfield image of the relaxed form and a heat map of traction stress applied to the substrate calculated from the mean of the traction stress vectors (corresponding to Supplementary video 2). **D.** Traction stress and **E.** cell area of single spontaneously contracting iPSC-derived cardiomyocytes from two control (Con1 [n=47] and Con2 [n=36]) and three MYBPC3 mutation lines (HCM1 [n=44], HCM2 [n=54] and HCM3 [n=43]). Unless otherwise stated the n signifies the number of individual cells measured, acquired over 3 independent experiments. Statistical significance was tested with a one-way ANOVA with Tukey's multiple comparison test in D and E, comparing either control against the HCM lines independently, and a Dunnett's correction in g and h. Comparison to both controls in d are statistically significant *P<0.05. Scale bar = 10 μm. See also Figure S5.

which could explain the increase in ΔΨp observed here. T3 also affects sarcomeric gene expression, stimulating expression of α-MHC, the fast ATPase activity MHC isoform, and repressing the expression of β-MHC, the slow ATPase activity isoform [41,42]. This effect was also shown in hESC-CMs by Yang et al. (2014), and confirmed here. These changes in MHC isoform expression may contribute to the increased contractile force generation observed with T3, as also previously reported by Yang et al. (2014). However, from this base condition we were able to extend these findings with the identification of additional physiologically relevant factors important for hPSC-CM function. IGF-1 also circulates in the developing heart and has an important role in myocardial cell growth and metabolism by signalling through the IGF-1 tyrosine kinase receptor [29]. We found that IGF-1 mildly increased the size of hPSC-CMs, but more importantly proved an essential factor in revealing a positive functional role for the glucocorticoid dexamethasone in this system. Synergistic effects for



IGF-1 and dexamethasone have been reported in skeletal muscle and heart, with pro-differentiation and anti-atrophic effects observed [43–45]. Glucocorticoids also promote the structural and functional maturation of fetal mouse cardiomyocytes [28,34], but have little effect on hPSC-CMs when added alone although do affect calcium handling (Kosmidis et al. unpublished results). Interestingly, the positive effect reported by Rog-Zielinska et al. in cultured cells was blocked by PGC-1α knockdown, a protein known to regulate mitochondrial respiration in cardiomyocytes [23]. Our observation here, that in combination with IGF-1 dexamethasone exerted a clear bioenergetic response, also supports the conclusion that the functional improvements in force generation and electrophysiology may at least partly be the result of enhanced energy production pathways. Basal respiration coupled to ATP synthesis was increased by TID, and as this rate remained proportionally sensitive to inhibitors of excitation and contraction these processes must be more active in these cells. Additionally, we showed that basal respiration was sensitive to inhibitors of both mitochondrial pyruvate uptake as well as fatty acid uptake, implying that substrate supply also exerts significant respiratory control in both basal and TID conditions. The higher respiratory rate in TID suggests that both pyruvate and fatty acid usage was increased. TID also stimulated anaerobic glycolysis which will provide additional pyruvate for mitochondria but can also drive the synthesis of biomass through precursor synthesis [46], and increase NADPH production important for ROS detoxification[47]. Reduced DHE oxidation in cells treated with TID indeed indicated lower ROS levels. Mitochondrial ROS production may also be lower as a result of the increased ATP turnover[48]. While ROS have been shown to have an important role in cardiomyocyte development[49], elevated levels can be inhibitory to cell function so a balance may be important[23,50–52].

At the electrophysiological level, in the presence of T3, the addition of IGF-1 and dexamethasone caused a large increase in hESC-CM AP upstroke velocity not explained solely by the MDP. This was not associated with increased SCN5A expression and was therefore predicted to involve altered cardiac sodium channel regulation. The functional improvement was highly sensitive to small molecule inhibition of the glucocorticoid-inducible kinase SGK1 which is known to regulate degradation of the channel through inactivation of the ubiquitin ligase NEDD4-2 [36,53]. This result supports a role for SGK1 in hPSC-CM function and will be an important avenue for future investigation. A further improvement was seen in the AP amplitude by TID, a parameter known to correlate with contractile force generation at a single cell level [9]. Indeed, TID substantially increased the traction force of hPSC-CMs as well as their sarcomeric structural organization, showing that all core aspects of cell function were enhanced.

Having identified conditions for maximising traction force, we were able to apply the system to a cardiac disease model. HCM is caused by mutations in sarcomeric protein-encoding genes important for contractile function, of which mutation in MYBPC3 accounts for approximately 35% of cases. While animal models of MYBPC3-deficiency and patient-derived cells have been well studied [54–60], a widely accessible human *in vitro* model has been lacking. Here, using two independent approaches, we assessed the impact of MYBPC3-deficiency on hPSC-CM contractile force generation. Cardiomyocytes from patient-derived

hiPSCs carrying a non-sense mutation in MYBPC3 had <50% of normal MYBPC3 levels and were found to exert significantly less force at the single cell level. Our results are supported by measurements in adult patient-derived cells assessed *in vitro* where a 30-40% decrease in maximum Ca2+-activated force development has been observed in cells with the c.2373insG mutation, and a mechanism of haploinsufficiency suggested [59–61]. Importantly, the force generation defects we observed here were in non-hypertrophic cells, suggesting a primary event not consequential to hypertrophy and related maladaptive processes. This observation is consistent with the diastolic dysfunction reported in non-hypertrophic cardiomyocytes of mice heterozygous for a point mutation in mybpc3 [62]. Together these results support the possibility that the contractile dysfunction is an early initiating event in HCM disease pathogenesis. The specific initiating cause of the force generation defect in the hPSC-CMs studied here is unknown, as in all other models of MYBPC3 mutation studied so far. Potential causes could include a defect in sarcomerogenesis leading to a reduced myofibril density, perturbed cross bridge cycling or increased sarcomere calcium sensitivity leading to diastolic dysfunction, or more general metabolic disturbance. Having a human model where this phenotype can be genetically induced and studied in a developmental context will present new opportunities to address this question. This could in turn lead to new therapeutic strategies for HCM, which is currently without cure.

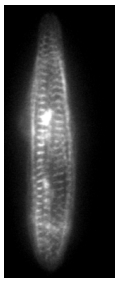
In summary, providing functionally important physiological factors to hPSC-CMs may be critical for achieving robust baseline function and maximising their use in applications of disease modelling, drug discovery and development, and toxicity screening. These are major goals for the stem cell field. Here we found that three defined factors were sufficient to markedly improve the function of hPSC-CMs and facilitated their use in a disease model of HCM. The advance in culture conditions towards a fully defined formulation also revealed the potential of the single cell traction force measurement technology for studying diseases of contractility in a highly controllable system.

Experimental Procedures

hPSC culture and differentiation

H3 NKX2-5eGFP/w hESCs or M1 NKX2-5eGFP/w hESCs as previously generated [21], were maintained on mouse embryonic fibroblasts and passaged using TrypLE select (Life Technologies). The generation of transgene-free hiPSCs from skin fibroblasts of one healthy male donor (LUMC0004iCtrl [Con1]) and three patients each with a c.2373dupG mutation in MYBPC3 (LUMC0033iMyBPC [HCM1], LUMC0034iMyBPC [HCM2] and LUMC0035iMyBPC [HCM3]) was previously reported [17]. A second transgene-free control hiPSC line (LUMC0047iCtrl [Con2]) generated from another healthy male donor was included in this study. hiPSCs were maintained on Matrigel (growth factor reduced; Corning 354230) in mTeSR1 medium (Stem Cell Technologies) and passaged with 1 mg/ml Dispase (Life Technologies). NKX2-5eGFP/w hiPSCs (RPD, CLM unpublished) were maintained in Essential 8 medium (Life Technologies) and differentiated as previously described (van den Berg 2015).

Cardiac differentiation was induced from monolayer cultures on Matrigel in a serum-free



medium (BSA, polyvinyl alcohol, essential lipids [BPEL]) as described in Supplemental information. Contracting cultures were dissociated on day 13 and replated on Matrigel-coated 24-well plates. The following experimental factors were added on day 16, refreshed on day 20 and measured on day 21: 100 ng/ml Long R3 IGF-1 (in the main text: IGF-1), 1 μM SAG (Millipore), 1 μM dexamethasone, 100 nM triiodothyronine hormone, 10 μM phenylephrine, 1 μM isoproterenol, 1-1000 nM norepinephrine. Unless otherwise stated all factors were obtained from Sigma

Flow cytometry measurements for plasma membrane potential and reactive oxygen species

For relative plasma membrane potential measurement, differentiated cultures were dissociated on day 21 (after treatment as above from day 16) using 5x TrypLE Select and resuspended in 2.5 nM TMRM (Life Technologies) in warm assay medium. Cells were incubated for 8 minutes at 37°C before being measured by flow cytometry. For superoxide detection, dissociated cells were labelled with 5 μM DHE for 30 mins at 37°C and then measured by flow cytometry. Appropriate compensation to correct from cross-bleed was performed for each.

Respiration and acidification rates measured with the Seahorse XF-24 Analyzer

Respiration and acidification rates were measured on adherent cells using a Seahorse XF-24 or an XF-96 Analyzer (Seahorse Bioscience). Cells were seeded on Matrigel-coated assay plates in BPEL medium 7 days before measurement. The assay was performed in bicarbonate-free DMEM as described in Supplemental information. The standard glucose concentration was 15 mM glucose and was supplemented with 0.5 mM sodium pyruvate. Cells were washed twice and pre-incubated in the assay medium for 1 h before measurement. For the standard profiling oligomycin was used at 0.5 μg/ml, FCCP titrated in 2 injections to 3 μM and rotenone and antimycin A were added at 1 μM and 2 μM respectively. A standard protein assay was used to normalize values to whole cell protein. Glycolytic rate calculations and ATP production rates are described in Supplemental information. To assess ATP demand for excitation and contractility nifedipine (10 μM) and blebbistatin (5 μg/ml) were co-injected and the respiration rate immediately recorded, followed by measurements after oligomycin and then rotenone and antimycin A injection. A vehicle-only injection was performed in parallel and the effect subtracted. Experiments analysing the effect of etomoxir and UK5099 were performed on the XF-96 format using an assay medium with the following modifications: the glucose concentration was 5.5 mM, sodium pyruvate 0.15 mM and palmitic acid was included at 100 μM conjugated to fatty acid-free BovoStar BSA as described in Supplemental information. 10 mM HEPES was also included in this assay medium to provide extra buffering (glycolytic rates were not calculated). Cells were washed twice and pre-incubated in this assay medium for 4 h before measurement. To assess the response to substrate uptake inhibitors, 40 μM etomoxir or 5 μM UK5099 were injected and respiration rates recorded after 45 mins, followed by injections of oligomycin, FCCP (3 μM) and then rotenone and antimycin A. A vehicle-only injection was performed in parallel and the effect subtracted.

Electrophysiological characterization

Action potential (AP) recordings were performed on single cardiomyocytes, 6-10 days after cell dissociation with the amphotericin perforated patch-clamp technique using an Axopatch 200B amplifier (Molecular Devices Corporation, Sunnyvale, CA, USA). Signals were filtered and digitized at 5 and 40 kHz, respectively. Data acquisition and analysis were accomplished using pClamp10.1 (Axon Instruments) and custom software. Potentials were corrected for the liquid junction potential. Cells were continuously perfused in a perfusion chamber at 37 0C (Cell MicroControls Norfolk VA, U.S.A.) using Tyrode's solution containing (mM): NaCl 140, KCl 5.4, CaCl2 1.8, MgCl2 1.0, glucose 5.5, HEPES 5; pH 7.4 (NaOH). Pipettes (borosilicate glass; resistance ~2.5 MΩ) were filled with solution containing (mM): K-gluconate 125, KCl 20, NaCl 5, amphotericin-B 0.22, HEPES 10; pH 7.2 (KOH).

APs were recorded at spontaneous beating frequencies and characterized by duration at 50 and 90% repolarization (APD50, and APD90, respectively), maximal diastolic potential (MDP), AP amplitude, maximal upstroke velocity and frequency. AP parameter values obtained from 8-9 consecutive APs were averaged and data were collected from at least 2 independent differentiations per condition.

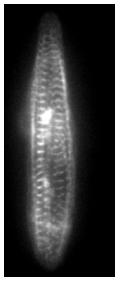
The SGK1-inhibitor GSK650394 [35] or vehicle-only control was applied at 6 μM 5 days before AP measurement. AP measurements were blinded in acquisition and analysis.

Traction force measurements

The traction force measurements were performed as previously described [8]. Cells were seeded onto the gelatine patterned acrylamide gels 4 days (see Supplemental information) before measurement in their normal culture medium in an environment maintained at 37°C with 5% CO2. Briefly, using a Leica AF-6000LX microscope, an image-series of aligned single spontaneously contracting cardiomyocytes was taken at 40x magnification at 20 frames per second, recording brightfield and fluorescent beads. Single frames from maximal relaxation and contraction of the brightfield and fluorescent beads image-series were analyzed by the LIBTRC software package (kindly provided by Dr. Micah Dembo), creating a mask of the cell outline from the brightfield image and a vector map from the difference between the relaxed and contracted fluorescent beads images. The vector map and the cell mask were used to calculate the total force that the cell applies on the substrate at its maximum peak of contraction. The traction stress generated by the cardiomyocyte during contraction was calculated by dividing the total force by the cell surface area. Measurements were blinded in acquisition and analysis.

Quantitative real-time PCR

RNA was isolated using a Minelute RNA extraction kit (Qiagen) and cDNA synthesized using an iScript cDNA synthesis kit (BioRad). Real-time PCR was performed on a BioRad CFX384 machine using IQ SYBR Green (BioRad). Gene expression values were normalized to the mean expression of the housekeeping genes human ribosomal protein (RPLP0), glucuronidase (GUSB), and RNF7. Primer sequences can be found in Supplemental information.



References

[1] Bellin M, Casini S, Davis RP, D'Aniello C, Haas J, Ward-van Oostwaard D, et al. Isogenic human pluripotent stem cell pairs reveal the role of a KCNH2 mutation in long-QT syndrome. EMBO J. 2013;32(24):3161–75.

[2] Drawnel FM, Boccardo S, Prummer M, Delobel F, Graff A, Weber M, et al. Disease Modeling and Phenotypic Drug Screening for Diabetic Cardiomyopathy using Human Induced Pluripotent Stem Cells. Cell Rep. 2014;810–20.

[3] Wang G, McCain ML, Yang L, He A, Pasqualini FS, Agarwal A, et al. Modeling the mitochondrial cardiomyopathy of Barth syndrome with induced pluripotent stem cell and heart-on-chip technologies. Nat Med. 2014;20(6):616–23.

[4] Zhang M, D'Aniello C, Verkerk AO, Wrobel E, Frank S, Ward-van Oostwaard D, et al. Recessive cardiac phenotypes in induced pluripotent stem cell models of Jervell and Lange-Nielsen syndrome: Disease mechanisms and pharmacological rescue. Proc Natl Acad Sci U S A. 2014;111(50):E5383–92.

[5] Sartiani L, Bettiol E, Stillitano F, Mugelli A, Cerbai E, Jaconi ME. Developmental changes in cardiomyocytes differentiated from human embryonic stem cells: a molecular and electrophysiological approach. Stem Cells. 2007;25(5):1136–44.

[6] Veerman C, Kosmidis G, Mummery C, Casini S, Verkerk A, Bellin M. Immaturity of human stem-cell derived cardiomyocytes in culture: fatal flaw or soluble problem? Stem Cells Dev. 2015;24(9):1035–52.

[7] Zhang J, Wilson GF, Soerens AG, Koonce CH, Yu J, Palecek SP, et al. Functional cardiomyocytes derived from human induced pluripotent stem cells. Circ Res. 2009;104(4):e30–41.

[8] Hazeltine LB, Simmons CS, Salick MR, Lian X, Badur MG, Han W, et al. Effects of substrate mechanics on contractility of cardiomyocytes generated from human pluripotent stem cells. Int J Cell Biol. 2012;2012:508294.

[9] Ribeiro MC, Tertoolen LG, Guadix JA, Bellin M, Kosmidis G, Aniello CD, et al. Functional maturation of human pluripotent stem cell derived cardiomyocytes in vitro e Correlation between contraction force and electrophysiology. Biomaterials. Elsevier Ltd; 2015;51:138–50.

[10] Magyar J, Iost N, Körtvély A, Bányász T, Virág L, Szigligeti P, et al. Effects of endothelin-1 on calcium and potassium currents in undiseased human ventricular myocytes. Pflügers Arch Eur J Physiol. 2000;441(1):144–9.

[11] Ma J, Guo L, Fiene SJ, Anson BD, Thomson JA, Kamp TJ, et al. High purity human-induced pluripotent stem cell-derived cardiomyocytes: electrophysiological properties of action potentials and ionic currents. Am J Physiol - Hear Circ Physiol. 2011;301(5):H2006–17.

[12] Synnergren J, Améen C, Jansson A, Sartipy P. Global transcriptional profiling reveals similarities and differences between human stem cell-derived cardiomyocyte clusters and heart tissue. Physiol Genomics. 2012;44(4):245–58.

[13] Glitsch HG. Electrophysiology of the sodium-potassium-ATPase in cardiac cells. Physiol Rev. 2001;81(4):1791–826.

[14] Tamargo J, Caballero R, Gómez R, Valenzuela C, Delpón E. Pharmacology of cardiac potassium channels. Cardiovasc Res. 2004;62(1):9–33.

[15] Maron BJ, Maron MS. Hypertrophic cardiomyopathy. Lancet. 381(9862):242–55.

[16] Eschenhagen T, Mummery C, Knollmann BC. Modelling sarcomeric cardiomyopathies in the

dish: from human heart samples to iPSC cardiomyocytes. Cardiovasc Res. 2015;105(4):424–38.

[17] Dambrot C, Braam SR, Tertoolen LGJ, Birket M, Atsma DE, Mummery CL. Serum supplemented culture medium masks hypertrophic phenotypes in human pluripotent stem cell derived cardiomyocytes. J Cell Mol Med. 2014;18(8):1509–18.

[18] Han L, Li Y, Tchao J, Kaplan AD, Lin B, Li Y, et al. Study familial hypertrophic cardiomyopathy using patient-specific induced pluripotent stem cells. 2014;258–69.

[19] Lan F, Lee AS, Liang P, Sanchez-Freire V, Nguyen PK, Wang L, et al. Abnormal calcium handling properties underlie familial hypertrophic cardiomyopathy pathology in patient-specific induced pluripotent stem cells. Cell Stem Cell. Elsevier Inc.; 2013;12(1):101–13.

[20] Birket MJ, Ribeiro MC, Verkerk AO, Ward D, Leitoguinho AR, den Hartogh SC, et al. Expansion and patterning of cardiovascular progenitors derived from human pluripotent stem cells. Nat Biotechnol. Nature Publishing Group; 2015;33(9):1–12.

[21] Elliott D a, Braam SR, Koutsis K, Ng ES, Jenny R, Lagerqvist EL, et al. NKX2-5(eGFP/w) hESCs for isolation of human cardiac progenitors and cardiomyocytes. Nat Methods. 2011;8(12):1037–40.

[22] Gerencser AA, Chinopoulos C, Birket MJ, Jastroch M, Vitelli C, Nicholls DG, et al. Quantitative measurement of mitochondrial membrane potential in cultured cells: calcium-induced de- and hyperpolarization of neuronal mitochondria. J Physiol. 2012;590(Pt 12):2845–71.

[23] Birket MJ, Casini S, Kosmidis G, Elliott DA, Gerencser AA, Baartscheer A, et al. PGC-1-alpha and Reactive Oxygen Species Regulate Human Embryonic Stem Cell-Derived Cardiomyocyte Function. Stem Cell Reports. 2013;1(6):560–74.

[24] Bisping E, Ikeda S, Sedej M, Wakula P, McMullen JR, Tarnavski O, et al. Transcription Factor GATA4 Is Activated but Not Required for Insulin-like Growth Factor 1 (IGF1)-induced Cardiac Hypertrophy. J Biol Chem. 2012;287(13):9827–34.

[25] Clement CA, Kristensen SG, Møllgård K, Pazour GJ, Yoder BK, Larsen LA, et al. The primary cilium coordinates early cardiogenesis and hedgehog signaling in cardiomyocyte differentiation. J Cell Sci. 2009;122(17):3070–82.

[26] El- Armouche A, Eschenhagen T. Beta-adrenergic stimulation and myocardial function in the failing heart. Heart Fail Rev. 2009;14(4):225–41.

[27] Li M, Iismaa SE, Naqvi N, Nicks A, Husain A, Graham RM. Thyroid hormone action in postnatal heart development. Stem Cell Res. 2014;13(3, Part B):582–91.

[28] Rog-Zielinska EA, Craig M-A, Manning JR, Richardson R V., Gowans GJ, Dunbar DR, et al. Glucocorticoids promote structural and functional maturation of foetal cardiomyocytes: a role for PGC-1α. Cell Death Differ. 2014;22(7):1106–16.

[29] Troncoso R, Ibarra C, Vicencio JM, Jaimovich E, Lavandero S. New insights into IGF-1 signaling in the heart. Trends Endocrinol Metab. 2014;25(3):128–37.

[30] Ng ES, Davis R, Stanley EG, Elefanty AG. A protocol describing the use of a recombinant protein-based, animal product-free medium (APEL) for human embryonic stem cell differentiation as spin embryoid bodies. Nat Protoc. 2008;3(5):768–76.

[31] Földes G, Matsa E, Kriston-Vizi J, Leja T, Amisten S, Kolker L, et al. Aberrant α-Adrenergic Hypertrophic Response in Cardiomyocytes from Human Induced Pluripotent Cells. Stem Cell Reports. 2014;3(5):905–14.

[32] Vidal M, Wieland T, Lohse MJ, Lorenz K. β-Adrenergic receptor stimulation causes cardiac hy-



pertrophy via a Gβγ/Erk-dependent pathway. Cardiovasc Res. 2012;96(2):255–64.

[33] Zhang Z, Liu R, Townsend PA, Proud CG. p90(RSK)s mediate the activation of ribosomal RNA synthesis by the hypertrophic agonist phenylephrine in adult cardiomyocytes. J Mol Cell Cardiol. 2013;59:139–47.

[34] Rog-Zielinska EA, Thomson A, Kenyon CJ, Brownstein DG, Moran CM, Szumska D, et al. Glucocorticoid receptor is required for foetal heart maturation. Hum Mol Genet. 2013;22(16):3269–82.

[35] Sherk AB, Frigo DE, Schnackenberg CG, Bray JD, Laping NJ, Trizna W, et al. Development of a small molecule serum and glucocorticoid-regulated kinase 1 antagonist and its evaluation as a prostate cancer therapeutic. Cancer Res. 2008;68(18):7475–83.

[36] Boehmer C, Wilhelm V, Palmada M, Wallisch S, Henke G, Brinkmeier H, et al. Serum and glucocorticoid inducible kinases in the regulation of the cardiac sodium channel SCN5A. Cardiovasc Res. 2003;57(4):1079–84.

[37] Alders M, Jongbloed R, Deelen W, van den Wijngaard A, Doevendans P, Cate F Ten, et al. The 2373insG mutation in the MYBPC3 gene is a founder mutation, which accounts for nearly one-fourth of the HCM cases in the Netherlands. Eur Heart J. 2003;24(20):1848–53.

[38] Biondi B, Klein I. Hypothyroidism as a risk factor for cardiovascular disease. Endocrine. 2004;24(1):1–13.

[39] Forini F, Nicolini G, Balzan S, Ratto GM, Murzi B, Vanini V, et al. Amiodarone inhibits the 3,5,3′-triiodothyronine-dependent increase of sodium/potassium adenosine triphosphatase activity and concentration in human atrial myocardial tissue. Thyroid Off J Am Thyroid Assoc. 2004;14(7):493–9.

[40] Sakaguchi Y, Cui G, Sen L. Acute effects of thyroid hormone on inward rectifier potassium channel currents in guinea pig ventricular myocytes. Endocrinology. 1996;137(11):4744–51.

[41] Danzi S, Ojamaa K, Klein I. Triiodothyronine-mediated myosin heavy chain gene transcription in the heart. Am J Physiol Heart Circ Physiol. 2003;284(6):H2255–62.

[42] Iwaki H, Sasaki S, Matsushita A, Ohba K, Matsunaga H, Misawa H, et al. Essential role of TEA domain transcription factors in the negative regulation of the MYH 7 gene by thyroid hormone and its receptors. PLoS One. 2014;9(4):e88610.

[43] Chrysis D, Chagin A, Sävendahl L. Insulin-like growth factor-1 restores dexamethasone-induced heart growth arrest in rats: the role of the ubiquitin pathway. Hormones. 2011;10(1):46–56.

[44] Pansters NA, Langen RC, Wouters EF, Schols AM. Synergistic stimulation of myogenesis by glucocorticoid and IGF-I signaling. J Appl Physiol. 2013;114(9):1329–39.

[45] Schakman O, Kalista S, Bertrand L, Lause P, Verniers J, Ketelslegers JM, et al. Role of Akt/GSK-3beta/beta-catenin transduction pathway in the muscle anti-atrophy action of insulin-like growth factor-I in glucocorticoid-treated rats. Endocrinology. 2008;149(8):3900–8.

[46] Chen X, Qian Y, Wu S. The Warburg effect: Evolving interpretations of an established concept. Free Radic Biol Med. 2015;79:253–63.

[47] Hamanaka RB, Chandel NS. Warburg Effect and Redox Balance. Science (80-). 2011;334(6060):1219–20.

[48] Goncalves RLS, Quinlan CL, Perevoshchikova I V., Hey-Mogensen M, Brand MD. Sites of Superoxide and Hydrogen Peroxide Production by Muscle Mitochondria Assessed ex Vivo under Conditions Mimicking Rest and Exercise. J Biol Chem. 2015;290(1):209–27.

[49] Puente BN, Kimura W, Muralidhar SA, Moon J, Amatruda JF, Phelps KL, et al. The Oxygen-Rich Postnatal Environment Induces Cardiomyocyte Cell-Cycle Arrest through DNA Damage Response. Cell. 2014;157(3):565–79.

[50] Guerra L, Cerbai E, Gessi S, Borea PA, Mugelli A. The effect of oxygen free radicals on calcium current and dihydropyridine binding sites in guinea-pig ventricular myocytes. Br J Pharmacol. 1996;118(5):1278–84.

[51] Liu M, Liu H, Dudley SC. Reactive Oxygen Species Originating From Mitochondria Regulate the Cardiac Sodium Channel. Circ Res. 2010;107(8):967–74.

[52] Mao W, You T, Ye B, Li X, Dong HH, Hill JA, et al. Reactive Oxygen Species Suppress Cardiac NaV1.5 Expression through Foxo1. PLoS One. 2012;7(2):e32738.

[53] Lang F, Stournaras C, Alesutan I. Regulation of transport across cell membranes by the serum- and glucocorticoid-inducible kinase SGK1. Mol Membr Biol. 2014;31(1):29–36.

[54] Barefield D, Kumar M, Gorham J, Seidman JG, Seidman CE, Tombe PP De, et al. Haploinsufficiency of MYBPC3 exacerbates the development of hypertrophic cardiomyopathy in heterozygous mice. J Mol Cell Cardiol. 2015;79:234–43.

[55] Harris SP, Bartley CR, Hacker T a., McDonald KS, Douglas PS, Greaser ML, et al. Hypertrophic cardiomyopathy in cardiac myosin binding protein-C knockout mice. Circ Res. 2002;90:594–601.

[56] McConnell BK, Fatkin D, Semsarian C, Jones KA, Georgakopoulos D, Maguire CT, et al. Comparison of Two Murine Models of Familial Hypertrophic Cardiomyopathy. Circ Res. 2001;88(4):383–9.

[57] Pohlmann L, Kröger I, Vignier N, Schlossarek S, Krämer E, Coirault C, et al. Cardiac myosin-binding protein C is required for complete relaxation in intact myocytes. Circ Res. 2007;101(9):928–38.

[58] Stöhr A, Friedrich FW, Flenner F, Geertz B, Eder A, Schaaf S, et al. Contractile abnormalities and altered drug response in engineered heart tissue from Mybpc3-targeted knock-in mice. J Mol Cell Cardiol. 2013;63:189–98.

[59] Witjas-Paalberends ER, Piroddi N, Stam K, van Dijk SJ, Oliviera VS, Ferrara C, et al. Mutations in MYH7 reduce the force generating capacity of sarcomeres in human familial hypertrophic cardiomyopathy. Cardiovasc Res. 2013;99(3):432–41.

[60] van Dijk SJ, Dooijes D, Remedios C dos, Michels M, Lamers JMJ, Winegrad S, et al. Cardiac Myosin-Binding Protein C Mutations and Hypertrophic Cardiomyopathy Haploinsufficiency, Deranged Phosphorylation, and Cardiomyocyte Dysfunction. Circulation. 2009;119(11):1473–83.

[61] van Dijk SJ, Boontje NM, Heymans MW, Cate FJ Ten, Michels M, Remedios C Dos, et al. Preserved cross-bridge kinetics in human hypertrophic cardiomyopathy patients with MYBPC3 mutations. Pflügers Arch Eur J Physiol. 2014;466(8):1619–33.

[62] Fraysse B, Weinberger F, Bardswell SC, Cuello F, Vignier N, Geertz B, et al. Increased myofilament Ca2+ sensitivity and diastolic dysfunction as early consequences of Mybpc3 mutation in heterozygous knock-in mice. J Mol Cell Cardiol. 2012;52(6):1299–307.



Supplementary information

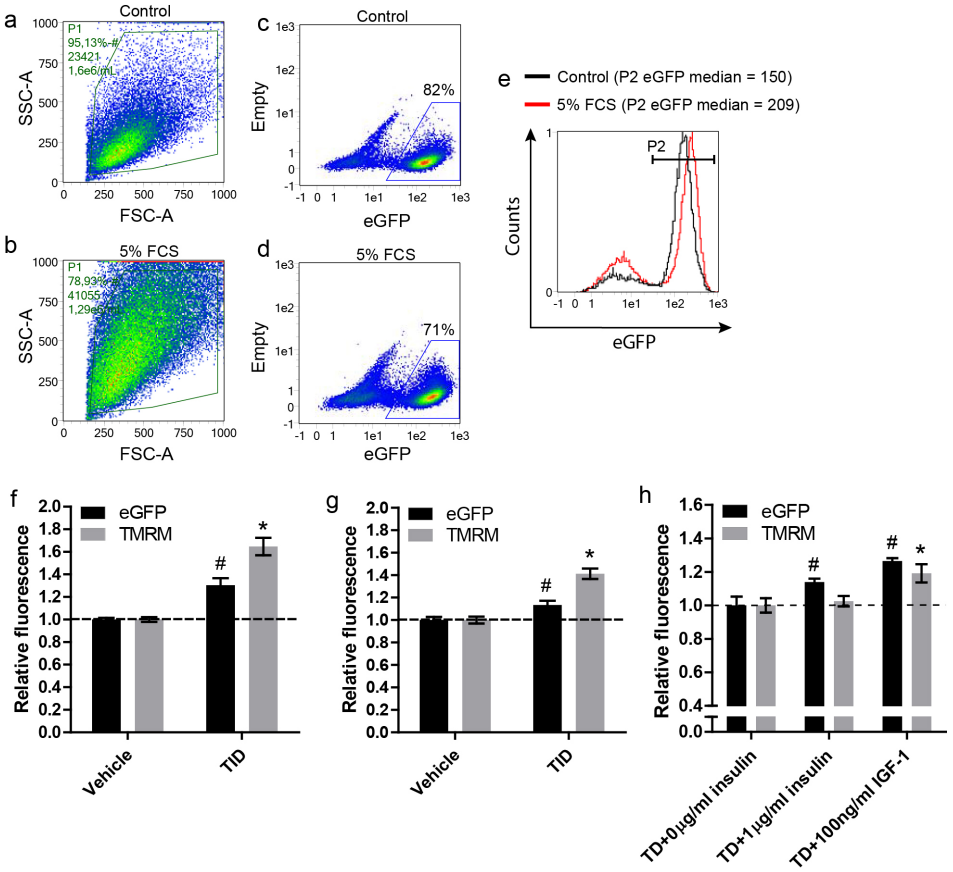


Figure S1- GFP and TMRM measurements in hPSC-derived cardiomyocytes maintained in different conditions. Related to **Figure 1**. FACS measurement after cardiac differentiation of NKX2-5eGFP/w hESCs and maintenance for 5 days under control conditions or in the presence of 5% FCS. **(a)** Scatter plots and P1 gating of control and (b) 5% FCS treated cells, **(c)** eGFP fluorescence of the P1 population of control and **(d)** FCS treated cells, **(e)** eGFP fluorescence histogram showing an overlay of the two P1 populations. The median eGFP fluorescence value within the P2 gate is shown above the histogram. **(f)** Relative TMRM and eGFP fluorescence values of M1 NKX2-5eGFP/w hESC-derived cardiomyocytes and **(g)** NKX2-5eGFP/w hiPSC-derived cardiomyocytes after 5 days of treatment with vehicle-only or TID medium. **(h)** Relative TMRM and eGFP fluorescence of cardiomyocytes after 5 days of treatment with T3+Dex (TD) plus insulin or IGF-1. Data are mean±SEM, n=6 **(f)**, n=8 **(g)**, n=9 **(h)**. The n signifies the number of wells (cell populations) measured. Statistical significance was calculated using a one-way ANOVA with Dunnett's correction, # P<0.05 for eGFP fluorescence, * P<0.05 for TMRM fluorescence.

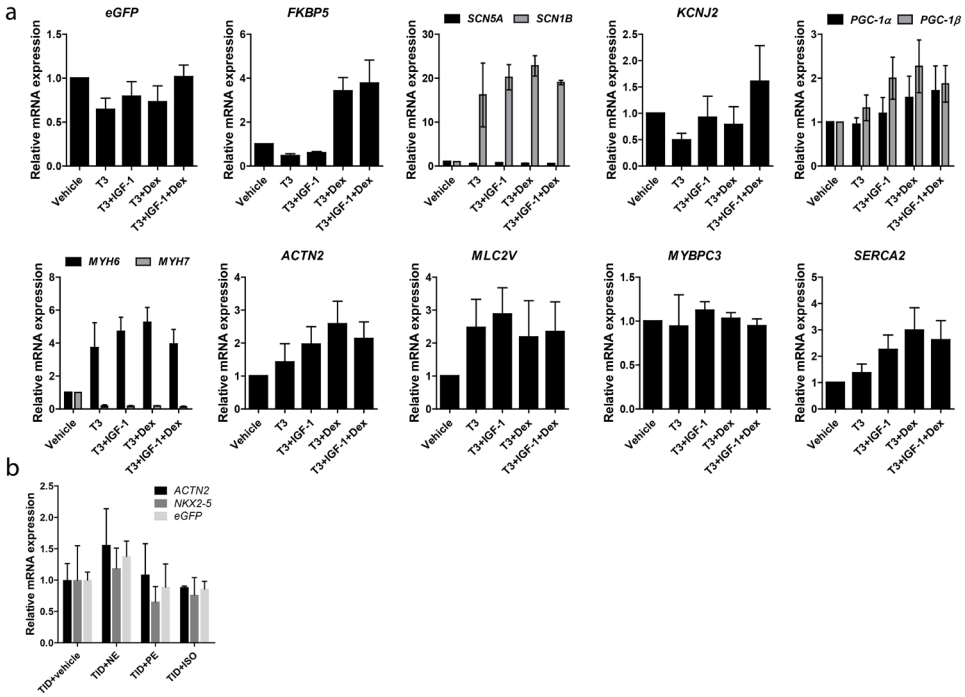


Figure S2- Gene expression profiles in hESC-derived cardiomyocytes maintained in different conditions. Related to **Figure 1. (a)** hESC-derived NKX2-5eGFP+ cardiomyocytes were isolated by FACS after 7 days of treatment with the conditions shown. Gene expression is normalized to the housekeeping gene RPLP0 and shown relative to the vehicle-only treated control. **(b)** Gene expression in cardiomyocytes treated for 5 days with T3+IGF-1+Dex (TID) plus vehicle, 1 μM norepinephrine (NE), 10 μM phenylephrine (PE) or 1 μM isoproterenol (ISO). Gene expression is normalized to the housekeeping gene RPLP0 and shown relative to the TID+vehicle treated control. Data are mean±SEM from three independent experiments in a, and mean±SD for 3 replicate wells in b.

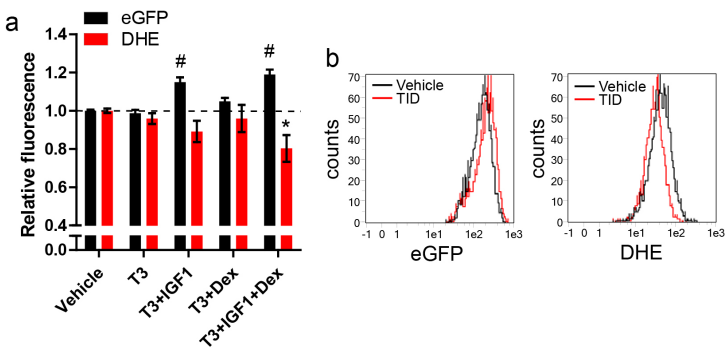


Figure S3- Modulation of reactive oxygen species levels in hESC-derived cardiomyocytes. Related to **Figure 2. (a)** Dihydroethidium (DHE) fluorescence measurements reporting superoxide radical levels in eGFP+ cardiomyocytes shown relative to a vehicle-only control after 5 days of maintenance with the factors shown. **(b)** Histograms of eGFP and DHE fluorescence intensity in eGFP+ cells maintained with vehicle-only or T3+IGF-1+Dex (TID). Note that eGFP is slightly increased while DHE is decreased by TID. Data are mean±SEM from three independent experiments. Statistical significance was calculated using a one-way ANOVA with Dunnett's correction, # P<0.05 for eGFP fluorescence, * P<0.05 for DHE fluorescence.



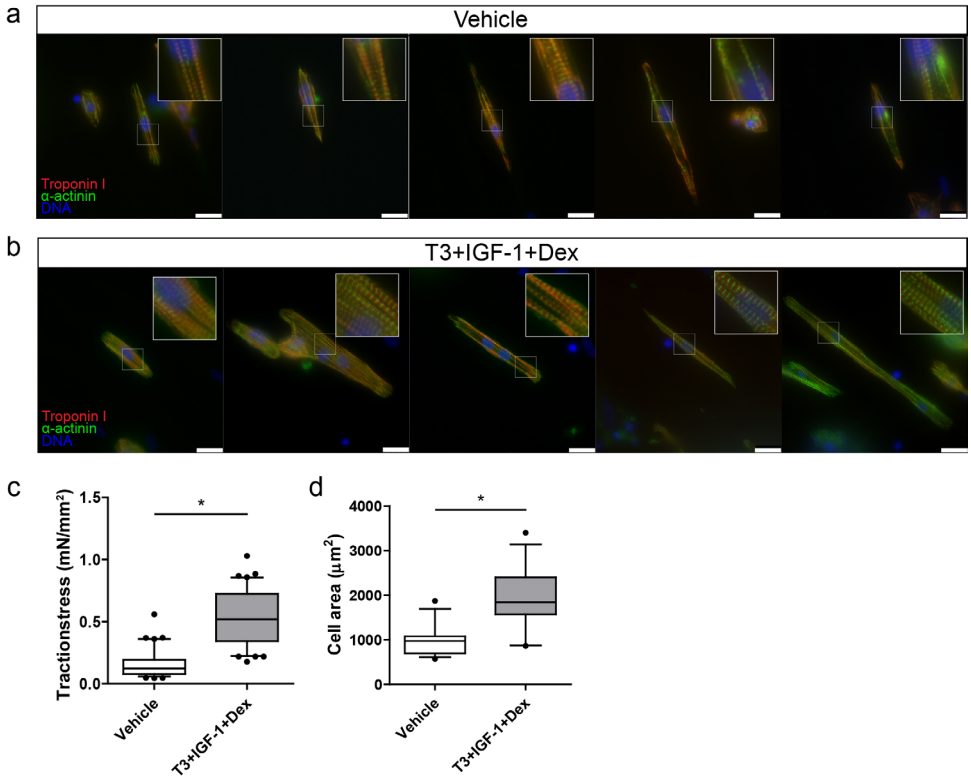


Figure S4- Structural imaging of hESC-derived cardiomyocytes and traction force analysis in an additional cell line. Related to **Figure 4. (a)** Immunostaining of Troponin I and α-actinin in cardiomyocytes maintained in **(a)** vehicle-only and **(b)** TID-medium, aligned on micropatterned PDMS gels. **(c)** Traction stress and **(d)** cell area of M1 hESC-derived cardiomyocytes maintained in vehicle or TID medium (n=15 individual cell measurements for each condition). Box and whisker plots show the median, interquartile range and 10-90 percentile range. Statistical significance was calculated with an unpaired t-test, * P<0.05.

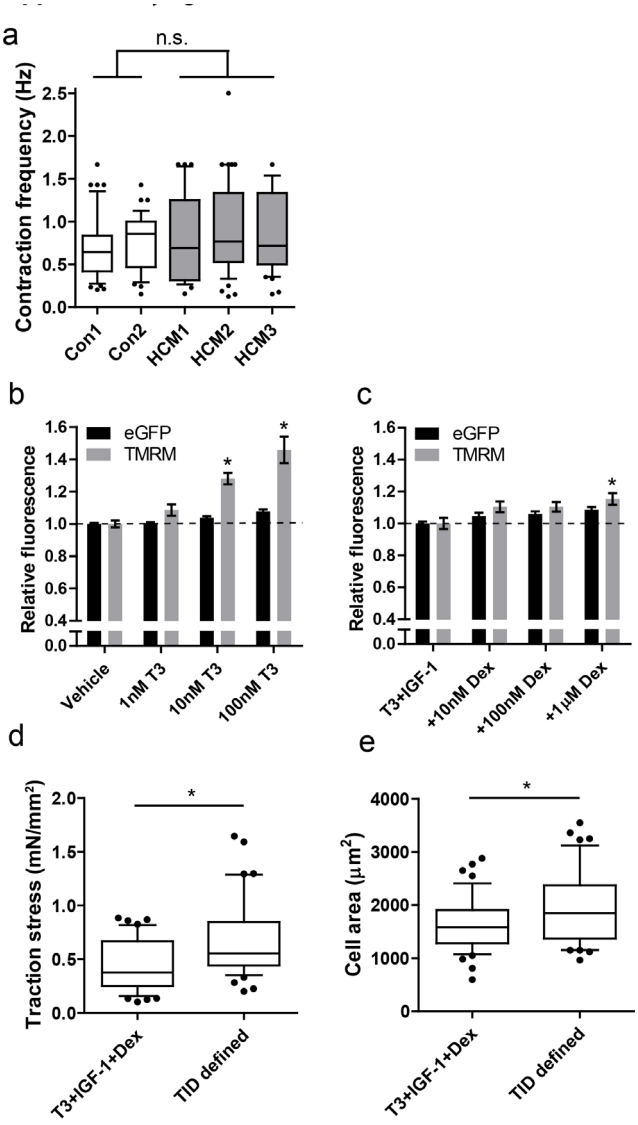


Figure S5- HCM cardiomyocyte frequency analysis and testing TID in a defined, albumin-free, basal medium. Related to **Figure 5. (a)** Contraction frequency of single spontaneously contracting iPSC-derived cardiomyocytes from two control (Con1 [n=47] and Con2 [n=36]) and three MYBPC3 mutation lines (HCM1 [n=44], HCM2 [n=54] and HCM3 [n=43]). Box and whisker plots show the median, interquartile range and 10-90 percentile range. **(b)** eGFP and TMRM fluorescence values in eGFP+ cardiomyocytes relative to a vehicle-only control after 5 days of incubation with the concentrations of T3 shown (n=6). **(c)** eGFP and TMRM fluorescence values in eGFP+ cardiomyocytes maintained in T3 (100 nM) +IGF-1 supplemented with a range of dexamethasone concentrations, measured relative to the T3+IGF-1+vehicle control (T3+IGF-1). **(d)** Traction stress and **(e)** cell size of single spontaneously contracting cardiomyocytes maintained in T3+IGF-1+Dex (n=45) and T3+IGF-1+Dex in defined medium (n=43). The n signifies independent experimental replicates in b and c and the number of individual cells in a, d and e acquired over three independent experiments. Statistical significance was calculated with a one-way ANOVA with Tukey's multiple comparison test in a, a one-way ANOVA with Dunnett's correction in b and c, and an unpaired t-test in d and e. n.s. = not significant, * P<0.05.

Table S1. Clinical Data of HCM patients with 2373insG mutation in *MYBPC3*. Related to Figure 5.

Patient	Age	Sex	Interventricular Septum in Diastole, mm	LVEDD, mm	LVESD, mm	% FS	LVEF%
HCM1	44	m	13	54	32.9	39	56
HCM2	14	m	35	41	24	41	58
HCM3	42	m	24	55	42	24	48
Healthy Range			<13	36-56	20-40	25-43	55-70

LVEDD = left ventricular end diastolic diameter; LVESD = left ventricular end systolic diameter; % FS = fraction shortening (LVEDD-LVESD)/LVEDD*100%; LVEF% = left ventricular ejection

Supplemental Experimental Procedures

hPSC culture and differentiation

H3 NKX2-5eGFP/w hESCs or M1 NKX2-5eGFP/w hESCs as previously generated (Elliott et al., 2011), were maintained on mouse embryonic fibroblasts and passaged using TrypLE select (Life Technologies). The generation of transgene-free hiPSCs from skin fibroblasts of one healthy male donor (LUMC0004iCtrl [Con1]) and three patients each with a c.2373dupG mutation in MYBPC3 (LUMC0033iMyBPC [HCM1], LUMC0034iMyBPC [HCM2] and LUMC0035iMyBPC [HCM3]) was previously reported (Dambrot et al., 2014). A second transgene-free control hiPSC line (LUMC0047iCtrl [Con2]) generated from another healthy male donor was included in this study. hiPSCs were maintained on Matrigel (growth factor reduced; Corning 354230) in mTeSR1 medium (Stem Cell Technologies) and passaged with 1 mg/ml Dispase (Life Technologies).

Cardiac differentiation was induced from monolayer cultures on Matrigel in serum-free medium (BSA, polyvinyl alcohol, essential lipids [BPEL]) as previously described (Ng et al., 2008). The formulation was as follows: 44% IMDM, 44% Ham's F12, 5% protein-free hybridoma medium (PFHM-II), 0.25% BovoStar BSA (Bovogen, Australia), 0.125% polyvinyl alcohol, 1x chemically defined lipids, 400 μM α-thioglycerol (Sigma-Aldrich), 50 μg/ml L-ascorbic acid 2-phosphate (AA-2P), 2mM Glutamax, 0.1x Insulin-transferrin-selenium-ethanolamine (ITS-X) and 0.5% Pen/Strep. All BPEL components were obtained from Life Technologies unless otherwise stated. The following factors were present for the first 3 days 20 ng/ml BMP4 (R&D), 20 ng/ml Activin A (Miltenyi Biotech) and 1.5 μM CHIR 99021 (Axon Medchem). 5 μM XAV 939 (Tocris Bioscience) was present on days 3-6. NKX2-5eGFP/w hiPSCs (RD, CLM unpublished) were maintained in Essential 8 medium (Life Technologies) and differentiated as previously described (van den Berg 2015).

Contracting cultures were dissociated on day 13 and replated on Matrigel-coated 24-well plates. The following experimental factors were added on day 16, refreshed on day 20 and measured on day 21: 100 ng/ml Long R3 IGF-1 (in the main text: IGF-1), 1 μM SAG (Millipore), 1 μM dexamethasone, 100 nM triiodothyronine hormone, 10 μM phenylephrine, 1 μM isoproterenol, 1-1000 nM norepinephrine. The above factors were obtained from Sigma Aldrich unless otherwise stated.

Patterned Polyacrylamide gel fabrication

Patterned polyacrylamide gels were prepared as previously described (Rape et al., 2011). Briefly, a 1% gelatin solution was activated with 3.5 mg/mL Sodium Periodate (both Sigma-Aldrich). A polydimethylsiloxane (PDMS) stamp was casted from a SU8 master produced by standard soft lithography techniques and incubated with the activated 1% gelatin solution for 45 mins. The excess of gelatin was removed with a nitrogen gun and the stamp was used to μcontact-print a pattern of 20 μm thick with 20 μm spacing gelatin lines onto 10mm (electrophysiology) or 15 mm (contraction assay) coverslips. The polyacrylamide solution was prepared with a final concentration of 0.1% bis-acrylamide (Bio-Rad), 5% acrylamide (Bio-Rad) and 10 mM HEPES pH 8.5 in distilled water, followed by centrifugation for 1 min at 10.000 RPM for degassing. 0.006% (m/v) of ammonium persulfate (Sigma-Aldrich) and a 1:1000 dilution of 0.2-μm fluorescent beads (Ex/Em: 660/680nm - Molecular Probes) were added to the solution (for the contraction assay) and

briefly vortexed. The gel polymerization was initiated with TEMED (Bio-Rad) and 4.08 µl/9.2 µl of the final solution was added to a 15 mm/25 mm coverslip treated with plus Bind-Silane solution (GE Healthcare). The µcontact-printed coverslip was applied on top of the drop with the gelatin lines facing the gel. After 20mins of polymerization the 10 mm/15 mm coverslip was removed. Each 25mm coverslip was mounted onto a well of a glassbottom 6-well plate (Mattek), replacing the initial glass. The 15mm coverslips were used directly. Plates were UV-sterilized and re-hydrated with culture medium for 30 mins before use. The polymerized gel has a Young's modulus of 5.8 kPa (Frey et al., 2007).

Flow cytometry measurements for plasma membrane potential and reactive oxygen species

For relative plasma membrane potential measurement, differentiated cultures were dissociated on day 21 (after treatment as above from day 16) using 5x TrypLE Select and resuspended in 2.5 nM TMRM (Life Technologies) in warm assay medium. Cells were incubated for 8 minutes at 37°C before being measured by flow cytometry. eGFP and TMRM fluorescence intensities were recorded. For superoxide detection, dissociated cells were labelled with 5 µM DHE for 30 mins at 37°C and then measured by flow cytometry. Samples were measured with a MACSQuant VYB (Miltenyi Biotech) equipped with a blue (488nm) and yellow (561nm) laser. eGFP and DHE fluorescence intensities were recorded. Appropriate compensation to correct from cross-bleed was performed for each.

Respiration and acidification rates measured with the Seahorse XF-24 Analyzer

Respiration and acidification rates were measured on adherent cells using a Seahorse XF-24 or an XF-96 Analyzer (Seahorse Bioscience). The assay plates were coated with Matrigel (1:100). Cells were seeded in BPEL medium at a density of 6.5x104 (XF-24) or 2.5x104 (XF-96) cells/well 7 days before measurement. The assay was performed in bicarbonate-free DMEM (D5030; Sigma Aldrich), containing 0.25% fatty acid-free BovoStar (Bovogen, Australia), 1 mM sodium lactate, 0.15 mM sodium hydroxybutyrate, 2 mM GlutaMAX (Life Technologies) and 0.5 mM L-carnitine. The standard glucose concentration was 15 mM glucose and was supplemented with 0.5 mM sodium pyruvate. Cells were washed twice and pre-incubated in the assay medium for 1 h before measurement. For the standard profiling oligomycin was used at 0.5 µg/ml, FCCP titrated in 2 injections to 3 µM and rotenone and antimycin A were added at 1 µM and 2 µM respectively. A standard protein assay was used to normalize values to whole cell protein. Acid titration experiments were performed to calculate the buffering capacity of the Seahorse assay media and gave a value of 0.1 pmoles H+/mpH in the 7 µl measuring volume. ECAR values were converted to anaerobic glycolyis/lactate production rates as previously described (Mookerjee et al., 2015), using a max H+/O2 value of 1.0 and converted 1:1 to an ATP production rate. The oligomycin-sensitive oxygen consumption was converted to an ATP production rate using a P/O ratio of 2.3 (Brand, 2005). To assess ATP demand for excitation and contractility nifedipine (10 µM) and blebbistatin (5 µg/ml) were co-injected and the respiration rate immediately recorded, followed by measurements after oligomycin and then rotenone and antimycin A injection. A vehicle-only injection was performed in parallel and the effect subtracted. Experiments analysing the effect of etomoxir and UK5099 were performed on the XF-96 format using an assay medium with the following modifications: the glucose concentration was 5.5 mM, sodium pyruvate 0.15 mM and palmitic acid was included at 100 µM conjugated to fatty acid-free BovoStar BSA in a 2.8:1 molar ratio. To prepare this a 4 mM palmitic acid solution was made in assay medium by heating at 65°C for 30 mins, then combined 1:1 with a 10% Bovostar BSA solution and heated at 37°C for 30 mins with mixing. 10 mM HEPES was also included in this assay medium to provide extra buffering (glycolytic rates were not calculated). Cells were washed twice and pre-incubated in this assay medium for 4 h before measurement. To assess the response to substrate uptake inhibitors, 40 µM etomoxir or 5 µM UK5099 were injected and respiration rates recorded after 45 mins, followed by injections of oligomycin, FCCP (3 µM) and then rotenone and antimycin A. A vehicle-only injection was performed in parallel and the effect subtracted.

Electrophysiological characterization

Action potential (AP) recordings were performed on single cardiomyocytes, 14-16 days after cell dissociation with the amphotericin perforated patch-clamp technique using an Axopatch 200B amplifier (Molecular Devices Corporation, Sunnyvale, CA, USA). Signals were filtered and digitized at 5 and 40 kHz, respectively. Data acquisition and analysis were accomplished using pClamp10.1 (Axon Instruments) and custom software. Potentials were corrected for the liquid junction potential. Cells were continuously perfused in a perfusion chamber at 37 0C (Cell MicroControls Norfolk VA, U.S.A.) using Tyrode's solution containing (mM): NaCl 140, KCl 5.4, CaCl2 1.8, MgCl2 1.0, glucose 5.5, HEPES 5; pH 7.4 (NaOH). Pipettes (borosilicate glass; resistance ~2.5 MΩ) were filled with solution containing (mM): K-gluconate 125, KCl 20, NaCl 5, amphotericin-B 0.22, HEPES 10; pH 7.2 (KOH).

APs were recorded at spontaneous frequencies and characterized by duration at 50 and 90% repolarization (APD50, and APD90, respectively), maximal diastolic potential (MDP), AP amplitude, maximal upstroke velocity and frequency. AP parameter values obtained from 8-9 consecutive APs were averaged and data were collected from at least 2 independent differentiations per condition.



Traction force measurements

The traction force measurements were performed as previously described (Hazeltine et al., 2012). Cells were seeded on gelatine patterned acrylamide gels 4 days before and measured in their normal culture medium in an environment maintained at 37°C with 5% CO2. Briefly, using a Leica AF-6000LX microscope, an image-series of aligned single spontaneously contracting cardiomyocytes was taken at 40x magnification at 20 frames per second, recording bright-field and fluorescent beads. Single frames from maximal relaxation and contraction of the brightfield and fluorescent beads image-series were analyzed by the LIBTRC software package (kindly provided by Dr. Micah Dembo), creating a mask of the cell outline from the brightfield image and a vector map from the difference between the relaxed and contracted fluorescent beads images. The vector map and the cell mask were used to calculate the maximum total force that the cell applies on the substrate at its peak of contraction. The traction stress generated by the cardiomyocyte during contraction was calculated by dividing the total force by the cell surface area. Measurements were blinded in acquisition and analysis.

Quantitative real-time PCR

RNA was isolated using a Minelute RNA extraction kit (Qiagen) and cDNA synthesized using an iScript cDNA synthesis kit (BioRad). Real-time PCR was performed on a BioRad CFX384 machine using IQ SYBR Green (BioRad). Gene expression values were normalized to the mean expression of the housekeeping genes human ribosomal protein (RPLP0), glucuronidase (GUSB), and RNF7. Primer sequences were as follows:

Gene	Forward primer	Reverse primer
RPLP0	CACCATTGAAATCCTGAGTGATGT	TGACCAGCCCAAAGGAGAAG
GUSB	CCACCTAGAATCTGCTGGCTAC	GTGCCCGTAGTCGTGATACCAA
RNF7	ACGCACCGAATAGTTACGG	CCAGGTCCACGGGCAGA
eGFP	GTGAGCAAGGGCGAGGAG	CCGTAGGTCAGGGTGGTC
FKBP5	TTCTCCTTGCTGCCTTTCTG	ACCCTTGGCTGACTCAAACTC
SCN5A	GAGCTCTGTCACGATTTGAGG	GAAGATGAGGCAGACGAGGA
SCN1B	GTGGTTGTAGGTGACATTGGTG	GAAGGGCACTGAGGAGTTTGT
KCNJ2	ACCGCTACAGCATCGTCTCT	TCCACACACGTGGTGAAGAT
PGC-1α	AACACTTACAAGCCAAACCA	GGGTTCAATAGTCTTGTTCTC
PGC-1β	TCCTCAACTATCTCGCTGAC	CTCACTGTCAATCTGGAAGAG
MYH6	CTTCTCCACCTTAGCCCTGG	GCTGGCCCTTCAACTACAGA
MYH7	CGACCTTCTTCTCTTGCTC	GAGGACAAGGTCAACACCCT
ACNT2	CTGCTGCTTTGGTGTCAGAG	TTCCTATGGGGTCATCCTTG
MYL2/MLC2V	TACGTTCGGGAAATGCTGAC	TTCTCCGTGGGTGATGATG
MYBPC3	GGCATGCTAAAGAGGCTCAA	TCTTGTGGCCTTTGCTCAC
SERCA2	ACCCACATTCGAGTTGGAAG	CCAACGAAGGTCAGATTGGT

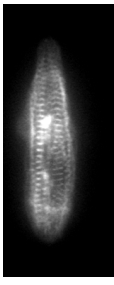
Western blotting

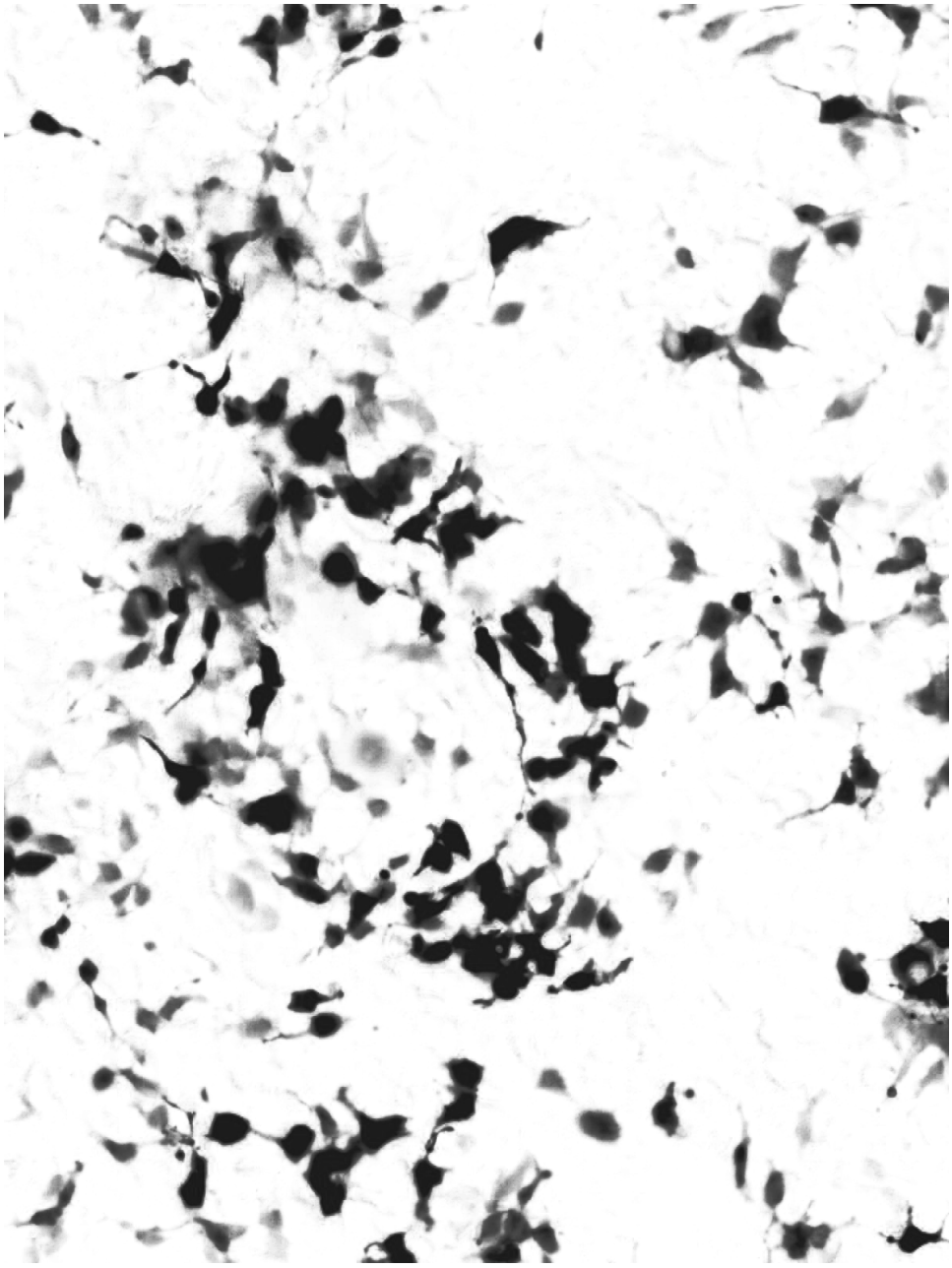
The samples were lysed with ice cold ELB (50mM HEPES pH 7.0; 250mM NaCl; 5mM EDTA; 0.1% NP-40) with 1:100 Protease Inhibitor Cocktail (Sigma-Aldrich) for 30 mins on ice. The samples were centrifuged at 7,000g for 10 mins and the supernatant was quantified for protein content using the Bio-Rad Protein Assay (based on the Bradford dye-binding method). 100μg of the hiPSC-CM lysates were run in a 6% polyacrylamide gel and 30μg of the hESC-CM with the shRNA lysates were run in a 10% polyacrylamide gel together with the protein ladder (Precision Plus Protein dual colour – Bio-Rad). The protein was transferred to an Amersham Hybond membrane (GE Heathcare- Life Sciences) overnight. The membrane was blocked with blocking buffer (2% milk in PBS) and each protein was detected with the specific antibody: Rabbit IgG anti- cMyBP-C (1:2000) kindly provided by Dr. Sakthivel Sadayappan from the Department of Cell and Molecular Physiology, Health Sciences Division, Loyola University Chicago, followed by Horse anti-Rabbit IgG – HRP (1:2000) (Cell Signaling). Mouse IgG anti-Actin (1:1000) (MAB1501 – Millipore) and Mouse IgG anti-α-actinin (A7811-Sigma-Aldrich), followed by Goat anti-mouse IgG-HRP (1:2000) (Cell Signaling).

Supplemental references

Frey, M.T., Engler, A., Discher, D.E., Lee, J., and Wang, Y.-L. (2007). Microscopic methods for measuring the elasticity of gel substrates for cell culture: microspheres, microindenters, and atomic force microscopy. Methods Cell Biol. 83, 47–65.

Rape, A.D., Guo, W.-H., and Wang, Y.-L. (2011). The regulation of traction force in relation to cell shape and focal adhesions. Biomaterials 32, 2043–2051.





Chapter 5

Alpha-Actinin-mCherry fusion protein
Building a paramount new tool for cardiomyocyte analysis



Marcelo C. Ribeiro[1], Mervyn Mol[1], Olga Drawska[1], Leon Tertoolen[1], Jantine Monshouwer-Kloots[1], Christine L. Mummery[1] and Robert Passier[1]

[1]Department of Anatomy & Embryology, Leiden University Medical Center, Leiden, The Netherlands.

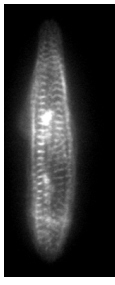
Manuscript in preparation

Abstract

Sarcomeric organization is crucial for function of cardiomyocytes and is used as a hallmark of maturation and cardiac diseases such as hypertrophic cardiomyopathies. One approach to determine sarcomeric organization is through visualization by immunofluorescent staining. This requires cell fixation and does therefore not allow assessment of sarcomere dynamics. Another approach is visualization in live cardiomyocytes by phase contrast imaging, which is only suitable for high degrees of sarcomeric organization, and therefore not suitable for immature cardiomycoytes such as those from human pluripotent stem cells (hPSC-CM). In order to visualize sarcomerogenesis and sarcomere dynamics in living cells, we generated a fusion protein, consisting of the sarcomeric α-actinin and a red fluorescent protein, mCherry. When overexpressed in hPSC-CM, the α-actinin-mCherry was incorporated into the sarcomeres, enabling the assessment and analysis of sarcomere movement during contraction. This new tool is potentially very useful for studies related to cardiomyocyte differentiation, maturation and cardiac disease modeling.

Introduction

The sarcomere is the smallest contractile unit of striated muscle. The concatenation of sarcomere units forms myofibers, which are the constituents of skeletal and cardiac muscle. Sarcomerogenesis occurs during early embryonic muscle development and following postnatal maturation controls sarcomeric organization[1], as shown in chapter 3 in relation to cardiomyocyte function. Besides during development from fetal to adult, sarcomeric organization also changes in cardiac disease, such as in hypertrophic cardiomyopathy[2] (either sarcomeric hypertrophy or disorganization). Myogenesis can thus be considered a hallmark of hPSC derived cardiomyocyte maturation[3] and hypertrophic cardiomyopathy. The sarcomeres are composed of different sets of proteins with a high degree of organization. The Z-disks mark the borders of the sarcomeric units, of which α-actinin is a major component. Alpha-actinin is a 104kDa protein member of the spectrin superfamily and consists of an N-terminal actin-binding domain, multiple spectrin repeats and a C-terminal calmodulin (CaM)-like domain[4]. This protein is functional as an anti-parallel homodimer that crosslinks actin filaments of adjacent sarcomere units forming a lattice-like structure that stabilizes the muscle contractile machinary[5]. This structure is evident by immunofluorescence microscopy as anti-parallel bands along the cell, providing cardiomyocytes with their characteristic striated appearance. Nevertheless, these immunofluorescent images only allow analysis of cardiomyocytes under static conditions. Therefore, we genetically engineered α-actinin fused with a fluorescent protein to be able to assess sarcomere structure and length in living cardiomyocytes, thus creating a useful tool to study sarcomere dynamics during maturation and disease. This fusion approach has been employed in studies of whole-cell stiffness in human osteoblasts[6].



To combine the sarcomeric reporter with the cardiac hESC-NKX2-5-eGFP reporter line, we fused alpha-actinin with mCherry that has an excitation/emission spectrum (587/610nm) distinct from GFP and has high photo stability[7]. The expression of fusion proteins is generally driven by constitutive promoters, from which the cytomegalovirus immediate-early promoter (CMV), mouse phosphoglycerate kinase 1 promoter (PGK) and human elongation factor 1a promoter (EF1A) are among the most commonly used. Despite their ubiquitous expression, activity of these promoters differs depending on the cell type in which they are expressed[8]. Furthermore, although these constitutively active promoters can be used for multiple purposes, they do not allow protein expression in time-controlled manner. In 1992 the tetracycline-controlled transcriptional activation (tetO) was described which induced coupled gene expression in the presence of tetracycline or its derivative[9,10]. This technology enables the production of clonally stable hESC lines carrying the α-actinin-mCherry in a repressed state, which can later be induced in differentiated cardiomyocytes.

Materials and methods

RNA isolation and cDNA synthesis

RNA was isolated from hESC derived cardiomyocytes using TRIzol Reagent (Invitrogen) and cleaned up with DNA free kit (Ambion). iScript kit (BioRad) was used to make cDNA.

α-Actinin and mCherry amplification

Primers were designed to amplify hACTN2 from cDNA template isolated from hESC-CM using PCR. The PCR reaction mix was prepared using Phusion Taq following manufacturer's guidelines (ThermoScientific) (Table S1). The PCR cycle was performed as shown in Table S2, where the annealing time was changed depending on the length of the DNA sequence being amplified. The samples were cleaned using the PCR cleaning kit (Qiagen). Afterwards, the samples were digested with the appropriate enzymes in conditions provided by manufacturer (O/N, usually 37ºC; Table S3), and separated on agarose gel. The right band was excised from the gel (QIAquick Gel Extraction Kit, QIAGEN).

Ligation

The vector was digested with the specific enzymes (Table S3) and then cleaned with the PCR cleaning kit (Qiagen). If second digestion was needed it was conducted after cleaning. The open vector was excised from agarose gel, and isolated using QIAquick Gel Extraction Kit (Qiagen). Vector and insert were ligated in the following Equation 1 with the molecular ratios (insert:vector): 3:1, 1:1 in standard protocol. In some cases more than two fragments were assembled, what is referred as multi-ligation. This method was conducted as all-in-one reaction using similar molecular ratio (insert1:insert2:vector=3:3:1, 1:1:1). The ligation was kept at 14ºC, O/N.

([ng of vector] x [size of insert in kb])/([size of vector in kb])=(3 or 1x insert)/(1x vector)
Equation 1

Transformation

Ligation mix used to transform Escherichia coli One Shot® TOP10 chemically competent cells for each transformation. 1-5 μl of DNA (10pg-100ng) was added to a vial of One Shot® cells, mixed gently and incubated on ice for 30 minutes. The samples were heated to 42°C for 30 seconds without shaking followed by 2mins on ice. 250 μl of pre-warmed S.O.C medium was added to the vial without antibiotics and incubated for 1 hour at 37°C shaking. The transformed bacteria were spread on Luria-Bertani (LB) + selection antibiotic (ampicilin - Amp or carbanicilin - Carb) plates and incubated O/N, 37ºC. Colonies (usually 24) were picked up and cultured in 3.0ml LB + Amp/Carb (O/N, 37ºC, 225rpm). DNA was isolated (PureLink Quick Plasmid Miniprep, Invitrogen) and evaluated by restriction analysis (Appendix III).. Clones were sequenced following Sanger method (Appendix X, XI). Correct clones were further expanded in larger volumes. DNA was isolated using the NucleBond Xtra Midi Kit (Macherey-Nagel).

Transfection

pcDNA3.1-hACTN2-mCherry was transfected into hESC-derived cardiomyocytes and human embryonic kidney (HEK) using transfection agents – FuGENE and GJ reagents (Appendix VIII). The control wells contained a pcDNA3.1-mCherry construct (purified or, purified and gel extracted). The amount of DNA was 1, 2, and 3μg. Cells were observed for 48hrs under the fluorescent microscope.

Immunocytochemistry

The cells were fixed with 4% paraformaldehyde for 20 mins and washed three times with PBS. Cells were permeabilized with 0.1% Triton for 8mins and blocked with 4% swine serum for 1h at room temperature (RT). For identification of sarcomeres the samples were incubated with the primary antibody Rabbit anti Troponin I (Santa Cruz sc-15368) diluted 1:500 for 1h at RT. The samples were washed three times 10 mins with PBS with 0.05% tween20 and incubated with the secondary antibodies donkey anti rabbit IgG A488 (Invitrogen A-21206) both diluted 1:200 for 1h at RT.

Lentivirus production

On day 1 HEK 293T cells were plated on 10cm dishes at density of 6 million per dish in DMEM (Gibco) plus 10% FBS (Invitrogen) plus antibiotics. Cells were cultured at 10% CO2 at 37 C overnight. On day 2 the cells were transfected in OptiMEM (Gibco) with the Lentiviral vector and the packaging constructs VSV-G, RRE and REV (added to a total of 40μg per dish) together with 50ul of Lipofectamine 2000. The medium was changed on day 3 with DMEM plus 10% FBS plus penicilline and streptavidin. On day 5 the medium was collected, combined and centrifuge at 1000 x g for 15 mins at 4°C. The supernatant was filtered through a 0.45 μm filter into sterile polyallomer centrifuge tube (Beckman Coulter). The tubes were inserted into a SW28 rotor (cat. #326823) and centrifuge at 20 000 RPM for 120 mins at 4°C. After centrifugation the supernatant was aspirated and the pellet resuspend in PBS. The final solution was aliquoted and stored at -80°C.

Mammalian expression vectors

pcDNA3.1 is a commercially available cloning/expression vector (Invitrogen). It was developed from pcDNA3 to permit high level of stable expression of recombinant protein in mammalian hosts using a CMV promoter. Despite of its small size (5.4kb), the vector has sequences of two selection markers: bacterial ampicillin and mammalian neomycin. Features of this vector are described **Figure S1** (Invitrogen).

pENTR1A is a Gateway® entry vector from Life Technologies (**Figure S2**). This vector contains multiple restriction sites flanking a ccdB gene (control of cell death), allowing multiple cloning possibilities and selection for positive clones. The multiple cloning sites are flanked by the attL1 and attL2 sites, which are used for site-specific recombination with a Gateway® destination vector, ensuring a fast and simple cloning step of the gene of interest in the correct orientation for expression.

pLenti CMVTRE3G Neo is a 3rd generation lentiviral vector containing a minimal CMV promoter preceded by TRE (Tetracycline Response Element), which is activated by tTA (Tetracycline-controlled activator) protein in presence of doxycycline. This promoter requires a co-expression of a vector encoding for the tTA protein. The attR1 and attR2 sites are present in front of the promoter for easy cloning by recombination with the entry vectors (see above). In addition a neomycin selection cassette for positive selection is included.

pLenti CMV rtTA3 Blast is a 3rd generation lentiviral vector expressing the reverse tetra-



cycline-controlled transactivator 3 (rtTA3) driven by a CMV promoter. This vector has a blasticidin selection cassette.

pLenti CMV Puro DEST is a 3rd generation lentiviral expression vector driven by a CMV promoter. The attR1 and attR2 sites are present in front of the promoter for easy cloning by recombination with the entry vectors. This vector has a puromycin selection cassette.

pLV-H1TetO-RFP-Puro (Biosettia) is a 3rd generation lentiviral vector for inducible expression of shRNA. The vector contains an EF1α promoter driving the expression of tTA protein followed by and IRES (Internal ribosome entry site) inducing the translation of a RFP fused to a puromycin. The shRNA expression is induced via a H1 promoter that can only be active in presence of doxycycline (TetON).

Human embryonic stem cell culture and differentiation

The human embryonic stem cell (hESC) line HES3-NKX2-5-eGFP was used for cardiac differentiation. This cardiac reporter line allows visualization and sorting of hESC-derived cardiomyocytes on the basis of GFP expression[11]. The cell line was maintained on irradiated mouse embryonic fibroblasts (MEFs). Differentiation was performed by two different methods. Monolayer differentiation was performed in a Matrigel coated plastic 6-well format where 300.000 hESC were seeded at day 0 in a BSA polyvinylalcohol essential lipids medium (BPEL)[12] together with 20ng/ml BMP4 (R&D), 20ng/ml Activin A (Miltenyi), 1.5μM chir99021 (Axon Medchem). The medium was refreshed after 3 days with BPEL supplemented with 5μM XAV-939. Alternatively, cardiomyocytes were generated using a "spin embryoid body (spin-EB)" method of differentiation[11]. Briefly, spin-EBs were formed by centrifugation of 30.000 hESCs in a 96-well format (Greiner) with BSA polyvinylalcohol essential lipids medium (BPEL) together with 35ng/ml BMP4 (R&D), 30ng/ml Activin A (Miltenyi), 30ng/ml VEGF (Miltenyi), 40ng/ml SCF (Miltenyi), 1.5μM chir99021 (Axon Medchem). The medium was refreshed on day 3. GFP positive spin-EBs started beating between day 7 and 10 of differentiation. Dissociation of both monolayers and spin EB derived cardiomyocytes was performed at day 20 with 1x TryplE select for 10 mins at 37C.

Single cell sorting

Four hours before start the sort Rock inhibitor (Fasudil, 5mM) was added, 1:1000 = 5uM. Undifferentiated hESCs were dissociated into single cells using TryplE (Gibco), resuspended in FACS buffer and passed through a cell strainer. The cells were pelleted and resuspended in FACS buffer, 2% FCS (Gibco), 1% normal goat serum and either primary SSEA4 (sc59368) antibody or isotype control. After 30mins on ice cells were washed 1x with FACS buffer containing 2% FCS and resuspended in FACS buffer, 2% FCS plus normal goat serum 1% and secondary goat anti-mouse IgG1 (H+L)-APC. After 30mins on ice, cells were washed and resuspended in FACS buffer plus 2% FCS and PI (1:1000). The cells were sorted to single well in a 96 well plate containing 9000 MEF/well plus Rock inhibitor 1:1000.

Analysis of sarcomere dynamics

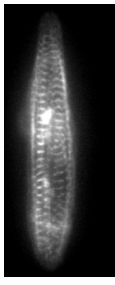
Image series of transduced cardiomyocytes were recorded with a Leica AF 6000 image

workstation (Leica Microsystems GmbH Wetzlar, Germany). A 40x dry objective with an internal 1.6x magnification extra was used to record images of 500x500 pixels during at least 6 contractions with a time resolution of 17 milliseconds. After export to uncompressed TIF format, Image stacks were constructed with the program of ImageJ or Fiji (National Institute of Health NIH U.S.A). The intrinsic function Z-profile of the program was used to construct a line-profile exactly perpendicular to the sarcomeres over the length of one cardiomyocyte. A plugin for ImageJ was written to export the profiles to a time-Z data set. A second program was developed for the interactive analysis using LabVIEW (National Instruments Corporation Austin, U.S.A.) - Power Spectral Analysis. A power spectral analysis per frame (Z-profile) was computed using a Hanning window output. Visual inspection of the power spectra always revealed a single peak and its successive second harmonics. The individual power spectral profiles were then fitted according a Gaussian function using the Levenberg–Marquardt algorithm with a ten times increased time resolution. The center frequency of this fitting (first peak in the spectrum) was used to compute the actual spacing (1/frequency) between the sarcomeres. Finally a graph was made of all computed points against time. From this graph speed of contraction, the speed of relaxation, the contraction duration and the repetition frequency was extracted. Requests for the ImageJ plugin and the Power Spectral.

Results

We have followed several strategies for introducing α-actinin-mCherry in human stem cell-derived cardiomyocytes for live imaging of sarcomeres during differentiation, assembly of sarcomeres and contractility. As a first step we cloned α-actinin into a mammalian expression vector pcDNA3.1 driven by the CMV promoter (**Figure S1**). The coding sequence of mCherry was has been previously incorporated into this vector. Human α-actinin was amplified by PCR from cDNA generated from hESC derived cardiomyocytes in a PCR reaction using primers FWamp1 + RVamp1 (**Figure 1A**, **Table S4**), followed by digestion with KpnI and subsequent ligation at the N-terminal side of mcherry. Positive clones (3 out of 24) were verified by sequence analysis (**Figure 1B** and **C**). In order to test whether α-actinin-mCherry was expressed and correctly incorporated in sarcomeres, we transfected the expression construct into HEK293T cells and hESC derived cardiomyocytes (hESC-CM), respectively. Although α-actinin-mCherry was clearly expressed in HEK 293T cells, expression was not observed in hESC-CM (**Figure 1D** and **E**). Lack of α-actinin-mCherry expression in hESC-CM could be due to multiple reasons, nonetheless, since it is expressed in the HEK 293T cells we assumed that the main issue was related to the lack of efficiency of the transfection procedure in cardiomyocytes.

In a next step we generated lentiviral vectors incorporating α-actinin-mCherry under control of the CMV promoter in order to obtain a higher transduction efficiency in hESC-CMs. For this, α-actinin and mCherry coding sequences were subcloned into a pENTR1A vector (**Figure S2**), which enables efficient recombination in the destination vector of choice using Gateway® technology. Alpha-actinin and mCherry were amplified using the FWamp2 and RVamp1 and FWamp3 and RVamp2 primer pair, respectively (**Figure 2A** and **Table**



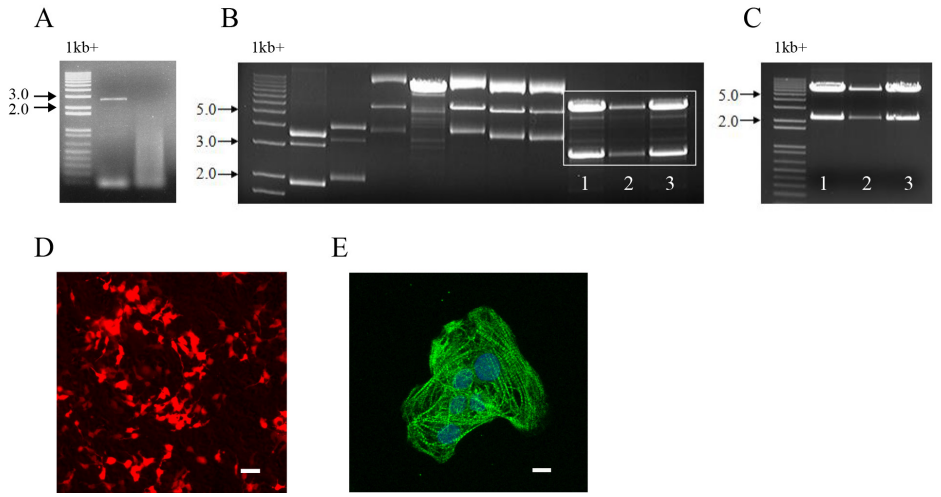


Figure 1- Cloning α-actinin-mCherry into pcDNA3.1. **A.** Band of the amplified α-actinin (2.7kb). **B.** Clone check after ligation with KpnI digestion with predicted bands at 2.7 and 5.4kb. **C.** Confirmation of correct clones with SalI digestion with predicted bands at 2.2 and 6.2kb. D. Expression of α-actinin-mCherry in HEK 293T cells in red (bar-50μm). **E.** Troponin I immunostaining in hESC-CM (green), nuclei (blue) with no expression of α-actinin-mCherry (red) (bar-10μm).

S4). PCR products were extracted from agarose gel and digested with either SalI and KpnI (α-actinin) or KpnI and XhoI (mCherry). The pENTR1A was digested with SalI and XhoI and ligated to both inserts in one reaction. Correct insertions (5 out of 6 clones, **Figure 2B** and **C**) were verified by sequence analysis and recombined into the pLenti CMVTRE3G Neo destination vector (**Figure S3**) using the LR Gateway® reaction. This vector allows inducible expression of α-actinin-mCherry in the presence of doxycycline (TetON system), avoiding a possible interference of this fusion protein during the process of cardiomyocyte differentiation. All clones recombined correctly (**Figure 2D**). Once clone was selected for further expansion and virus production.

Additionally, virus was produced for the pLenti CMV rtTA3 Blast expression vector. hESC-CM were transduced with both viruses in a glass bottom plate and doxycycline was added 48h post transduction. The expression and sarcomeric localization of α-actinin-mCherry was clearly visible by fluorescence microscopy. The movement of sarcomeres from contracting cardiomyocytes was recorded, demonstrating the feasibility to use this fusion protein for functional analysis of cardiomyocytes (**Figure 2E**). In order to generate a stable hESC line with the inducible α-actinin-mCherry expression both pLenti CMVTRE3G α-actinin-mCherry and pLenti CMV rtTA3 vectors (**Figure S3** and **S4**) were transduced into the HES3-NKX2-5-eGFP line and cultured for a week in the presence of antibiotics (Blasticidin and G418), followed by treatment with doxycycline (Dox). After 72h of Dox treatment only about ≈20% of the cells were expressing α-actinin-mCherry (**Figure 2F**), indicating silencing of the promoters. After differentiation to cardiomyocytes no overlap between GFP and mCherry expression was observed, indicating further silencing of expression in cardiomyocytes. In order to select for clonally derived cell lines displaying inducible mCherry expression, we performed FACS sorting based on mCherry and SSEA4 (pluripotency marker)

expression and seeded single cells in a 96 well plate (containing mouse feeders). Clonal expansion was successful in 51% (46 out of 90) of the wells, from which the cells were transferred by cut and paste both to a new well of feeders for expansion and to a matrigel-coated plate for cardiac differentiation. At day 10 of differentiation Dox was added to all wells and after 72h only 36% (18 out of 50) of the wells displayed mCherry positive cells. These positive wells displayed approximately 10% to 50% of mCherry positive cells. Unfortunately, we did not observe overlap between GFP and mCherry expression in the same cell (data not shown), suggesting silencing of α-actinin-mCherry expression, in particular in cardiomyocytes. Therefore, we decided to perform transient lentiviral-transduced expression of hESC-CMs in future experiments.

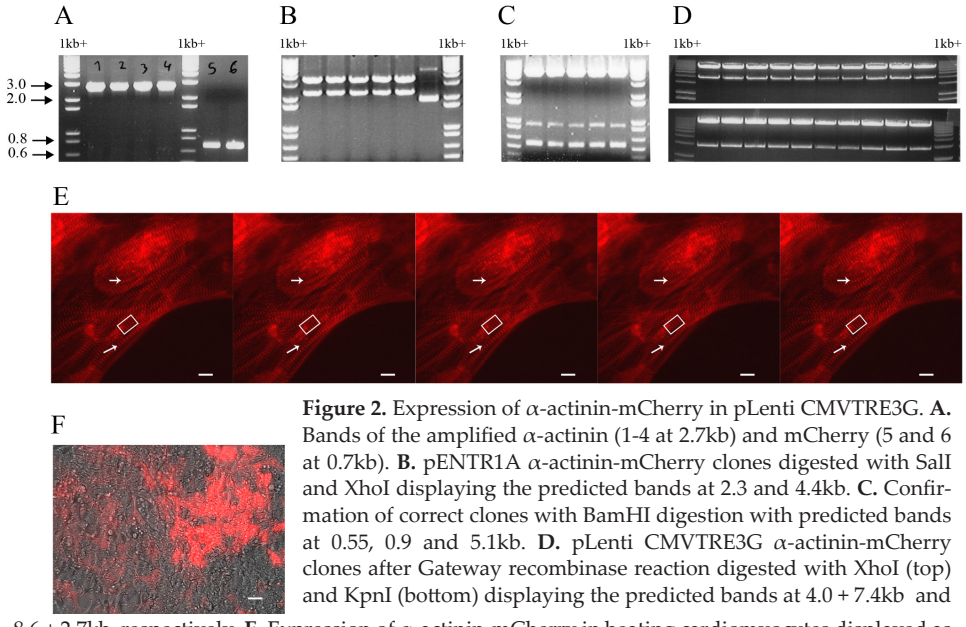


Figure 2. Expression of α-actinin-mCherry in pLenti CMVTRE3G. **A.** Bands of the amplified α-actinin (1-4 at 2.7kb) and mCherry (5 and 6 at 0.7kb). **B.** pENTR1A α-actinin-mCherry clones digested with SalI and XhoI displaying the predicted bands at 2.3 and 4.4kb. **C.** Confirmation of correct clones with BamHI digestion with predicted bands at 0.55, 0.9 and 5.1kb. **D.** pLenti CMVTRE3G α-actinin-mCherry clones after Gateway recombinase reaction digested with XhoI (top) and KpnI (bottom) displaying the predicted bands at 4.0 + 7.4kb and 8.6 + 2.7kb, respectively. **E.** Expression of α-actinin-mCherry in beating cardiomyocytes displayed as different frames of one contraction (bar-10μm). **F.** Merge between brightfield and fluorescent images of hESC expressing of α-actinin-mCherry after antibiotic selection (bar-50μm).

For this approach we generated a pLenti CMV α-actinin-mCherry viral vector following LR Gateway® recombination of pENTR1-α-actinin-mCherry and pLenti CMV Neo vectors (**Figure S5** and **3A**). HESC-CMs were transduced at day 15 of differentiation. Transduced cardiomyocytes were cultured in defined maturation medium during 7 days for phenotypical improvement (see Chapter 4), followed by dissociation and seeding on 1% gelatine 20x20 lines printed on a polyacrylamide gel. After four days beating single cardiomyocytes were imaged at 37°C - 5%CO2 at a speed of 56 frames per second, represented in selected frames in **Figure 8B**. In order to analyse the sarcomere movement during contraction, the frame sequence was loaded into the software Image J as a stack and a pixel intensity profile was made across the sarcomere length for each frame (**Figure 3C**). Subsequently the pixel intensity plot of every frame was uploaded into the Power Spectral Analysis software (**Figure 8D** left panel) and the most frequent distance between peaks was calculated using



a power spectrum analysis (Hanning) fitted with a Gaussian distribution (**Figure 3D** right panel) (see materials and methods). The distance corresponding to the peak of the power spectrum of each frame was plotted in function of time (**Figure 3E**). This data format enables the assessment of the sarcomere spacing in its relaxed (y0- 1.79μm) and contracted (y1- 1.51μm) form, the distance covered by the sarcomeres during contraction (shortening amplitude) (Δy- 0.27μm) and relaxation (elongation amplitude) (Δy2- 0.27μm) as well as the time taken by the sarcomeres during both actions (Δt- 0.11s and Δt2- 0.27s, respectively), which allow us to analyse kinetics of sarcomere movement during contraction and relaxation with a shortening speed of - 2.45μm/s and a elongation speed of - 1.01μm/s (**Figure 3E**).

Discussion

Here we generated an α-actinin-mCherry fusion protein following various cloning strategies and demonstrated proof of concept for its use as a tool to accurately identify the dynamic changes of Z-disks in live hPSC-CM. We further developed power spectral analysis software to calculate the length of each sarcomere during contraction, which we used to assess the kinetics of sarcomere movement during contraction.

Currently sarcomere length measurements are mostly based on observations made on fixed cells, which obviously interferes with assessment of dynamic changes of the sarcomeres. Other approaches such as laser diffraction techniques[13] or the use of 2-photon microscopes[14] have been applied to measure dynamics of sarcomere length in single cells or live tissue. Nevertheless, these techniques are rooted on the extremely well defined periodicity of the sarcomeres as they are based on a constant light diffraction pattern or on the presence of T-tubules, both traits of fully matured cardiomyocytes, which are currently non-existent or at least difficult to achieve in hPSC-CM. On the other hand, our approach of genetic labelling sarcomeres with a fluorescent reporter not only allows the assessment of sarcomeres kinetics but also of sarcomerogenesis during hPSC-CM maturation or disease modelling. With this approach we intended to develop a stable hESC line with temporal control of the α-actinin-mCherry expression by the use of a doxycycline inducible CMV promoter (TetON). Although the expression of the α-actinin-mCherry was present initially in undifferentiated hESC, its level decreased over time during cardiomyocyte differentiation due to an event of vector transcriptional silencing as previously reported in these cell types[8]. Most interestingly, even after clonal selection of undifferentiated hESC expressing α-actinin-mCherry, upon cardiac differentiation mCherry expression could no longer be detected in a large percentage of the cell population. This observation has been previously reported in another study[8] and can be explained by chromatin remodelling-induced silencing occurring during differentiation[15]. An alternative strategy to generate a stable reporter line is to genetically modify, for example by CRISPR/Cas9 system[16], the genomic locus of α-actinin by inserting a fluorescent reporter in frame in order to create a fluorescent sarcomeric fusion protein, which is regulated by endogenous genomic regulatory elements. This avoids not only transcriptional silencing of exogenous inserted DNA, but also non-specific over-expression of α-actinin in both cardiomyocytes and non-cardiomyocytes.

To circumvent the silencing problems that we encountered with generating stable cell lines,

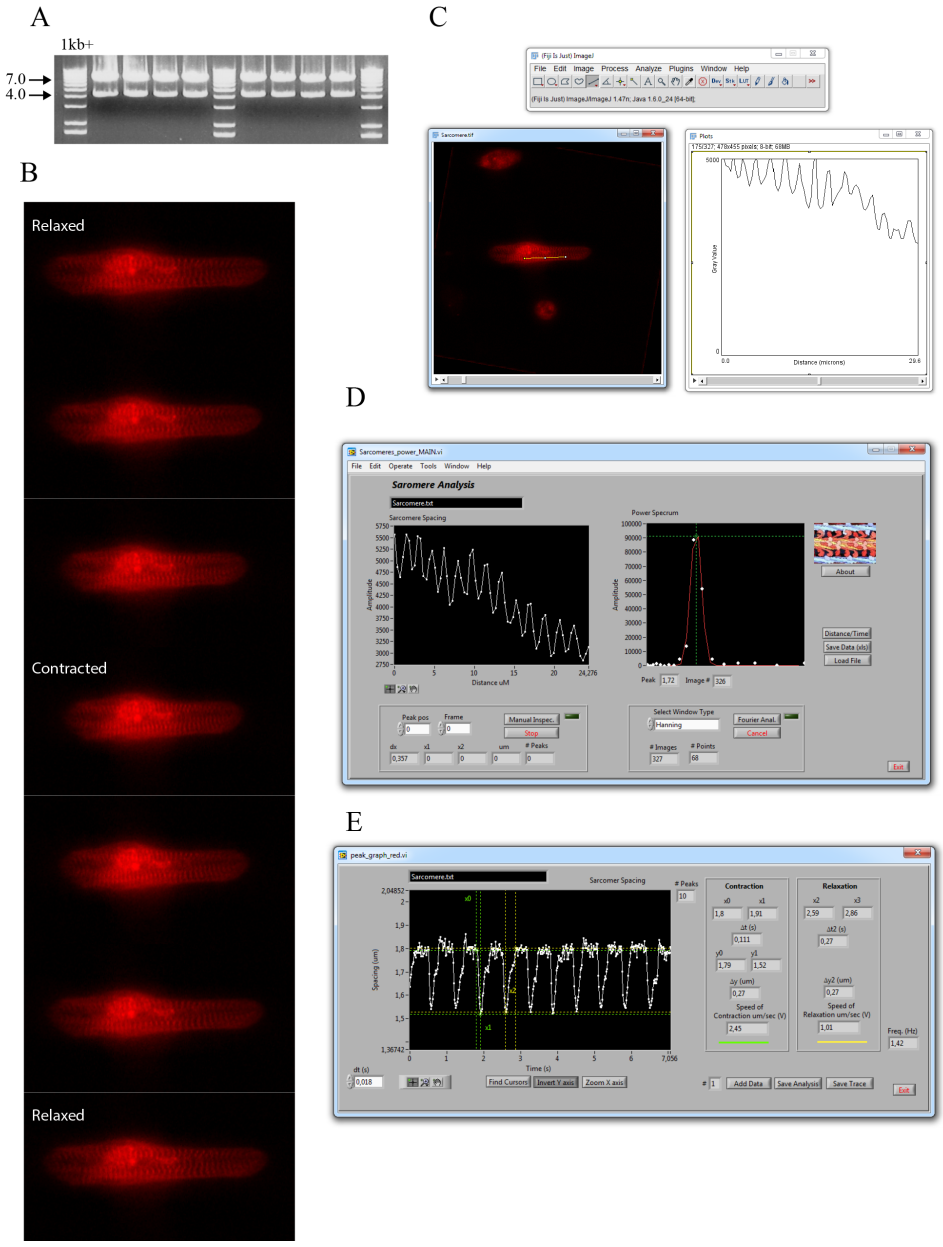


Figure 3- Sarcomere analysis. **A.** pLenti CMV α-actinin-mCherry clones after Gateway recombinase reaction digested with EcoRI displaying the predicted bands 4.2 and 7.4kb. **B.** Representative image sequence of a single cardiomyocyte contraction cycle (top-Relaxed, middle-Contracted and bottom-Relaxed form) – α-actinin-mCherry in Red. **C.** Image sequence loaded to software Image J as image stack (left); Pixel intensity profile of the line crossing the sarcomere length plotted over distance for each frame (right). **D.** Power Spectral Analysis software displaying on the left panel the pixel intensity profile with the user input of pixel size (dx) and on the right panel the power spectrum analysis output (white dots) fitted with a Gaussian distribution (red line), displaying the most frequent spacing observed (Peak) for each image and the possibility to change the window type. **E.** Sarcomere spacing of each frame plotted over time with user input of time resolution. Green lines - x0 and x1 are cursors that allow manual picking the interval between relaxed and contracted sarcomere form during active contraction; Yellow lines – x2 and x3 are cursors that allow manual picking the interval between contracted and relaxed sarcomere form during active relaxation.

we studied the use of a sarcomeric fluorescent reporter in hESC-CMs by transient over-expression of the sarcomeric reporter construct. Although the cells were selected for transduction based on the neomycin cassette, not every cell visibly expressed the α-actinin-mCherry. Moreover, there was a clear variation of sarcomeric-mCherry intensity between cardiomyocytes of the same well. Of note, regardless of the sarcomeric-mCherry intensity, all cardiomyocytes displayed no or low non-sarcomeric expression of α-actinin-mCherry, mostly localized around the nucleus as shown in **Figure 8b**, indicating an immediate degradation of the non-assembled α-actinin-mCherry inside the cardiomyocytes. This observation suggests that the variation in sarcomeric-mCherry intensity between each cardiomyocyte may not be caused by differences in expression of the α-actinin-mCherry but by the different amount of α-actinin-mCherry assembled onto the sarcomeres versus the endogenous α-actinin. Although the number of clearly visible and measurable α-actinin-mCherry positive cardiomyocytes is enough to conduct a single cell study, the variation of sarcomeric-mCherry intensity increases the number of wells and time needed to obtain enough measurable cells, especially when used in combination with other vectors (e.g. shRNA or protein over-expression). A possible solution to increase signal-to-noise ratio of the sarcomeric-mCherry intensity in this approach is to replace the mCherry by a more recently developed mRuby2 or TagRFP-T fluorescent proteins, which are 2.5x and 3x, respectively, brighter than mCherry[17,18].

After capturing good quality image sequence of contracting α-actinin-mCherry sarcomeres the most intuitive method to analyse sarcomere distances would be to measure the average distance between the consecutive sarcomeres using the intensity peak of each sarcomeric-mcherry as reference. However, the output of this method was extremely noisy due to the background created by the movement of the sarcomeres in each frame (data not shown), impairing the analysis of sarcomere kinetics. Different studies have employed the Fourier transformation to decompose the signal derived from pixel intensity plot made across the sarcomere length into a frequency spectrum, which can be used further to assess the most dense wavelength corresponding to the sarcomere distance[14,19,20]. The use of this tool fitted with a Gaussian distribution and enabled the assessment hESC-CM sarcomere velocity of shortening and relaxation. The preliminary data suggest that hESC-CM sarcomeres contract 5x slower than the observed velocities for Cat and Rat cardiac sarcomeres[13], most probably due to hESC-CM immature stage and/or to physiologic differences between species.

Conclusion

This chapter describes the development of α-actinin-mCherry fusion protein as a tool for sarcomere kinetics analysis in hPSC-CM. The use of the α-actinin-mCherry as a sarcomeric reporter tool was accomplished by lentiviral transiently delivery directly into hESC-CM, establishing a proof of concept of α-actinin-mCherry fusion assembly into functional sarcomeres. Power spectra analysis software was developed to determine the sarcomere spacing of each frame in a high-speed movie of a contracting cardiomyocyte, enabling the assessment of movement kinetics of single sarcomeres. In conclusion, we successfully developed a multifunctional tool, which will enable to study hPSC-CM contractile function in healthy and diseased conditions, responses to drugs and sarcomerogenesis and maturation.



References

[1] Yang X, Pabon L, Murry CE. Engineering adolescence: maturation of human pluripotent stem cell-derived cardiomyocytes. Circ Res. 2014;114(3):511–23.

[2] Abraham MR. Hypertrophic cardiomyopathy : a heart in need of an energy bar ? 2014;5(August):1–8.

[3] Pasqualini FS, Sheehy SP, Agarwal A, Aratyn-Schaus Y, Parker KK. Structural Phenotyping of Stem Cell-Derived Cardiomyocytes. Stem Cell Reports. The Authors; 2015;4:4–11.

[4] Sjöblom B, Salmazo a, Djinović-Carugo K. Alpha-actinin structure and regulation. Cell Mol Life Sci. 2008;65(17):2688–701.

[5] Squire JM. Architecture and function in the muscle sarcomere. Curr Opin Struct Biol. 1997;7(2):247–57.

[6] Jackson WM, Jaasma MJ, Baik AD, Keaveny TM. Over-expression of alpha-actinin with a GFP fusion protein is sufficient to increase whole-cell stiffness in human osteoblasts. Ann Biomed Eng. 2008;36(10):1605–14.

[7] Shaner NC, Campbell RE, Steinbach P a, Giepmans BNG, Palmer AE, Tsien RY. Improved monomeric red, orange and yellow fluorescent proteins derived from Discosoma sp. red fluorescent protein. Nat Biotechnol. 2004;22(12):1567–72.

[8] Norrman K, Fischer Y, Bonnamy B, Sand FW, Ravassard P, Semb H. Quantitative comparison of constitutive promoters in human ES cells. PLoS One. 2010;5(8).

[9] Gossen M, Bujard H. Tight control of gene expression in mammalian cells by tetracycline-responsive promoters. Proc Natl Acad Sci U S A. 1992;89(12):5547–51.

[10] Lycett GJ, Kafatos FC, Loukeris TG. Conditional expression in the malaria mosquito Anopheles stephensi with Tet-on and Tet-off systems. Genetics. 2004;167(4):1781–90.

[11] Elliott D a, Braam SR, Koutsis K, Ng ES, Jenny R, Lagerqvist EL, et al. NKX2-5(eGFP/w) hESCs for isolation of human cardiac progenitors and cardiomyocytes. Nat Methods. 2011;8(12):1037–40.

[12] Ng ES, Davis R, Stanley EG, Elefanty AG. A protocol describing the use of a recombinant protein-based, animal product-free medium (APEL) for human embryonic stem cell differentiation as spin embryoid bodies. Nat Protoc. 2008;3(5):768–76.

[13] de Tombe PP, ter Keurs HE. Sarcomere dynamics in cat cardiac trabeculae. Circ Res. 1991;68(2):588–96.

[14] Botcherby EJ, Corbett A, Burton R a B, Smith CW, Bollensdorff C, Booth MJ, et al. Fast measurement of sarcomere length and cell orientation in langendorff-perfused hearts

using remote focusing microscopy. Circ Res. 2013;113(7):863–70.

[15] Mok H-P, Lever AM. Chromatin, gene silencing and HIV latency. Genome Biol. 2007;8(11):228.

[16] Cong L, Ran FA, Cox D, Lin S, Barretto R, Habib N, et al. Multiplex Genome Engineering Using CRISPR/Cas Systems. Science (80-). 2013;339(February):819–24.

[17] Kredel S, Oswald F, Nienhaus K, Deuschle K, Röcker C, Wolff M, et al. mRuby, a bright monomeric red fluorescent protein for labeling of subcellular structures. PLoS One. 2009;4(2):1–7.

[18] Siegel AP, Baird M a., Davidson MW, Day RN. Strengths and weaknesses of recently engineered red fluorescent proteins evaluated in live cells using fluorescence correlation spectroscopy. Int J Mol Sci. 2013;14(10):20340–58.

[19] Bub G, Camelliti P, Bollensdorff C, Stuckey DJ, Picton G, Burton R a B, et al. Measurement and analysis of sarcomere length in rat cardiomyocytes in situ and in vitro. Am J Physiol Heart Circ Physiol. 2010;298(5):H1616–25.

[20] Zhang D, Shadrin IY, Lam J, Xian H-Q, Snodgrass HR, Bursac N. Tissue-engineered cardiac patch for advanced functional maturation of human ESC-derived cardiomyocytes. Biomaterials. Elsevier Ltd; 2013;34(23):5813–20.



Supplementary figures

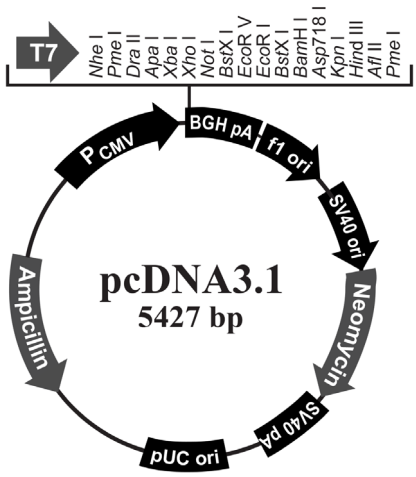


Figure S1. Vector map of pcDNA3.1 (Authorized by Thermo Fisher Scientific).

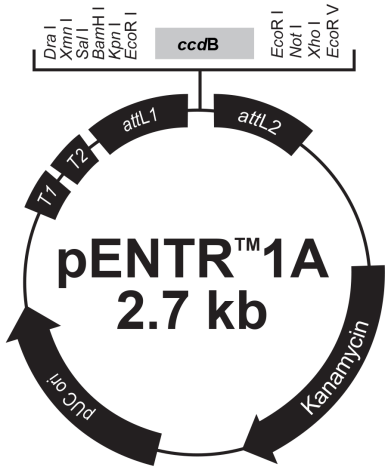


Figure S2. Vector map of pENTR1A (Authorized by Thermo Fisher Scientific).

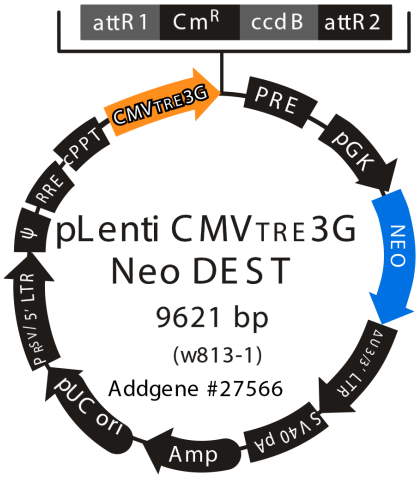


Figure S3. Vector map of pLenti CMVTRE3G Neo destination (provided by Dr. Eric Campeau and authorized by Addgene).

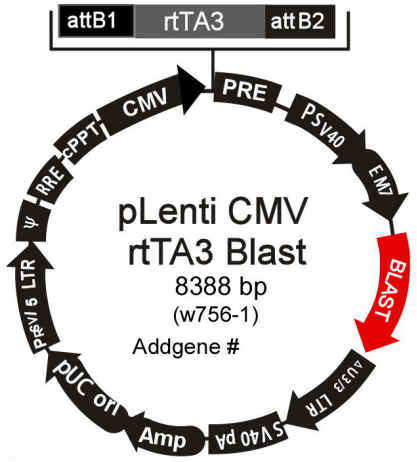


Figure S4. Vector map of pLenti CMV rtTA3 Blast (provided by Dr. Eric Campeau and authorized by Addgene).



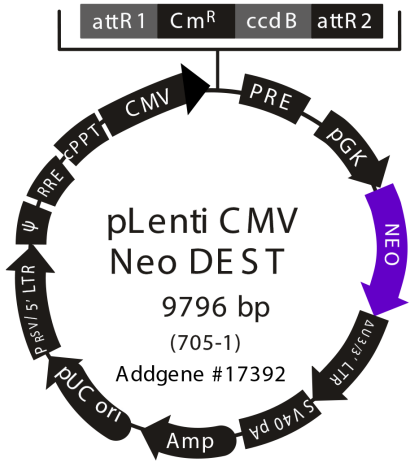


Figure S5. Vector map of pLenti CMV Neo (provided by Dr. Eric Campeau and authorized by Addgene).

Table S1 - Polymerase Chain Reaction

	Final concentration
Phusion Taq (ThermoScientific)	0.02U/µl
5x Phusion HF Buffer	1x
DMSO	3%
dNTP	200.0µM each
Fw primer	0.5µM
Rv primer	0.5µM
DNA	1.0pg-10.0ng (≥1.0 µl)
MQ	to 50.0µl
Total	50.0µl

Table S2 - PCR cycle program

Cycle step	*Temperature*	*Time*	*Cycles*
Initial denaturation	98°C	02:00	1x
Denaturation	98°C	00:30	25x
Annealing	X°C	00:30	
Extension	72°C	0:15-0:30s/kb	
Final extension	72°C	10:00	1x
Hold	12°C	∞	

Table S3 - Digestion reaction

Enzyme*	1.0-1.5µl
DNA	2-10µg
Buffer 10x**	1x
BSA 10x***	1x
MQ	to final volume
Total	20.0-50.0µl

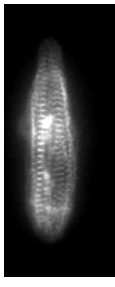
*Enzyme's volume should not exceed 10% of the final volume. It is possible to use two enzymes in one reaction, if they are active in similar conditions (reaction buffer, temperature)

**Reaction buffer should be chosen following a producer's table of enzymes' activity

***BSA intensifies the reaction, but is not recommended for all enzymes (check producer's table of enzymes' activity)

Table S4 – Amplification primers

Name	Sequence	Restriction site	binding end
FWamp1	CGGGTACCACCATGAACCAGATAGAGCCC	KpnI	5'
RVamp1	CGGGTACCGCCAGATCGCTCTCCCCGTA	KpnI	3'
FWamp2	CAGTCGACCACCATGAACCAGATAGAGC	SalI	5'
FWamp3	TGGGTACCATGGTGAGCAAGGGCGAGGA	KpnI	5'
RVamp2	ATCTCGAGTTACTTGTACAGCTCGTCCA	XhoI	3'





Chapter 6

Hypertrophic Cardiomyopathy - Impaired sarcomeric motion and contractile dysfunction caused by defective MYBPC3 in hPSC derived cardiomyocytes



Marcelo C. Ribeiro[1], Matthew J. Birket[1], Leon Tertoolen[1], Jantine Monshouwer-Kloots[1], Christine L. Mummery[1] and Robert Passier[1]

[1]Department of Anatomy & Embryology, Leiden University Medical Center, Leiden, The Netherlands.

Manuscript in preparation

Abstract

Hypertrophic Cardiomyopathy (HCM) is a cardiac disease, morphologically characterized by cardiac hypertrophy, fibrosis and impaired heart function. HCM is primarily associated with mutations in sarcomeric proteins. Mutations in sarcomeric Myosin Binding Protein C (MYBPC3) account for approximately 25% of all HCM patients. The majority of mutations in MYBPC3 are nonsense mutations, predicted to produce truncated proteins. However, instead of truncated proteins, lower levels of full-length protein of MYPBC3 are frequently found in heart samples of patients with mutations in MYBPC3, strongly suggesting that haploinsufficiency is responsible for the cardiac disease phenotype. In Chapter 4 we described a contractile defect in human induced pluripotent stem cell derived cardiomyocytes (hiPSC-CM) from HCM patients carrying a MYBPC3 mutation. In this chapter we demonstrate that decreasing the MYBPC3 protein level through short-hairpin RNA knock-down in normal hPSC-CM induces contractile dysfunction similar to the observations on MYBPC3 mutated hiPSC-CM. Additionally, we observed a decrease in diastolic sarcomere length together with a decrease in shortening and elongation amplitude of the sarcomeres of MYBPC3 deficient hPSC-CM. Knock-down of MYBPC3 did not affect calcium handling of hPSC-CMs, but reduced the ATP consumption per contraction cycle. In summary, we successfully developed a human *in vitro* model for cardiac MYBPC3 haploinsufficiency in combination with state of the art biophysical and imaging techniques, which will allow us future investigation of the molecular mechanisms responsible for HCM.

Introduction

Hypertrophic Cardiomyopathy (HCM) is the most common inherited cardiac disease with an estimated prevalence of 1:500 in the general population[1]. HCM is characterized morphologically by thickening of cardiac walls, mainly induced by hypertrophy and disarray of cardiomyocytes as well as cardiac fibrosis, leading to asymmetric ventricular hypertrophy and obstruction of the left ventricular outflow tract[1]. The clinical symptoms are variable among patients, ranging from asymptomatic individuals to patients with chest angina, cardiac dyspnea, atrial fibrillation and sudden cardiac death[1,2]. Several causal mutations for HCM have been identified in genes encoding sarcomeric proteins such as cardiac myosin binding protein C (MYBPC3) (42%), β-myosin heavy chain (40%), troponin T (6.5%), and myosin light chain 2 (<1%), all with an autosomal dominant inheritance[3]. The different mutations found in each protein can be divided into: 1) missense mutations (causing a single amino acid substitution); 2) nonsense mutations (insertion or deletion of a nucleotide, causing a shift of the open reading frame shifts and consequent a premature stop codon; 3) in-frame insertion or deletion of a number of nucleotides[4]. A nonsense mutation generated by a guanine duplication at the nucleotide position 2373 of the myosin binding protein C (MYBPC3) gene is responsible for nearly one fourth of the HCM cases in the Netherlands and is therefore being considered as a Dutch founder mutation[5]. This mutation is predicted to create a premature stop codon and consequently a truncated protein at the C-terminus[6]. However, a truncated MYBPC3 protein has not been found in heart samples derived from these patients, suggesting that the truncated protein is degraded. A decrease in total amount of MYBPC3 was also found in these patients compelling the thought of a disease-causing haploinsufficiency[6,7].

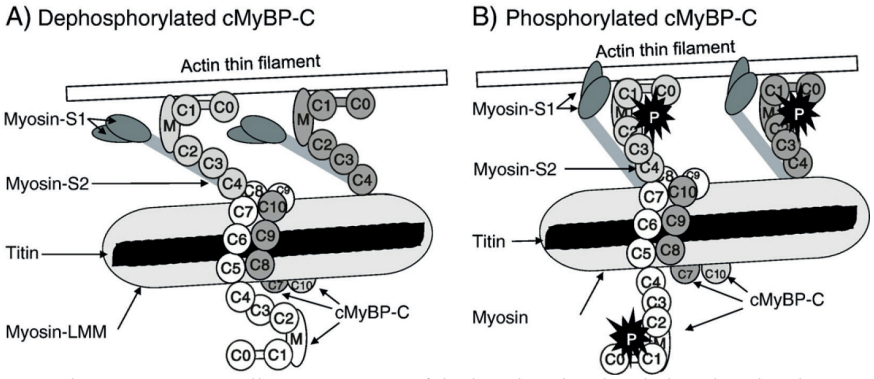
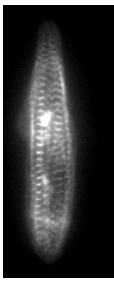


Figure 1- Schematic trimeric collar organization of dephosphorylated and phosphorylated MYBPC3 in the sarcomere. The C5–C10 domains of three MYBPC3 molecules (white, light gray and dark gray) are wrapped around the filament of light meromyosin (myosin-LMM, in light gray) and titin (in black). The overlapping is stabilized by interactions between domains C5:C8 and C7:C10 of two adjacent MYBPC3 molecules. The C0–C4 domains of MYBPC3 are extended into the interfilament space. **A.** when MYBPC3 is dephosphorylated in the MyBP-C motif (M), the C1–M–C2 domains are tightly bound to myosin-S2 (gray rectangles) and actin (white rectangle); this prevents cross-bridges formation. **B.** when MYBPC3 is phosphorylated, M domain releases its interaction with myosin-S2 and actin. This allows myosin heads (myosin-S1) to get ordered and extended to the thin filaments, which results in strong actin–myosin interactions. In contrast to the M domain, C1 domain binds to actin irrespective of the phosphorylation state of MYBPC3 (Taken from Schlossarek S. et. al 2011 with permition).



The MYBPC3 is a 140kDa protein, localized transversally in the A-band of cardiac sarcomeres. This protein comprises 11 domains (C0-C10) that connect the thin (actin) to the thick filaments (myosin) through binding of the C0 and C1 domains to the actin filament and C5 to C10 domains to the myosin, titin and light meromyosin (LMM)[4]. Moreover, the C2 to C4 domains together with the MYBPC motif have an important role in modulating contraction as they are tightly bound to the myosin head, preventing its cross-bridge binding the actin during the relaxed state. The MYBPC motif contains three phosphorylation sites that are phosphorylated upon contraction, releasing the interaction with myosin-S2 (**Figure 1**) This release allows the myosin heads to extend and strongly interact with the actin on the thin filament[4]. Even though sarcomeric organization has been well described, the precise function of MYBPC3 during contraction is still not completely understood and direct consequences of various mutations or change in levels of expression have been subject of intensive research. The absence of MYBPC enables the movement of the myosin heads closer to the actin filament[8], increasing the probability of the myosin head being weakly bound to the actin at any given contraction stage. These random cross bridge have been shown to impair the full relaxation of the sarcomere[9] and decrease the strong myosin-actin interactions and force generation during contraction[10]. Random cross bridges not only impair the generation of contractile force but also use energy that is not converted into contraction, which translates to a decreased cardiac output while consuming the same amount of energy. Patients who carry a MYBPC3 mutation display reduced myocardial work relative to oxygen consumption[11]. The impairment of myocardial work indicates that the link between sarcomere mutations and the development of HCM may be related to bioenergetics demand. Further research is needed to fully verify and understand the mechanisms of this disease. Since patient-derived cardiac samples are extremely difficult to obtain and controlled experimental design using primary cardiomyocyte cultures are hampered by the inability to proliferate and the challenging task to maintain viable functional cardiomyocytes *in vitro*. The use of patient-derived induced pluripotent stem cells (iPSC) provides an excellent opportunity to study this. In chapter 4 we showed that cardiomyocytes derived from hiPSC (hiPSC-CM) of patients carrying the 2373dupG mutation display decrease contraction stress when compared to cardiomyocytes derived from hiPSC of healthy donors. In order to have a better understanding of the underlying working mechanism of the disease we established an isogenic human *in vitro* model of MYBPC3 haploinsufficiency using short-hairpin RNAs (shRNAs). Using a multiplex platform we analyzed changes in calcium, sarcomere and contraction kinetics as well as energy consumption caused by the MYBPC3 knockdown in single cardiomyocytes.

Materials and methods

hESC culture and differentiation

The previously described cardiac reporter NKX2-5eGFP/w hESC line[12], was maintained on mouse embryonic fibroblasts (MEFs) and passaged using TrypLE select (Life Technologies). Cardiac differentiation was induced from monolayer cultures on Matrigel in

a serum-free medium (BSA, polyvinyl alcohol, essential lipids [BPEL]) as previously described[13]. The following factors were present for the first 3 days 20 ng/ml BMP4 (R&D), 20 ng/ml Activin A (Miltenyi Biotech) and 1.5 μM CHIR 99021 (Axon Medchem). 5 μM XAV 939 (Tocris Bioscience) was present on days 3-6. Beating cardiomyocyte cultures were dissociated on day 13 and replated on Matrigel-coated 24-well plates. At day 16 cardiomyocyte cultures were refreshed in defined cardiomyocyte culture medium (CCM), which is composed of the following: DMEM (Sigma D5030), 15 mM glucose, 0.5 mM sodium pyruvate, 0.19 mM sodium hydroxybutyrate, 0.5 mM L-carnitine, 1 mM creatine, 5 mM taurine, phenol red (0.011 g/l), 1x Trace elements (A, B and C; Corning), 1x chemically defined lipids (Life Technologies), 2 mM Glutamax, 400 μM α-thioglycerol, 0.1x ITS-X, 50 μg/ml AA-2P, 0.5% Pen-Strep, 3.5 g/l sodium bicarbonate, 100 nM T3, 100 ng/ml Long R3 IGF-1 and 1 μM dexamethasone (TID).

Lentiviral transduction

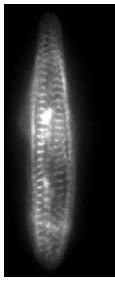
shRNAs against MYBPC3 (NM_000256) were obtained from Open Biosystems in the pLKO Puro vector (#1 - TRCN0000082906 (AGCCAGAATATGGTTGGCTTT) and #2 - TRCN0000082903 (CCTCCCTACTGTTGGATGTAT). A scrambled control shRNA was used as control (Sarbassov et al., 2005) (Addgene plasmid: 1864). The lentivirus containing pLenti CMV Puro DEST α-actinin-mCherry was described in chapter 5. Cardiomyocytes were transduced with lentiviruses on day 15 of differentiation and subsequently selected with puromycin before single cell dissociation and analysis.

Western blotting

Samples were lysed with ice cold ELB (50mM HEPES pH 7.0; 250mM NaCl; 5mM EDTA; 0.1% NP-40) with 1:100 Protease Inhibitor Cocktail (Sigma-Aldrich) for 30 mins on ice. The samples were centrifuged at 7,000g for 10 mins and supernatant was quantified for protein content using the Bio-Rad Protein Assay (based on the Bradford dye-binding method). 100μg of the hiPSC-CM lysates were run on a 6% polyacrylamide gel and 30μg of the hESC-CM with the shRNA lysates were run on a 10% polyacrylamide gel together with the protein ladder (Precision Plus Protein dual colour – Bio-Rad). Proteins were transferred to an Amersham Hybond membrane (GE Heathcare- Life Sciences) overnight. The membrane was blocked with blocking buffer (2% milk in PBS) and MYBPC3 protein was detected using a specific antibody: Rabbit IgG anti- MYBPC3 (1:2000) overnight at 4C kindly provided by Dr. Sakthivel Sadayappan (Department of Cell and Molecular Physiology, Health Sciences Division, Loyola University Chicago), followed by incubation with a Horse anti-Rabbit IgG – HRP (1:2000) (Cell Signaling). As an internal control for protein levels, and more specifically cardiomyocytes, we used a mouse IgG anti-Actin (1:1000) (MAB1501 – Millipore) and mouse IgG anti-α-actinin (A7811-Sigma-Aldrich) overnight at 4C, respectively. As a second antibody we used a goat anti-mouse IgG-HRP (1:2000) (Cell Signaling).

Contraction stress, sarcomere dynamics and calcium transients measurements on single cardiomyocytes

Contraction stress



As described in chapter 2 cells were seeded onto gelatine patterned acrylamide gels 4 days before measurements at 37°C and 5% CO2. Briefly, using a Leica AF-6000LX microscope, image-series of aligned single contracting cardiomyocytes paced at 1Hz were taken at a 40x magnification at 20 frames per second, recording brightfield and fluorescent beads (660/680nm). Single frames from maximal relaxation and contraction of the brightfield and fluorescent beads image-series were analyzed by the LIBTRC software package (kindly provided by Dr. Micah Dembo), creating a mask of the cell outline from the brightfield image and a vector map from the difference between the relaxed and contracted fluorescent beads images. The vector map and the cell mask were used to calculate the total force that the cell applies on the substrate at its maximum peak of contraction. The contraction stress generated by the cardiomyocyte during contraction was calculated by dividing the total force by the cell surface area.

Sarcomere dynamics

Contraction cycles of cardiomyocytes were recorded in image series of 500x500 pixels using a 40x dry objective with an internal 1.6x magnification displaying clearly visible and measurable α-actinin-mCherry (587/610nm) expression during at least 6 contractions with a time resolution of 17 milliseconds (56 frames/second). After export to uncompressed TIF format, Image stacks were constructed with the program of ImageJ or Fiji (National Institute of Health NIH U.S.A). The intrinsic function Z-profile of the program was used to construct a line-profile exactly perpendicular to the sarcomeres over the length of one cardiomyocyte. A plugin for ImageJ was written to export the profiles to a time-Z data set. A second program was developed for the interactive analysis using LabVIEW (National Instruments Corporation Austin, U.S.A.) - Power Spectral Analysis. A power spectral analysis per frame (Z-profile) was computed using an Hanning window output. Visual inspection of the power spectra always revealed a single peak and its successive second harmonics. The individual power spectral profiles were then fitted according a Gaussian function using the Levenberg–Marquardt algorithm with a ten times increased time resolution. The center frequency of this fitting (first peak in the spectrum) was used to compute the actual spacing (1/frequency) between the sarcomeres. Finally, all computed points were plotted against time. From this graph, the speed of contraction and relaxation, the contraction duration and the repetition frequency was extracted.

Calcium transients

After recording images for contraction stress and sarcomere dynamics cells were incubated in 5μM of Fluo-4 AM (Invitrogen), unless mentioned otherwise, for 20mins at 37°C and 5%CO2. The change in Fluo-4 intensity (485/520nm) was recorded for each contracting cardiomyocytes paced at 1Hz with a time resolution of 17 milliseconds (56 frames/second) for at least 6 full contractions. Transient recordings were analysed using ImageJ-Fiji in combination with a custom-made software generated to convert raw data to dF/F0 results. The calcium transient duration (from peak amplitude until 90% return to base level, CaT90), amplitude, slope and decay were determined. The time constant of calcium transient decay (τ) was obtained by fitting the decay phase with a single exponential function (y=A0+A1ex-

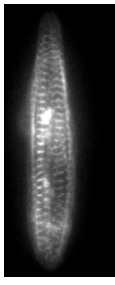
p[-t/τ]).

Respiration measurements with the Seahorse XF-24 Analyzer

GFP+ cardiomyocytes were sorted by FACS and seeded on Matrigel-coated assay plates at a density of 7x104 cells per well of a Seahorse XF plate, 7 days before measurement. At the time of seeding cells were transduced with lentivirus expressing the scrambled shRNA or the B7 MYBPC3 shRNA. Measurements were performed in bicarbonate-free DMEM (D5030; Sigma Aldrich), containing 0.25% fatty acid-free BovoStar (Bovogen, Australia), 15 mM glucose, 0.5 mM sodium pyruvate, 1 mM sodium lactate, 0.15 mM sodium hydroxybutyrate, 2 mM GlutaMAX (Life Technologies) and 0.5 mM L-carnitine. Cells were washed twice and pre-incubated in assay medium 1 h before measurement. Contraction frequencies of each well were recorded manually at 37°C just before measurement. To assess ATP demand for contraction, after recording the basal respiration rate 5 μg/ml blebbistatin was injected and the respiration rate immediately recorded, followed by measurements after injection of oligomycin to inhibit ATP synthase and then rotenone and antimycin A to interfere with the electron transport chain. A vehicle-only injection was performed in parallel for normalization. In addition, a standard protein assay was used to normalize values to whole cell protein. The oligomycin-sensitive oxygen consumption was converted to an ATP production rate using a P/O ratio of 2.3 as previously described [14].

Statistical analysis

Differences between the different groups were assessed by Student's t-test for comparison of two groups or one-way ANOVA followed by Bonferroni post-test for comparison of three or more groups. The differences in cell structure classification were assessed using Chi2 test.



Results

In chapter 4 we described an *in vitro* model that effectively mimics the contractile dysfunction observed in patients. However, this model was based on hiPSC-CM derived from different individuals with different genetic background. In order to minimize the phenotypical differences due to genetic background, we decreased MYBPC protein levels by shRNAs knock down in single hESC lines.

Two different shRNAs specifically targeting MYBPC3 and one scrambled were delivered by lentiviral transduction into cardiomyocytes differentiated form the Hes3-NKX2-5eGFP/w hESC line. Both shRNA constructs effectively decreased mRNA levels and protein expression of MYBPC3 in these cells, when normalized for the effects of control scrambled shRNA (**Figure 2A, B** and **C**). Further experiments were performed in a cardiomyocyte culture medium (CCM) containing TID with entirely defined basal components and no serum albumin (see Experimental procedures) to maximize functional output. In order to analyse changes in the sarcomere dynamics, hESC-CM were co-transduced with a lentivirus carrying the α-actinin-mCherry as described in chapter 5. The cells were cultured for 10 days after virus transduction in CCM before seeding on the patterned lines for contraction stress

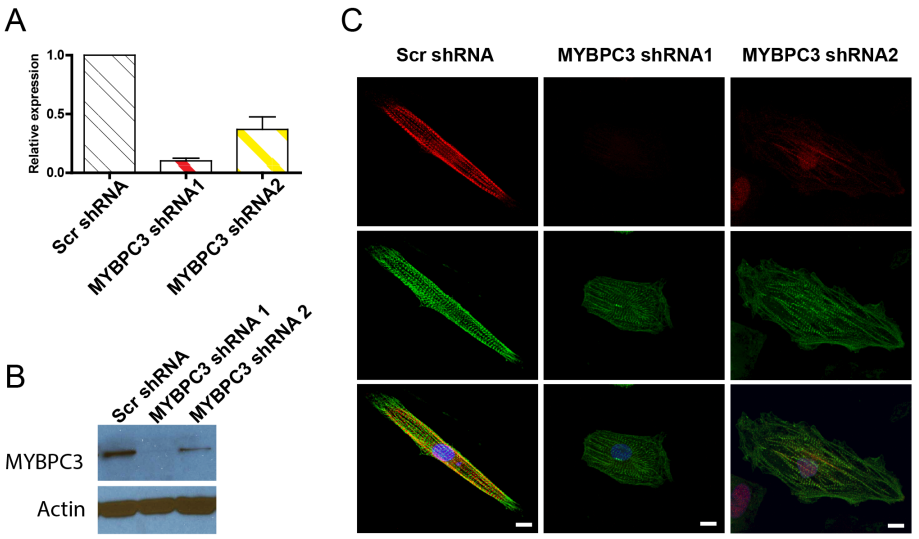


Figure 2- Knocking down MYBPC3 in hESC-CM. **A.** Relative MYBPC3 mRNA expression in hESC-CM transfected with scrambled (SCR) shRNA or two distinct MYBPC3 shRNA (N=3). Expression levels were normalized to RPLP expression. **B.** Western blot assessment of MYBPC3 protein expression after knockdown. C. Sarcomeric immunostaining on hESC-CM after MYBPC3 knockdown; Red-MYBPC3; Green-Troponin I; Blue-Nucleus.

measurements. Since the contraction force setup is based on optical recordings at excitation/emission 660/680nm, additional measurements can be recorded at other wavelengths, such as sarcomere dynamics at 587/610nm and calcium kinetics at 485/520nm on the same cardiomyocytes (**Figure 3**).

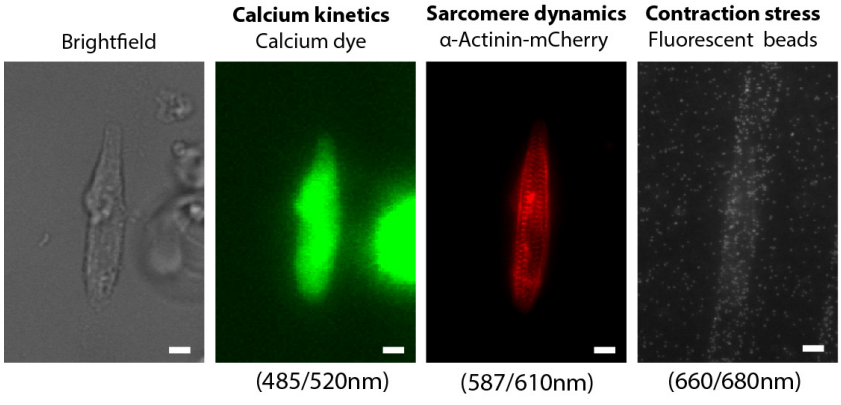


Figure 3 – Example of the single cell multiplex platform. Grey left- Brightfield picture of a beating cardiomyocytes. Green middle- Single frame of calcium transients measurements using Fluo-4; Red middle- α-Actinin-mCherry used to analyse sarcomere dynamics; B&W right- Fluorescent beads embedded on the polyacrylamide gel for contraction stress measurements.

Knocking down MYBPC3 (shRNA) induced a significant decrease in contraction stress of hESC-CM but no changes in cell size were observed (**Figure 4A** and **B**), which is consistent with our previous findings using hiPSC-CM from patients with the c.2373dupG mutation, as described in chapter 4. This suggest that contractile defects are indeed due to haploinsufficiency for MYBPC3. To determine whether the decrease in contraction stress was caused by changes in sarcomere dynamics, movement of α-actinin-mCherry positive Z-disks during contraction were recorded on the same cardiomyocytes. Although the majority of the cardiomyocytes were transduced, only the minority of cardiomyocytes assembled α-actinin-mCherry to a level that is clearly visible and measurable (Chapter 5). Preliminary data showed that the shRNA induced a significant reduction in the diastolic sarcomere length together with a decrease in shortening and elongation amplitude (average distance migrated by each sarcomere during contraction and relaxation, respectively) (**Figure 5A**, **B** and **C**). Additionally, there is a trend in the decrease of the shortening and elongation speeds of sarcomeres in the shRNA cardiomyocytes (**Figure 5D** and **E**), suggesting both impaired relaxation and contraction of the sarcomeres. Additional experiments need to be performed in order to analyse the relation between sarcomere dynamics and contractile force generation for each group. Nevertheless, if both shRNA and Scr groups are combined there is a correlation between force generation of individual cardiomyocytes and the amplitude of sarcomere shortening, amplitude of sarcomere relaxation as well as with the sarcomere diastolic length. However, this correlation does not exist between force generation and systolic length (**Figure 6 A, B, C** and **D**).

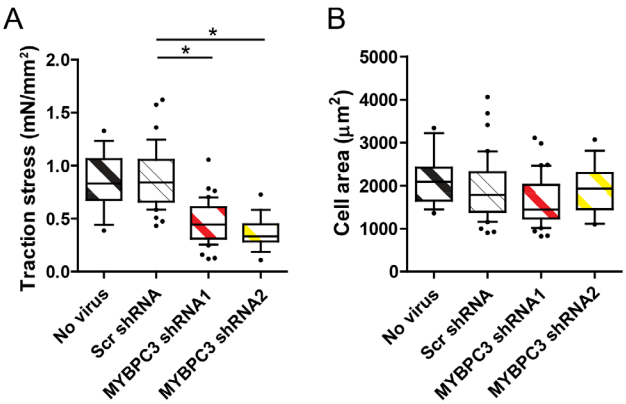


Figure 4- Contractile force changes of cardiomyocytes with MYBPC3 knockdown **A.** Contraction stress and **B.** cell size measured on single hESC-CM with no virus (n=15) or transduced with a scrambler (n=32) or two different MYBPC3 shRNA (n=26 and 16); . *P<0.05.

Several studies have described changes in calcium handling as an important characteristic of hypertrophic cardiomyocytes[9,15–17]. Therefore, assessing the impact of MYBPC3 knock down on calcium handling properties may shed some light on the HCM disease state of this human *in vitro* model. After contraction stress measurements, the cardiomyocytes were loaded with 5µM Fluo-4 for 20mins and the fluorescence intensity change was recorded in each contracting cardiomyocyte. To control for the effect of the calcium buffering by the Fluo-4 each cardiomyocyte was measured again for contraction stress after Fluo-4 load-

ing. No changes in any calcium kinetics parameters were observed on the shRNA treated cardiomyocytes in comparison with the controls (**Figure 7A, B, C, D** and **E**). Nevertheless, the effect of calcium buffering of the Fluo-4 on the single cardiomyocytes greatly affected the contraction stress generation of the cardiomyocytes from all groups (**Figure 7F**), indicating that the high concentration of dye was compromising the contractile machinery of the cardiomyocytes.

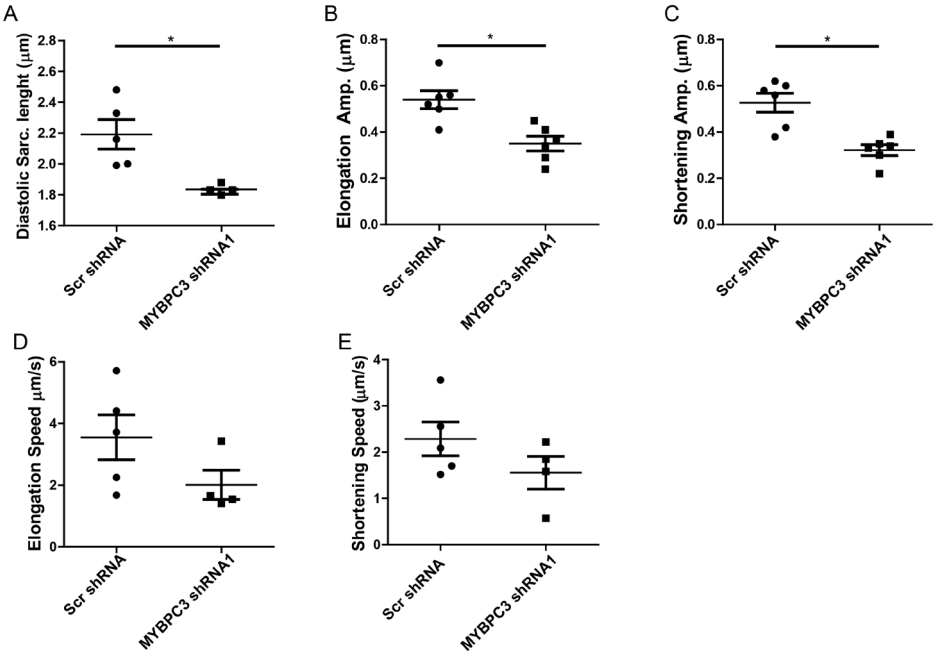


Figure 5- Changes in sarcomere dynamics of cardiomyocytes with MYBPC3 knockdown. **A.** Sarcomere length at relaxed state. **B**. and **C.** Average distance migrated by one sarcomere during relaxation and during contraction, respectively. **D.** and **E.** Average speed at which one sarcomere moves during relaxation and contraction, respectively (Scr n=6; MYBPC3 shRNa1 n=6). *P<0.05.

Recent studies suggested that MYBPC3 deficiency may give rise to HCM because of an increased energy requirement for muscle contraction[11,18]. To test this, bioenergetic profiles of contracting cardiomyocyte monolayers were determined using the Seahorse XF24 Analyzer on cardiomyocytes from the same experimental groups. Contraction rates, measured prior to analysis, were not significantly different between groups. Under standard conditions (15 mM glucose, 0.5 mM sodium pyruvate) normalized to total cell protein, the basal respiration rate and the ATP turnover appeared slightly but not significantly decreased in cardiomyocytes transduced with MYBPC3 shRNA (**Figure 8A, B** and **C**). Moreover, blebbistatin-sensitive respiration rate per contraction cycle was decreased significantly, which is translated to a reduction of ATP use by the actomyosin ATPase for each contraction cycle (**Figure 8D**).

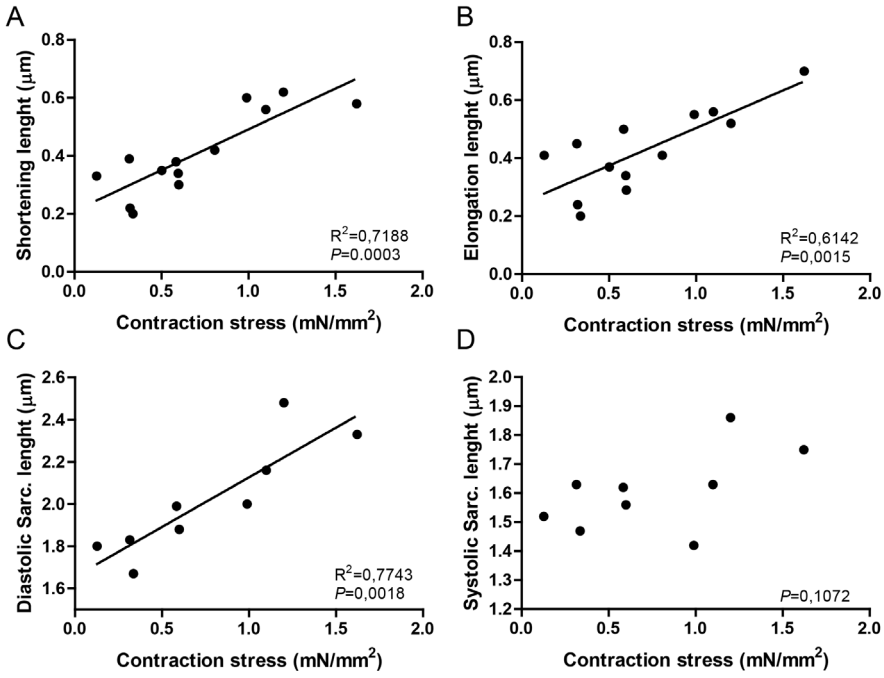


Figure 6- Relation between total contraction stress and sarcomere dynamics. **A.** and **B.** Correlation between contraction stress and average distance migrated by one sarcomere during relaxation or during contraction, respectively. **C.** Correlation between contraction stress and sarcomere length at relaxed state. **D.** Contraction stress does not correlate with sarcomere length at contracted state. With P<0.05* and P<0.01** a correlation was considered existent and a linear regression line was drawn (black line) with the respective R2; With P >0.05 no correlation was considered existent and therefore no linear regression line was drawn.



Discussion

In the work described we developed a human stem cell derived model for multiplex analysis of cardiomyocyte function in disease-simulating conditions. Knockdown of MYBPC3, which mimics the reduced levels of MYBPC3 in HCM patients, resulted in contractile impairment, defects in sarcomeric relaxation and contractile properties and a decrease in bioenergetic demand in hESC-derived cardiomyocytes. We combined different tools developed in previous chapters creating a multiplex platform for measuring contraction stress, sarcomere dynamics and calcium transients in individual cells.

This was a follow up study to chapter 4 where we demonstrated impaired contractile stress in patient derived hiPSC-CM with mutations in MYBPC3. Although the effects on contractile stress were evident, it was unclear whether reduced levels of MYBPC3 were sufficient for the cause of the observed phenotype. Furthermore, we also investigated in more detail the underlying mechanism, by measuring various functional assays in control and diseased cardiomyocytes. For this we knocked down MYBPC3 protein in hESC-CM, enabling us to study the specific role of this protein in cardiomyocyte function by comparing isogenic hESC-CMs with and without knockdown. Alternatively, to determine the causal relation-

ship between the affected protein and the disease phenotype, diseased hiPSC bearing the mutation could be genetically rescued by correcting the mutation, creating an isogenic control. It has been shown previously that the 2373dupG mutation resulted in a decrease of MYBPC3 protein levels human myectomy samples[7], suggesting that the disease is caused by haploinsufficiency of MYBPC3. The contractile defect observed in the cardiomyocytes with decreased MYBPC3 content is consistent with the phenotype observed in patients' cardiac samples[11]. Although the contractile force measurement is a direct consequence of sarcomeric function, a correlation has not been previously shown in hPSC-CM models. The shorter diastolic sarcomeric length and the impairment of shortening and lengthening amplitudes caused by the reduction of MYBPC3 is congruent with previously reported findings in mouse models[9], which substantiates the notion that this protein plays a crucial role in sarcomere function and stability. Moreover, the positive correlation observed between these parameters of sarcomere dynamics and the total contractile force suggests that reduction of MYBPC3 levels impairs contraction stress by disrupting sarcomere function. Furthermore, it would be interesting to determine differences in the relationship between contraction stress and sarcomere dynamics in the diseased model versus control. For this we would need to increase the number of samples in order to make robust conclusions.

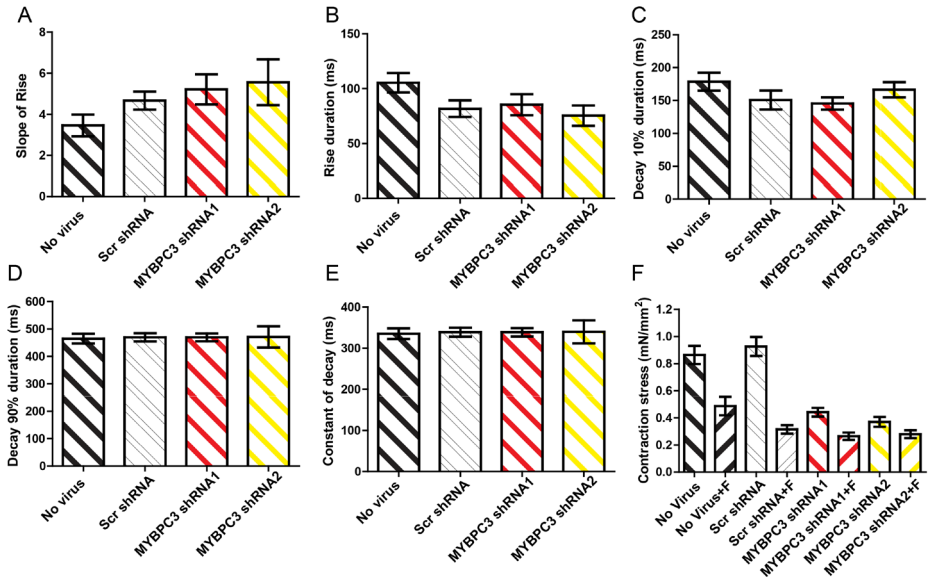


Figure 7- Changes in calcium handling of cardiomyocytes with MYBPC3 knockdown. **A.** and **B.** Slope and duration of rise in intracellular calcium, respectively. **C.**, **D.** and **E.** 10%, 90% and decay constant of intracellular calcium, respectively. **F.** Contraction stress of the same cardiomyocytes before and after (+F) Fluo-4 incubation of each group. No virus-n=10; Scr-n=17; MYBPC3shRNA1-n=16; MYBPC3shRNA2-n=8.

Most individuals carrying a MYBPC3 ultimately develop HCM. Recent studies using patient derived hPSC-CM models of HCM have described this disease phenotype *in vitro* as increased cell size and calcium handling defects[15,17]. However, in our model none of these characteristics are observed in the MYBPC3 deficient cardiomyocytes, which may

indicate that sarcomeric and contractile dysfunction precede an adaptive hypertrophic response. This notion is supported by the fact that HCM is mostly observed later in life of MYBPC3 mutation carriers[11]. It is important to note that the calcium dye evidently affects the excitation-contraction coupling of single cardiomyocytes by buffering the calcium. These observations are reason for concern that Fluo-4 interferes with the calcium handling kinetics: this could be responsible for masking possible differences between disease and control previously described in other HCM causing mutations[15]. The use of calcium dyes has been well established for multicellular platforms in which calcium chelation does not affect the contractile output[19]. On the other hand, single cardiomyocytes are more sensitive to the accumulation of calcium dye inside the cell, which can easily disturb the calcium handling kinetics.

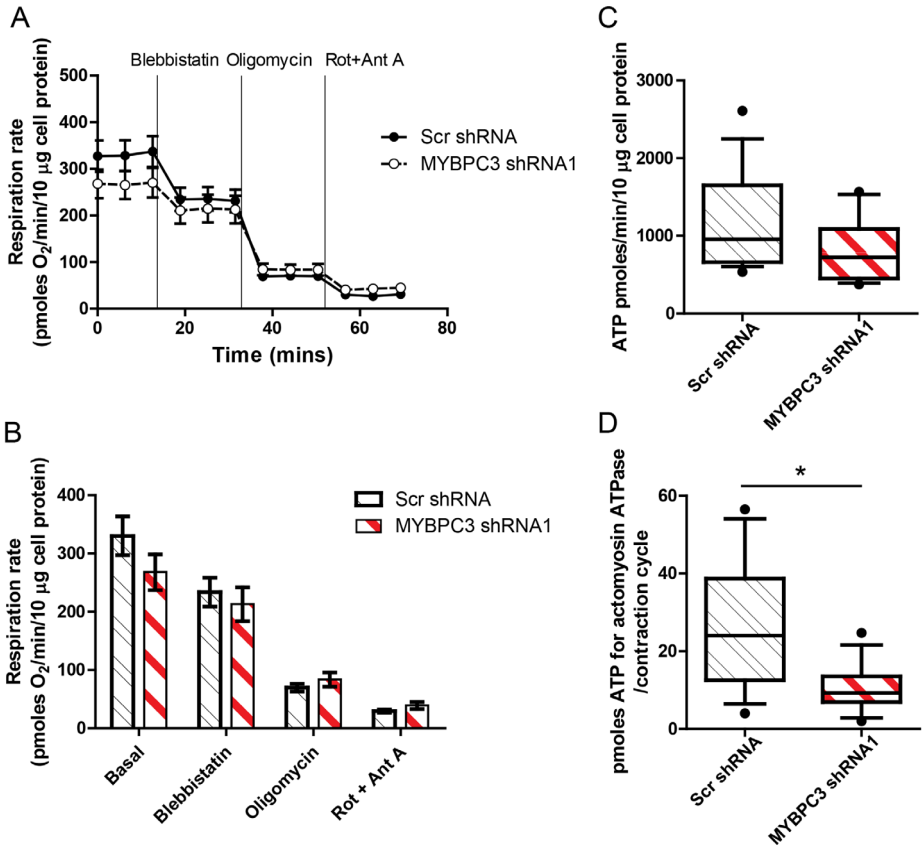


Figure 8- Energy demand for contraction in cardiomyocytes with MYBPC3 knockdown. **A.** Real-time respiration measurements and response to injection of blebbistatin, then oligomycin, and finally rotenone and antimycin A. **B.** Summary data of respiration rates measured at basal activity or in the presence of the factors indicated. **C.** Theoretical ATP production rates from oxidative phosphorylation calculated from the values in **B. D**. Theoretical ATP used by the actomyosin ATPase per contraction cycle. Data in **A** and **B** show mean±sem. The box and whisker plots in **C** and **D** show the median, interquartile range and 10-90 percentile range. n=12-18 measurements acquired over 3 independent experiments. Statistical significance was calculated with an unpaired t-test in **B**, **C** and **D** comparing the scrambled versus the MYBPCshRNA1 rates. *p<0.05.

The knockdown of MYBPC3 induced a decrease of about 50% in the energy usage per contraction cycle, matching the decrease in contractile force generation, meaning that there is similar energy usage per contraction cycle (contractile work) between control and disease groups. This result is not congruent with the theory of increased energy costs per contraction observed in human cardiac samples[11]. One possible explanation for this could be the immature contractile machinery of the hPSC-CM, which might become less function in the absence of MYBPC3 and therefore use less energy.

Conclusion

In this chapter we developed a new disease model for MYBPC3 deficiency using hPSC-derived cardiomyocytes. Knocking down the MYBPC3 in these human cardiomyocytes induced a reduction in contractile force generation, which was correlated with specific changes in sarcomere dynamics. The reduction of MYBPC3 did not affect the calcium handling properties but diminished the energy used per contraction cycle. In conclusion, by applying different tools developed in previous chapters we were able to create a multiplex platform for measuring cardiomyocyte function in individual cells enabling the development of an *in vitro* hPSC-derived disease model for MYBPC3 that recapitulates important functional characteristics of the disease as observed in HCM patients with mutations for MYBPC3, making it a step forward towards studying and understanding the mechanism of cardiomyopathies.

References

[1] [1] Maron BJ, Olivotto I, Bellone P, Conte MR, Cecchi F, Flygenring BP, et al. Clinical profile of stroke in 900 patients with hypertrophic cardiomyopathy. J Am Coll Cardiol. 2002;39(2):301–7.

[2] Maron BJ, Maron MS. Hypertrophic cardiomyopathy. Lancet. 381(9862):242–55.

[3] Richard P, Charron P, Carrier L, Ledeuil C, Cheav T, Pichereau C, et al. Hypertrophic cardiomyopathy: distribution of disease genes, spectrum of mutations, and implications for a molecular diagnosis strategy. Circulation. 2003;107(17):2227–32.

[4] Schlossarek S, Mearini G, Carrier L. Cardiac myosin-binding protein C in hypertrophic cardiomyopathy: mechanisms and therapeutic opportunities. J Mol Cell Cardiol. Elsevier Ltd; 2011;50(4):613–20.

[5] Alders M. The 2373insG mutation in the MYBPC3 gene is a founder mutation, which accounts for nearly one-fourth of the HCM cases in the Netherlands. Eur Heart J. 2003;24(20):1848–53.

[6] Moolman JA, Reith S, Uhl K, Bailey S, Gautel M, Jeschke B, et al. A Newly Created Splice Donor Site in Exon 25 of the MyBP-C Gene Is Responsible for Inherited Hypertrophic Cardiomyopathy With Incomplete Disease Penetrance. Circulation. 2000;

[7] Marston S, Copeland O, Jacques A, Livesey K, Tsang V, McKenna WJ, et al. Evidence from human myectomy samples that MYBPC3 mutations cause hypertrophic cardiomyopathy through haploinsufficiency. Circ Res. 2009;105(3):219–22.

[8] Colson B a, Bekyarova T, Fitzsimons DP, Irving TC, Moss RL. Radial displacement of myosin cross-bridges in mouse myocardium due to ablation of myosin binding protein-C. J Mol Biol. 2007;367(1):36–41.

[9] Pohlmann L, Kröger I, Vignier N, Schlossarek S, Krämer E, Coirault C, et al. Cardiac myosin-binding protein C is required for complete relaxation in intact myocytes. Circ Res. 2007;101(9):928–38.

[10] Lecarpentier Y, Vignier N, Oliviero P, Guellich A, Carrier L, Coirault C. Cardiac Myosin-binding protein C modulates the tuning of the molecular motor in the heart. Biophys J. 2008;95(2):720–8.

[11] Witjas-Paalberends ER, Güclü A, Germans T, Knaapen P, Harms HJ, Vermeer AMC, et al. Gene-specific increase in the energetic cost of contraction in hypertrophic cardiomyopathy caused by thick filament mutations. Cardiovasc Res. 2014;103:248–57.

[12] Elliott D a, Braam SR, Koutsis K, Ng ES, Jenny R, Lagerqvist EL, et al. NKX2-5(eGFP/w) hESCs for isolation of human cardiac progenitors and cardiomyocytes. Nat Methods. 2011;8(12):1037–40.



[13] Ng ES, Davis R, Stanley EG, Elefanty AG. A protocol describing the use of a recombinant protein-based, animal product-free medium (APEL) for human embryonic stem cell differentiation as spin embryoid bodies. Nat Protoc. 2008;3(5):768–76.

[14] Birket MJ, Casini S, Kosmidis G, Elliott D a, Gerencser A a, Baartscheer A, et al. PGC-1α and Reactive Oxygen Species Regulate Human Embryonic Stem Cell-Derived Cardiomyocyte Function. Stem Cell Reports. The Authors; 2013;1(6):560–74.

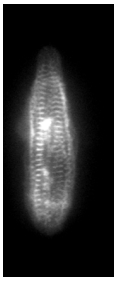
[15] Lan F, Lee AS, Liang P, Sanchez-Freire V, Nguyen PK, Wang L, et al. Abnormal calcium handling properties underlie familial hypertrophic cardiomyopathy pathology in patient-specific induced pluripotent stem cells. Cell Stem Cell. Elsevier Inc.; 2013;12(1):101–13.

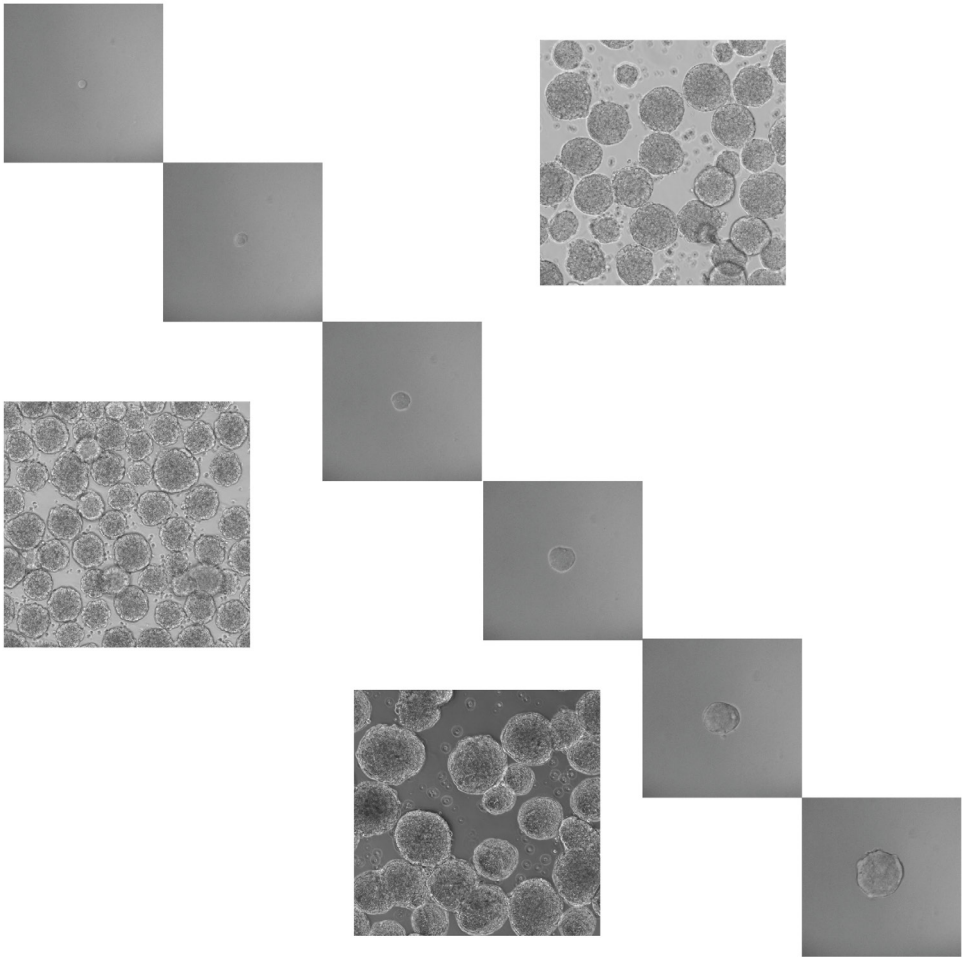
[16] Abraham MR. Hypertrophic cardiomyopathy : a heart in need of an energy bar ? 2014;5(August):1–8.

[17] Han L, Li Y, Tchao J, Kaplan AD, Lin B, Li Y, et al. Study familial hypertrophic cardiomyopathy using patient-specific induced pluripotent stem cells. 2014;258–69.

[18] Timmer S a J, Germans T, Brouwer WP, Lubberink M, Van Der Velden J, Wilde A a M, et al. Carriers of the hypertrophic cardiomyopathy MYBPC3 mutation are characterized by reduced myocardial efficiency in the absence of hypertrophy and microvascular dysfunction. Eur J Heart Fail. 2011;13(12):1283–9.

[19] Stoehr A, Neuber C, Baldauf C, Vollert I, Friedrich FW, Flenner F, et al. Automated analysis of contractile force and Ca2+ transients in engineered heart tissue. Am J Physiol Heart Circ Physiol. 2014;306(9):H1353–63.





Chapter 7

Expansion and developmental patterning of human PSC-derived cardiovascular progenitors

Matthew J Birket[1], Marcelo C Ribeiro[1], Arie Verkerk[2], Dorien Ward[1], Ana Rita Leitoguinho[1], Sabine den Hartogh[1], Milena Bellin[1], Valeria V Orlova[1], Harsha D Devalla[1], Verena Schwach[1], Robert Passier[1], Christine L Mummery[1]

[1] Leiden University Medical Center, Leiden, The Netherlands.

[2] Amsterdam Medical Center, Amsterdam, The Netherlands.



Nature Biotechnology 2015 33(9):1–12

Abstract

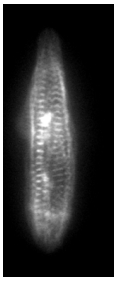
The inability of multipotent cardiovascular progenitor cells (CPCs) to undergo more than a few divisions in culture has precluded stable expansion of precursors of (human) cardiomyocytes and vascular cells. This contrasts with neural progenitors, which can be expanded robustly and are a renewable source of their derivatives. Here, we used human pluripotent stem cells (hPSCs) in which CPCs are genetically marked to show that regulated MYC expression enables their robust expansion through IGF-1 and hedgehog signalling. These CPCs can be patterned with morphogens, recreating features of heart field assignment, and controllably differentiated to relatively pure populations of pacemaker-like or "working" ventricular-like cardiomyocytes with strikingly different physiological characteristics. The cells are clonogenic and can be expanded over 40 population doublings yet still be directed to differentiate to cardiomyocytes as well as vascular cells. Together, this tractable model reveals the potential of hPSC-derived CPCs for precisely recreating elements of heart development in vitro.

Introduction

Human pluripotent stem cells (hPSCs) can recapitulate aspects of development in vitro and produce cell types not routinely available from primary tissue. This has already proven useful in modeling disease, screening compound libraries to identify drug targets and developing cell therapies [1–3]. The heart is of particular relevance because of its vital function and inaccessibility. Differentiation of hPSCs to cardiomyocytes and vascular cells can contribute to understanding the nature of congenital defects in development and disease and in safety pharmacology, as the heart is a crucial target of toxicity [4]. The availability of expandable hPSC-derived multipotent CPCs with the ability to form cardiomyocytes and vascular cells in culture could advance all of these areas by providing renewable precursors without the need to return to the hPSC source. This goal has been challenging because the culture requirements of CPCs are uncertain and their molecular identity is poorly defined [5].

In heart development, CPC populations arise within bilateral cardiogenic areas of mesoderm. Following prior lineage segregation, one CPC population, called the first heart field (FHF), forms the myocardium of the linear heart tube, and the remaining pool of undifferentiated CPCs, called the second heart field (SHF), are added later, providing further cardiomyocytes, smooth muscle and endothelial cells to the developing heart [6]. The genes ISL1 and NKX2-5 (the vertebrate homolog to tinman), which encode homeobox transcription factors, are two of the earliest genes identifying CPCs and may be expressed at least transiently in the majority of these cells [7–9]. Both have been used to isolate multipotent CPCs from embryonic or neonatal hearts and hPSCs, and the potential of these cells for differentiation has been demonstrated in short-term experiments [10–12]. However, the difference between the isolated populations in these respective studies is unclear, and heterogeneity in clonal experiments suggests that there is a need for additional markers and better methods for robustly maintaining discrete populations at different stages of commitment. Expression of Nkx2-5 in mice, for example, is present in the majority of CPCs destined to form 'working' myocardium but is thought to be absent in the SHF lineage destined for the sinoatrial node (SAN) [13]. These SAN progenitors, however, express Isl1 and may also express Tbx18, which encodes a T-box transcription factor14. Conversely, in mice, the FHF CPC population, which gives rise mainly to primitive left ventricular progenitors, may be uniquely marked by early Hcn4 expression [15,16]. Hcn4 is expressed later and then maintained in the $Isl1^{+}Nkx2\text{-}5^{-}Tbx18^{+}$ SHF-CPC–derived SAN. These important commitment steps and their regulatory mechanisms are not resolved in the hPSC model. Generating pure populations of pacemaker cells is crucial for modeling sinus node dysfunction and could be useful in the future development of biological pacemakers; pure populations of ventricular or atrial working myocardial cells would similarly benefit other applications.

The practical challenge for more effectively directing cardiac progression from hPSCs is to slow the otherwise rapid and uncontrolled transition from the appearance of CPCs, marked by increasing expression of platelet-derived growth factor receptor-α (PDGFR-α)[17], to their differentiation, predominantly to cardiomyocytes of heterogeneous identity. Here, taking advantage of $NKX2\text{-}5^{eGFP/w}$ human embryonic stem cells (hESCs) in which the emergence of $NKX2\text{-}5^{+}$ cells can be followed by eGFP expression, we report a solution through



regulated MYC expression. This enables the expansion of primitive pre–NKX2-5$^+$ CPCs, their patterning through regulation of fibroblast growth factor (FGF) and bone morphogenetic protein (BMP) signaling and their directed differentiation to NKX2-5–eGFP$^+$ working ventricular-like cells, NKX2-5–eGFP$^-$ pacemaker-like cells and endothelial and, later, smooth muscle cells, mimicking the cardiac developmental program.

Results

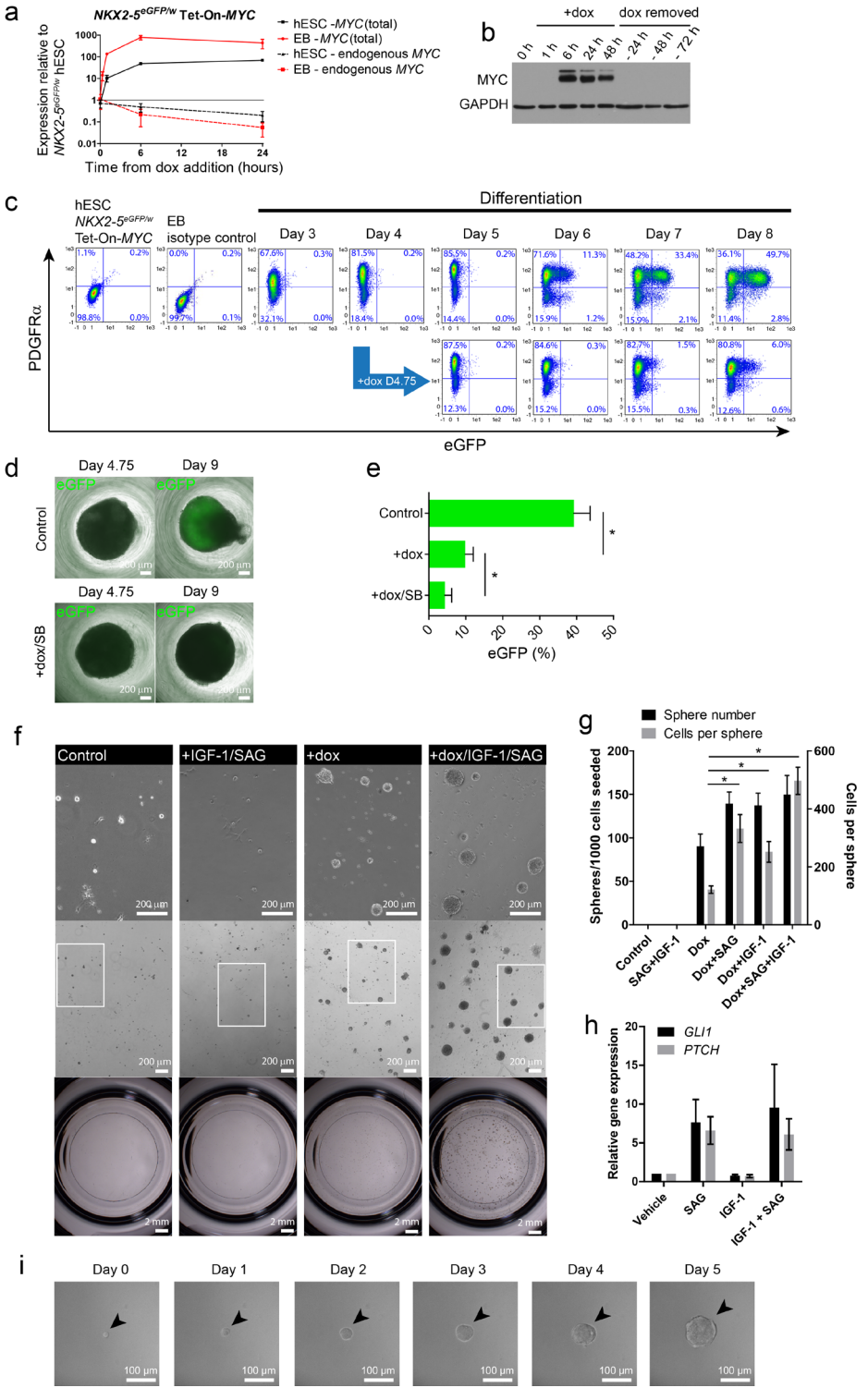
Regulated MYC expression restrains cardiac differentiation

A doxycycline-inducible MYC transgene (Tet-On-MYC) was introduced into an NKX2-5$^{eGFP/w}$ hESC line to allow MYC expression to be controlled during differentiation. In NKX2-5e$^{GFP/w}$ Tet-On-MYC hESCs and day 5 embryoid bodies (EBs) derived from them, MYC expression could be tightly regulated by doxycycline (dox) (**Figure 1a,b** and **Supplementary Figure 1**). High transgene expression was also evident given the autosuppression of endogenous MYC [18]. In the absence of dox these hESCs could differentiate to beating cardiomyocytes in EBs with similar efficiency as the parent line, making ~60% eGFP$^+$ cells by day 9 of differentiation (**Supplementary Figure 2a,b**). Activation of MYC expression by addition of dox during cardiac differentiation at day 5.5 or beyond had little impact on the expression of NKX2-5–eGFP (**Supplementary Figure 2c**), whereas dox addition at day 4.75 significantly blocked differentiation from the PDGFR-α^+ state to the NKX2-5–eGFP$^+$ state (**Figure 1c,e and Supplementary Figure 2e**). There was no such effect of dox on eGFP expression in the parent line (**Supplementary Figure 2b**). We also analyzed the expression kinetics of the posterior heart field marker podoplanin (PDPN) (**Supplementary Figure 2d**). PDPN was highly expressed in undifferentiated hESCs and was maintained in derivative NKX2-5–eGFP$^+$ cardiomyocytes, whereas in the heart myocardium PDPN expression is restricted largely to the SAN [19]. These data suggest that PDPN may have utility as a marker of both primitive CPCs and SAN-like derivatives in this system.

With the aim of further restricting CPC differentiation–inducing signaling, we added SB431542 (SB) together with dox to inhibit endogenous transforming growth factor-β (TGF-β)–activin signaling; this further restrained NKX2-5–eGFP induction as measured on day 8 (**Figure 1d,e**).

CPCs proliferate with defined mitogenic stimulation

To investigate the proliferative capacity of this largely PDGFR-α^+, pre–NKX2-5$^+$, putative CPC-encompassing population, we seeded cells at day 6 of EB differentiation at low density on a soft basement membrane. With maintained MYC expression in the continued presence of dox, cells proliferated to form small spheres (**Figure 1f**). If dox was not added or was removed on seeding, spheres did not form, and cell proliferation was not apparent on this substrate. Yet dox combined with SB was insufficient to robustly sustain the culture in a growing state beyond this first expansion, so additional mitogenic stimulants or supportive factors were sought.


a
NKX2-5eGFP/w Tet-On-MYC
hESC -MYC(total)
EB -MYC(total)
hESC - endogenous MYC
EB - endogenous MYC
Expression relative to NKX2-5eGFP/w hESC
Time from dox addition (hours)
b
+dox
dox removed
0 h
1 h
6 h
24 h
48 h
- 24 h
- 48 h
- 72 h
MYC
GAPDH
c
hESC
NKX2-5eGFP/w
Tet-On-MYC
EB
isotype control
Differentiation
Day 3
Day 4
Day 5
Day 6
Day 7
Day 8
PDGFRα
+dox D4.75
eGFP
d
Day 4.75
Day 9
Control
+dox/SB
eGFP
200 µm
e
Control
+dox
+dox/SB
eGFP (%)
f
Control
+IGF-1/SAG
+dox
+dox/IGF-1/SAG
200 µm
2 mm
g
Sphere number
Cells per sphere
Spheres/1000 cells seeded
Cells per sphere
Control
SAG+IGF-1
Dox
Dox+SAG
Dox+IGF-1
Dox+SAG+IGF-1
h
GLI1
PTCH
Relative gene expression
Vehicle
SAG
IGF-1
IGF-1 + SAG
i
Day 0
Day 1
Day 2
Day 3
Day 4
Day 5
100 µm

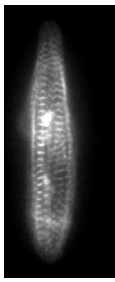


Figure 1- The expansion of early pluripotent stem cell derived cardiac cells. **A.** Time-course of MYC mRNA induction by doxycycline (dox) in NKX2-5eGFP/w Tet-On-MYC hESCs and embryoid bodies (EB). Expression is shown relative to the parent line. The lower panel shows the MYC protein induction time-course in EBs and reversal on dox removal. **B.** FACS plots for PDGFRα and **C.** Podoplanin in undifferentiated NKX2-5eGFP/w Tet-On-MYC hESCs and during a time-course of cardiac differentiation. eGFP fluorescence, reporting NKX2-5 expression, is shown on the horizontal axis. The lower panel of each shows the time-course following dox addition from day 4.75. **D.** Representative EBs imaged at day 4.75 and again at day 9 showing the effect of dox/SB addition on eGFP induction. **E.** The percentage of eGFP+ cells on day 8, with EBs maintained in the indicated conditions from day 4.75. **F.** Cultures maintained in the indicated conditions, imaged 6 days after dissociation (of day 6 EBs). The bottom panel shows the whole well. The upper images are magnifications at 4X and 10X (highlighted area). **G.** Quantification of sphere number and size (cells/sphere) after 6 days. **H.** Relative mRNA expression of hedgehog pathway response genes measured in spheres after expansion in dox/SB plus the factors indicted. **I.** Time-lapse imaging showing a single cell proliferating to form a sphere. Error bars signify SEM. *P<0.05 Paired t-test.

Roles have been proposed for IGF-1 and hedgehog signaling in CPC proliferation during cardiac development [20,21]. Dox combined with SB and IGF-1 or SAG (an agonist of Smoothened, part of the hedgehog signaling pathway) increased proliferation within spheres by 2.1-fold or 2.7-fold, respectively (**Figure 1f,g**). Whereas dox combined with SB, IGF-1 and SAG had an additive effect, increasing proliferation by 4.1-fold, MYC remained essential. The expression of SAG-induced hedgehog response genes GLI1 and PTCH1 was not modified by IGF-1, suggesting that the additive potentiation was not due to enhanced hedgehog signaling (**Figure 1h**). Time-lapse imaging showed that spheres were typically clonal (**Figure 1i** and **Supplementary Video 1**) and remained NKX2-5–eGFP^{-} under these conditions.

Concerted FGF and BMP signaling induce NKX2-5 expression

As these sphere-forming cells might be in a developmental state equivalent to pre–NKX2-5^{+} CPCs, we tested whether expression of NKX2-5–eGFP could be induced in this population by FGF and BMP signaling, as occurs during heart development [22–26]. For this experiment, spheres were generated in medium containing dox, SB, IGF-1 and SAG (DSIS) in the presence or absence of basic FGF (bFGF) and/or BMP4. SB does not interfere with BMP signaling [27]. After 6 d, bFGF had potently induced NKX2-5–eGFP expression in a concentration-dependent manner yet also reduced the number of spheres formed (**Figure 2a–d**). BMP4 alone had little impact on NKX2-5–eGFP expression but markedly potentiated induction by bFGF and, when combined with 1 ng/ml bFGF, was sufficient to induce NKX2-5–eGFP expression in >95% of cells and to a higher intensity. BMP4 in combination with bFGF also increased sphere formation compared to bFGF alone (**Figure 2c**). Inhibition of BMP signaling with dorsomophin-homolog 1 (DMH1) restricted NKX2-5–eGFP induction by bFGF and completely blocked sphere formation at higher concentrations of bFGF. A time-course experiment showed eGFP expression after 48 h of exposure to bFGF and BMP4, and this expression reverted on factor withdrawal (**Supplementary Figure 3**). Both the CPC marker PDGFR-α and the primitive CPC–SAN marker PDPN were downregulated with increasing concentrations of bFGF and BMP4, creating heterogeneity in addition to the variation in NKX2-5–eGFP levels (**Figure 2a,b**).

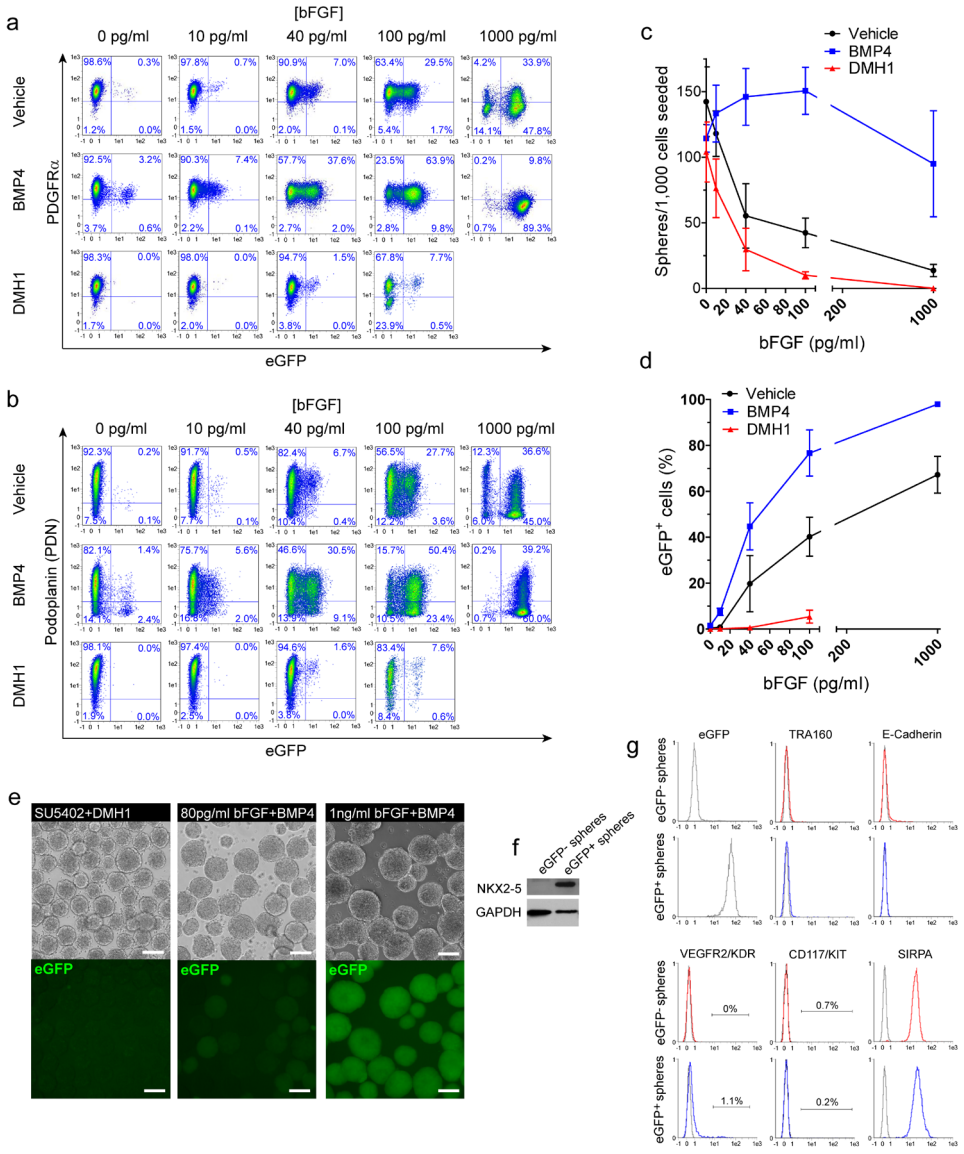
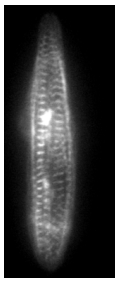


Figure 2- NKX2-5eGFP expression is activated in spheres by concerted FGF and BMP signalling. **A.** FACS measurements for PDGFRα and **B.** Podoplanin (PDN) together with eGFP, of spheres expanded in: vehicle, BMP4 or the BMP signalling-inhibitor DMH1, in concert with a range of bFGF concentrations. **C.** Sphere number in each condition. **D.** eGFP$^+$ cells in spheres of each condition. **E.** Representative spheres (in suspension after collection) following expansion in the indicated conditions. SU5402 = FGF receptor inhibitor. **F.** FACS measurement of eGFP$^-$ and eGFP$^+$ spheres for additional cell surface makers. Unlabelled/isotype control-labelled cells are shown in grey and specific antibody-labelled cells in red (eGFP$^-$) or blue (eGFP$^+$).



To additionally suppress endogenous FGF signaling and minimize differentiation, we pro-

duced NKX2-5-eGFP$^-$PDPN$^+$ spheres in the presence of an FGF receptor inhibitor (SU5402) as well as DMH1 (**Figure 2e**). Differences in NKX2-5 expression were confirmed by western blotting (**Figure 2f** and **Supplementary Figure 4**). **Figure 2g** shows an analysis of surface markers in NKX2-5–eGFP$^-$PDPN$^+$ cells expanded in DSIS with SU5402 and DMH1, compared to the most divergent NKX2-5–eGFP$^+$ cells expanded in DSIS with 1 ng/ml bFGF and BMP4. The pluripotent markers TRA160 and E-cadherin were absent, as were vascular endothelial growth factor receptor 2 (VEGFR2, here referred to as KDR) and stem cell factor receptor c-Kit (CD117); however, the CPC marker SIRPA was expressed in both sphere populations (data on additional surface markers are shown in **Supplementary Figure 5**). Downregulation of KDR and CD13 is consistent with their being earlier mesodermal markers [28–30], and the absence of CD117 is consistent with cardiac lineage–tracing data [31].

CPC patterning mimics features of heart field development

By regulating FGF and BMP signaling, we generated seven putative CPC sphere populations and isolated them by fluorescence-activated cell sorting (FACS) for gene expression and differentiation analysis (**Figure 3a**). Inhibition of both signaling pathways enriched the NKX2-5–eGFP$^-$PDPN^{high} (population 1), whereas exposure to BMP4 alone (with FGF signaling inhibited) or BMP4 and bFGF (80 pg/ml or 1 ng/ml) allowed isolation of cells with different NKX2-5–eGFP and PDPN expression: eGFP$^-$PDPN$^+$ (population 2), eGFP$^-$PDPN$^-$ (population 3), eGFP^{low}PDPN$^+$ (population 4), eGFP^{low}PDPN$^-$ (population 5), eGFP$^+$PDPN$^+$ (population 6) and eGFP$^+$PDPN$^-$ (population 7) (**Figure 3a,b**).

Comparison of these cells with earlier MESP1$^+$ mesodermal cells isolated from a MESP1 reporter derivative of the same hESC line28 showed much lower expression of MESP1 in all sphere populations (**Figure 3c**). NKX2-5 and PDPN expression confirmed expectations based on eGFP levels and sorting and antibody fidelity. The genes ISL1, MEF2C, SMARCD3 and TBX5, encoding cardiac transcriptional regulators, were all upregulated compared to their expression in the MESP1$^+$ cells and were expressed in the NKX2-5–eGFP$^-$PDPN^{high} population before BMP exposure. Whereas expression of the SAN-regulatory genes TBX3 and SHOX2 was lower in spheres, TBX18 was induced, most notably in the NKX2-5–eGFP$^-$PDPN$^+$ populations. Notably, HCN4, which in vivo in the mouse marks early differentiating FHF CPCs that give rise to primitive left ventricular progenitors [14,16], was induced by BMP4 exposure in this system and remained low in the NKX2-5–eGFP$^-$PDPN^{high} population. These data raise the testable hypothesis that BMP signaling, together with FGF, controls the transition from a multipotent CPC (SHF-like) to a ventricular-specified progenitor (FHF-like). Microarray analysis of five of the populations revealed a large number of genes differentially regulated by BMP4 or bFGF and BMP4, and very close clustering of the subsets positive or negative for PDPN (**Supplementary Figure 6** and **Supplementary Data Set 1**).

To induce differentiation, we removed dox to turn off MYC transgene expression and plated cells in defined endothelial- or cardiomyocyte-promoting conditions. Endothelial induction was based on vascular endothelial growth factor (VEGF) and SB (to block the TGF-β activity from the substrate) [32], with a low concentration of bFGF to preserve viability.

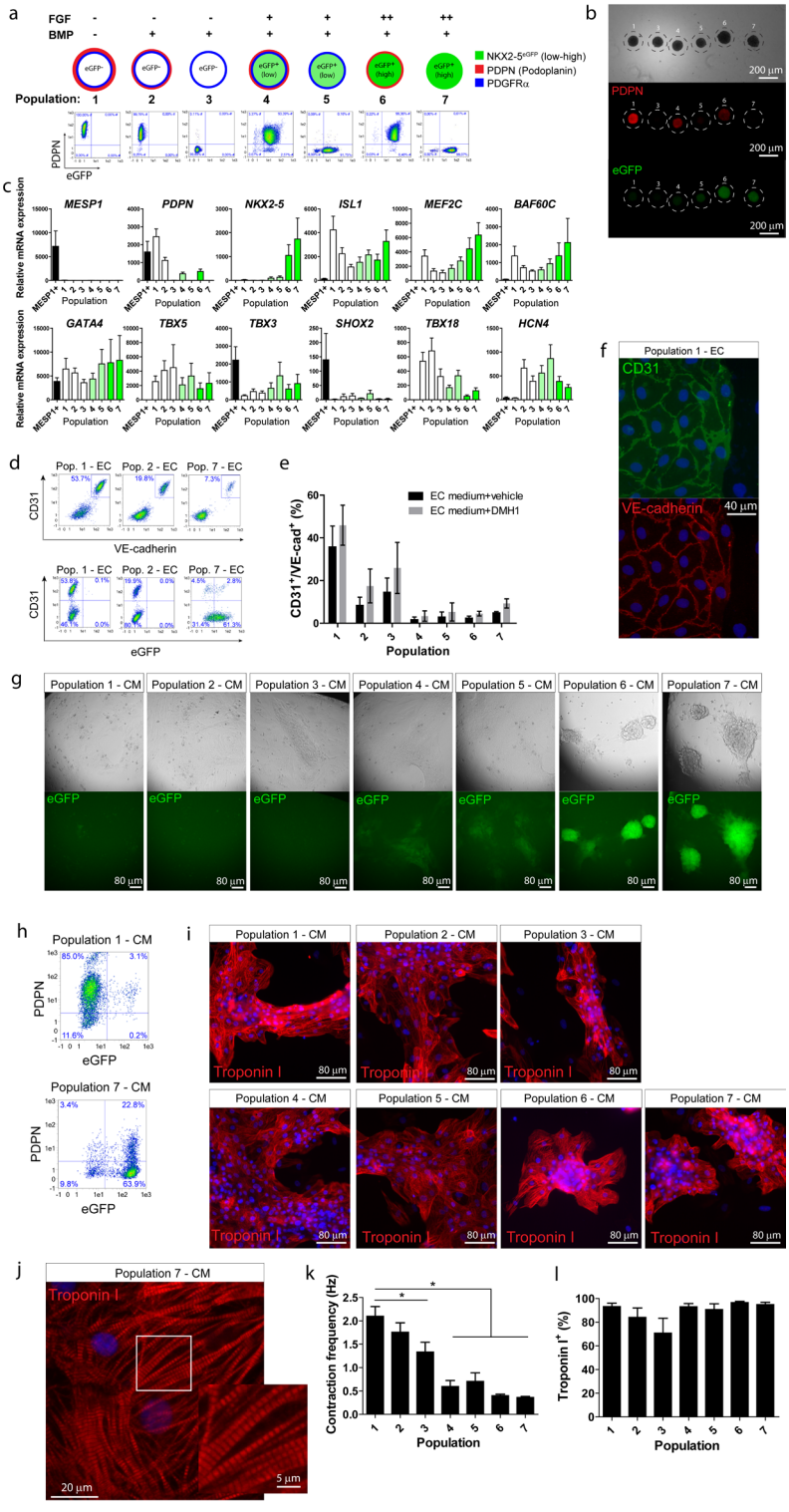

a
FGF
BMP
Population: 1 2 3 4 5 6 7
NKX2-5eGFP (low-high)
PDPN (Podoplanin)
PDGFRα
PDPN
eGFP
b
PDPN
eGFP
200 µm
c
Relative mRNA expression
MESP1
PDPN
NKX2-5
ISL1
MEF2C
BAF60C
GATA4
TBX5
TBX3
SHOX2
TBX18
HCN4
Population
d
Pop. 1 - EC
Pop. 2 - EC
Pop. 7 - EC
CD31
VE-cadherin
eGFP
e
EC medium+vehicle
EC medium+DMH1
CD31+/VE-cad+ (%)
Population
f
Population 1 - EC
CD31
VE-cadherin
40 µm
g
Population 1 - CM
Population 2 - CM
Population 3 - CM
Population 4 - CM
Population 5 - CM
Population 6 - CM
Population 7 - CM
eGFP
80 µm
h
Population 1 - CM
Population 7 - CM
PDPN
eGFP
i
Troponin I
80 µm
j
Population 7 - CM
Troponin I
20 µm
5 µm
k
Contraction frequency (Hz)
Population
l
Troponin I+ (%)
Population

Figure 3- Characterization of sphere heterogeneity and differentiation potential. **A.** Schematic showing seven sphere identities and the signalling configuration used to enrich for each. Beneath each are FACS plots showing population purity after sorting by the above markers. **B.** Individual spheres labelled live with an anti-PDN-PE antibody demonstrating the range of clonal identities. **C.** Gene expression analysis for the sorted sphere populations compared to earlier MESP1+ mesodermal progenitors (n=4). **D.** FACS measurements after differentiation of sorted populations towards endothelial cells. The upper and lower panel of each population are the same cells showing different channels. **E.** Mean percentage of endothelial cells on differentiation with or without DMH1 (n=3). **F.** Immunostaining showing typical CD31+/VE-cadherin+ endothelial cells derived from 'Population 1'. **G.** Live cell images of brightfield and eGFP after differentiation of sorted populations towards cardiomyocytes. All fields contained substantial areas of contraction. Corresponding to the areas in Supplementary video 2. **H.** FACS measurement of Population 1 and 7 for PDN and eGFP, after differentiation towards cardiomyocytes. **I.** Immunofluorescence for Troponin I after cardiomyocyte differentiation of sorted populations. **J.** Higher magnification of Population 7 to highlight the sarcomeric organization. **K.** Average contraction frequency of beating areas measured 10 days after differentiation (n=3). **L.** Mean percentage of Troponin I^+ cells (n=3). Error bars signify SEM. *P<0.05 One-way ANOVA with Bonferroni's correction.

Cardiomyocyte induction involved transient FGF and BMP signaling [33,34], with Wnt signaling inhibited [35] and exposure to TGF-β between 24 and 72 h to promote full differentiation [36]. A minimal change in bFGF concentration from the specific growth medium to the initial cardiomyocyte induction medium (i.e., in the first 24 h after dox removal) gave optimal viability and differentiation. IGF-1 and hedgehog signaling have additional roles in cardiac differentiation and so were kept active. The NKX2-5–eGFP$^-$PDPN^{high} population gave rise to VE-cadherin$^+$ (VE-cad$^+$) CD31$^+$ endothelial cells with the highest efficiency (46 ± 9%, s.e.m.), whereas eGFP$^+$ cells were much more restricted (**Figure 3d–f**). The presence of the BMP inhibitor DMH1 throughout differentiation improved endothelial differentiation efficiency in every population. In cardiomyocyte-promoting conditions, all populations differentiated with very high efficiency to spontaneously contracting cells. NKX2-5–eGFP expression status was largely maintained on differentiation, with NKX2-5–eGFP$^-$ CPCs unexpectedly giving rise primarily to NKX2-5–eGFP$^-$ cardiomyocytes (**Figure 3g–i** and **Supplementary Video 2**). The bFGF and BMP4 present in this window of differentiation as cardiomyocyte-inducing factors were apparently insufficient to induce substantial stable NKX2-5–eGFP expression in these populations. A time-course experiment during differentiation of these CPCs showed that eGFP induction was low (detected in <10% of cells) and mostly transient during this exposure period (**Supplementary Figure 7**), contrasting with the higher sensitivity of proliferating CPCs. On differentiation of populations 6 and 7, NKX2-5–eGFP expression was maintained and became stable and independent of bFGF and BMP4. Apart from derivatives of population 3, all cultures were >80% troponin I+ (**Figure 3l**). Sarcomeric organization was evident in cardiomyocytes from all populations but was particularly striking in cardiomyocytes from populations 6 and 7 (**Figure 3j** and **Supplementary Figure 8**). Contraction frequency was much higher in the cardiomyocyte monolayers from CPC population 1 (**Figure 3k**). Contractility of these cells also seemed to have more limited dynamic range, contrasting with the lower frequency and more highly dynamic contractility of the NKX2-5–eGFP$^+$ cultures.

Together with the observation of greater potential for endothelial differentiation, these data suggested that the ISL1-expressing NKX2-5– eGFP−PDPNhigh CPCs might resemble primitive SHF-like CPCs and, consequently, be competent for SAN lineage specification.

CPC differentiation to pacemaker and ventricular myocytes

To better characterize the two most divergent populations, we compared gene expression after cardiomyocyte differentiation of NKX2-5–eGFP^{-}PDPN^{high} and NKX2-5–eGFP^{+}PDPN^{-} CPCs, with standard hESC-derived cardiomyocytes from the parental line used as a reference (Supplementary Table 1). Sarcomere-related transcripts from TNNT2 and MYL7 were induced equally in both populations, consistently with a general cardiomyocyte identity (**Figure 4a**). Equal α-actinin protein expression was also observed (**Figure 4b** and **Supplementary Figure 9**). By contrast, the ventricular marker MYL2 (encoding MLC2V) was 40-fold higher in the NKX2-5–eGFP^{+}PDPN^{-} than in the NKX2-5–eGFP^{-}PDPN^{+} cardiomyocytes ($P < 0.05$), and SCN5A, encoding cardiac sodium channel, was also significantly higher in the same population ($P < 0.05$). The difference in MLC2V expression was confirmed by immunostaining (**Supplementary Figure 10**). Expression of the genes TBX5, MEF2C, GATA4, SMARCD3, HAND1, HAND2 and MYOCD, encoding cardiac transcriptional regulators, was increased similarly in each lineage and these genes were also expressed at similar levels in the reference cardiomyocytes. However, consistently with the premise that the NKX2-5–eGFP−PDPNhigh CPCs tend toward a SAN fate under these conditions, this lineage showed much higher induction of TBX3 and SHOX2 (11-fold and 289-fold, respectively) ($P < 0.05$), TBX18 (3.6-fold) and HCN4, the dominant HCN transcript underlying the hyperpolarization-activated current (If) in SAN [37] (4.3-fold). Despite these differences, which suggest regional specification, the chamber myocardial marker NPPA was induced on differentiation of both populations, and CX40 and CX43, which encode gap junction proteins, were equally expressed. Whether a functional pacemaker phenotype would develop despite seemingly inappropriate expression of such genes requires further validation.



Contracting monolayers of NKX2-5–eGFP^{+}PDPN^{-} and NKX2-5–eGFP^{-}PDPN^{+} cardiomyocytes were dissociated to single cells on micropatterned polyacrylamide gels for electrophysiological and contraction stress measurement (**Figure 4c,d**). Spontaneously active and virtually quiescent single cells were subsequently observed in both groups. After electrophysiological analysis, the quiescent cells could be subdivided into those with a depolarized (higher than −50 mV) maximal diastolic potential (MDP) (**Figure 4e**) or an MDP of approximately −75 mV (**Figure 4f**). Action potentials (APs) could be elicited by suprathreshold current pulses through the patch pipette in the latter group (**Figure 4f**) but not in those that were depolarized. Quiescent cells with an MDP of around −75 mV were observed only in the NKX2-5–eGFP^{+}PDPN^{-} group. **Figure 4g** shows typical examples of spontaneous APs of NKX2-5–eGFP^{+}PDPN^{-} and NKX2-5–eGFP−PDPN+ cells (average AP parameters are summarized in Table 1). AP parameters were notably different between the spontaneously active cells of each group. NKX2-5–eGFP^{-}PDPN^{+} cells had a higher MDP and a faster diastolic depolarization rate (DDR), which resulted in pacemaker activity with a shorter intrinsic cycle length (CL). Their maximal AP upstroke velocity (dV/dtmax) was also lower. In both cell types APs overshot the zero potential value, but the AP amplitude (APA) was lower in NKX2-5–eGFP^{-}PDPN^{+} cells. APs of NKX2-5–eGFP^{-}PDPN^{+} cells repolarized earlier and faster, resulting in shorter AP duration at 20%, 50% and 90% repolarization (APD20, APD50 and APD90, respectively). Of note, the stimulated (previously quiescent) NKX2-5–eGFP^{+}PDPN^{-} cells had a more polarized MDP and higher APA and dV/dtmax than did the

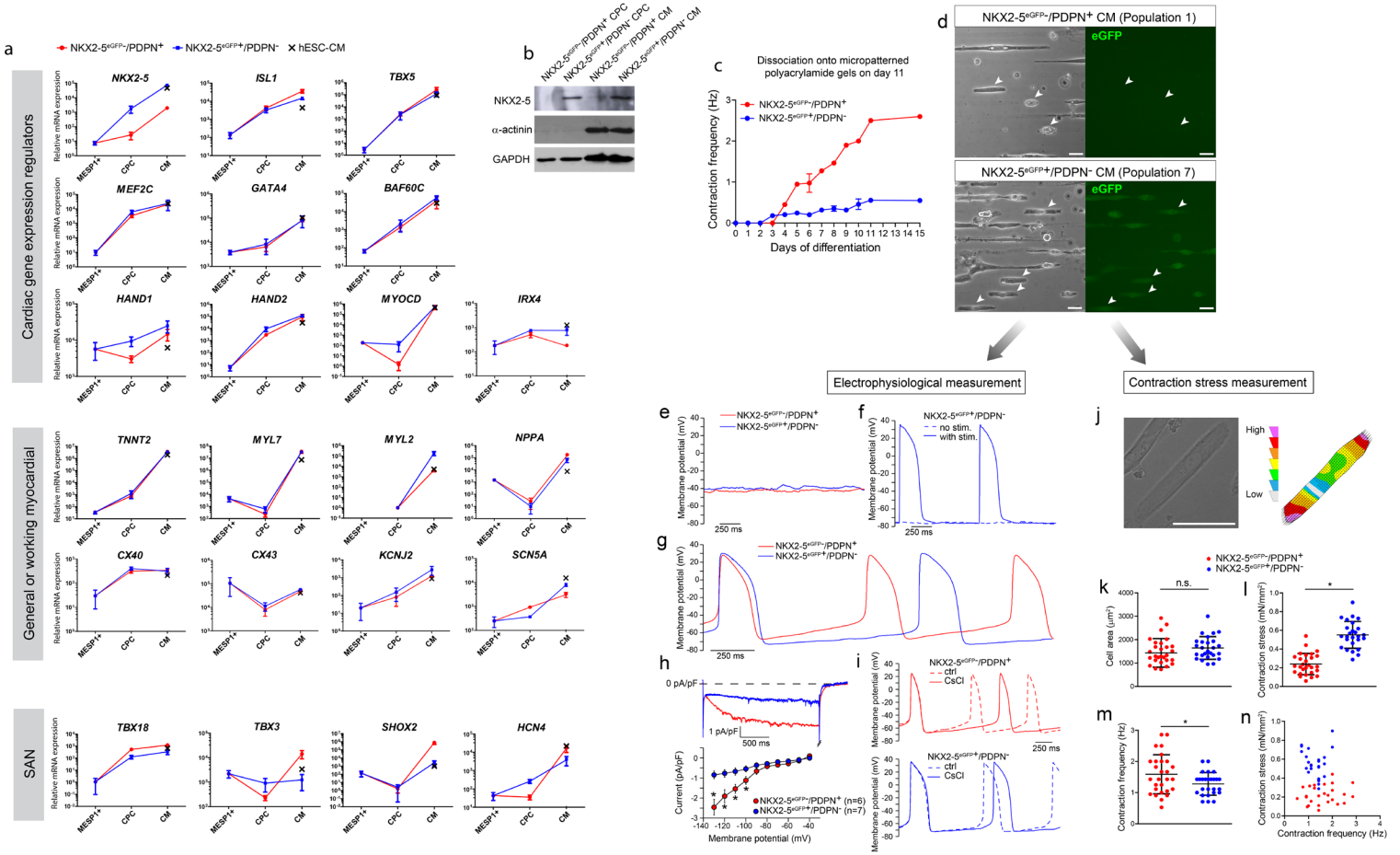

a
NKX2-5eGFP-/PDPN+
NKX2-5eGFP+/PDPN-
hESC-CM
Cardiac gene expression regulators
General or working myocardial
SAN
Relative mRNA expression
MESP1+
CPC
CM
NKX2-5
ISL1
TBX5
MEF2C
GATA4
BAF60C
HAND1
HAND2
MYOCD
IRX4
TNNT2
MYL7
MYL2
NPPA
CX40
CX43
KCNJ2
SCN5A
TBX18
TBX3
SHOX2
HCN4
b
NKX2-5eGFP-/PDPN+ CPC
NKX2-5eGFP+/PDPN- CPC
NKX2-5eGFP-/PDPN+ CM
NKX2-5eGFP+/PDPN- CM
NKX2-5
α-actinin
GAPDH
c
Dissociation onto micropatterned polyacrylamide gels on day 11
NKX2-5eGFP-/PDPN+
NKX2-5eGFP+/PDPN-
Contraction frequency (Hz)
Days of differentiation
d
NKX2-5eGFP-/PDPN+ CM (Population 1)
NKX2-5eGFP+/PDPN- CM (Population 7)
eGFP
Electrophysiological measurement
Contraction stress measurement
e
NKX2-5eGFP-/PDPN+
NKX2-5eGFP+/PDPN-
Membrane potential (mV)
250 ms
f
NKX2-5eGFP+/PDPN-
no stim.
with stim.
g
h
0 pA/pF
1 pA/pF
500 ms
Current (pA/pF)
NKX2-5eGFP-/PDPN+ (n=6)
NKX2-5eGFP+/PDPN- (n=7)
Membrane potential (mV)
i
NKX2-5eGFP-/PDPN+
ctrl
CsCl
NKX2-5eGFP+/PDPN-
j
High
Low
k
n.s.
Cell area (μm²)
l
*
Contraction stress (mN/mm²)
m
*
Contraction frequency (Hz)
n
Contraction stress (mN/mm²)
Contraction frequency (Hz)

Figure 4- "Working" ventricular-like and pacemaker-like cardiomyocyte functions recapitulated. **A.** Gene expression analysis, grouped into three gene categories, showing 3 stages of cardiac differentiation: MESP1$^+$ mesodermal progenitors, NKX2-5eGFP$^-$/PDN$^+$ or NKX2-5eGFP$^+$/PDN$^-$ CPCs, and the cardiomyocytes derived from differentiation of each CPC population. The expression of normal/control hESC-derived cardiomyocytes (hESC-CM) is shown for reference. **B.** Contraction frequency measured over time from the induction of cardiomyocyte differentiation (n=2). **C.** Brightfield and eGFP images of typical aligned cells on micropatterned soft polyacrylamide, following dissociation of high density cultures. Contracting cells are indicated with arrows. Left panel: Electrophysiological measurement. **D.** Typical recordings of quiescent cells with a depolarized (>-50 mV) MDP. **E.** Representative example of a quiescent NKX2-5eGFP+/PDN- cell with a MDP of around -75 mV without and with suprathreshold stimulation. **F.** Typical examples of spontaneously active NKX2-5eGFP$^+$/PDN$^-$ and NKX2-5eGFP$^-$/PDN$^+$ cells. **G.** Typical If recordings in response to hyperpolarizing voltage steps from -40 to -130 mV (top panel) and average current-voltage relationships of If (bottom panel). **H.** Representative examples of action potentials in the absence (ctrl) and presence (after 5 mins) of 2 mM CsCl. Right panel: Contraction stress measurement. **I.** Representative contracting cell and conversion to vector displacement values. **J.** Single cell surface area values. **K.** Single cell contraction stress values. **L.** Single cell contraction frequency values. **M.** Single cell contraction stress values plotted against frequency. Error bars signify SEM. P<0.05 Student's t-test. n.s. = not significant.

spontaneously active ones (Table 1).

If is an important characteristic of pacemaker cells, including those of humans [37]. In NKX2-5–eGFP$^-$PDPN$^+$ cells, If density was ~100% higher than in NKX2-5–eGFP$^+$PDPN$^-$ cells ($P < 0.05$) (**Figure 4h**). In 6 out of the 9 NKX2-5–eGFP$^-$PDPN$^+$ cells and in 7 out of the 15 NKX2-5–eGFP$^+$PDPN$^-$ cells measured under current clamp conditions (Table 1), we assessed the contribution of If to pacemaker activity. If block by CsCl induced a reduction of DDR, as expected, and prolongation of the CL (**Figure 4i**). The DDR was reduced by an average of 43 ± 7% and 16 ± 7% (s.e.m.), whereas the CL was prolonged by 36 ± 6% and 14 ± 7% in NKX2-5–eGFP$^-$PDPN$^+$ and NKX2-5–eGFP$^+$PDPN$^-$ cells, respectively. The more pronounced decrease in DDR and prolongation of CL in NKX2-5–eGFP$^-$PDPN$^+$ cells is probably due to the higher If and HCN4 density in these cells.



Another difference between pacemaker and working myocardial cells is in their contractile force. We measured this using traction force microscopy (**Figure 4j**). Although spontaneously active NKX2-5–eGFP$^-$PDPN$^+$ and NKX2-5–eGFP$^+$PDPN$^-$ cardiomyocytes were of similar size (**Figure 4k**), the mean contraction stress was much lower in the NKX2-5–eGFP$^-$ cardiomyocytes ($P < 0.05$) (**Figure 4l** and **Supplementary Video 3**). The lower contraction stress in the NKX2-5–eGFP$^-$ cardiomyocytes was not due to their higher beating frequency (**Figure 4m**, $P < 0.05$), as shown by the frequency-contraction stress relationships (**Figure 4n**). The absence of a positive force-frequency relationship in either population is consistent with previous measurements in PSC-derived cardiomyocytes, which display a fetal level of maturity [38].

CPCs are clonogenic and possess long-term multipotency

We next tested how frequently clonal lineages of expanded NKX2-5–eGFP$^-$PDPN$^+$ cells retain the capacity to become NKX2-5–eGFP$^+$ as well as self-renew, and whether heterogeneity in differentiation potential existed across this population. Clonal NKX2-5–eGFP$^-$PDPN$^+$ spheres were dissociated into DSIS with SU5402 and DMH1 (self-renewal condition) or DSIS with 1 ng/ml bFGF and BMP4 (NKX2-5 inducing condition). After 6 d, eGFP was

Table 1. Action potential parameters of single NKX2-5^{eGFP+}/PDN^{-} and NKX2-5^{eGFP-}/PDN^{+} cells.

	NKX2-5^{eGFP+}/PDN^{-} cells		**NKX2-5^{eGFP-}/PDN^{+} cells**
	Stimulated at 1 Hz (n=6)	Spontaneous (n=15)	Spontaneous (n=9)
MDP (mV)	–78.7±1.4†	–74.4±0.7	–68.9±1.9*
dV/dt_{max} (V/s)	44.7±10.6†	16.0±2.7	6.7±1.3*
APA (mV)	105±3†	97±2	84±4*
APD_{20} (ms)	123±16	119±16.9	79±9*
APD_{50} (ms)	179±18	178±12	124±11*
APD_{90} (ms)	207±18	217±13	172±12*
Cycle length (ms)	–	1330±155	642±108*
DDR_{100} (mV/s)	–	21.6±2.4	37.3±6.2*

Data are mean±SEM; n=number of cells, MDP=maximal diastolic potential, DDR100=diastolic depolarization rate over the 100-ms time interval starting at MDP+1 mV, dV/dtmax=maximal upstroke velocity, APA=action potential amplitude, APD20, APD50, and APD90=action potential duration at 20, 50, and 90% repolarization, respectively. † $p<0.05$ stimulated vs spontaneously active NKX2-5^{+}/PDN^{-} cells. * $p<0.05$ spontaneously active NKX2-5eGFP+/PDN- vs spontaneously active NKX2-5eGFP^{-}/PDN^{+} cells.

induced in >95% of cells from clones expanded in bFGF and BMP4 and in none of those maintained in the inhibitors, where the NKX2-5–eGFP^{-}PDPN^{+} status was largely preserved (**Supplementary Figure 11**). Endothelial differentiation capacity remained stronger in NKX2-5–eGFP^{-}PDPN^{+} spheres, whereas both populations could generate a high percentage of cardiomyocytes (median troponin I^{+}, ≥90%). Clone-to-clone variation was relatively small, indicating that the initial NKX2-5–eGFP^{-}PDPN^{+} sphere population may be uniform. The self-renewal of this early SHF-like progenitor population presents an opportunity for applying patterning with retinoic acid to direct CPC specification toward the atrial lineage. The expression profile of cardiomyocytes generated from CPCs exposed to 10 nM retinoic acid prior to differentiation suggested that this response may be present in these cells (**Supplementary Figure 12**).

To assess the long-term potential of NKX2-5–eGFP^{-}PDPN^{+} spheres and their NKX2-5–eGFP^{+} derivative spheres, we expanded the cultures over multiple passages (**Figure 5a,b**). Cells maintained in DSIS with bFGF and BMP4 had a shorter doubling time that did those in DSIS with SU5402 and DMH1 (15.3 h versus 18.6 h, respectively). In three separate experiments the lifespan of NKX2-5–eGFP^{-}PDPN^{+} spheres in DSIS with SU5402 and DMH1 was ~50 population doublings, at which point the cells abruptly stopped growing, whereas cells in DSIS with bFGF and BMP4 grew for >80 doublings without reaching senescence. NKX2-5–eGFP induction capacity was well preserved in NKX2-5–eGFP^{-}PDPN^{+} CPCs maintained with SU5402 and DMH1, with ~80% of cells, on average, capable of full induction beyond 40 doublings (**Figure 5c,d**). These cells could also generate >30% endothelial cells beyond 35 doublings, whereas CPCs induced to NKX2-5–eGFP^{+} status were progressively restricted (**Figure 5e**), as observed above (**Figure 3e**). Cardiomyocyte differentiation was >80% efficient up to around 30 doublings in all three populations (**Figure 5f**), beyond which distinctly striated α-SMA^{+} smooth muscle–like cells (troponin I^{-}) became increasingly prevalent, resulting in more mixed populations (**Figure 5g**). NKX2-5–eGFP expression was difficult to maintain uniformly beyond 50 doublings (**Supplementary Figure 13**).

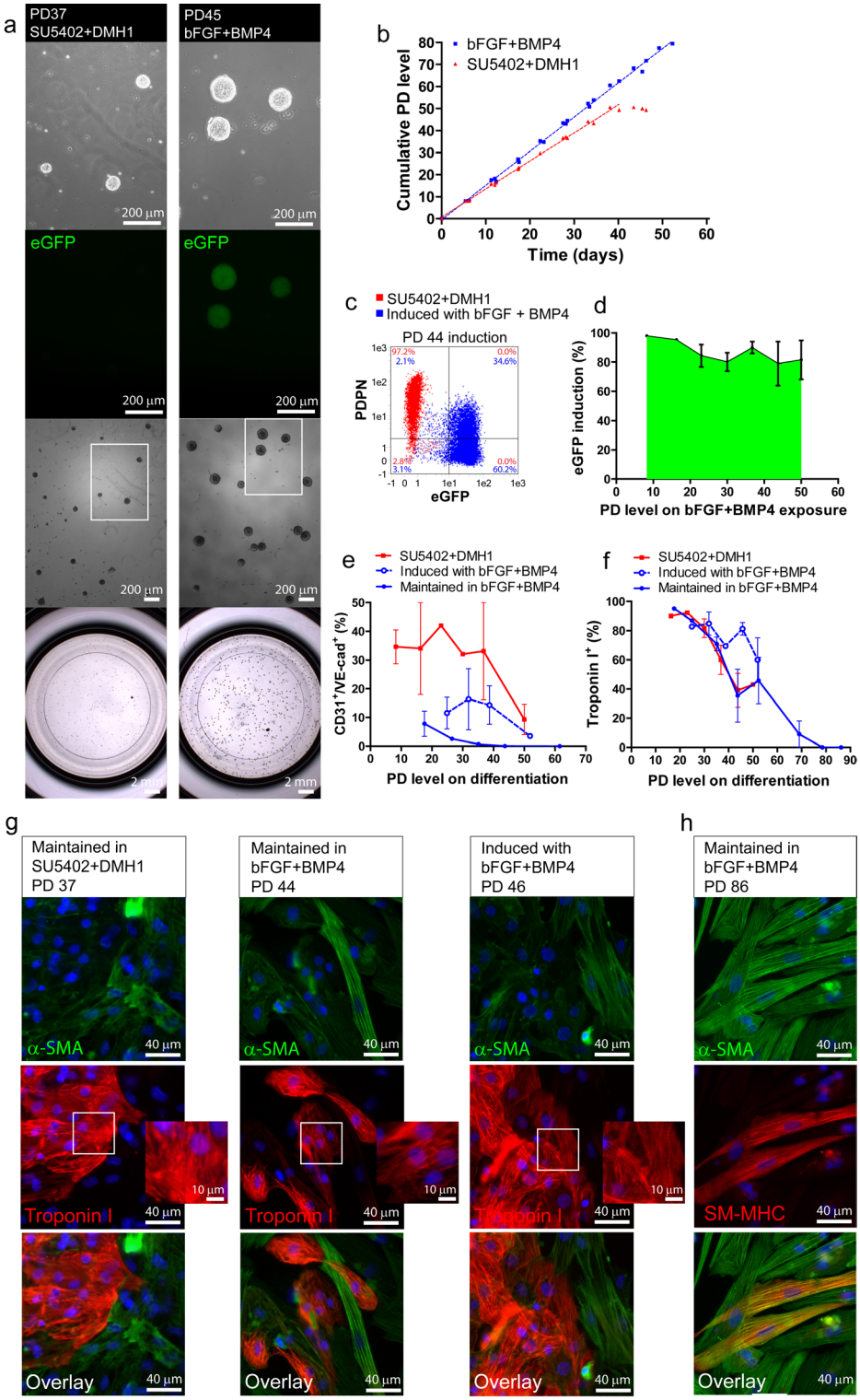

a
PD37
SU5402+DMH1
PD45
bFGF+BMP4
200 µm
eGFP
2 mm
b
bFGF+BMP4
SU5402+DMH1
Cumulative PD level
Time (days)
c
SU5402+DMH1
Induced with bFGF + BMP4
PD 44 induction
PDPN
eGFP
97.2%
2.1%
0.0%
34.6%
2.8%
3.1%
0.0%
60.2%
d
eGFP induction (%)
PD level on bFGF+BMP4 exposure
e
SU5402+DMH1
Induced with bFGF+BMP4
Maintained in bFGF+BMP4
CD31+/VE-cad+ (%)
PD level on differentiation
f
SU5402+DMH1
Induced with bFGF+BMP4
Maintained in bFGF+BMP4
Troponin I+ (%)
PD level on differentiation
g
Maintained in SU5402+DMH1 PD 37
Maintained in bFGF+BMP4 PD 44
Induced with bFGF+BMP4 PD 46
h
Maintained in bFGF+BMP4 PD 86
α-SMA
Troponin I
SM-MHC
Overlay
40 µm
10 µm

Figure 5- Clonal analysis of NKX2-5eGFP^{-}/PDN^{+} spheres shows self-renewal and universal potential for endothelial and cardiomyocyte differentiation. **A.** Individual clonal NKX2-5eGFP^{-}/PDN^{+} spheres were isolated and dissociated for expansion in **B.** (**i**) DSIS+SU5402+DMH1 or (**ii**) DSIS+1 ng/ml bFGF+BMP4. Representative images are shown after expansion of one clone. **C.** (**i**) eGFP and Podoplanin (PDN) measurement in each clone after expansion in (**i**) DSIS+SU5402+DMH1 or (**ii**) DSIS+bFGF+BMP4. FACS plots are shown for 3 clones. **D.** Representative brightfield images taken 4 days after the start of endothelial or cardiomyocyte differentiation for clone 27, after expansion in (**i**) DSIS+SU5402+DMH1 or (**ii**) DSIS+bFGF+BMP4. The cell clustering seen in the cardiomyocyte-promoting condition is strongly associated with a cardiomyocyte fate. **E.** Percentage of CD31+ endothelial cells derived from each clone expanded in (**i**) DSIS+SU5402+DMH1 or (**ii**) DSIS+bFGF+BMP4. FACS plots are shown for 3 clones. **F.** Percentage of Troponin I+ cells from each clone after expansion in (**i**) DSIS+SU5402+DMH1 or (**ii**) DSIS+bFGF+BMP4. Immunofluorescence images of two clones are shown, and were representative.

Spheres induced over one passage with bFGF and BMP4 gave the highest percentage of cardiomyocytes at higher doubling levels. Beyond 78 doublings, only smooth-muscle cells were generated. The more definitive smooth-muscle marker SM-MHC was also evident in many of these cells (**Figure 5h**).

Discussion

Studies in developmental biology have provided the foundation for the understanding and control of hPSC differentiation. This has led to effective methods for generating cardiac cell types, but difficulties in maintaining CPCs have hindered specific reconstruction of some aspects of heart development [5]. In this study we developed a system enabling the isolation and robust expansion of pure populations of hPSC-derived CPCs. A central feature of our method is the use of controlled MYC expression to facilitate the maintenance of CPCs. When expressed in a defined time window, MYC arrested CPCs at a pre–NKX2-5^{+} multipotent stage and acted as an essential permissive element in their continued expansion through IGF-1 and hedgehog signaling. In mouse development, c-Myc mRNA is clearly detectable in the embryonic heart and decreases markedly in the neonate [39].

Cardiogenesis is regulated by the tight spatial and temporal control of secreted factors at specific concentrations [40]. Although the early cardiogenic roles of cytokines including BMP, activin and Wnt have been well characterized in the PSC system [17,35,41], control of CPC specification has not be as well studied. The expression of FGF and BMP, particularly by endoderm and ectoderm adjacent to the heart-forming region, is thought to underlie early NKX2-5 expression [22,24–26]. These tissues may have similar inducing roles on the later-differentiating SHF progenitor population, with additional signaling sources being the SHF progenitors themselves and the primary myocardium [7,42]. Here we show that the developmental roles of FGF and BMP are reenacted in hPSC CPCs, and by modulating these signaling pathways we were able to recreate the gene expression signatures of early heart field development (**Figure 6**) and direct the patterned CPCs toward NKX2-5–eGFP^{-} PDPN^{+} pacemaker-like myocytes or NKX2-5–eGFP^{+} ventricular-like working myocytes with appropriate electrophysiological and contractile characteristics. CPC-derived NKX2-5–eGFP^{+} cardiomyocytes had well-organized sarcomeres and encompassed a population of highly polarized quiescent cells excitable by stimulation—the signature of mature working myocytes. By contrast, the pacemaker-like cells exhibited rapid spontaneous activity owing to their higher If. Additionally, we found that NKX2-5–eGFP^{-}PDPN^{+} CPCs were uniquely

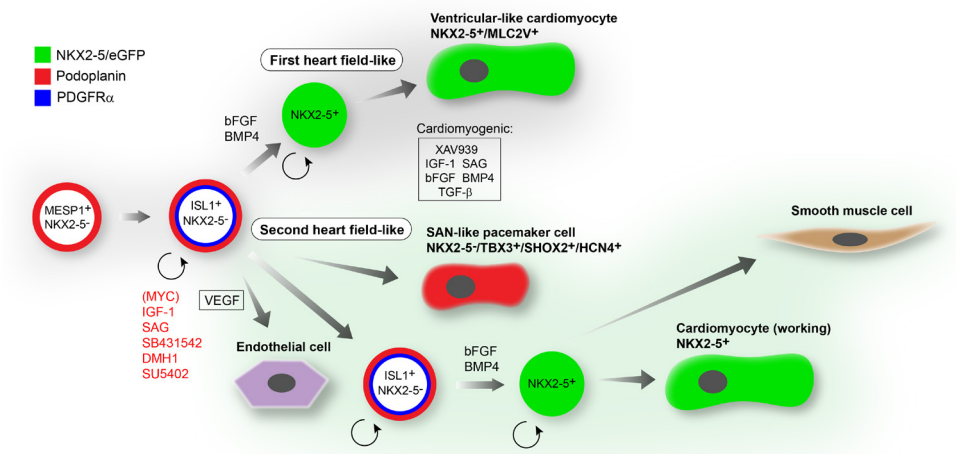
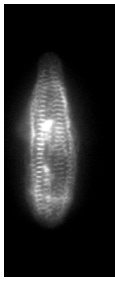


Figure 6- Long term expansion and differentiation analysis of CPCs. **A.** CPC spheres expanded for 37 population doublings (PD) in DSIS+SU5402+DMH1 (eGFP-) or 45 PD in 1 ng/ml bFGF+BMP4 (eGFP+). Images for each condition are of one dish at different magnifications. **B.** Growth curves for each culture condition (n=3 expansions). **C.** NKX2-5eGFP induction capacity from DSIS+SU5402+DMH1 on exposure to bFGF+BMP4, measured at progressive population doubling levels. **D.** CPCs expanded to PD 44 in DSIS+SU5402+DMH1 (red), tested for NKX2-5eGFP-induction capacity by bFGF+BMP4 exposure (blue). Podoplanin (PDN) is measured on the vertical axis. Each quadrant shows the frequency of each population coded by colour. **E.** Percentage of CD31+/VE-cadherin+ endothelial cells, or **F.** Troponin I+ cardiomyocytes, generated from each three culture conditions at progressive population doubling levels. **G.** Immunofluorescence of α-smooth muscle actin (α-SMA) and Troponin I after cardiomyocyte differentiation of spheres at the indicated doubling level in the condition shown. Note: eGFP fluorescence (in the bFGF+BMP4 conditions) is weak after fixation and does not interfere with interpretation of filament labelling by the α-SMA antibody. **H.** Immunofluorescence images of α-SMA and smooth muscle myosin heavy chain (SM-MHC) after differentiation of spheres at PD 86.



susceptible to differentiation to an endothelial fate despite having undetectable levels of KDR expression, which is therefore not essential for this capability. This competence might shed light on the origin of the endocardium [43]. The generation of atrial cardiomyocytes was not the focus of this study, but we showed that retinoic acid may have a role in directing this lineage commitment when applied initially to the self-renewing SHF-like NKX2-5–eGFP^{-}PDPN^{+} CPCs, consistently with earlier reports [44,45].

CPCs could be expanded to >40 population doublings while retaining multipotent differentiation capacity, a substantial extension compared with previous reports [11,12,29,30,46–51]. Although the use of a MYC transgene limits the translational applicability of our approach, the growth stability achieved creates an opportunity to identify factors enabling the expansion of either pre–NKX2-5^{+} or NKX2-5^{+} CPCs in the absence of exogenous MYC (i.e., dox-independent growth) or genes that restrain self-renewal, such as those governing cell-cycle arrest mechanisms. This tractable system could be used to help identify the genes conferring CPC potential, and hence the nature of the apparent 'clock' we have observed, which we define as the progressive time-dependent shift in differentiation affinity toward smooth muscle, perhaps in relation to the development of smooth muscle in the heart [52].

We replicated the essential elements of these results in induced hPSCs (Supplementary

Figure 14 and Supplementary Video 4). Such applications could benefit studies aiming to model cardiac disease, for example, by isolating and cryopreserving CPCs, which are later differentiated to the necessary target population. Realizing the potential shown here means that an expansion of more than 107-fold from the starting CPC population is feasible. In summary, the identification of MYC as a permissive factor in CPC self-renewal should enable the use of expandable PSC-derived CPCs for a variety of applications relating to modeling or regenerating the human heart.

Methods

Tet-On-MYC hPSC line generation and maintenance

NKX2-5eGFP/w hESCs generated previously [37], or hiPSCs generated previously (LQT-hiPSCsN9961 and LQT2-hiPSCsCORR) [41], were maintained on mouse embryonic fibroblasts in DMEM/F12-based medium containing 20% Knockout Serum Replacement (Invitrogen) and 10 ng/ml bFGF (Miltenyi Biotech). hPSCs were passaged using TrypLE Select (Invitorgen). A Tet-On-MYC system was introduced into each line by transducing the hPSCs with two lentiviruses, one carrying a MYC T58A transgene under the control of a TRE-CMV promoter (Addgene plasmid #19775), and the second carrying the tetracycline transactivator (Addgene plasmid #19780) [42]. Titres giving transduction efficiencies of approximately 40% (based on a GFP expressing control lentivirus) were used to avoid multiple viral insertions. Clones were isolated following single cell FACS deposition and selected for their ability to efficiently upregulate MYC on exposure to doxycycline.

hPSC differentiation

Differentiations were performed in serum-free "BPEL" medium using an embryoid body (EB) system as previously described [43]. The following growth factors were present for the first 3 days of differentiation: 30 ng/ml BMP4 (R&D), 25 ng/ml Activin A (Miltenyi Biotech), 30 ng/ml VEGF (Miltenyi Biotech), 40 ng/ml SCF (Miltenyi Biotech) and 1.5 μM CHIR99021 (Axon Medchem). On day 4.75 control wells were refreshed again with plain medium ± vehicle, or for MYC induction with medium containing 1 μg/ml doxycycline (Sigma Aldrich) ± 5 μM SB431542 (Tocris Bioscience). EBs were either maintained in these conditions for subsequent FACS, RNA or protein analysis, or dissociated on day 6 for progenitor expansion.

CPC culture maintenance and differentiation

CPCs were seeded on a thin layer (14 μl/cm2) of undiluted Matrigel (BD Bioscience) in organ culture dishes (BD Falcon) in BPEL medium containing 5 μM SB431542 with or without experimental factors: 1 μg/ml doxycycline, 100 ng/ml LONG R3 IGF-1 (hereafter, IGF-1), 1 μM SAG (Millipore), 0.5 μM DMH1 44, 5 μM SU5402, bFGF (Miltenyi Biotech), BMP4 (R&D). Reagents were obtained from Sigma-Aldrich unless stated otherwise. Cultures were refreshed every 2 days. Growing cell spheres were manually collected after 6 days under a dissecting microscope, dissociated using TrypLE Select and either plated for differentiation or replated on fresh Matrigel at a density of 350-1700 cells/cm^2 depending on the condition. Long term expansions were carried out at 3% O2 to minimise cellular senescence. For clonal

analysis, single cell deposition of eGFP$^-$/PDN$^+$ cells into 96-well plates was performed by FACS, from EBs at day 6 of differentiation. Clonal spheres were then picked after 6 days for propagation.

Cardiomyocyte differentiation was induced by plating cells at a density of 105 cells/cm^2 on either Matrigel-coated (1:100 dilution) 96-well plates (BD Falcon) in BPEL medium supplemented with 100 ng/ml IGF-1, 1 μM SAG, 1 μM XAV 939 (Tocris Bioscience), 100 or 1000 pg/ml bFGF (for NKX2-5GFP$^-$ and NKX2-5GFP$^+$ CPCs respectively) and 20ng/ml BMP4. From 24-72 h of differentiation cells were all in the same medium above containing 100 pg/ml bFGF plus the addition of 2.5 ng/ml TGFβ1 (Peprotech). At 72 h the medium was changed to 100 ng/ml IGF-1, 1 μM XAV 939 and 10 pg/ml bFGF. At 96 h onwards the beating cardiomyocytes were maintained in contractility-promoting medium (MJB unpublished data) containing 100 ng/ml IGF-1, 30 μM 3,3',5-Triiodo-L-thyronine sodium salt (T3) and 1 μM dexamethasone (all Sigma Aldrich).

Endothelial differentiation was induced by plating cells at a density of 0.6x105 cells/cm^2 on Matrigel-coated 96-well plates (BD Falcon) in BPEL medium supplemented with 100 ng/ml IGF-1, 50 ng/ml VEGF, 50 pg/ml bFGF, 5 μM SB431542 and 0.5 μM DMH1. Medium was refreshed at 48 h. At 96 h DMH1 was removed. Cells were analysed by FACS or fixed after a further 2 days.

Flow cytometry and cell sorting

Staining was performed in PBS containing 1 mM EDTA and 0.5% BSA. The antibodies and dilutions used were as follows: anti-PDGFRα-BV421 (BD Bioscience cat no. 562799; 1:50), anti-Podoplanin-PE (eBioscience cat no. 12-9381-41; 1:500), anti-VEGFR2-PE (R&D cat no. FAB357P; 1:50), anti-VEGFR3-PE (R&D cat no. FAB3492P; 1:50), , anti-VE-cadherin-PE (eBioscience cat no.12-1449-80; 1:150), anti-CD31-APC (eBioscience cat no. 17-0319-42; 1:150), anti-CD90-PE (BD cat no. 555596; 1:500), anti-CD146-PE (BD cat no. 550315; 1:20), anti-NG2-PE (R&D cat no. FAB2585P; 1:20), anti-PDGFRβ-PE (BD cat no. 558821; 1:20), anti-E-cadherin-APC (R&D cat no. FAB18381A; 1:40), anti-TRA-1-60-PE (Miltenyi Biotec cat no. 130-100-347; 1:100), anti-CD73-PE (BD cat no. 550257; 1:20), anti-CD105-PE (Life Technologies cat no. MHCD10504; 1:20), anti-CD13-BV421 (Biolegend cat no. 301716; 1:50), anti-CKIT-APC (BD Bioscience cat no. 550412; 1:100), anti-SIRPα (Biolegend cat no. 323801; 1:500), anti-mouse IgG PE (Jackson Immuno Research cat no: 115-116-146; 1:200), mouse IgG1 (BD Bioscience cat no. 556650), mouse IgG2a-BV421 (BD Bioscience), mouse IgG1-PE isotype control (Miltenyi Biotec 130-098-845), mouse IgG2b-APC isotype control (R&D cat no. IC0041A). Samples were measured with a MACSQuant VYB (Miltenyi Biotech) equipped with a violet (405nm), blue (488nm) and yellow (561nm) laser.

Immunostaining and microscopy

Cells were fixed with 2% paraformaldehyde and permeabilised with 0.1% Triton X. Blocking was achieved with 4% normal goat serum. Primary antibody incubations were overnight in 4% normal goat serum at 4°C using the following antibodies: anti-troponin I (clone H170, Santa Cruz; 1:500) together with α-smooth muscle actin (Sigma A2547; 1:300), or



VE-cadherin (Cell Signalling; 1:200) together with CD31 (DAKO M0823; 1:20). Secondary antibodies were: Alexa 488 anti-mouse and Alexa 555 anti-rabbit (Invitrogen). GFP fluorescence was reduced to background levels after fixation and could be differentiated from the specific smooth muscle type-α-smooth muscle actin staining.

Quantitative real time PCR

RNA was isolated using a Minelute RNA extraction kit (Qiagen) and cDNA synthesized using an iScript cDNA synthesis kit (BioRad). Real time PCR was performed on a BioRad CFX96 machine using IQ SYBR Green (BioRad). Gene expression values were normalized to the mean expression of the housekeeping genes human acidic ribosomal phosphoprotein (hARP), glucuronidase (GUS), and RNF7. RNA from MESP1-expressing sorted cells was obtained from a derivative knock-in reporter line and used as a reference [23]. The hESC-cardiomyocyte control RNA was obtained from eGFP+ sorted cells from a standard monolayer differentiation of the NKX2-5$^{eGFP/w}$ hESC line .

Primer sequences were as follows:

Gene	Forward primer	Reverse primer
hARP	CACCATTGAAATCCTGAGTGATGT	TGACCAGCCCAAAGGAGAAG
GUS	CCACCTAGAATCTGCTGGCTAC	GTGCCCGTAGTCGTGATACCAA
MYC (endogenous only)	AGAAATGTCCTGAGCAATCACC	AAGGTTGTGAGGTTGCATTTGA
MYC (total)	ACGCACCGAATAGTTACGG	CCAGGTCCACGGGCAGA
MESP1	CTCTGTTGGAGACCTGGATG	CCTGCTTGCCTCAAAGTG
PDPN	AGTGTCATCTTCTGGCTGGC	AGCAACAACTCAACGGGAAC
NKX2-5	TCTATCCACGTGCCTACAGC	GTTGTCCGCCTCTGTCTTCT
ISL1	TGATGAAGCAACTCCAGCAG	GGACTGGCTACCATGCTGTT
MEF2C	CCACTGGCTCACCCTTCTCTGC	ACCCGTTCCCTGCACTAGTG
BAF60C	GCGCGCAAAGCCACGAAA	ATCCGGGCTCCAGACGGCATC
GATA4	GACAATCTGGTTAGGGGAAGC	GAGAGATGCAGTGTGCTCGT
TBX5	TACCACCACACCCATCAAC	ACACCAAGACAGGGACAGAC
FGF8	TACATCTGCATGAACAAGAAGGG	TTCTCCAGCACAATCTCCGT
HAND1	TGAACTCAAGAAGGCGGATG	AATCCTCTTCTCGACTGGGC
HAND2	ACATCGCCTACCTCATGGAC	TGGTTTTCTTGTCGTTGCTG
TBX3	AAAGGAGAATGGGACCTCTG	CGCTGGGACATAAATCTTTGAG
TBX18	TTGCTAAAGGCTTCCGAGAC	AGGTGGAGGAACTTGCATTG
SHOX2	AATCAAGCAGAGGCGAAGTC	TCTCGTCAAAAAGCCTCTCC
MYOCD	CAACACCGATTCAGCTACCT	TTCAGAGACCTTCAGATCCAG
MYL2/MLC2V	TACGTTCGGGAAATGCTGAC	TTCTCCGTGGGTGATGATG
MYL7/MLC2A	CTTGTAGTCGATGTTCCCCG	TCAAGCAGCTTCTCCTGACC
TNNT2	TTCGACCTGCAGGAGAAGTT	GCGGGTCTTGGAGACTTTCT
ACTN2	CTGCTGCTTTGGTGTCAGAG	TTCCTATGGGGTCATCCTTG
MYBPC3	GGCATGCTAAAGAGGCTCAA	TCTTGTGGCCTTTGCTCAC

Western blot

Samples were lysed with ice cold ELB (50mM HEPES pH 7.0; 250mM NaCl; 5mM EDTA; 0.1% NP-40) or RIPA (25mM Tris-HCl pH 7.6; 150mM NaCl; 1% Triton X100; 0.1% SDS; 1% Sodium Deoxycholate) with 1:100 Protease Inhibitor Cocktail (Sigma-Aldrich) for 30 mins on ice. The samples were centrifuged at 7000g for 10 mins and the supernatant was quantified for protein content (Bradford dye-binding method). 30μg of each sample was

run in a 10% polyacrylamide gel together with the protein ladder (Precision Plus Protein dual colour – Bio-Rad). The protein was transferred to an Amersham Hybond membrane (GE Heathcare- Life Sciences) overnight. The membrane was blocked with blocking buffer (2% milk in PBS) and probed with a Rabbit IgG anti-cMYC 1:1000 (Cell Signaling 5605S) detected with a Goat anti-Rabbit IgG – HRP (Cell Signaling 7074s).

Patterned Polyacrylamide gel fabrication

Patterned polyacrylamide gels were prepared as previously described [45]. Briefly, a 1% gelatin solution was activated with 3.5mg/mL Sodium Periodate (both Sigma-Aldrich). A polydimethylsiloxane (PDMS) stamp was casted from a SU8 master produced by standard soft lithography techniques and incubated with the activated 1% gelatin solution for 45 mins. The excess of gelatin was removed with a nitrogen gun and the stamp was used to μcontact-print a pattern of 20μm thick with 20μm spacing gelatin lines onto 10mm (electrophysiology) or 15mm (contraction assay) coverslips. The polyacrylamide solution was prepared with a final concentration of 0.1% bis-acrylamide (Bio-Rad), 5% acrylamide (Bio-Rad) and 10mM HEPES pH 8.5 in distilled water, followed by centrifugation for 1 min at 10.000RPM for degassing. 0.006% (m/v) of ammonium persulfate (Sigma-Aldrich) and a 1:1000 dilution of 0.2-μm fluorescent beads (Ex/Em: 660/680nm - Molecular Probes) were added to the solution (for the contraction assay) and briefly vortexed. The gel polymerization was initiated with TEMED (Bio-Rad) and 4.08μl/9.2μl of the final solution was added to a 15mm/25mm coverslip treated with plus Bind-Silane solution (GE Healthcare). The μcontact-printed coverslip was applied on top of the drop with the gelatin lines facing the gel. After 20mins of polymerization the 10mm/15mm coverslip was removed. Each 25mm coverslip was mounted onto a well of a glassbottom 6-well plate (Mattek), replacing the initial glass. The 15mm coverslips were used directly. Plates were UV-sterilized and re-hydrated with culture medium for 30 mins before use. The polymerized gel has a Young's modulus of 5.8 kPa [46].



Contraction force measurements

The contraction force measurements were performed as previously described [47]. Briefly, using a Leica AF-6000LX microscope with controlled temperature and CO2, 40x image series of brightfield and fluorescent beads were taken at 20 frames per second of aligned single self-pacing cardiomyocytes. Single frames from maximal relaxation and contraction of the brightfield and fluorescent beads image series were analyzed by the LIBTRC software package (kindly provided by Dr. Micah Dembo), creating a mask of the cell outline from the brightfield image and a vector map from the difference between the relaxed and contracted fluorescent beads images. The vector map and the cell mask were used to calculate the total force that the cell applies on the substrate at its maximum peak of contraction. The contraction stress generated by the cardiomyocyte during contraction was calculated by dividing the total force by the cell surface area.

Cellular electrophysiology

Recording procedures. Action potentials and the hyperpolarization-activated current, If,

were recorded in single cells by the amphotericin-perforated patch-clamp technique using an Axopatch 200B amplifier (Molecular Devices, USA) 5-7 days after dissociation on day 11 of differentiation. Coverslips containing the cells were put in a recording chamber on the stage of an inverted microscope and superfused with Tyrode's solution (36±0.2°C) containing (in mM): NaCl 140, KCl 5.4, CaCl2 1.8, MgCl2 1.0, glucose 5.5, and HEPES 5.0; pH 7.4 (NaOH). Patch pipettes (borosilicate glass, 2-3 MΩ) were filled with solution containing (in mM): K-gluc 120, KCl 20, NaCl 5, amphotericin-B 0.44, HEPES 10, pH 7.2 (KOH). Series resistance was compensated by ≥80%, and potentials were corrected for the calculated liquid junction potential. Action potentials were low-pass filtered (cut-off frequency: 2 kHz) and digitized at 10 kHz, while If was filtered and digitized at 1 kHz and 4 kHz, respectively. Voltage control, data acquisition and analysis were accomplished using custom software. Cell membrane capacitance (Cm) was estimated by dividing the time constant of the decay of the capacitive transient in response to 5 mV hyperpolarizing voltage clamp steps from -40 mV by the series resistance.

Action potentials measurements. In both cell groups we observed spontaneously active as well as virtually quiescent single cells. We recorded spontaneous action potentials or action potentials were elicited at 1 Hz by 3-ms, ≈1.2Ω threshold current pulses through the patch pipette. Action potentials were characterized by duration at 20, 50, and 90% repolarization (APD20, APD50, and APD90, respectively), maximum diastolic potential (MDP), action potential amplitude (APA), maximum upstroke velocity (dV/dtmax), and, in case of spontaneously active cells, cycle length (CL) and diastolic depolarization rate measured over the 100-ms time interval starting at MDP+1 mV (DDR100). Parameter values obtained from 10 consecutive action potentials were averaged.

If measurements. If was activated upon 2-s hyperpolarizing pulses from a holding potential of –40 mV. If amplitude was calculated as the difference between the current at the beginning and end of the voltage step. Current densities were calculated by dividing current amplitudes by Cm.

Statistical analyses

Data are mean±SEM. Groups of HF SAN cells were compared with groups of CTRL SAN cells using Fisher's exact test, Two-Way Repeated Measures ANOVA followed by pairwise comparison using the Student-Newman-Keuls test, and unpaired t-test. Paired t-tests were used to compare drug effects within a group. An F-test was used to compare frequency dependency between groups. $P<0.05$ is considered statistically significant

References

[1] Drawnel, F.M. et al. Disease modeling and phenotypic drug screening for diabetic cardiomyopathy using human induced pluripotent stem cells. Cell Reports 9, 810–820 (2014).

[2] Matsa, E., Burridge, P.W. & Wu, J.C. Human stem cells for modeling heart disease and for drug discovery. Sci. Transl. Med. 6, 239ps6 (2014).

[3] Lundy, S.D., Gantz, J.A., Pagan, C.M., Filice, D. & Laflamme, M.A. Pluripotent stem cell derived cardiomyocytes for cardiac repair. Curr. Treat. Options Cardiovasc. Med. 16, 319 (2014).

[4] Bhave, M., Akhter, N. & Rosen, S.T. Cardiovascular toxicity of biologic agents for cancer therapy. Oncology 28, 482–490 (2014).

[5] Birket, M.J. & Mummery, C.L. Pluripotent stem cell derived cardiovascular progenitors—a developmental perspective. Dev. Biol. 400, 169–179 (2015).

[6] Vincent, S.D. & Buckingham, M.E. How to make a heart: the origin and regulation of cardiac progenitor cells. Curr. Top. Dev. Biol. 90, 1–41 (2010).

[7] Cai, C.-L. et al. Isl1 identifies a cardiac progenitor population that proliferates prior to differentiation and contributes a majority of cells to the heart. Dev. Cell 5, 877–889 (2003).

[8] Lints, T.J., Parsons, L.M., Hartley, L., Lyons, I. & Harvey, R.P. Nkx-2.5: a novel murine homeobox gene expressed in early heart progenitor cells and their myogenic descendants. Development 119, 419–431 (1993).

[9] Ma, Q., Zhou, B. & Pu, W.T. Reassessment of Isl1 and Nkx2–5 cardiac fate maps using a Gata4-based reporter of Cre activity. Dev. Biol. 323, 98–104 (2008).

[10] Laugwitz, K.-L. et al. Postnatal isl1+ cardioblasts enter fully differentiated cardiomyocyte lineages. Nature 433, 647–653 (2005).

[11] Moretti, A. et al. Multipotent embryonic isl1+ progenitor cells lead to cardiac, smooth muscle, and endothelial cell diversification. Cell 127, 1151–1165 (2006).

[12] Wu, S.M. et al. Developmental origin of a bipotential myocardial and smooth muscle cell precursor in the mammalian heart. Cell 127, 1137–1150 (2006).

[13] Mommersteeg, M.T.M. et al. Molecular pathway for the localized formation of the sinoatrial node. Circ. Res. 100, 354–362 (2007).

[14] Wiese, C. et al. Circ. Res. 104, 388–397 (2009).

[15] Liang, X. et al. HCN4 dynamically marks the first heart field and conduction system precursors. Circ. Res. 113, 399–407 (2013).



[16] Später, D. et al. A HCN4+ cardiomyogenic progenitor derived from the first heart field and human pluripotent stem cells. Nat. Cell Biol. 15, 1098–1106 (2013).

[17] Kattman, S.J. et al. Stage-specific optimization of activin/nodal and BMP signaling promotes cardiac differentiation of mouse and human pluripotent stem cell lines. Cell Stem Cell 8, 228–240 (2011).

[18] Wierstra, I. & Alves, J. The c-myc promoter: still mysterY and challenge. Adv. Cancer Res. 99, 113–333 (2008).

[19] Gittenberger-De Groot, A.C. et al. Nkx2.5 negative myocardium of the posterior heart field and its correlation with podoplanin expression in cells from the developing cardiac pacemaking and conduction system. Anat. Rec. 290, 115–122 (2007).

[20] Dyer, L.A. et al. BMP signaling modulates hedgehog-induced secondary heart field proliferation. Dev. Biol. 348, 167–176 (2010).

[21] Gude, N. et al. Akt promotes increased cardiomyocyte cycling and expansion of the cardiac progenitor cell population. Circ. Res. 99, 381–388 (2006).

[22] Keren-Politansky, A., Keren, A. & Bengal, E. Neural ectoderm-secreted FGF initiates the expression of Nkx2.5 in cardiac progenitors via a p38 MAPK/CREB pathway. Dev. Biol. 335, 374–384 (2009).

[23] Liberatore, C.M., Searcy-Schrick, R.D., Vincent, E.B. & Yutzey, K.E. Nkx-2.5 gene induction in mice is mediated by a Smad consensus regulatory region. Dev. Biol. 244, 243–256 (2002).

[24] Reifers, F., Walsh, E.C., Leger, S., Stainier, D.Y. & Brand, M. Induction and differentiation of the zebrafish heart requires fibroblast growth factor 8 (fgf8/acerebellar). Development 127, 225–235 (2000).

[25] Schultheiss, T.M., Burch, J.B. & Lassar, A.B. A role for bone morphogenetic proteins in the induction of cardiac myogenesis. Genes Dev. 11, 451–462 (1997).

[26] Barron, M., Gao, M. & Lough, J. Requirement for BMP and FGF signaling during cardiogenic induction in non-precardiac mesoderm is specific, transient, and cooperative. Dev. Dyn. 218, 383–393 (2000).

[27] Inman, G.J. et al. SB-431542 is a potent and specific inhibitor of transforming growth factor-β superfamily type I activin receptor-like kinase (ALK) receptors ALK4, ALK5, and ALK7. Mol. Pharmacol. 62, 65–74 (2002).

[28] Den Hartogh, S.C. et al. Dual reporter MESP1mCherry/w-NKX2–5eGFP/w hESCs enable studying early human cardiac differentiation. Stem Cells 33, 56–67 (2015).

[29] Yang, L. et al. Human cardiovascular progenitor cells develop from a KDR+ embryonic-stem-cell-derived population. Nature 453, 524–528 (2008).

[30] Ardehali, R. et al. Prospective isolation of human embryonic stem cell-derived cardiovascular progenitors that integrate into human fetal heart tissue. Proc. Natl. Acad. Sci. USA 110, 3405–3410 (2013).

[31] van Berlo, J.H. et al. c-kit+ cells minimally contribute cardiomyocytes to the heart. Nature 509, 337–341 (2014).

[32] James, D. et al. Expansion and maintenance of human embryonic stem cell-derived endothelial cells by TGFβ inhibition is Id1 dependent. Nat. Biotechnol. 28, 161–166 (2010).

[33] Marques, S.R., Lee, Y., Poss, K.D. & Yelon, D. Reiterative roles for FGF signaling in the establishment of size and proportion of the zebrafish heart. Dev. Biol. 321, 397–406 (2008).

[34] de Pater, E. et al. Bmp signaling exerts opposite effects on cardiac differentiation. Circ. Res. 110, 578–587 (2012).

[35] Ueno, S. et al. Biphasic role for Wnt/β-catenin signaling in cardiac specification in zebrafish and embryonic stem cells. Proc. Natl. Acad. Sci. USA 104, 9685–9690 (2007).

[36] Goumans, M.-J. et al. TGF-β1 induces efficient differentiation of human cardiomyocyte progenitor cells into functional cardiomyocytes in vitro. Stem Cell Res. 1, 138–149 (2007).

[37] Verkerk, A.O., van Ginneken, A.C.G. & Wilders, R. Pacemaker activity of the human sinoatrial node: role of the hyperpolarization-activated current, I(f). Int. J. Cardiol. 132, 318–336 (2009).

[38] Xi, J. et al. Comparison of contractile behavior of native murine ventricular tissue and cardiomyocytes derived from embryonic or induced pluripotent stem cells. FASEB J. 24, 2739–2751 (2010).

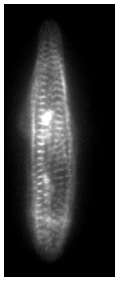
[39] Jackson, T. et al. The c-myc proto-oncogene regulates cardiac development in transgenic mice. Mol. Cell. Biol. 10, 3709–3716 (1990).

[40] Noseda, M., Peterkin, T., Simões, F.C., Patient, R. & Schneider, M.D. Cardiopoietic factors extracellular signals for cardiac lineage commitment. Circ. Res. 108, 129–152 (2011).

[41] Cai, W. et al. Coordinate Nodal and BMP inhibition directs Baf60c-dependent cardiomyocyte commitment. Genes Dev. 27, 2332–2344 (2013).

[42] Waldo, K.L. et al. Conotruncal myocardium arises from a secondary heart field. Development 128, 3179–3188 (2001).

[43] Milgrom-Hoffman, M. et al. The heart endocardium is derived from vascular endothelial progenitors. Development 138, 4777–4787 (2011).



[44] Zhang, Q. et al. Direct differentiation of atrial and ventricular myocytes from human embryonic stem cells by alternating retinoid signals. Cell Res. 21, 579–587 (2011).

[45] Devalla, H.D. et al. Atrial-like cardiomyocytes from human pluripotent stem cells are a robust preclinical model for assessing atrial-selective pharmacology. EMBO Mol. Med. 7, 394–410 (2015).

[46] Kattman, S.J., Huber, T.L. & Keller, G.M. Multipotent Flk-1+ cardiovascular progenitor cells give rise to the cardiomyocyte, endothelial, and vascular smooth muscle lineages. Dev. Cell 11, 723–732 (2006).

[47] Qyang, Y. et al. The renewal and differentiation of Isl1+ cardiovascular progenitors are controlled by a WNT/β-catenin pathway. Cell Stem Cell 1, 165–179 (2007).

[48] Bu, L. et al. Human ISL1 heart progenitors generate diverse multipotent cardiovascular cell lineages. Nature 460, 113–117 (2009).

[49] Domian, I.J. et al. Generation of functional ventricular heart muscle from mouse ventricular progenitor cells. Science 326, 426–429 (2009).

[50] Moretti, A. et al. Mouse and human induced pluripotent stem cells as a source for multipotent Isl1+ cardiovascular progenitors. FASEB J. 24, 700–711 (2010).

[51] Elliott, D.A. et al. NKX2–5eGFP/w hESCs for isolation of human cardiac progenitors and cardiomyocytes. Nat. Methods 8, 1037–1040 (2011).

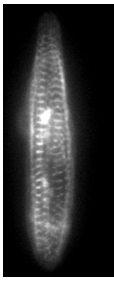
[52] Miano, J.M., Cserjesi, P., Ligon, K.L., Periasamy, M. & Olson, E.N. Smooth muscle myosin heavy chain exclusively marks the smooth muscle lineage during mouse embryogenesis. Circ. Res. 75, 803–812 (1994).





Chapter 8

General discussion and future perspectives



Summary

This thesis described how the symbiosis between biochemistry, biomaterials and stem cell technologies (**Chapter 2**) can be used to determine maturation and disease states of human pluripotent stem cell derived cardiomyocytes (hPSC-CM) (**Chapter 3**). The functional improvement inherent from this process enabled the revelation of a contractile defect caused by a MYBPC3 mutation in hiPSC-CM derived from patients with the disorder(**Chapter 4**). In order to further investigate how this can be attributed to this MYBPC3 mutation in human cardiomyocytes, several genetic tools were developed (**Chapter 5**) to mimic and analyse the underlying mechanisms (**Chapter 6**). The thesis ends with the development of a novel tool to expand cardiac progenitors and study their differentiation into the different cell types (**Chapter 7**).

Discussion

The use of human pluripotent stem cells (hPSC) to generate different organ-specific cell types creates enormous possibilities for developing disease modelling platforms, tissue engineering and drug toxicity studies. A major advantage of using hPSC is that functional human cell-types or tissue can in principle be generated with higher predictivity for disease modelling and drug responses when compared to non-human cell lines or animal models [1]. In the heart for example, human cardiomyocytes exhibit electrophysiological signals, which are very distinct from those, for example, in mice. Differences in the contribution of ion channels at different phases during the contraction-relaxation cycle are indicated by their differences in shape and duration of their respective action potentials (APs) and electrocardiogram (ECG) [2]. Mice have a tenfold faster beating rate and a much shorter AP, lacking a distinct plateau phase and have a shorter QT interval (100ms) when compared to that of the human heart (400ms). Variations in cardiac electrophysiological profiles between species translate into differences in susceptibility to drug-induced cardiotoxicity, caused by interference with ion channels and their respective ion currents, which has been identified as one of the major reason for drugs failing clinical trials[3]. Furthermore, these limitations not only affect drug toxicity assessment, but also the study of human cardiac diseases in which ion channel functions are impaired (i.e. channelopathies such as long-QT syndrome), which may be difficult to analyse in experimental animal models. Moreover, interspecies variations regarding other aspects of cardiac function complicate establishing reliable and predictable animal models of cardiac disease. For example, mice with only one copy of sarcomeric myosin binding protein c 3 (MYBPC3) do not develop cardiac hypertrophy whilst a non-sense mutation in one allele of MYBPC3, causing a decrease in the protein in humans, ultimately leads to hypertrophic cardiomyopathy and heart failure [4,5]. Additionally, despite specific human cardiac diseases being linked to coding/non-coding DNA variants through genome-wide association studies, the exact role of these gene variants have been difficult to assess due to absence of clear orthologs in mice or in other species [6].

Another advantage of hPSC technology is the ability to derive stem cells from any individual, enabling their generation from patients with specific genetic mutations and/or a disease phenotype (**Chapter 4**) [7,8]. The use of optimized and defined protocols for the production

of specialized functional cell-types, including those of the heart, enables in vitro modeling of patient diseases, making it feasible to study any associations between phenotype(s) observed in vitro and clinic symptoms. Additionally, the mechanism of disease can be further explored by the use of genome editing techniques such as Zinc finger nucleases (ZFNs), Transcription Activator-Like Effector Nucleases (TALENs) or the CRISPR/Cas system9. These techniques enable the correction of the disease causing mutation in order to create isogenic control cell lines or vice versa, introducing mutations in healthy control cell lines to directly analyse the functional and phenotypic consequences10.

To analyse the diverse aspects of the hiPSC-derived cardiomyocyte (hiPSC-CM) phenotype several technologies are widely used. Electrical activity, responsible for cardiomyocyte excitation, is often measured by single cell patch clamp, multi-electrode array (MEA) and most recently by optical mapping with the use of voltage sensitive dyes [11]. The electrical excitation induces the fast release of calcium from the sarcoplasmic reticulum, promoting force generation by the contractile machinery. Calcium transients can be measured using calcium sensitive dyes[12]. In the heart the contractile force production of each cardiomyocyte exerts the work necessary to pump the blood out of the cardiac ventricles into the circulation system. Methods available to measure contraction force in vitro vary from the use of force transducers for cardiac tissue strips measurements [13], micro-pillars [14] to beads embedded on acrylamide gels for single cardiomyocytes measurements (**Chapter 3**). Although, each measurement provides valuable information on each particular cardiac parameter, it would be of greater interest if multiple parameters could be determined simultaneously in a multiplexed system, comparable to the complex cardiomyocyte function in vivo. Such integration of simultaneous measurements in a single cell or tissue will enable the assessment of the interdependence and inter-regulation of the different cardiac parameters in each single beat. For example, assessing how does one slower/arrhythmic action potential influence the calcium transients and contraction force or does a defective contraction affect the next action potential and/or calcium transients? This information allows a deeper look onto the mechanisms through which channelopathies affect heart function or cardiomyopathies cause arrhythmias. Additionally, such analysis can be used as a sensitive and highly informative assay for drug cardiotoxicity screening. **Chapter 3** describes a platform that allows the assessment of the relation between different electrophysiological parameters and contractile forces, whereas in **Chapter 6** this platform is optimized for measuring calcium kinetics, sarcomere dynamics and contraction force in the same cardiomyocyte. Recently different platforms have been developed to simultaneously measure electrophysiology together with calcium transients [15,16] or calcium transients with contraction force [17]. Nevertheless, further development is needed to integrate more simultaneous measurements in a single cell or tissue. With the use of a polyacrylamide-based platform it is theoretically possible to measure five parameters in a single cardiomyocyte employing optical reporters as voltage sensitive dyes for electrophysiology, calcium indicator dye for calcium handling, the α-actinin-mCherry for the sarcomere dynamics and the fluorescent beads for contraction force, followed by single cell Q-PCR for gene expression analysis. This platform would create added value for understanding the interconnected mechanisms during development, disease or for drug-induced toxicity studies.



Despite the great potential of human stem cell-derived cardiomyocytes there are several hurdles that need to be overcome. One major issue is the immature or fetal-like phenotype of hPSC-CMs (**Chapter 3**). Micro-environmental aspects present in vivo, such as blood flow, cell-cell interactions, dynamic fluctuations of blood components, stretch, electrical fields, geometry of cells, softness of tissue, etc. are absent or suboptimal in cell-based in vitro assays; these are likely to affect differentiation and function of cells. It is therefore important to mimic the in vivo situation as closely as possible. Temporal and spatially-dependent activation of specific signalling pathways responsible for cell differentiation during development have been mimicked in vitro to successfully differentiate stem cells into different cardiomyocyte subtypes (**Chapter 7**). Nevertheless, these pathways are just few threads in the network of development signalling. Such incomplete input impairs the differentiation process, restraining cells from reaching an adult phenotype. In order to mimic more aspects of in vivo development, in **Chapter 2** we studied the use of biocompatible polymers with different stiffness (including conditions that mimic the stiffness of heart tissue) in combination with micro-contact printing of ECM proteins, enabling controlled geometry and cell shape. Although morphological and functional improvements towards a more adult phenotype were observed, the induction of cardiogenic promoting pathways in combination with soft substrates and controlled cell shape, were not sufficient to promote a fully mature state. However, we found that addition of T3 hormone in optimized cardiomyocyte maturation medium resulted in significant molecular, morphological and functional improvement of hPSC-CMs, comparable to human fetal primary cardiomyocytes from second trimester of gestation (**Chapter 3**). Moreover, in **Chapter 4** a fully defined medium containing T3, Insulin-like Growth Factor 1 (IGF1) and a synthetic glucocorticoid Dexamethasone (Dex) among other components was described to induce an increase in hPSC-CM contractile force to a level twice that in 2nd trimester human fetal cardiomyocytes (**Chapter 3** and **4**). Although these improvements of electrophysiological and contractile properties are still far from adult cardiomyocytes[18,19], the importance of this advance in maturation of cardiomyocytes is indicated by the fact that this optimized culture condition allowed us to detect contractile defects in patient-derived hiPSC-CMs carrying a mutation in MYBPC3, which were consistent with studies from patients[13].

To further characterize the phenotype of MYBPC3 deficiency in hPSC-CMs, a reporter line expressing an α-actinin-mCherry fusion protein, incorporated at the Z-disc of sarcomeres was produced in order to analyze changes in sarcomeric organization and sarcomere dynamics (**Chapter 5**). Congruent with previous observations in mouse models[20], the deficiency of MYBPC3 causes a reduction in the diastolic sarcomere length and a decrease in shortening and lengthening amplitudes. Moreover, this phenotype was accompanied by a decrease in ATP usage per contraction cycle. However, the changes in calcium handling or increase in cardiomyocyte area, characteristic of hypertrophic cardiomyopathy, were not observed in these cells (**Chapter 6**). This may be related to the relative immaturity of hPSC-CMs in a two dimensional in vitro setting, which contrasts with hypertrophic cardiomyopathy that normally emerges at a later stage in life in a three dimensional heart. Although important advances have been made, culture conditions need to be further improved in order to mimic physiologically revenant conditions and to ensure the ability to analyze

disease related phenotypes in vitro. Besides adjustment of culture conditions, generation of defined cardiac subpopulations need to accomplished. In **Chapter 7** we show for the first time an effective way to arrest cardiac differentiation and expand cardiac progenitors, which could be to further differentiated into endothelial cells, smooth muscle cells, working myocardium (atrium and ventricular-like NKX2.5 positive cardiomyocytes) and pacemaker-like cardiomyocytes depending on the downstream signaling events in defined differentiation protocols. A better understanding of these processes that control cardiac progenitors cells and direct differentiation to specific cell-types may have a great impact on further research of cardiac development and tissue engineering, as it allows the production of different "pieces of the puzzle" for reconstitution of the heart.

Future directions

Integration of Biology and Engineering

Ultimately the best model of a human heart is the organ itself. Although current technology is not close to such an achievement, small steps have been made towards this direction. In 1997 the engineered heart tissue (EHT) concept was first introduced using chicken cardiomyocytes, but it was only until 2011 that hPSC-derived cardiomyocytes were used in three dimensional (3D) systems[21,22]. The 3D culture format has been shown to induce improvements in electrophysiology, cell size and orientation, structural organization and drug response of hPSC-CM[23,24]. Nevertheless, contraction force (0.37±0.29mN/mm2)[17] and electrophysiology parameters (RMP -49±1.2mV; Upstroke 10.4±1.2V/s)[22] of this 3D system are still far from the reality of the adult heart (Contraction force 44±11.7 mN/mm2; RMP -85mV; Upstroke 270V/s)[18,19], indicating that the 3D structure alone is not enough to direct hPSC-CM towards the adult stage. Other studies have demonstrated the importance of the contribution of non-cardiomyocyte populations of cardiac fibroblasts, endothelial and smooth muscle cells on the phenotype of hPSC-CMs in engineered tissues[25–27]. The main cardiac output measured in EHTs is calcium handling and contractile function in order assess drug responses or disease modeling[22,23,28]. However, in patients, disease symptoms or adverse drug effects in the heart are assessed through different parameters such as electrocardiography (ECG), ventricular wall thickness assessment, the ventricular volume intake, diastolic ventricular function left ventricular ejection fraction and blood pressure[29,30]. In order to progress towards more clinically relevant readouts it may have added value if the fluidic pump function of the heart can be mimicked in vitro.



3D Bioprinting

3D printing is a rapid evolving technology with an increasing number of applications. Recently, it was used for generation of biological material using viable cells and supporting substrates. This so-called 3D bioprinting technology potentially enables reconstruction of complex tissues by emulating the 3D architectural composition of the tissue of interest using the right cell types and supporting matrix components[31]. Currently there are different types of 3D bioprinters (e.g. Inkjet, Microextrusion and Laser assisted) that have been shown to generate not only multiple tissue types like skin[32], liver[33] and cartilage[34] but also diverse biological structures such as branched tumor models[35], vascular trees[36]

and aortic valves[37]. Despite the promising applicability of this technique in tissue engineering, there are major hurdles related to the materials and scaffolds that are currently used for 3D bioprinting. Generating complex functional tissues demands materials or scaffolds that are biocompatible, printable and have structural and mechanical properties that mimic the heart environment, which is very challenging[31].

Decellularized Heart

Another approach to build a 3D heart model is to start from a base structure which will serve as a fundament and an architectural blueprint for the heart. This can be achieved by decellularization of heart tissue[38]. This process involves the perfusion of cadaveric hearts with different types of detergents and/or enzymes that degrade and remove the intercellular content of the cells constituting the tissue, leaving the ECM structure intact for subsequent recellularization. The advantages of this approach are that the intact skeleton of the heart is being used to guide the assembly of the new cellular population, avoiding the hurdle of designing and building the correct heart structures and the use of complex synthetic scaffolds, together with non-inducing immunologic response of the native ECM structure on the new host in case of future transplantation application[38,39]. Nevertheless, the challenges of this approach are the poor delivery and low retention of repopulating cells together insufficient understanding how to produce and organize the different types and sub-types of cells in order to form a well-integrated functional multicellular heart tissue[40]. Some attempts have successfully been made on a smaller scale by repopulating decellularized mouse hearts with hiPSC-CM, which contracted and responded to adrenergic stimuli[40]. Perhaps in a short term basis the recellularization of single cavities of rodent hearts with hiPSC-CM can become a novel effective tool for drug development and toxicity studies.

Although at the long term any of these approaches may have the potential to successfully mimic the function of a pumping heart in vitro, most likely combinations of the above mentioned technologies could lead to formation of 3D functional heart model resembling the human heart in vivo, which will provide us more detailed information about drug responses and disease mechanisms. In the near future the hPSC-derived cardiac models will rise to a better and more predictive platform for drug discovery and development.

References

[1] Braam SR, Tertoolen L, van de Stolpe A, Meyer T, Passier R, Mummery CL. Prediction of drug-induced cardiotoxicity using human embryonic stem cell-derived cardiomyocytes. Stem Cell Res. Elsevier B.V.; 2010;4(2):107–16.

[2] Nerbonne JM. Studying cardiac arrhythmias in the mouse - A reasonable model for probing mechanisms? Trends Cardiovasc Med. 2004;14(3):83–93.

[3] Braam SR, Passier R, Mummery CL. Cardiomyocytes from human pluripotent stem cells in regenerative medicine and drug discovery. Trends Pharmacol Sci. 2009;30(10):536–45.

[4] Carrier L, Knöll R, Vignier N, Keller DI, Bausero P, Prudhon B, et al. Asymmetric septal hypertrophy in heterozygous cMyBP-C null mice. Cardiovasc Res. 2004;63:293–304.

[5] Harris SP, Bartley CR, Hacker T a., McDonald KS, Douglas PS, Greaser ML, et al. Hypertrophic cardiomyopathy in cardiac myosin binding protein-C knockout mice. Circ Res. 2002;90:594–601.

[6] Kathiresan S, Voight BF, Purcell S, Musunuru K, Ardissino D, Mannucci PM, et al. Genome-wide association of early-onset myocardial infarction with single nucleotide polymorphisms and copy number variants. Nat Genet. 2009;41(3):334–41.

[7] Takahashi K, Tanabe K, Ohnuki M, Narita M, Ichisaka T, Tomoda K, et al. Induction of pluripotent stem cells from adult human fibroblasts by defined factors. Cell. 2007;131(5):861–72.

[8] Jung CB, Moretti A, Schnitzler MMY, Iop L, Storch U, Bellin M, et al. Dantrolene rescues arrhythmogenic RYR2 defect in a patient-specific stem cell model of catecholaminergic polymorphic ventricular tachycardia. EMBO Mol Med. 2011;

[9] Esvelt KM, Wang HH. Genome-scale engineering for systems and synthetic biology. Mol Syst Biol. Nature Publishing Group; 2013;9(641):641.

[10] Bellin M, Casini S, Davis RP, D'Aniello C, Haas J, Ward-van Oostwaard D, et al. Isogenic human pluripotent stem cell pairs reveal the role of a KCNH2 mutation in long-QT syndrome. EMBO J. 2013;32(24):3161–75.

[11] Blazeski A, Zhu R, Hunter DW, Weinberg SH, Boheler KR, Zambidis ET, et al. Electrophysiological and contractile function of cardiomyocytes derived from human embryonic stem cells. Prog Biophys Mol Biol. Elsevier Ltd; 2012;110(2-3):178–95.

[12] Bootman MD, Rietdorf K, Collins T, Walker S, Sanderson M. Ca2+-sensitive fluorescent dyes and intracellular Ca2+ imaging. Cold Spring Harb Protoc. 2013;8(2):83–99.

[13] Witjas-Paalberends ER, Güclü A, Germans T, Knaapen P, Harms HJ, Vermeer AMC,



et al. Gene-specific increase in the energetic cost of contraction in hypertrophic cardiomyopathy caused by thick filament mutations. Cardiovasc Res. 2014;103:248–57.

[14] Yang X, Rodriguez M, Pabon L, Fischer KA, Rei- H, Regnier M, et al. Tri-iodo-L-thyronine Promotes the Maturation of Human Cardiomyocytes-Derived from Induced Pluripotent Stem Cells. J Mol Cell Cardiol. Elsevier B.V.; 2014;

[15] Herron TJ, Lee P, Jalife J. Optical imaging of voltage and calcium in cardiac cells & tissues. Circ Res. 2012;110(4):609–23.

[16] Lee P, Klos M, Bollensdorff C, Hou L, Ewart P, Kamp TJ, et al. Simultaneous voltage and calcium mapping of genetically purified human induced pluripotent stem cell-derived cardiac myocyte monolayers. Circ Res. 2012;110(12):1556–63.

[17] Stoehr A, Neuber C, Baldauf C, Vollert I, Friedrich FW, Flenner F, et al. Automated analysis of contractile force and Ca2+ transients in engineered heart tissue. Am J Physiol Heart Circ Physiol. 2014;306(9):H1353–63.

[18] Hasenfuss G, Mulieri L a., Blanchard EM, Holubarsch C, Leavitt BJ, Ittleman F, et al. Energetics of isometric force development in control and volume- overload human myocardium. Comparison with animal species. Circ Res. 1991;68(3):836–46.

[19] Koncz I, Szél T, Bitay M, Cerbai E, Jaeger K, Fülöp F, et al. Electrophysiological effects of ivabradine in dog and human cardiac preparations: potential antiarrhythmic actions. Eur J Pharmacol. Elsevier B.V.; 2011;668(3):419–26.

[20] Pohlmann L, Kröger I, Vignier N, Schlossarek S, Krämer E, Coirault C, et al. Cardiac myosin-binding protein C is required for complete relaxation in intact myocytes. Circ Res. 2007;101(9):928–38.

[21] Eschenhagen T, Fink C, Remmers U, Scholz H, Wattchow J, Weil J, et al. Three-dimensional reconstitution of embryonic cardiomyocytes in a collagen matrix: a new heart muscle model system. FASEB J. 1997;11(8):683–94.

[22] Schaaf S, Shibamiya A, Mewe M, Eder A, Stöhr A, Hirt MN, et al. Human engineered heart tissue as a versatile tool in basic research and preclinical toxicology. PLoS One. 2011;6(10):e26397.

[23] Nunes SS, Miklas JW, Liu J, Aschar-Sobbi R, Xiao Y, Zhang B, et al. Biowire: a platform for maturation of human pluripotent stem cell-derived cardiomyocytes. Nat Methods. 2013;10(8):781–7.

[24] Eder A, Vollert I, Hansen A, Eschenhagen T. Human engineered heart tissue as a model system for drug testing. Adv Drug Deliv Rev. Elsevier B.V.; 2015;

[25] Naito H, Melnychenko I, Didié M, Schneiderbanger K, Schubert P, Rosenkranz S, et al. Optimizing engineered heart tissue for therapeutic applications as surrogate heart muscle. Circulation. 2006;114:72–9.

[26] Kim C, Majdi M, Xia P, Wei K a, Talantova M, Spiering S, et al. Non-cardiomyocytes influence the electrophysiological maturation of human embryonic stem cell-derived cardiomyocytes during differentiation. Stem Cells Dev. 2010;19(6):783–95.

[27] Thavandiran N, Dubois N, Mikryukov A, Massé S, Simmons CA, Deshpande VS, et al. Design and formulation of functional pluripotent stem cell-derived cardiac microtissues. Proc Natl Acad Sci. 2014;111(47):16973–16973.

[28] Tulloch NL, Muskheli V, Razumova M V., Korte FS, Regnier M, Hauch KD, et al. Growth of engineered human myocardium with mechanical loading and vascular coculture. Circ Res. 2011;109(1):47–59.

[29] Albini A, Pennesi G, Donatelli F, Cammarota R, De Flora S, Noonan DM. Cardiotoxicity of anticancer drugs: The need for cardio-oncology and cardio-oncological prevention. J Natl Cancer Inst. 2010;102(1):14–25.

[30] Gopinathannair R, Etheridge SP, Marchlinski FE, Spinale FG, Lakkireddy D, Olshansky B. Arrhythmia-Induced Cardiomyopathies. J Am Coll Cardiol. 2015;66(15):1714–28.

[31] Murphy S V, Atala A. 3D bioprinting of tissues and organs. Nat Biotechnol. Nature Publishing Group; 2014;32(8):773–85.

[32] Koch L, Kuhn S, Sorg H, Gruene M, Schlie S, Gaebel R, et al. Laser printing of skin cells and human stem cells. Tissue Eng Part C Methods. 2010;16(5):847–54.

[33] Ananthanarayanan A, Narmada BC, Mo X, McMillian M, Yu H. Purpose-driven biomaterials research in liver-tissue engineering. Trends Biotechnol. Elsevier Ltd; 2011;29(3):110–8.

[34] Gao G, Schilling AF, Hubbell K, Yonezawa T, Truong D, Hong Y, et al. Improved properties of bone and cartilage tissue from 3D inkjet-bioprinted human mesenchymal stem cells by simultaneous deposition and photocrosslinking in PEG-GelMA. Biotechnol Lett. Springer Netherlands; 2015;37(11):2349–55.

[35] Xu F, Celli J, Rizvi I, Moon S, Hasan T, Demirci U. A three-dimensional in vitro ovarian cancer coculture model using a high-throughput cell patterning platform. Biotechnol J. 2011;6(2):204–12.

[36] Norotte C, Marga FS, Niklason LE, Forgacs G. Scaffold-free vascular tissue engineering using bioprinting. Biomaterials. Elsevier Ltd; 2009;30(30):5910–7.

[37] Duan B, Hockaday LA, Kang KH, Butcher JT. 3D bioprinting of heterogeneous aortic valve conduits with alginate/gelatin hydrogels. 2013;101(5):1255–64.

[38] Ott HC, Matthiesen TS, Goh S-K, Black LD, Kren SM, Netoff TI, et al. Perfusion-decellularized matrix: using nature's platform to engineer a bioartificial heart. Nat Med. 2008;14(2):213–21.



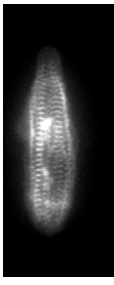
[39] GILBERT T, SELLARO T, BADYLAK S. Decellularization of tissues and organs. Biomaterials. 2006;27:3675–83.

[40] Lu T-Y, Lin B, Kim J, Sullivan M, Tobita K, Salama G, et al. Repopulation of decellularized mouse heart with human induced pluripotent stem cell-derived cardiovascular progenitor cells. Nat Commun. Nature Publishing Group; 2013;4:1–11.

Summary

Resumo

Samenvatting



Summary

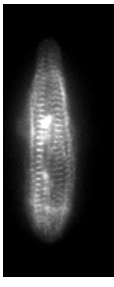
This thesis describes research about cells from the human heart. To provide some context to this research lets explain some basics of biology. All living beings are organisms. All living beings are built from cells, as the cell is the smallest living element containing all the information and function capable of creating a more complex organism such as the human being. The information inside each cell is stored in the DNA as code (sequence). All cells of each unique individual contain exactly the same DNA sequence. Consequently, what distinguishes a skin cell from a gut cell or a stem cell is its function. Taking into consideration this concept a group of scientist from a Japanese university, headed by Dr. Yamanaka, developed a technique in 2006 that enables the transformation of a skin cell into a stem cell (functional transformation of the cell). Dr. Yamanaka was given the Nobel Prize of Medicine in 2012 for this achievement. Currently, our laboratory in the Leiden University Medical Center is specialized, among other things, in transforming cells of any individual into stem cells using Dr. Yamanaka's method. The stem cell is the mother cell of our entire body, as this cell gets multiplied and transformed naturally (differentiates) into every single cell in our body (this process is the reversed of the one mentioned above), giving us life. Making use of this stem cell's special ability we, in our laboratory, differentiate the stem cells into cells of the heart through the use of a specific molecular cocktail. These heart cells are very much alike the cells present in our hearts as they generate electrical impulses (similar to the impulses described in the movies when the patient is connected to the machine in the hospital bed) and contract (heart beat) in the laboratory. However, these heart cells have the morphology of a thin layer of cells in a bottom of a laboratory dish, which is far from the shape and composition of an adult heart. The adult heart has very peculiar characteristics that are still not completely understood by the scientific community and is formed by millions of cells from various types. The type of cell responsible for the motion of contraction of the heart is called cardiomyocytes. These cardiomyocytes are generated in the first weeks of an embryo and further develop during both gestation inside the uterus and after birth until the individual becomes an adult. In this perspective it can be understood that the maturation state of the cardiomyocytes is dependent of the age of the embryo or individual. For example, the cardiomyocytes of a 7-month-old child are more developed when compared with the cardiomyocytes of an embryo of 16-week gestation. On the other hand, these cardiomyocytes are less mature than the ones from a 20-year-old adult. This difference is a major research topic and it characterizes the state of the art in this field: currently the cardiomyocytes produced in the laboratory have a maturation level identical of an embryo of 15 weeks of gestation, meaning that in our laboratory we produce cardiomyocytes equivalent to the ones of an fetus, which is quite far from the adult level. Using cell made in laboratory to study what happens in the human is the same as analyzing the movements of a newborn to study how an adult walks.

The **first chapter** is a theoretical introduction of this thesis as it describes the current "state of the art" in this field of biology.

The **second chapter** of this thesis focuses in the use of polymers that mimic the environment

inside the human body. It is commonly known that all tissues of our body are soft with the exception of bones. Therefore, most cells are in contact with soft tissue. This is not the reality in the laboratory dish where the cell cultures are maintained in stiff plastic or glass bottom dishes. We understand that this type of environment is not optimal for the development of the cardiomyocytes. With the use of some polymers like PDMS and acrylamide we are able to mimic certain characteristics of the living tissues. In this chapter we describe different techniques to use these polymers as a base to culture the cells with similar characteristics to the human body. One of the main characteristics of these polymers is the fact that they are soft enough to be deformed by cardiomyocytes upon contraction. Through this technique we are able to measure the force produced by the cardiomyocyte upon its contraction (Contraction Force). These techniques of cell culture and contraction force measurement are the basis for the research in the following chapters.

In the **third chapter** the state of maturation of the cardiomyocyte made in laboratory is evaluated. This evaluation is made thought the measurement of contraction force and electrical impulses generated by the cardiomyocytes. This evaluation was performed in comparison with the *in vivo* human heart. We compared these parameters between cardiomyocytes made in the laboratory and cardiomyocytes isolated from embryos between 15 and 19 weeks of gestation. We observed that the cardiomyocytes made in the laboratory contract with less force and similar speed of electrical impulses than the cardiomyocytes from embryos of 15 to 19 weeks of gestation. With the objective of improving the maturation level of the cardiomyocytes made in the laboratory we made use of commercially available culture medium, which composition induces the growth and maturation of the cardiomyocytes. With the help of this new culture medium the cardiomyocytes made in the laboratory increased their contraction force and their speed of electrical impulses to levels above the cardiomyocytes from embryos. We concluded that it is possible to increase the level of maturation of these cardiomyocyte *in vitro* (in the lab).



The **fourth chapter** describes the development of a new alternative culture medium to increase the maturation level of the cardiomyocytes made in the laboratory and its use to analyze a heart disease. The culture medium has great potential for maturing the cardiomyocytes all the way to levels close to the adult reality, therefore, we continued to further develop the medium having this goal in mind. In order to develop this new culture medium we sequentially added three molecules that are known to play a role in the growth and maintenance of the human body: A thyroid hormone (T3), a growth factor (IGF-1) and a synthetic glucocorticoid (Dexamethasone). The incremental addition of each molecule induced an increase in the force of contraction and in the speed of the electrical impulses generated by the cardiomyocytes made in the laboratory. One of the goals of developing the technology of producing the human cardiomyocytes in the laboratory is to enable the study of all heart diseases that affect human beings in the controlled situation of the laboratory. This technology will open the doors to the development of new medication that can prevent or cure diseases such as heart failure, fibrillation, hypertrophic cardiomyopathy, etc. At the moment, the low level of maturation of the cardiomyocytes made in the laboratory and their monolayer morphology hampers its use to model a large number of heart diseases *in*

vitro. Nevertheless, this new culture medium (T3+IGF-1+Dex) enabled the study of a heart disease named hypertrophic cardiomyopathy (HCM) using stem cells derived transformed from skin cells of patients with this disease. We further transformed these stem cells into cardiomyocytes that have the same defect as the patients' heart. Although this defect was not observable in initial experiments, after culturing the cardiomyocytes in the new medium we observed that the cardiomyocytes of the patients contract with significantly less force than the ones from the cardiomyocytes derived from stem cells of a normal person. These results opens the door to study this disease that affects 1 person in each 500, meaning that it is one of the most common heart diseases affecting humans.

The **fifth chapter** describes the development of a synthetic protein through genetic manipulation. The sarcomere is considered the "engine" of the heart as it enables the contraction of cardiomyocytes and consequently the contraction of the heart. This sarcomere is a type of Lego in which the pieces are proteins capable of moving simultaneously back and forth inside each cardiomyocyte. The way that his Lego is organized is used by the researchers as a scale to determine the state of maturation and health of a cardiomyocyte. In another words, by evaluating the organization of the sarcomeres (the Lego) we can assess the maturation state or disease state of cardiomyocytes. To evaluate the sarcomere organization with the currently available techniques it is necessary to kill the cells with a fixative. This procedure precludes the analysis of the sarcomeres while they are forming or moving during contraction (dynamic analysis). In order to make the dynamic analysis of the sarcomeres we took one of the proteins that constitutes the sarcomere and made it fluorescent so we could see the sarcomeres live under the microscope. In this project we used the sarcomeric protein "α-actinin" and we fused it with a red fluorescent protein. This fluorescent protein is a synthetic protein capable of emitting red light when its electrons are excited with green light. The fusion of these two proteins was done through genetic manipulation (cloning). After cloning, this fusion protein was placed into a virus that infects the cells and forces them to express the protein that we have created. The consequence of the expression of this fusion protein is its incorporation into the sarcomeres when the cell is alive. This new technology allows a dynamic evaluation of the maturation or disease level of the human cardiomyocytes.

The **sixth chapter** is the integration of all the previous chapters as it describes the usage of the technology developed in the chapters 2, 3, 4 and 5 to analyze the heart disease described in chapter 4. In this study we used the technology of the soft polymers, the contraction force measurements, the maturation medium and the fluorescent sarcomeres to describe and study the consequences of a defect in a protein responsible for regulating contraction (named Myosin Binding Protein C3 or MYBPC3). The results showed that MYBPC3 deficiency induces a reduction in contraction force of the cardiomyocytes and a reduction in the sarcomere movement during contraction. The technology developed here allows the analysis of contraction force and the sarcomere movement in the same cell, from which can be concluded that the contraction force of the cardiomyocytes is correlated with the movement of the sarcomeres. From this its inferred that the contraction force is affected by the reduction of the sarcomere movement, which in turn is affected by the MYBPC3 deficiency.

We also show that the MYBPC3 deficiency induces a reduction in energy consumption of the cardiomyocytes. In conclusion a characterization and evaluation of the cardiomyocytes with a MYBPC3 deficiency has been performed, creating a model that can be used for the discovery and development of new drugs that can revert the effects of the MYBPC3 deficiency in humans.

The **seventh chapter** describes the development of a new biotechnology that allows the expansion and characterization of cardiac progenitor cells. As mentioned above all cells from our body are derived from a single embryonic cell. This cell divides itself multiple times and the resulting cells of each division differentiate into the different organs and tissues. This differentiation occurs step by step, and at each step the cells become more and more specialized until they reach their final form/function. This differentiation occurs not only in living beings but can also be replicated in the laboratory through the differentiation of stem cells. In order to study and understand the differentiation of stem cells into specific organs it is necessary to collect the intermediate cells (named progenitor cells) so their biological characterization can be performed. Until now the only procedure used to obtain progenitor cells is done through its isolation at a specific time point counting from the start of the differentiation. However, the time needed to get to a specific time point of differentiation varies with each differentiation and with the cell line used. In this study we inserted a modified protein (cMYC) into the stem cells that allowed us to stop the differentiation and to expand the progenitor cells simply by adding a molecule (Doxycycline) to the culture medium. This molecule activated the cMYC which in turn initiates the propagation of the progenitor cells, stopping their differentiation. In the first part of this study we performed an optimization of the progenitor cell expansion using other supplementary molecules. In the second part of this study we characterized the progenitor cells based on specific markers such as NKX2-5; Podoplanin and PDGFRα. In the third part we tested the capacity of these progenitors to differentiate into the different cell types present in the heart such as pace-making cells, working myocardium, smooth muscle cells and endothelial cells. This progress has great impact on the scientific community that studies the heart as it allows the research on how the different cell types of the heart are generated at a molecular level.



The **last chapter** is a general discussion of the data of all the chapters in this thesis, taking into consideration the state of the art of this field of research. The chapter ends with my perspective regarding the future advances in the heart research using human stem cells.

Resumo

Esta tese desenvolve temas sobre células do coração as humano. Para contextualizar este tema comecemos por explicar alguns conceitos de biologia.

Todos os seres vivos são organismos. O organismo que compõe todos os seres vivos é a célula, sendo que a célula é o elemento vivo mais pequeno que detém toda a informação e funcionalidade capaz de originar um organismo mais complexo como o ser humano. A informação dentro de cada célula é armazenada no ADN sobre forma de código (sequencia). Todas as células de um único individuo contêm exatamente a mesma sequência de ADN, por consequência o que distingue uma célula do cérebro de uma célula do intestino é a sua funcionalidade. Tendo em conta este conceito um grupo de cientistas de uma universidade no Japão (liderado por Dr. Yamanaka) conseguiu, em 2006, transformar uma célula da pele numa célula estaminal (transformação funcional da célula), pelo qual ganhou o prémio Nobel da Medicina em 2012.

Presentemente, o nosso laboratório de investigação, no Leiden University Medical Center, é especializado em transformar células do corpo de qualquer individuo em células estaminais usando o método do Dr. Yamanaka. A célula estaminal é a célula mãe de todo o nosso organismo, é esta célula que no feto se multiplica e se transforma naturalmente (diferencia) em cada célula do nosso corpo (processo inverso ao acima descrito), dando-nos vida. Usando esta capacidade das células estaminais, no nosso laboratório, diferenciamos as células estaminais em células do coração (células cardíacas) através de um cocktail específico de compostos. Estas células cardíacas são em muito parecidas às células presentes no nosso coração uma vez que geram impulsos elétricos (iguais aos impulsos descritos nos filmes quando o paciente está ligado à maquina na cama de hospital) e contraem (batimento cardíaco) em laboratório. No entanto, o conjunto destas células cardíacas apresenta-se como uma camada fina de células num prato de laboratório, não sendo suficiente para obter a forma de um coração adulto.

O coração adulto humano tem uma forma específica muito complexa que ainda não é totalmente compreendida pela comunidade científica, sendo constituído por milhões de células de vários tipos. O tipo de células cardíacas responsáveis pelo batimento cardíaco são chamadas cardiomiócitos. Estes cardiomiócitos nascem nas primeiras semanas de vida do embrião dentro do útero que vão crescendo e desenvolvendo durante a gestação, continuando apos o nascimento até o individuo se tornar adulto. Nesta perspectiva entende-se que o estado de maturação dos cardiomiócitos é dependente da idade do embrião ou do individuo. Por exemplo os cardiomiócitos de uma criança de 7 meses estão mais desenvolvidos do que os cardiomiócitos de um embrião uterino de 16 semanas, mas por outro lado são mais imaturos quando comparados com os cardiomiócitos de um adulto de 20 anos.

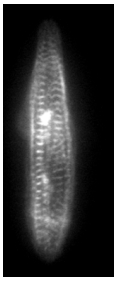
Daqui surge a questão fulcral que indica o estado do avanço científico:

Presentemente os cardiomiocitos produzidos em laboratório tem um nível de maturação idêntico ao de um embrião uterino com menos de 15 semanas, ou seja em laboratório produzimos cardiomiocitos equivalentes a cardiomiocitos dum feto, estando portanto muito

longe do nível adulto. Usar estas células feitas em laboratório para estudar o que se passa no corpo humano é o mesmo que analisar os movimentos de um recém-nascido para estudar como um ser adulto se movimenta, a comparação é válida mas com uma relevância pouco significativa.

O **primeiro capitulo** é uma introdução teórica a esta tese de doutoramento, pelo que descreve difíceis conceitos de biologia e o corrente "estado da arte" deste campo da biologia humana. Em poucas palavras, ler o primeiro capítulo não será tarefa fácil para quem não esteja familiarizado com a área, visto estar apresentado de forma técnica.

O **segundo capitulo** desta tese é focado no uso de polímeros que simulam o ambiente dentro do corpo humano. É de conhecimento geral que todos os tecidos do nosso corpo são moles com a excepção dos ossos, portanto as células estão em contacto com um tecido mole. Esta não é a realidade no prato de laboratório, já que este é feito de plástico ou vidro bastante rijo. Entende-se então que este tipo de ambiente rijo não é propício para as células se desenvolverem. Certos polímeros como o PDMS e Acrylamida são capazes de imitar as características dos tecidos vivos, sendo portanto bons precursores para o desenvolvimento e análise das células. Neste capítulo desenvolve-se diferentes técnicas para o uso destes polímeros como base de sustentação das células com características similares ou corpo humano. Uma das principais características destes polímeros é serem moles o suficiente para poderem ser deformados pelos cardiomiocitos quando estes contraem. Esta característica possibilita a medição da força exercida por cada cardiomiocito aquando da sua contração (Força de contração). Estas técnicas de cultura de células e medição de força de contração são a base dos progressos científicos dos capítulos seguintes.



No **terceiro capitulo** é feita a avaliação do estado de maturação dos cardiomiocitos feitos em laboratório. Esta avaliação é feita através da medição da força de contração dos cardiomiocitos e dos impulsos elétricos que estes geram. Este tipo de avaliações são feitas em comparação com a realidade do coração humano. Neste sentido comparámos os parâmetros referidos anteriormente entre os cardiomiocitos feitos em laboratório e cardiomiocitos de embriões de 15 a 19 semanas de gestação, observando que os cardiomiocitos feitos em laboratório contraem com menos força e geram impulsos elétricos equivamente lentos aos seus homólogos provenientes de embriões, de onde se conclui que os cardiomiocitos feitos em laboratório tem um nível de maturação abaixo ou proximo de um embrião de 15 semanas. Com o objectivo de melhorar o nível de maturação dos cardiomiocitos feitos em laboratório usou-se uma nova combinação de meios de cultura adquiridos comercialmente cuja composição estimula o crescimento e maturação dos cardiomiocitos. Com a ajuda destes novos meios de cultura de células os cardiomiocitos feitos em laboratório passaram a contrair com mais forca e a gerar impulsos elétricos mais rápidos que os seus homólogos provenientes de embriões, de onde se concluiu ser possível aumentar o nível de maturação destes cardiomiocitos em *in vitro* (em laboratório).

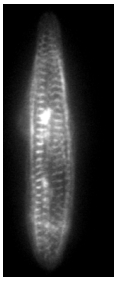
O **quarto capitulo** descreve o desenvolvimento de um meio de cultura celular alternativo para maturação dos cardiomiocitos em laboratório e o seu uso na análise de uma doença cardíaca. Meios de cultura para maturação tem um grande potencial para trazer os car-

diomiocitos para um nível de maturação semelhante ao de um humano adulto, por isso nós continuámos a desenvolver novos meios de cultura com este objectivo em mente. Para desenvolver este novo meio de cultura, adicionamos sequencialmente ao meio base três moléculas responsáveis pelo crescimento e manutenção do corpo humano: a hormona da tiróide (T3), um factor de crescimento (IGF-1) e um glucocorticoide sintético (Dexamethasone). A adição incremental de cada uma destas moléculas induziu um aumento na força de contração dos cardiomiocitos e da velocidade do seu impulso elétrico, concluindo-se que foi atingido um novo patamar de maturação dos cardiomiocitos em laboratório. Um dos objetivos em desenvolver a tecnologia de cardiomiocitos produzidos em laboratório é poder-se estudar todas as doenças cardíacas que afectam o ser humano nas condições controladas de laboratório. Tal tecnologia abrir-nos-á as portas para o desenvolvimento de novos medicamentos que podem vir a prevenir ou a tratar doenças como o enfarte cardíaco, fibrilação, hipertrofia cardíaca, etc. Neste momento, devido ao baixo nível de maturação e a forma destes cardiomiocitos impossibilita a reprodução da grande maioria das doenças cardíacas em laboratório. No entanto o uso este novo meio de cultura (T3+IGF+Dex) possibilitou o estudo duma doença cardíaca chamada cardiomiopatia hipertrófica (HCM) usando células estaminais provenientes da transformação das células da pele de pacientes com esta doença. Neste procedimento transformámos as células dos pacientes em células estaminais e por sua vez transformámos estas em cardiomiocitos com o mesmo defeito que o coração dos pacientes têm. Este defeito não era visível inicialmente mas depois de se aplicar o novo meio de cultura inferimos que os cardiomiocitos dos pacientes contraiam com significativamente menos força que os de uma pessoa normal. Este avanço científico abre portas para o estudo desta doença que afecta 1 pessoa em cada 500, ou seja é uma das doenças cardiacas mais comuns que afecta os seres humanos.

O **quinto capitulo** fala da construção de uma proteína sintética através de manipulação genética. O motor que faz os cardiomiocitos e consequentemente o coração contrair chama-se sarcómero. Este sarcómero é um tipo de lego em que as peças são proteínas que se movem em uníssono para traz e para a frente dentro de cada cardiomiocito. A forma como este lego está organizado é usada pelos cientistas como barómetro do estado de maturação e do estado de saúde dos cardiomiocitos. Ou seja, ao avaliar como os sarcómero estão organizados infere-se a avaliação do nível de maturação dos cardiomiocitos ou o nível de doença destas células. Para se poder avaliar estes sarcómeros com as técnicas existentes hoje em dia é necessário matar as células fixando-as. Este procedimento impede a análise dos sarcómeros enquanto estes se formam ou se movimentam durante a contração (analise dinâmica). Para podermos fazer a análise dinâmica dos sarcómeros decidimos pegar numa das proteínas que constitui os sarcómeros e torna-la fluorescente para se poder visualizar ao microscópio. Neste projeto usamos a proteína sarcomerica "α-actinin" e fundimo-la com uma proteína fluorescente vermelha. Esta proteína fluorescente é uma proteína sintética especial capaz de emitir luz vermelha quando os eletrões do seu interior são excitados com luz verde. A fusão destas duas proteínas foi feita através de manipulação genética (clonagem). Após a clonagem desta proteína para dentro de um vector viral produzimos um vírus que quando infecta as células alvo as obriga a expressar esta proteína que criámos. A consequência da expressão desta proteína fusão é que ela é incorporada nos sarcómeros

pela célula permitindo que possamos visualizar a formação e o movimento/contração dos sarcómeros enquanto a célula está viva. Esta nova tecnologia permite a avaliação dinâmica do nível de maturação e de doença dos cardiomiocitos humanos.

O **sexto capitulo** é o culminar de todos os capítulos anteriores pois descreve o uso da tecnologia desenvolvida nos capítulos 2, 3, 4, 5 para analisar a doença cardíaca descrita no capitulo 4. Neste estudo usou-se a tecnologia dos polímeros, da medição da contração das células, os meios de maturação e os sarcómeros fluorescentes para descrever e tentar entender o que realmente se passa quando o cardiomiocito tem uma deficiência numa proteína responsável por regular a sua contração (chamada Myosin Binding Protein C3 ou MYBPC3). Mostramos que a deficiência da MYBPC3 induz uma diminuição da força que os cardiomiocitos contraem e induz uma redução no movimento dos sarcómeros durante a contração. A nova tecnologia que desenvolvemos permite-nos analisar a força de contração e o movimento dos sarcómeros na mesma célula, pelo que podemos concluir que a força de contração dos cardiomiocitos é diretamente relacionada ao movimento dos sarcómeros. Dai infere-se que a força de contração das células é afectada pela redução do movimento dos sarcómeros que por sua vez são afectados pela deficiência da MYBPC3. Demonstramos também que a deficiência da MYBPC3 provoca uma redução no consumo de energia da célula. Em conclusão neste capítulo avaliamos e caracterizamos os cardiomiocitos com deficiência da MYBPC3, criando um modelo pode ser utilizado para o desenvolvimento de compostos que revertam os efeitos da deficiência da MYBPC3 em seres humanos.



O **sétimo capitulo** descreve o desenvolvimento de uma nova tecnologia biológica que permite a expansão e caracterização de células progenitoras do coração. Como descrito a cima, todas as células do nosso corpo provêem de uma só célula embrionária. Esta célula divide-se inúmeras vezes e as células provenientes de cada divisão vão-se diferenciando nos diferentes tecidos e órgãos. Esta diferenciação acontece passo a passo, sendo que a cada passo as células vão-se tornado cada vez mais especificas até atingirem a sua forma/função final. Esta diferenciação não só acontece nos seres vivos como é replicado em laboratório aquando da diferenciação das células estaminais. Para se estudar e compreender esta diferenciação das células estaminais nos diferentes órgãos é necessário obter grande número destas células intermediárias (chamadas células progenitoras) para se poder fazer a sua caracterização biológica. Até ao presente o único procedimento de se obter células progenitoras é através do isolamento destas células a um tempo fixo após o início da diferenciação. No entanto o tempo necessário para chegar a um determinado passo de diferenciação varia consoante a diferenciação e células usadas. Neste estudo inserimos uma proteína modificada (cMYC) nas células estaminais que nos permite parar a diferenciação e expandir as células progenitoras nos diferentes passos por apenas adicionar uma molécula (Doxycycline) ao meio de cultura. Esta molécula activa o cMYC que por sua vez inicia a multiplicação das células progenitoras, parando a diferenciação. Na primeira parte deste estudo é feita a otimização da expansão das células progenitoras com a ajuda de outras moléculas suplementares. Na segunda parte do estudo é feita a caracterização destas células progenitoras com base em marcadores específicos como NKX2-5; Podoplanin e PDGFRα. Na terceira parte a capacidade de diferenciação destes progenitores em diferentes tipos de células pre-

sentes no coração, como células pace-maker, cardiomiocitos ventriculares, células endoteliais e células musculares lisas, é testada aquando da remoção da Doxycycline. Em conclusão a tecnologia desenvolvida neste estudo abre as portas para uma melhor compreensão dos diferentes passos de diferenciação das células estaminais nas diferentes células do coração. Este avanço tem grande impacto na comunidade científica que investiga o coração uma vez que permite estudar o processo de como as diferentes células do coração humano são produzidas a nível molecular.

O **ultimo capitulo** é uma discussão geral dos resultados de todos os capítulos tendo em consideração o estado corrente da investigação científica desta área. O capítulo termina com as minhas perspectivas de futuros avanços na investigação do coração usando células estaminais humanas.

Samenvatting

Dit proefschrift beschrijft onderzoek dat gaat over de cellen van het menselijk hart. Om de lezer wat achtergrondinformatie te geven over de context van dit onderzoek, zal ik beginnen met het uitleggen van een aantal basisprincipes van de biologie. Alle levende wezens zijn organismen. Alle organismen zijn opgebouwd uit cellen; de cel is het kleinste levende element van het lichaam, waarin alle informatie is opgeslagen voor het creëren van een complex organisme zoals de mens. Deze informatie is opgeslagen in het DNA als code (sequentie). Alle cellen in het lichaam van een individu bevatten dezelfde DNA-sequentie. Maar toch zijn de cellen in het lichaam van de mens heel verschillend; bijvoorbeeld een hersencel en een darmcel verschillen sterk van vorm en functie. Dit in acht nemend, heeft een groep wetenschappers aan een Japanse universiteit, geleid door Dr. Yamanaka, in 2006 een techniek ontwikkeld waardoor een huidcel in een stamcel kon worden veranderd (functionele transformatie van de cel). Dr. Yamanaka kreeg voor deze prestatie de Nobelprijs voor de Geneeskunde in 2012. Ons laboratorium in het Leids Universitair Medisch Centrum is gespecialiseerd, in het transformeren van cellen naar stamcellen met behulp van de methode van Dr. Yamanaka.



Maar wat is nu precies een stamcel? De stamcel is de moedercel van ons lichaam, aangezien deze cel wordt vermenigvuldigd en omgezet in alle typen lichaamscellen. Het proces van ontwikkeling van de stamcel tot de uiteindelijke gespecialiseerde cel heet differentiatie. In ons lab maken wij gebruik van deze speciale eigenschap van stamcellen, en differentiëren de stamcellen naar cellen van het hart. Het volwassen hart heeft zeer specifieke eigenschappen die nog niet volledig worden begrepen door de wetenschappelijke gemeenschap, en bestaat uit verschillende typen cellen. Het type cel verantwoordelijk voor het kloppen van het hart wordt de hartspiercellen genoemd. Dit type cel ontstaat als het embryo slechts enkele weken oud is, en ontwikkeld zich verder, zowel tijdens de zwangerschap in de baarmoeder, als na de geboorte totdat het individu volwassen is. Hoever de hartspiercellen ontwikkeld zijn, is dan ook afhankelijk van de leeftijd van het embryo of individu. Zo zijn de hartspiercellen van een kind van 7 maanden verder ontwikkeld dan die hartspiercellen van een embryo van 16 weken, en zijn de hartspiercellen weer minder ontwikkeld dan die van een volwassene van 20 jaar oud. Momenteel zijn de hartspiercellen die geproduceerd worden in het laboratorium qua ontwikkelingsstadium vergelijkbaar met hartspiercellen van een embryo van 15 weken oud. Deze hartspiercellen bereiken dus nog lang niet het niveau van volwassen hartspiercellen. Verder zijn deze cellen zijn gekweekt in het laboratorium, en bestaan slechts uit een dunne laag cellen op de bodem van een glazen schaal, wat niet erg lijkt op de vorm en samenstelling van volwassen hartweefsel in een echt mens. Dit proefschrift gaat over manieren om de hartspiercellen die in het laboratorium worden gekweekt, verder te laten ontwikkelen, zodat ze meer gaan lijken op de hartspiercellen die te vinden zijn in het hart van een volwassen persoon.

Het **eerste hoofdstuk** is een theoretische inleiding van dit proefschrift, en beschrijft de huidige stand van zaken in dit gebied van de biologie.

Het **tweede hoofdstuk** is gericht op het gebruik van polymeren die het milieu in het

menselijk lichaam na bootsen. De meeste weefsels van ons lichaam zijn zacht, met uitzondering van de botten. De meeste cellen in ons lichaam, komen dan ook in contact met zachte weefsels. Echter, in het laboratorium is dit niet het geval; de laboratorium schaal waarin de cellen worden gekweekt is gemaakt van hard kunststof of glas. Deze omgeving is niet optimaal voor de ontwikkeling van de hartspiercellen. Met het gebruik van bepaalde polymeren zoals PDMS en acrylamide kunnen wij bepaalde kenmerken, zoals de zachtheid van de levende weefsels nabootsen. In dit hoofdstuk beschrijven we verschillende technieken die beschikbaar zijn om deze polymeren te gebruiken als basis om de cellen op te kweken, zodat de cellen kunnen groeien op structuren die lijken op structuren uit het menselijk lichaam. Eén van de belangrijkste eigenschappen van deze polymeren is dat ze zacht genoeg zijn om te kunnen worden vervormd door de hartspiercellen als deze samentrekken. Dit maakt het meten van de kracht die wordt veroorzaakt door de samentrekking van de hartspiercellen mogelijk. Deze technieken vormen de basis voor het onderzoek in de volgende hoofdstukken.

Het **derde hoofdstuk** beschrijft onderzoek naar de ontwikkeling van de hartspiercel in het laboratorium. Voor dit onderzoek werden hartspiercellen die in het laboratorium geproduceerd waren, vergeleken met hartspiercellen die geïsoleerd waren uit embryo's van 15 tot 19 weken oud (abortusmateriaal). Uit dit onderzoek bleek dat de hartspiercellen die ontwikkeld werden in het laboratorium met minder kracht en snelheid samentrokken dan hartspiercellen van embryo's van 15 tot 19 weken oud. Ons doel was om het ontwikkelingsniveau van de hartspiercellen in het laboratorium te verbeteren, door gebruik te maken van een combinatie van commercieel beschikbaar kweekmedium (vloeistof dat gebruikt wordt om de cellen in te laten groeien), waarvan de samenstelling de groei en ontwikkeling van de hartspiercellen verbetert. Met behulp van dit nieuwe kweekmedium, werden de samentrekkingskracht en de snelheid van de elektrische impulsen verbeterd, waardoor de hartspiercellen die werden gekweekt in het laboratorium zich ontwikkelden tot niveaus boven de hartspiercellen van de embryo's van 15 tot 19 weken. We konden hierdoor concluderen dat het mogelijk is om de mate van ontwikkeling van deze hartspiercellen in het laboratorium te verbeteren, met behulp van dit commercieel beschikbare kweekmedium.

Het **vierde hoofdstuk** beschrijft de ontwikkeling van een nieuw alternatief kweekmedium voor de ontwikkeling van hartspiercellen in het laboratorium, en het gebruik ervan voor de analyse van een hartaandoening. Op dit moment wordt onderzoek naar een groot aantal hartziekten in belemmerd door de langzame ontwikkeling van de hartspiercellen in het laboratorium. Verbetering van het kweekmedium, waardoor de hartspiercellen zich beter ontwikkelen, opent deuren naar de ontwikkeling van nieuwe geneesmiddelen die kunnen worden ontwikkeld ter voorkoming of genezing van hartziekten. Om een nieuwe kweekmedium te ontwikkelen, voegden wij achtereenvolgens drie moleculen toe waarvan bekend is dat ze een rol spelen in de groei en het onderhoud van het menselijk lichaam: een schildklier hormoon (T3), een groeifactor (IGF-1), en een synthetisch glucocorticoïde (dexamethason). Doordat deze moleculen werden toegevoegd aan het kweekmedium, namen de samentrekkingskracht en snelheid van de elektrische impulsen toe in de gekweekte hartspiercellen. Met behulp van dit nieuwe kweekmedium (T3 + IGF-1 + Dex) was het mo-

gelijk om een hartziekte genaamd hypertrofische cardiomyopathie (HCM) te onderzoeken, met behulp van stamcellen afkomstig uit de transformatie van huidcellen van patiënten met deze ziekte. Nadat hartspiercellen werden gekweekt in het nieuwe medium, zagen we dat de hartspiercellen die kwamen van patiënten met HCM, aanzienlijk minder krachtig samentrokken dan die van een normaal persoon. Resultaten van dit onderzoek openen de deuren naar verder onderzoek naar deze ziekte, die voorkomt bij 1 op de 500 mensen.

Het **vijfde hoofdstuk** beschrijft de ontwikkeling van een synthetisch eiwit door genetische manipulatie. Het gedeelte van de hartspiercel dat de samentrekking van het hart mogelijk maakt, heet de sarcomeer. Deze sarcomeer kan je zien als een LEGOsteen, die opgebouwd is uit meerdere laagjes: deze laagjes zijn eiwitten. De manier waarop deze eiwitten zijn opgebouwd (bijv. zijn ze rommelig of recht) wordt door onderzoekers gezien als een manier om vast te stellen hoever de hartspiercel is ontwikkeld en hoe gezond de cel is. De meest gebruikelijke methode om de opbouw van de sarcomeer goed te kunnen zien, is door de cellen te doden met een fixeermiddel (zodat ze precies dezelfde vorm houden). Echter, door deze fixatie is het niet meer mogelijk om de cellen te zien bewegen. Aangezien hartspiercellen kloppen, is het heel belangrijk om de beweging van de cellen te kunnen zien. Hier hebben wij een oplossing voor gevonden. Aan één van de eiwitten die het sarcomeer vormt, genaamd α-actinine, verbonden wij een lichtgevend (fluorescerend) eiwit, terwijl de cel nog in leven was. Deze nieuwe techniek maakte het mogelijk om de hartspiercellen te bekijken onder de microscoop terwijl ze nog in leven zijn en kloppen.



In het **zesde hoofdstuk** wordt de hartziekte HCM verder onderzocht, aan de hand van de technieken die beschreven zijn in de hoofdstukken 2, 3, 4 en 5. In dit onderzoek probeerden we te begrijpen wat er gebeurt in een hartspiercel die een tekort heeft aan een eiwit dat verantwoordelijk is voor het reguleren van samentrekking (genaamd myosine bindend eiwit C3, of MYBPC3). We hebben aangetoond dat MYBPC3 tekort zorgt voor een verminderde samentrekkingskracht, en een vermindering van de sarcomeer beweging tijdens de samentrekking. De nieuwe technologieën die we hebben ontwikkeld, stellen ons in staat om de samentrekkingskracht en de sarcomeer beweging in exact dezelfde cel te meten. Hierdoor konden wij zien dat de samentrekkingskracht wordt beïnvloed door de vermindering van de sarcomeer beweging, die op zijn beurt worden beïnvloed door de MYBPC3 tekort. We tonen ook aan dat het tekort aan MYBPC3 leidt tot een vermindering van het energieverbruik van de hartspiercellen. Door dit onderzoek hebben we een model ontwikkeld dat gebruikt kan worden voor de ontdekking en ontwikkeling van nieuwe geneesmiddelen die kunnen helpen bij een MYBPC3.

Het **zevende hoofdstuk** beschrijft de ontwikkeling van een nieuwe biotechnologie, die de groei en ontwikkeling van voorlopercellen van hartcellen mogelijk maakt. Zoals eerder beschreven, stammen alle cellen van ons lichaam af van een embryonale cel. Deze cel deelt zich miljoenen keren, en de cellen die ontstaan na elke celdeling ontwikkelen zich tot de verschillende organen en weefsels. Deze differentiatie gebeurt stapsgewijs, en bij elke stap worden de cellen meer gespecialiseerd, totdat ze hun uiteindelijke vorm / functie bereiken. Om deze differentiatie van stamcel tot orgaancel te bestuderen en begrijpen, is het noodzakelijk om de cellen die als tussenstap worden aangemaakt (genaamd voorloper-

cellen) te onderzoeken. Tot nu toe konden deze voorlopercellen alleen verkregen worden door isolatie op een bepaald tijdstip gerekend vanaf het begin van de differentiatie. Dit tijdstip verschilt per differentiatie en de gebruikte cellijn. In dit onderzoek bedachten we een methode om de voorlopercellen op een makkelijkere manier te isoleren en te vermenigvuldigen. We voegden het gemodificeerde eiwit cMYC, toe aan de stamcellen, en voegden het molecuul Doxycycline toe aan het kweekmedium. Dit molecuul activeert de cMYC, dat op zijn beurt zorgt dat de voorlopercellen stoppen met verder differentiëren, en toenemen in aantal. In het eerste deel van deze studie hebben we deze methode geoptimaliseerd door gebruik te maken van andere aanvullende moleculen. In het tweede deel van deze studie hebben we de kunnen bewijzen dat de gekweekte voorlopercellen daadwerkelijk de voorlopers zijn van hartspiercellen, door te laten zien dat ze de specifieke markers NKX2-5; Podoplanin en PDGFRα droegen. In het derde deel van de studie hebben we de capaciteit van deze voorlopers getest, om te zien of ze in alle verschillende celtypen van het hart kunnen differentiëren, zoals pace-maker cellen, hartspiercellen, gladde spiercellen en endotheelcellen. De resultaten van dit onderzoek hebben grote invloed op de wetenschappelijke wereld die zich richt op onderzoek naar het hart, omdat het aanwijzingen geeft naar de manier waarop de verschillende celtypen in het hart worden ontwikkeld op moleculair niveau.

Het **laatste hoofdstuk** is een algemene bespreking van de gegevens van alle hoofdstukken van dit proefschrift. Dit hoofdstuk eindigt met mijn perspectief op de toekomstige ontwikkelingen in onderzoek naar het hart, waarbij menselijke stamcellen worden gebruikt.

Acknowledgements

Em primeiro lugar quero agradecer aos meus pais António e Ângela Ribeiro por todo o apoio incondicional e aconselhamento a todos os níveis durante todo o meu percurso pessoal, académico e profissional. Sem vocês eu não chegava onde cheguei.

A warm thank you to Robert Passier for helping and guiding me through this PhD and for all the funny moments and fruitful discussions that eased it up and made this process very interesting.

A deep word of thank you to Christine Mummery for offering me the opportunity to do this PhD and for all the guidance and door opening that enabled me to successfully finish it.

-I would like to express my thankfulness to:

Georgios Kosmidis for always being there for me, in the good and bad moments. I very much appreciated our everyday lunch with all the interesting stories and discussions.

Pedro Contumelias por estares sempre disponivel e teres sempre uma prespectiva diferente. Apreciarei sempre as nossas caminhadas por telheiras até às tantas da manhã.

Pepijn Burgers for all your support thought out these years and for reminding me of how crazy I can be.

João Rodrigues por estares presente e me ouvires durante estes anos. Vou-me sempre recordar das tuas historias malucas sempre divertidas.

Luis Janeiro for enlightening me with valuable new concepts and always showing me a different perspective to every situation. You will always be my mentor.

Pedro Oliveira por sempre me vires visitar às terras frias. Apreciarei sempre os nossos "cafés" quando estou em Lisboa.

Matthew Birket for being my squash mate and my mentor in the lab. I highly appreciated all the help you have given me in my career.

Juan Antonio for making my time in the office/lab super fun. Thank you for all your help and good advice.

Margaux Bennett and (Super) Matt Schriock for taking such good care of me while I was in USA and for all the nice experiences we went through together.

Johnathan Hoijer and Ivan Poulina for teaching me how to dance and most of all for showing me a different world that is unlocked with Salsa.

Sija Stofberg for being such a good anchor during the roughest times of my PhD. I will never forget your kindness and support.

Steven de Maat for the fruitful dinners and stories we shared.



Tessa Sinnige for introducing me to Leiden and for the interesting discussions we had.

Marti Boss for the fun time we spent hanging out.

Caspar for letting me crash your birthday parties and for the fun times we spent.

Harsha-Deepti Devalla and Sabine den Hartogh for your help and support during my PhD. I am very happy for going through this PhD together with you! I really appreciated all the good times and scientific discussions we had throughout this journey.

Jantine, Verena, Tom, Chantal for your precious help in the lab and moral support when things went wrong.

Olga, Antonio, Mervijn for all the help that you gave me on my projects.

Leon and Berend for the help in different technical aspects but mostly for all the very interesting discussions "thinking outside the box" that showed me that imagination is the only limitation.

Milena for the peace of mind you always brought me by showing me that my sense of reality was not skewed.

Dorien for all the help and support throughout my PhD. Without you it would be nearly impossible to get this PhD done!

Kostas, Tim, Annelot, Emeline, Maria, Mathias, Susana, Cheryl, Sjord, Cathelijne, Valeria and Richard for all the good times, drinks and interesting conversations that enlightened my time in the lab

Adam Feinberg and everyone in Feinberg's Lab: Quentin Jallerat, John M. Szymanski, Rachelle N. Palchesko and Stephanie S. Chang for being such nice hosts and showing be the best time in Pittsburg and for the precious teachings of valuable new techniques.

Joop and Annelies for the valuable help and support during my long hours at in the microscope room.

Roeland Reitsema and Matthew Schriock for help with making the cover of this thesis, and to Maaike Alkema for translating my summary to Dutch.

Alkema family: Harco, Petra, Auke, Thijmen, Wouter, Eeke for the support and super nice that made the writing of this thesis bearable.

At last a very special thanks to my sweet Maaike Alkema for being such a happy person and for giving me such important moral support during the busiest times of my PhD.

Curriculum Vitae

Marcelo Catarino Ribeiro was born in the 18th of October 1987, in Lisbon, Portugal. In 2005 he started his studies in Biochemistry in the University of Lisbon. During a 4 month internship he worked in the forensics department of Portuguese Ministry of Justice (Instituto de Medicina Legal e Ciencias Forenses) optimizing ELISA protocols for detection of illegal drugs in human hole blood.

After finishing his bachelor in 2008 he moved to the Netherlands to pursue his Masters in Drug Innovation in the Utrecht University. During his master he performed two 9 month internships: The major was held in Dr. Frank Redegeld's lab in Utrecht, researching new approach to isolation of the Free Light Chain receptor in human mast cells. For his minor he moved to the University of California Berkeley, where he explored the tumour suppressor role of mir-34 in Kras and Braf lung cancer mouse models in Professor Dr. Lin He's lab. He finished his master by writing his thesis about the application of induced pluripotent stem cells in drug development under the supervision of Professor Dr. Christine Mummery.

His PhD was started in 2011 in the lab of Dr. Robert Passier, funded by FOM (Fundamenteel Onderzoek der Materie), in the department of Anatomy & Embryology of Leiden University Medical Center, headed by Professor Dr. Christine Mummery. In 2013 he did a month training in the lab of Dr. Adam Feinberg in Carnegie Mellon University over micro-contact printing and traction force microscopy techniques.

In the beginning of 2016 he moved to the department of Applied Stem cell Technologies in the University of Twente to start his Post Doc in 3D bioengineering of the human heart.



List of Publications

Ribeiro MC, Tertoolen LG, Guadix JA, et al. Functional maturation of human pluripotent stem cell derived cardiomyocytes in vitro e Correlation between contraction force and electrophysiology. **Biomaterials**. 2015; 51:138–50

Birket MJ, Ribeiro MC, Verkerk AO, et al. Expansion and patterning of cardiovascular progenitors derived from human pluripotent stem cells. **Nat Biotechnol**. 2015; 33(9):1–12;

Ribeiro MC*, Birket MJ*, Kosmidis G, et al. Contractile Defect Caused by Mutation in MYBPC3 Revealed under Conditions Optimized for Human PSC-Cardiomyocyte Function. **CellReports**. 2015; (13):1–13

Kosmidis G, Bellin M, Ribeiro MC, et al. Altered calcium handling and increased contraction force in human embryonic stem cell derived cardiomyocytes following short term dexamethasone exposure. **Biochem Biophys Res Commun**. 2015;467(4):998–1005

Okada N, Lin C-P, Ribeiro MC, Biton A, et al. A positive feedback between p53 and miR-34 miRNAs mediates tumor suppression. **Genes Dev**. 2014; 28(5):438–50

